

**BRAIN INFLAMMATION AND CELL DEATH FOLLOWING  
INTRACEREBRAL HEMORRHAGE IN RODENTS**

A Thesis Presented to the Faculty of Graduate Studies and Research in Partial  
Fulfillment of the Requirements for the Degree of Doctor of Philosophy in the

Department of Human Anatomy and Cell Sciences

University of Manitoba

By

Mengzhou Xue, MD, MSc

2004

©Copyright by Mengzhou Xue, 2004.

All rights reserved.

**THE UNIVERSITY OF MANITOBA**  
**FACULTY OF GRADUATE STUDIES**  
\*\*\*\*\*  
**COPYRIGHT PERMISSION PAGE**

**Brain Inflammation and Cell Death Following Intracerebral Hemorrhage in Rodents**

**BY**

**Mengzhou Xue**

**A Thesis/Practicum submitted to the Faculty of Graduate Studies of The University**

**of Manitoba in partial fulfillment of the requirements of the degree**

**of**

**DOCTOR OF PHILOSOPHY**

**MENGZHOU XUE ©2004**

**Permission has been granted to the Library of The University of Manitoba to lend or sell copies of this thesis/practicum, to the National Library of Canada to microfilm this thesis and to lend or sell copies of the film, and to University Microfilm Inc. to publish an abstract of this thesis/practicum.**

**The author reserves other publication rights, and neither this thesis/practicum nor extensive extracts from it may be printed or otherwise reproduced without the author's written permission.**

## ACKNOWLEDGMENTS

First of all, I would like to express my deepest gratitude to my supervisor, Dr. Marc R. Del Bigio. His excellent guidance, advice, encouragement, and full support have made the completion of this thesis possible.

I wish to thank the members of my Graduate Advisory Committee, Drs. Jim Peeling, Hugo Bergen, and Jerry Vriend for their time and helpful suggestions on the study, and Dr. Fred Colbourne for serving as my external examiner.

I thank all the members and students from Dr. Del Bigio's lab for their help and friendship. I would like particular to thank Ms. Janani Balasubramaniam and Mr. Ossama Khan for their kind and enthusiastic help over those years.

I gratefully acknowledge receipt support from Canadian Institutes of Health Research (CIHR), Heart and Stroke Foundation of Canada (HSF), Postdoctoral fellowship from Manitoba Health Research Council (MHRC), Faculty of Graduate Studies of University of Manitoba, and Manitoba Institute for Child Health (MICH) for my PhD training. The experiments were carried out in Department of Pathology and MICH.

A special mention should be made for the excellent technological assistant provided by Sharon Allen and Susan Janeczko in the Department of Pathology at the Health Sciences Centre.

Finally, I thank my wife, Binghua, and my daughters, Che (Qi) and Sara (Shan), for their unconditional support and love, and always being there when I need them. I am also grateful to my parents and parents-in-law in China for their understanding and love.

## ABSTRACT

Intracerebral hemorrhage (ICH) associated with stroke, head trauma and premature birth often predicts poor prognosis. The goals of the experiments described in this thesis are to investigate the role of inflammation and proteolytic enzymes in brain following ICH. Several animal models of ICH, magnetic resonance imaging, pathological, histological and immunological techniques, and behavioral tests were applied to rats and mice of various ages. We found that whole blood causes brain inflammation and brain cell death that is maximal from 48-72 hours. There is a prolonged period of brain reaction over at least 4 weeks. Different specific models of ICH are associated with similar temporal patterns of cell death and inflammation, although the magnitude of inflammation differs. "Activated" leukocytes seem to exacerbate the brain injury in adult rats, as does systemic immune pre-activation in mouse, particularly in 2-day old mice. Thrombin and plasmin are harmful to brain cells in rodents in a dose and age dependent manner. The neonatal brain is relatively more sensitive to proteolytic enzymes than blood. Hirudin can significantly reduce the brain injury following ICH in the acute stage and trends to be mildly protective the neonatal mouse brain. These data suggest that inflammation and proteolytic enzymes play an important role in the pathogenesis of brain damage following ICH. Therefore inhibition of thrombin and inflammation may represent potential targets for therapeutic intervention.

## TABLE OF CONTENTS

TABLE OF CONTENTS.....	iv
ACKNOWLEDGEMENTS.....	ii
ABSTRACT.....	iii
ABBREVIATIONS.....	x

CHAPTERS.....	PAGE
---------------	------

### CHAPTER 1

GENERAL INTRODUCTION.....	1
1.1 Introduction and definitions (stroke, hemorrhage).....	1
1.2 Hemorrhagic stroke in the clinical setting.....	2
1.2.1 Brain hemorrhage in the adult brain.....	2
1.2.2 Hemorrhage in the immature brain.....	4
1.3 Animal models of hemorrhagic stroke.....	5
1.3.1 Microballoon insertion models.....	5
1.3.2 Autologous whole blood injection models.....	6
1.3.3 Collagenase animal models of ICH.....	7
1.3.4 Hypertensive stroke models.....	8
1.3.5 Models of neonatal PVH/IVH and IVH.....	9
1.3.6 Other animal models of ICH.....	9
1.4 Histopathology of ICH.....	10

1.5	Pathophysiology of brain damage after ICH.....	10
1.6	Brain inflammation following ICH (published by Xue M, Balasubramaniam J, Del Bigio MR. "Brain inflammation following ICH." in Current Neuropharmacology. 2003;1: 325-332) .....	12
1.6.1	General aspects of the immune response.....	12
1.6.2	Brain inflammation following ICH in humans.....	13
1.6.3	Early inflammatory mediators following ICH.....	16
1.6.4	Cytokines following ICH.....	16
1.6.5	Adhesion molecules following ICH.....	17
1.6.6	Leukocytes infiltration following ICH.....	18
1.6.7	Brain inflammation following ICH in immature brain .....	19
1.6.8	Treatment of ICH with anti-inflammatory agents .....	19
1.6.9	Summary and conclusion of brain inflammation.....	21
1.7	Brain cell death following ICH.....	22
1.7.1	Brief introduction of cell death in the brain.....	22
1.7.2	Apoptotic cell death pathway.....	25
1.7.3	Intrinsic caspase-dependent pathway.....	25
1.7.4	Extrinsic caspase-dependent pathway.....	25
1.7.5	Caspase-independent pathways.....	26
1.7.6	Bcl-2 family.....	27
1.7.7	BNIP3-mediated neuronal cell death pathway.....	28
1.7.8	Cell death detection methods.....	28
1.7.9	Brain cell death following ICH in humans.....	30

1.7.10	Brain cell death following ICH in animal models.....	31
1.7.11	Proteolytic enzymes involved in cell death following ICH.....	33
1.7.12	Treatment of ICH with pharmacological agents.....	35
1.7.13	Brain cell death following the ICH in immature brain.....	37
1.7.14	Summary and conclusions of brain cell death.....	37
1.8	Proteolytic enzymes in brain development.....	38
1.9	Cell migration from germinal matrix.....	39
1.10	Brain injury in the developing brain in ICH and other brain injury.....	39
1.11	Age-dependent brain response following brain injury.....	41
1.12	Summary.....	42
1.13	General hypotheses .....	43
1.14	Specific goals .....	43

## CHAPTER 2

SPECIFIC EXPERIMENTS.....	45
---------------------------	----

2.1	INTRACEREBRAL INJECTION OF AUTOLOGOUS WHOLE BLOOD IN RATS: TIME COURSE OF INFLAMMATION AND CELL DEATH. (Xue M, Del Bigio MR. Neurosci Lett. 2000;283(3):230-232).....	45
-----	---	----

2.2	COMPARISON OF BRAIN CELL DEATH AND INFLAMMATORY REACTION IN THREE MODELS OF INTRACEREBRAL HEMORRHAGE IN ADULT RATS.	
-----	---	--

	(Xue M, Del Bigio MR. J. Stroke Cerebrovasc. Dis. 2003;12: 152-159).....	54
2.3	INTRACORTICAL HEMORRHAGE INJURY IN RATS: RELATIONSHIP BETWEEN BLOOD FRACTIONS AND BRAIN CELL DEATH. (Xue M, Del Bigio MR. Stroke. 2000;31(7):1721-1727) .....	72
2.4	ACUTE TISSUE DAMAGE AFTER INJECTIONS OF THROMBIN AND PLASMIN INTO RAT STRIATUM. (Xue M, Del Bigio MR. Stroke. 2001;32(9):2164-2169).....	94
2.5	PERIVENTRICULAR / INTRAVENTRICULAR HEMORRHAGE IN NEONATAL MOUSE CEREBRUM. (Xue M, Balasubramaniam J, Buist R. Del Bigio MR, Peeling J. J Neuropath Exp Neur. 2003;62: 1154–1165).....	114
2.6	NEONATAL MOUSE BRAIN IS MORE SEVERELY DAMAGED THAN MATURE BRAIN BY INJECTIONS OF BLOOD, THROMBIN, AND PLASMINOGEN. (Xue M, Del Bigio MR. Submitted to Brain Pathology).....	146
2.7	IMMUNE PREAMPLIFICATION EXACERBATES HEMORRHAGIC BRAIN INJURY IN IMMATURE MOUSE BRAIN. (Xue M, Del Bigio MR. Submitted to Stroke).....	172

2.8	INHIBITION OF THROMBIN ACTIVATION REDUCES BRAIN DAMAGE FOLLOWING INTRACEREBRAL BLOOD INJECTIONS IN NEONATAL MICE.  (Xue M, Balasubramaniam J, Parsons K, McIntyre I, Peeling J, Del Bigio MR. Submitted to J Neuropath Exp Neur).....	196
-----	---	-----

CHAPTER 3

	GENERAL DISCUSSION.....	236
3.1	Animal models play an important role in ICH research.....	236
3.2	Brain inflammation play a role in brain injury following ICH.....	238
3.2.1	Brain inflammation is significant following ICH.....	238
3.2.2	Brain inflammation along with cell death is time-dependent following ICH.....	239
3.2.3	Brain cell death accompanies inflammation following ICH.....	242
3.2.4	Immune preactivation exacerbates the brain damage following ICH.....	242
3.3	Proteolytic enzymes are involved in the pathogenesis of brain damage following ICH.....	244
3.3.1	Brain inflammation and damage caused by thrombin and plasmin are dose and age-dependent manner.....	244
3.3.2	Hirudin reduces brain injury following ICH.....	246
3.4	Brain responses are age-dependent following ICH.....	247
3.5	Shortcomings of these experiments and alternate approaches.....	248

3.6 Conclusions.....250

REFERENCES.....252

## LIST OF ABBREVIATIONS

AIF - Apoptosis induce factor

AVM - arterialvenous malformation

ANOVA - analysis of variance

BBB - blood brain barrier

BDNF - brain-derived neurotrophic factor

BCG - bacillus Calmette-Guerin

BSA – bovine serum albumin

CD - cluster of differentiation (standardized nomenclature for designation of leukocyte surface molecules)

CBF - cerebral blood flow

cm - centimeter

ConA - concanavalin A

CNS - central nervous system

CNTF - generation ciliary neurotrophic factor

CPP - cerebral perfusion pressure

CSF - cerebrospinal fluid

CTL - cytotoxic T lymphocyte

DNA - deoxyribonucleic acid

ELISA - enzyme-linked immunosorbent assay

EOM – enzyme overlay membrane

FGF - fibroblast growth factor

GFAP - glia fibrillary acidic protein

GM - germinal matrix

H&E - hematoxylin and eosin

HLA - human leukocyte antigen

ICAM - intracellular adhesion molecule

ICH - intracerebral hemorrhage

ICV - intracerebroventricular

ICP- intracranial pressure

IFN - interferon

IL - interleukin

iNOS - inducible nitric oxide synthase

ISNT - in situ nick translation

IVH - intraventricular hemorrhage

IUI - intrauterine infection

kg - kilogram

LPS - lipopolysaccharide

MAP - mean arterial pressure

MAPK - mitogen-activated protein kinase

MBP - myelin basic protein

MCA – middle cerebral artery

mg - milligram

MHC - major histocompatibility complex

MIF - macrophage/microglial inhibitory factor

ml - milliliter

mm - millimeter

MMPs - matrix metalloproteinases

MRI - magnetic resonance imaging

mRNA - messenger ribonucleic acid

MS - multiple sclerosis

MTT - 3-(4,5-dimethyl-2-thiazolyl)-2,5-diphenyl-2H tetrazolium bromide]

NF- $\kappa$ B - nuclear factor kappa B

NK - natural killer lymphocytes

NMDA - N-methyl D-aspartate

NO - nitric oxide

PAI - plasminogen activator inhibitor

PAR - protease activated receptors

PBS - phosphate buffered saline

PDGF - platelet derived growth factor

PN-1 - protease nexin-1

PolyI:C - Polyinosinic-polycytidilic acid

PS - phosphatidylserine

PVH - periventricular hemorrhage

PVH/IVH - periventricular/intraventricular hemorrhage

RCA-1 - Ricinus communis agglutinin lectin

ROS - reactive oxygen species

SAH - subarachnoid hemorrhage

SCID - severe combined immune deficient

SEB - staphylococcal enterotoxin B

SHR - spontaneously hypertensive rats

TBI - trauma brain injury

TGF - transforming growth factor

TIMP - tissue inhibitors of metalloproteinases

TNF - tumor necrosis factor

tPA - tissue plasminogen activator

TUDCA - tauroursodeoxycholic acid

TUNEL - terminal deoxynucleotidyl transferase (TdT)-mediated deoxyuridine

triphosphate (dUTP)-biotin nick end labeling

VCAM - vascular adhesion molecule

uPA - urokinase-type plasminogen activator

$\mu\text{g}$  - microgram

$\mu\text{l}$  - microliter

$\mu\text{m}$  - micrometer

## Chapter 1      GENERAL INTRODUCTION

### 1.1      Introduction and definitions

Stroke is defined as any acute clinical event, related to impairment of cerebral circulation, that lasts for more than 24 hours and can cause a loss of the ability to move particular parts of the body. The sudden death of some brain cells is due either to lack of oxygen when the blood supply to the part of the brain is suddenly interrupted (ischemic stroke) or to bursting of a blood vessel in the brain, which spills blood into the spaces surrounding the brain cells (hemorrhagic stroke, intracerebral hemorrhage, ICH). Subarachnoid hemorrhage (SAH) implies the presence of blood within the subarachnoid space from some pathologic process. The nontraumatic types of SAH are usually from rupture of a berry aneurysm or arteriovenous malformation (AVM). We will not discuss SAH because blood does not necessarily enter brain parenchyma. Brain cells are damaged when stroke happens. These damaged cells can linger for several hours in the penumbra area, which surrounds the damaged core and contains functionally impaired but still viable brain tissue supplied with blood from collateral vessels. This area may be transformed into infarction due to secondary neuronal damage induced by deleterious biochemical cascades, resulting in cytotoxic and excitotoxic effects. With timely treatment, these cells can be saved.

ICH differs from ischemic stroke in that blood enters the brain parenchyma and may extend into the ventricles (Figure 1-1a, see page 15). The amount of research concerning ICH is lacking compared to the work done on ischemic stroke. Delayed

clinical deterioration may occur after ICH but the mechanism is not fully understood. After ICH blood components (i.e. leukocytes, hemoglobin, thrombin, plasmin, complement, plasma, and fibrin degradation products) enter into the brain parenchyma. This is followed by an inflammatory response and brain cell death, which may involve enzyme activation, cytokine release, leukocyte migration, and brain tissue breakdown and repair. Some aspects of the brain damage following ICH are well documented, for example, disruption of tissue by the enlarging hematoma <sup>1</sup>, reduction of blood flow in surrounding tissue <sup>2</sup>, and destruction of cells by proteolytic enzymes including thrombin, plasmin, and matrix metalloproteinases (MMPs) <sup>3,4</sup>.

Although ICH is a disease of the brain, it can affect the entire body due to neurological deficit. The consequences following ICH depend on the area of the brain affected. The most common neurological deficit is weakness or paralysis of one side of the body with partial or complete loss of voluntary movement or sensation in a leg or arm. There can be speech problems, cognitive deficits, emotional difficulties, daily living problems, and pain. Numbness or tingling is very common. An ICH involving the brain stem can affect balance, vision, swallowing, breathing, and even consciousness.

## 1.2 Hemorrhagic stroke in the clinical setting

### 1.2.1 Brain hemorrhage in the adult brain

The worldwide annual incidence of primary (spontaneous) ICH is 12-35/100,000 population, which accounts for approximately 15% of cerebral strokes and is associated with a higher mortality rate <sup>5,6</sup> than to brain ischemia. ICH is more common in men than

in women, particularly those older than 55 years of age <sup>7</sup> and of African American and/or Japanese origin <sup>8</sup>. A high prevalence of hypertension and alcohol use in the Japanese population may account for the incidence <sup>9</sup>. ICH associated with hypertension <sup>10</sup> remains the most common form of ICH. ICH may also be associated with coagulopathy <sup>11, 12</sup>, cerebral amyloid angiopathy <sup>10</sup>, brain tumors <sup>13</sup>, vascular anomalies <sup>14</sup>, brain trauma <sup>1</sup>, or premature birth <sup>15</sup>. Stroke associated with ICH has a worse prognosis than ischemic stroke <sup>16</sup>, the mortality rate at 30 days is 43-51% <sup>17</sup>; and recovery following ICH is poor; most surviving patients retain a considerable functional handicap related to the specific site of hemorrhage <sup>18</sup>. The most common sites of hypertensive ICH are the caudate / putamen (basal nuclei), thalamus, cerebellum, and pons (the locations may differ with other etiologies).

There is no proven effective treatment for ICH <sup>19</sup>. However, the clinical therapeutic strategies include medication and surgery. Drug therapy is the most common treatment for ICH. This includes prevention of ICH based on treating an individual's underlying risk factors, for example, control of hypertension. The blood glucose in diabetics is often quite high after a stroke; controlling the glucose level may minimize the size of a stroke <sup>20</sup>. Oxygen is given as needed. Surgery can be used to prevent ICH by repairing vascular damage or malformations in and around the brain or to treat acute ICH by evacuating the hematoma, but the surgical treatment is still controversial <sup>21, 22</sup> due to very few controlled randomized trials. Rehabilitation may help overcome disabilities that result from ICH damage <sup>23</sup>. Initial severity of disability, age, and duration of therapy best predict functional outcome after rehabilitation.

### 1.2.2 Hemorrhage in the immature brain

The developing brain lacks mechanical rigidity and is readily deformed during birth or following trauma. Fragile blood vessels within the brain are thereby easily ruptured. Hemorrhage can arise from the arterial, capillary, or venous systems. It may be due to intravascular hypertension, thrombosis, or breakdown of vessel integrity following infarction or physical trauma<sup>24</sup>. The location and type of hemorrhage are dictated at least in part by the stage of development<sup>25</sup>. Periventricular hemorrhage (PVH) refers to bleeding adjacent to the lateral ventricles. Intraventricular hemorrhage (IVH) refers to blood collections within the ventricles, which are usually extensions of ganglionic eminence hemorrhage. PVH and IVH frequently occur in combination (PVH/IVH). Blood can extend into the ventricles causing hydrocephalus, or it can cause secondary ischemic injury in the adjacent tissue<sup>15</sup>. Even a small hemorrhage may be associated with cognitive deficits<sup>26</sup>. Detectable PVH/IVH with extensive hemorrhage occurs in approximately half of the affected infants born <28 weeks while only one tenth of those affected at >35 weeks have severe bleedings<sup>27</sup>. The highest risk periods are within the first 3 hours after birth, 2 days, and around 10 days after birth<sup>28</sup>. The main risk factor for IVH is young gestational age, although maternal / fetal sepsis<sup>27, 29-32</sup>, and delivery with excessive head distortion may contribute<sup>25</sup>.

The desirable therapy is prevention of brain hemorrhage through the avoidance of preterm birth, chorioamnionitis, and improved understanding of the physiologic determinants of hemorrhage. Many medical treatments have been attempted to prevent initial or progressive IVH in preterm infants, but none appear to be effective<sup>33, 34</sup>. Digestion of intraventricular clots with proteolytic agents such as urokinase and tPA has

been attempted with minimal success although new trials are being designed <sup>35, 36</sup>. Subdural hemorrhage can be managed surgically if necessary.

### 1.3 Animal models of hemorrhagic stroke

To understand the pathogenesis of ICH and to evaluate preventive or therapeutic strategies, animal models of ICH have been developed and used. Experimental ICH models have been studied in several species including mouse <sup>37</sup>, rat <sup>38-42</sup>, rabbit <sup>9, 43</sup>, cat <sup>44</sup>, pig <sup>45</sup>, and primate <sup>46</sup>.

#### 1.3.1 Microballoon insertion models

An acute expanding lesion model using a mechanical microballoon to simulate the space-occupying effect of ICH was developed by Sinar in the adult rat in 1987 (although this model lacks the effects of blood components) <sup>47</sup>. The microballoon system consisted of an embolization balloon mounted on a 20 gauge venous cannula using its own previously blunted guide. The microballoon was then inflated with saline in a syringe. Immediately following balloon inflation in the caudate nucleus of rats, there was a significant increase in intracranial pressure accompanied by a reduction in cerebral blood flow (CBF) in the ipsilateral frontal cortex and the ipsilateral caudate nucleus <sup>2</sup>. There was little change in intracranial pressure (ICP) with microballoons (25 microliters and 50 microliters in volume) equivalent in size to those lesions which occur with this disorder in man. With larger volumes (100 microliters) there is an increase in ICP which is associated with systemic effects on cerebral perfusion pressure (CPP) <sup>48</sup>. The rats with an intracerebral mass exhibited a 10-fold increase in the volume of ischemic damage in

the ipsilateral caudate nucleus compared to the sham-treated group <sup>47</sup>. The quantity of damaged neurons was significantly higher in the permanent groups than in transient inflation groups <sup>49</sup>. Deflation of balloon after 10 minutes was shown to improve clinical outcome and reduces CBF abnormalities in rats <sup>50</sup>. Therefore, in this model evacuation of an extensive acute expanding subcortical (hematoma-like) mass must be performed within a limited time window to prevent the development of irreversible neurological deficits or death. Similarly a microballoon inserted into the ventral posterolateral nucleus of the thalamus in cat, caused a rapid reduction in CBF following gradual balloon inflation <sup>51</sup>.

### 1.3.2 Autologous whole blood injection models

Although autologous blood does not reproduce the rupturing of a blood vessel in spontaneous ICH, this method allows anatomically localized hematomas to be created without artificial agents <sup>39-41</sup>. The autologous whole blood may be obtained from the animal's tail or femoral artery, then directly injected into the selected brain areas. Sometimes the femoral artery may be attached directly to a cannula to simulate pressure/pulsation. Several groups have studied the brain injury mechanism following ICH by using this model. In the rat, autologous blood can cause brain edema, cell death, inflammation and behavioral impairment <sup>38-40, 52-54</sup>. Studies in the dog have shown that despite a prominent increase in intracranial pressure (ICP) and mean arterial pressure (MAP) after ICH, there is no evidence to support the presence of an ischemic penumbra in the first 5 hours after ICH <sup>55</sup>. Increased intracranial pressure as well as compromised CBF and metabolism following ICH have been shown <sup>56</sup> in the cats, rabbits, monkeys,

and pigs. Pigs have been frequently studied for clot evacuation <sup>57, 58</sup>. For instance, a tPA-induced clot lysis study showed that reduction in clot size was significantly greater than mechanical aspiration alone. In the rabbit model <sup>59</sup>, urokinase treated animals showed 86 % of clot lysis compared to injection of saline into clot (23 %).

Rat models have been used to compare effects of blood components, such as thrombin, plasmin, plasma, serum, leukocyte fractions and erythrocytes individually <sup>40-42</sup>. Leukocytes, activated leukocytes, thrombin and plasminogen caused brain edema, inflammation, and brain cell death when they were injected into the brain <sup>38</sup>. Components of the coagulation system can modulate inflammation <sup>60</sup>. Activation of the complement system <sup>61</sup> and injections of hemoglobin as well as erythrocytes into the brain may lead to brain edema <sup>41, 42</sup>.

### 1.3.3 Collagenase animal models of ICH

This model was developed by Rosenberg's group. Bacterial collagenases, which are proteolytic enzymes, are injected into basal ganglia to induce ICH by destruction of the capillary basal lamina in the brain <sup>62, 63</sup>. The advantage of using this model is that it produces highly reproducible hemorrhages and mimics spontaneous ICH without significant blood leakage along the needle track. In studies of adult rat following collagenase induced ICH, behavioral improvement is rapid during resolution of the edema but incomplete at 3 weeks <sup>52</sup>. This model is also used to study treatment following ICH <sup>4, 62-65</sup>. A disadvantage of using the collagenase model is that it involves introduction of a foreign protein that seems to cause more inflammatory reaction than autologous

blood injection or venous hemorrhage due to avulsion of surface vessels of brain <sup>54</sup>. Addition of heparin to collagenase injection enhances the inflammation in rat brain <sup>52</sup>.

#### 1.3.4 Hypertensive stroke models

Hypertension is the most common cause of primary ICH. Hypertension also causes changes in the walls of small vessels in the brain and leading to rupture, which make the blood bleed into the brain parenchyma. To understand the effect of hypertension induced hemorrhage and to develop treatment for it, several animal models have been developed <sup>66</sup>. Renal artery constriction in which the roots of both renal arteries are constricted by ring-shaped silver clips, causes renovascular hypertension <sup>67</sup>. The rate of stable hypertension was 100% and the incidence of spontaneous stroke including ICH and brain infarct was 61.8% at 40 weeks after renal artery constriction <sup>67</sup>. The hypertension is stable and not renin dependent, apparently involving brain angiotensin and perhaps circulating vasopressin <sup>66</sup>. Stroke prone spontaneously hypertensive rats (SHR) may also develop cerebral hemorrhage as well as cerebral infarct <sup>68</sup>. The brain lesions in this model include old and fresh cerebral hemorrhage and infarcts with or without subarachnoid effusion. These models simulate hypertensive ICH in humans and offer the chance to study the mechanism of brain injury following hypertensive ICH. The disadvantages are that brain lesions are unpredictable with regard to size and position.

#### 1.3.5 Models of neonatal PVH/IVH and IVH

Using immature rabbits, dogs, cats, and sheep, the mechanisms of germinal matrix hemorrhage have been elucidated. Fluctuations in arterial and venous blood

pressure can cause PVH <sup>69</sup>. IVH has been induced using glycerol to create intracranial hypotension in prematurely born rabbits (27 - 30 days gestation) <sup>70, 71</sup>. In a newborn beagle model, injection of phenylephrine hydrochloride intravenously induced hypertension which can cause IVH <sup>72</sup>. Intraventricular injection of blood into newborn dog brains has been used to study the effect of acute ventricular distension on the surrounding blood flow patterns <sup>73</sup>. Dog models have played an important role in understanding the physiologic factors that predispose to PVH/IVH <sup>69</sup>. A mouse model of neonatal hypoxia develops superficial foci of bleeding unlike those seen in humans <sup>74</sup>. We recently developed a novel PVH/IVH model in newborn mice by injection of autologous whole blood into periventricular tissue including germinal matrix (GM) and striatum <sup>37</sup>. All mice exhibited extension of the hematoma into the ventricles, which mimics germinal matrix hemorrhage in humans at 24-28 weeks gestation age. This model provides an opportunity to study mechanisms of cellular injury after PVH/IVH. Posthemorrhagic hydrocephalus can be modeled by injection of blood into the ventricles of 7-day old rats <sup>75</sup>.

#### 1.3.6 Other animal models of ICH

In addition to the above-mentioned ICH animal models, other models have also been developed. Cortical vessel avulsion by tearing the pia can cause mixed brain damage including ischemic and hemorrhagic <sup>54</sup>. Hemorrhage related to shaking injury in 6-day old rats has been studied as a model of child abuse <sup>76</sup>. Some forms of traumatic brain injury (TBI) also cause bleeding into the brain parenchyma <sup>77-79</sup>. None of the above-mentioned ICH models completely reproduce the brain injury response following

human ICH. However, these models have significantly contributed to the overall knowledge of the pathophysiology of human ICH including edema, inflammation, cell death, brain damage, compromised CBF, and metabolism as well as pathogenesis.

#### 1.4 Histopathology of ICH

Following ICH, blood components, including cells and plasma, intermingle with brain cells adjacent to the hematoma, which is a contiguous collection of clotted blood. Brain tissue surrounding the core of damaged area appears pale due to edema. After 24 h, degenerating erythrocytes and fragmented nuclear debris are seen. Hemosiderin is evident in macrophages as early as 3 days after the bleed<sup>80</sup>. The surrounding tissue may become necrotic if the hematoma is large and secondary infarction ensues<sup>81</sup>. In intact brain tissue surrounding the hematoma, neutrophils adhere to vessel walls or pass through capillaries and small veins. Neutrophils are rarely present within the necrotic tissue except at the periphery of hematoma. Neutrophil infiltration and reactive glial changes including astrocyte activation and microglia reaction in the brain adjacent to the hematoma are obvious at 2-3 days after ICH. Large clots degrade very slowly because the macrophage ingestion of debris takes place only at the surface. For months after clot resolution, residual hemosiderin and mineralization may be detected along the hematoma cavity. In the IVH, blood debris may obstruct the cerebral aqueduct. This may cause hydrocephalus.

#### 1.5 Pathophysiology of brain damage after ICH

Several mechanisms are involved in ICH-related brain damage. Mechanical

destruction of brain tissue is caused by the enlarging hematoma <sup>1</sup>. Local cerebral blood flow (CBF) surrounding the hematoma may be compromised through mechanical and chemical factors. Cerebral edema raises intracranial pressure and reduces cerebral perfusion pressure <sup>2</sup>. In this regard ICH has similarities to ischemic stroke particularly in the penumbra region that surrounds the hematoma <sup>82, 83</sup>. ICH is associated with entry of proteolytic enzymes including thrombin, plasmin, and complement proteins <sup>84</sup> from plasma into the brain parenchyma. Matrix metalloproteinases (MMPs) are a family of proteolytic enzymes with relative specificity for components of the extracellular matrix. Following brain injury MMPs such as MMP3 and MMP9 are produced by infiltrating inflammatory cells, microglia, and astroglia <sup>85</sup>. Plasmin can promote the activity of MMPs <sup>86, 87</sup>. MMPs can directly damage brain cells, cause cell injury by processing death molecules (e.g. FasL), disrupting the myelin, and perpetuating of inflammation <sup>86, 87</sup>. MMPs may contribute to the brain damage following ICH. To a lesser extent this may occur after ischemia when the blood brain barrier (BBB) becomes permeable to large molecular weight proteins <sup>88-91</sup> such as plasminogen and prothrombin. They may contribute to brain edema <sup>92, 93</sup> (e.g. albumin), cellular necrosis (e.g. thrombin and plasmin), and inflammation <sup>38</sup> (e.g. complement). However, the brain may also be a source of prothrombin <sup>91</sup> and plasminogen <sup>88, 89</sup>, which are the precursors of thrombin and plasmin, respectively. When erythrocytes begin to break down 2-3 days after ICH, hemoglobin is released. It can cause brain damage through iron-dependent formation of oxidizing agents <sup>42, 94</sup>. Reactive oxygen species (ROS), which come from neutrophils, reactive microglia/macrophages, and the damaged brain cells, also contribute to the brain cell damage following ICH <sup>1</sup>.

1.6 Brain inflammation following ICH (published by Xue M, Balasubramaniam J, Del Bigio MR. "Brain inflammation following ICH." in *Current Neuropharmacology*. 2003;1: 325-332)

#### 1.6.1 General aspects of the immune response

Response of the immune system to tissue injury occurs in two phases: an early, non-adaptive (or innate) response and a later adaptive response<sup>95</sup>. Vascular permeability increases immediately, in part due to histamine release from mast cells. Minutes to hours after injury mediators such as chemokines and cytokines promote cell activation and attract immune cells. Adhesion molecules on endothelial cells mediate extravasation of leukocytes. Neutrophils, which release proteolytic and oxidizing agents, attack cells with bound complement, a plasma protein that adheres to damaged cells. Natural killer (NK) cells can kill injured cells that have downregulated their major histocompatibility (MHC) class I molecules. Cytotoxic T lymphocytes (CTLs) and NK cells express CD95 ligand (CD95L or FasL) which binds to CD95 (Fas) on target cells to induce apoptosis; CD95 is upregulated following cell injury. In the adaptive immune response, antigen-presenting cells (e.g. microglia or macrophages) process proteins released from damaged cells. MHC class I molecules present cytosolic antigens to T lymphocytes that express the CD8 antigen on their surface. MHC class II molecules present lysosomal antigens to CD4 T lymphocytes. Subsequent activation and proliferation of cells directed against the specific antigen occurs over the next 3-5 days in lymph nodes. In the brain, some T cell proliferation occurs locally<sup>96</sup>. Activated CTLs bind to target cells that express

appropriate peptide/MHC class I complexes and costimulatory molecules. Then they release perforin and deliver granzymes to induce apoptosis<sup>97</sup>.

#### 1.6.2 Brain inflammation following ICH in humans

Clinical studies show that the increase in circulating leukocytes is greater<sup>98</sup> and persists longer (3-5 days) following hemorrhagic brain lesions than following ischemic brain lesions<sup>99</sup>, although it is not clear that the data are adjusted for coma level. The leukocyte count at 24 hours correlates with factors such as hematoma size<sup>100</sup>. In contrast, peripheral neutrophil activation determined by chemiluminescence occurs within the first hours following ischemic stroke but not following ICH<sup>101</sup>. Infants with intraventricular hemorrhage (IVH) display an increase in total leukocytes and absolute neutrophils in peripheral blood compared to infants without IVH<sup>102</sup>. Cerebrospinal fluid (CSF) neutrophil counts are frequently elevated after ICH<sup>103</sup>. High plasma levels of tumor necrosis factor alpha (TNF $\alpha$ ) within 24 hours of ICH are correlated with the magnitude of perihematoma brain edema<sup>104</sup>. Elevated levels of the pro-inflammatory cytokines interleukin (IL)-10, IL-6, and transforming growth factor-beta (TGF- $\beta$ ) have been detected in the CSF or serum of patients with ICH; the levels correlated with hematoma volume<sup>105, 106</sup>. Patients with ICH exhibit increased IL-6 secretion by leukocytes after ex vivo stimulation with endotoxin (lipopolysaccharide, LPS)<sup>107</sup>. Leukemia inhibitory factor (LIF) is induced in germinal brain cells of premature humans with ICH<sup>108</sup>. Cysteinyl-leukotriene (cys-LT), which is a proinflammatory lipid molecule, is increased in the urine of patients following ICH, and the amount of cys-LT release depends on the hematoma volume<sup>109</sup>. This agent can promote vascular permeability<sup>110</sup>. Serum soluble

vascular cell adhesion molecule-1 (sVCAM-1) was higher at 24 hours in patients with infarct than ICH<sup>111</sup>.

Concerning the histological changes in human brain following ICH, there are few studies and most make little or no mention of inflammation<sup>112</sup>. Contused brain tissue from adult humans has been studied more frequently<sup>113, 114</sup>. The inflammatory response consists of monocytes/macrophages, reactive microglia, neutrophils, and CD4- and CD8-positive T lymphocytes appearing 3 to 5 days after trauma<sup>115</sup>. Following ICH in adults, neutrophils were identified in the penumbra region beginning at 5-8 hours and disappearing by 72 hours. However, they were sparsely distributed and the authors expressed the opinion that neutrophils "have no major role in the development of cellular changes around hematomas"<sup>116</sup> (see Figure 1-1b). Lymphocytes also appear early and persist for weeks (see Figure 1-1c). Macrophages in the brain are derived from either microglia or monocytes in the circulating blood<sup>1</sup>. Macrophages with hemosiderin appear at 3-6 days after ICH<sup>1, 117</sup> and persist for many months (see Figure 1-1d). Microglial cells also ingest a range of plasma proteins after ICH<sup>118</sup>. Whether post-contusion changes are directly comparable to post-ICH changes is unclear.

Less is known about inflammation in the premature human brain after hemorrhage than is known about inflammation in the adult. The inflammatory reaction in this situation has been described as "negligible" with few details offered<sup>119</sup>. In a pilot investigation, neutrophils appear from 1-4 days and CD3 positive lymphocytes from 1-100 days after ICH. Both are in small quantities, but are more abundant than after ischemic damage (Del Bigio, unpublished). Macrophages appear in the periventricular germinal tissue 4 days after hemorrhage in premature infants<sup>120, 121</sup>. Some cytokines may

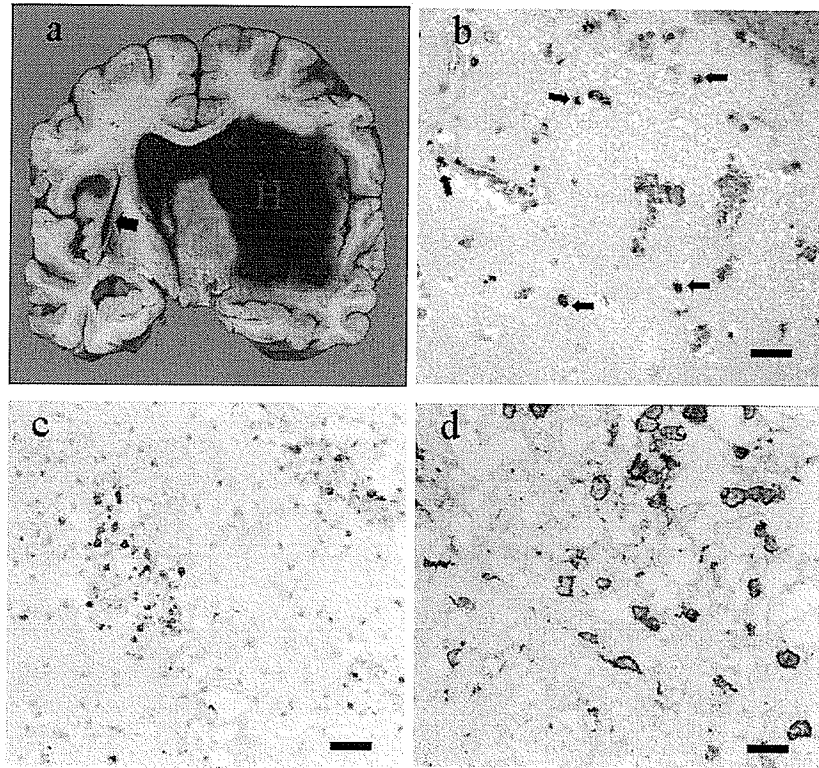


Figure 1-1. Intracerebral hemorrhage and inflammatory cell infiltration in adult human brain. a. Photograph showing coronal slice through the brain of an adult who died hours after ICH. A large hematoma (H) centered around the right basal nucleus extends into the ventricles (intraventricular hemorrhage). There is a cavity in the left putamen (arrow) that is the result of an old resolved hemorrhage. b. Photomicrograph showing neutrophils stained red (arrows) in brain tissue adjacent to a hematoma, 3 days after ICH (Leder stain for chloracetate esterase activity. Bar = 40  $\mu$ m). c. Photomicrograph showing CD8 $\alpha$  immunoreactive lymphocytes (brown) in brain tissue adjacent to a hematoma, 42 days after ICH. (Bar = 50  $\mu$ m). d. Photomicrograph showing HLA-DR immunoreactive macrophages and activated microglia (brown) in brain tissue adjacent to a hematoma 42 days, after ICH. (Bar = 20  $\mu$ m.)

play a role in the brain damage <sup>122</sup>.

### 1.6.3 Early inflammatory mediators following ICH

Although there are mast cells in the brain <sup>123</sup> and histamine seems play a role in ischemic stroke <sup>124</sup>, there appear to be no studies of histamine after ICH despite the fact that it could play a role in BBB opening and brain edema <sup>125</sup>. Following ICH, complement enters the brain and is activated to form membrane attack complexes that can precipitate neutrophil attack <sup>61</sup>.

### 1.6.4 Cytokines following ICH

The production of cytokine and chemokine messenger ribonucleic acids (mRNA) coincident with or preceding the infiltration of neutrophils and monocytes has suggested a role in the pathology of brain injury <sup>126, 127</sup>. Cytokines are small peptides potentially released by almost all immune cell types (e.g. leukocytes, neurons, microglia, and astroglia). Often cytokines are divided into pro- and anti-inflammatory mediators based on their ability to promote or suppress immunoactivation. However, recent data showed that some cytokines possess a dual action and their presence is fundamental for the processes of tissue repair, regeneration and neurological recovery <sup>77, 78</sup>. The role of individual cytokines in brain disease has been studied by injecting them into the brain or by studying mutant mice.

TNF $\alpha$  exerts a diverse array of biological activities, including stimulation of acute phase protein production and vascular permeability <sup>128</sup>. TNF $\alpha$  is released by many cell types in the brain such as neurons, astrocytes, and microglia upon appropriate stimulation <sup>129</sup>. Immunohistochemical labeling indicated that collagenase-induced ICH in rats was

accompanied by elevated expression of TNF $\alpha$  in neutrophils, macrophages, and microglia. Inhibiting expression of TNF $\alpha$  using antisense oligodeoxynucleotides reduced inflammation and brain injury<sup>130</sup>. There was no significant expression of cytokines IL-6, IL-1 $\beta$ , and TNF $\alpha$  found one hour after autologous blood ICH in brain, CSF, or serum in dogs<sup>131</sup>; however, this results do not include that cytokine expression may be delayed and may not be measurable within the 1 hour time frame. One technical problem that should be mentioned is that antihuman antibodies might be inappropriate to detect the canine expression.

#### 1.6.5 Adhesion molecules following ICH

Adhesion molecules on vascular endothelium mediate binding and extravasation of blood-borne inflammatory cells. Activated endothelial cells in the vicinity of damaged or infarcted brain rapidly present selectins on the luminal surface<sup>132-134</sup>. Those molecules cause neutrophils to roll onto the endothelial surface. Stable binding of neutrophils occurs when intracellular adhesion molecule 1 (ICAM-1) and vascular cell adhesion molecule 1 (VCAM-1) are upregulated on the endothelium. This occurs in rats and humans following brain trauma and infarction<sup>135, 136</sup>. Once stable binding is achieved the leukocytes can pass through or between endothelial cells in postcapillary venules. Then they migrate to the injured tissue following a path of chemoattractant substances (chemokines)<sup>79</sup>. However, only sparse data are available concerning the role of adhesion molecules following ICH. Immunohistochemical detection of ICAM-1 expression in rats following whole blood injection showed that ICAM-1 was presented in blood vessels adjacent to

the hematoma 1 to 7 days after ICH, as well as in activated microglia and neurons in the ipsilateral hemisphere 1 to 10 days after ICH<sup>137</sup>.

#### 1.6.6 Leukocyte infiltration following ICH

The intensity of inflammation is greater in hemorrhagic lesions than in non-hemorrhagic brain lesions in rats<sup>40</sup>. In rat brain adjacent to autologous blood hematomas, neutrophil infiltration begins before 1 day, peaks at 2 days and is gone by 3 days<sup>39, 40</sup>. Activated neutrophils are known to die by apoptosis within 2 days<sup>138</sup>. Monocytes come from blood beginning at about 3 days to become macrophages and ingest hematoma breakdown products<sup>39, 52</sup>. CD8 $\alpha$  immunoreactive lymphocytes, possible CTL or NK cells, enter brain at 2 days and persist until 7 days<sup>39</sup>. The same temporal sequence of inflammation occurs after collagenase-induced hemorrhage<sup>52</sup>. Similar findings have been reported by other groups in rats<sup>137, 139</sup> and rabbits<sup>140</sup>.

Leukocytes included in the hematoma, as well as those infiltrating from the blood, could release vasoactive mediators, such as superoxide anion, thromboxane A<sub>2</sub>, endothelin-1, prostaglandin I<sub>2</sub> and prostaglandin H<sub>2</sub>, TNF $\alpha$ , nitric oxide (NO), and interferon-gamma (INF $\gamma$ )<sup>141, 142</sup>. We showed that injection of whole blood, leukocytes, or activated leukocytes into adult rat brain caused more inflammation and brain damage than comparable plasma, serum, or saline injections<sup>40</sup>. A similar pattern of B- and T-lymphocyte infiltration peaking at 2 days and persisting for 7 days has been documented following brain trauma in mice<sup>143</sup> and rats<sup>144</sup>.

Activated microglial cells or macrophages can produce a number of cytotoxic compounds, including NO, chemokines, and cytokines<sup>145</sup>. Microglia might also have

trophic effects on neurons through release of growth factors such as FGF and TGF- $\beta$  <sup>146</sup>. In rats microglial cells are activated as early as 4 hours after ICH, they reach a maximal state of activation after 3 days. Their condition remains altered for at least 1-3 weeks following whole blood injection <sup>39</sup>. Similar timing of microglial activation has been documented in human brains following traumatic ICH <sup>147</sup>. The potentially deleterious or beneficial roles of microglia after ICH may be related to when and where the microglia are activated.

#### 1.6.7 Inflammation following the ICH in immature brain

Following periventricular blood injection into brains of neonatal mice, reactive microglia were evident by 8 hours, their quantity was maximal at 2-7 days, and they had decreased by 28 days. By 7 days macrophages were adjacent to the hematoma. Neutrophils and lymphocytes in the brain tissue surrounding the hematoma were detected in only very small quantities using immunolabeling with anti-CD3, CD3 $\epsilon$ , CD4, and CD8 antibodies <sup>37</sup>.

#### 1.6.8 Treatment of ICH with anti-inflammatory agents

There are few studies using anti-inflammatory agents in humans with ICH. Dexamethasone, an anti-inflammatory steroid, did not improve outcomes of unselected patients with ICH and the complication rate was higher <sup>148</sup>. In a randomized trial there was no statistically significant difference between treated and untreated patients <sup>149</sup>. A trial of methylprednisolone in ICH also failed <sup>150</sup>. Enlimomab (murine anti human ICAM-1 antibody) has been given to patients with ICH in an uncontrolled safety trial;

there was no increased risk of adverse events <sup>151</sup>. However, the drug, which failed clinical trials for ischemic stroke <sup>152</sup>, has not been formally tested for protection in ICH.

Experimental animals seem to benefit by reduction of inflammation following ICH. Whole body irradiation to deplete leukocytes reduces cerebral edema around small balloons inflated in the striatum of rats suggesting a role for inflammation in generation of edema <sup>153</sup>. Several drugs have been studied in rats with collagenase-induced ICH, because this model is most consistent. Quenching free radicals with systemically administered dimethylthiourea or alpha-phenyl-N-tert-butyl nitron slightly improved outcome; however, treatment did not significantly affect edema, resolution of the hematoma, or neuronal injury in tissue adjacent to the hematoma. Furthermore, alpha-tocopherol/ascorbic acid had no effect <sup>154</sup>. Fucoidan, which can block selectin-mediated binding of leukocytes, significantly improved early recovery of motor function following ICH and was associated with memory retention in the passive avoidance test <sup>155</sup>. However, the drug also caused hemodilution, which could itself be neuroprotective. Administration of ORF4-PE (a TNF $\alpha$  antisense oligodeoxynucleotide) directly into rat striatum, decreased levels of TNF $\alpha$  mRNA and protein in brain tissue surrounding hematoma. Brain cell death was also reduced and neurobehavioral scores improved <sup>130</sup>. Systemic FK-506 (tacrolimus), a potent immunosuppressant, reduced neutrophil infiltration and cell death around the hematoma. The decreased inflammatory response was accompanied by functional improvement <sup>156</sup>. However, FK-506 can be directly neuroprotective independent of inflammation <sup>156</sup>. Minocycline, a tetracycline derivative that crosses the BBB, significantly reduced neutrophil and macrophage infiltration, microglia activation, and cell death. Neurobehavioral outcomes were also improved <sup>157</sup>.

Injection of metalloproteinase inhibitors reduced hemorrhagic edema following collagenase-induced ICH<sup>4, 64</sup>. Interpretation of these data is confounded by the fact that collagenase-induced ICH is associated with artificially enhanced inflammation<sup>54</sup>.

Therapeutic studies of rats with ICH induced by whole blood injection have shown that N-acetyl heparin, a complement activation inhibitor, decreased perihematomal edema<sup>61</sup>. Systemic depletion of complement with cobra venom factor reduced brain edema in rats with autologous blood ICH<sup>158</sup>.

#### 1.6.9 Summary and conclusions of brain inflammation

Published data indicate that an inflammatory response occurs in and around brain hematomas following ICH. Far less information is available for ICH than for ischemic stroke or trauma, with which there may be overlap and similarities. Brain inflammation seems to be more severe after ICH than that after ischemic stroke. Infiltration of leukocytes, activation of microglia, and production of cytokines may participate in the absorption of the blood clot and the removal of injured brain cells. Macrophages and microglia in the central nervous system (CNS) have been considered by some to have predominantly destructive effects. They might, however, also have a neuroprotective role through their ability to clear debris<sup>159</sup>. T cells directed against myelin-associated proteins appear to have a beneficial effect by promoting regrowth and reducing the post-traumatic spread of damage in the injured rat optic nerve or spinal cord<sup>159, 160</sup>. However, the T cells probably need well-controlled stimulation in order to be effective<sup>159</sup>. Infiltrations of neutrophils seem more likely to have only harmful side effects. Experimental blockade of leukocyte entry and inhibition of pro-inflammatory cytokines

provide weak evidence that ICH-induced brain injury may be amenable to treatment with anti-inflammatory agents. However, the few clinical trials using corticosteroids are uniformly negative. It seems naïve to try to block inflammation in general. More work is needed to define the harmful role of inflammation, if any, as well as the age-dependent variables <sup>161</sup> before embarking on pharmacological anti-inflammatory therapy in human ICH.

## 1.7 Brain cell death following ICH

### 1.7.1 Brief introduction of cell death in the brain

Acute brain injury can lead to significant neuronal cell death resulting in a loss in neurological functions. Despite their causative differences, the ultimate cell death mechanisms and pathways from brain injuries are largely similar. Cellular death includes both necrosis and apoptosis. Accumulating data have been shown that autophagy, another type of cell death, may play an important role in brain development <sup>162</sup>. Autophagy is an intracellular lysosome-mediated catabolic mechanism that is responsible for the bulk degeneration and recycling of damaged or dysfunctional cytoplasmic components and intracellular organelles <sup>162, 163</sup> (Table 1-1). There are no data showings that autophagy occurs in ICH, and therefore it will not be discussed here.

Necrosis is characterized by cellular swelling and lysis, involves the death of a group of cells and evokes a significant inflammatory response. Mechanisms of cell necrosis include acute stresses directly acting on the cells such as toxic chemicals, extreme temperature, free radicals, and lack of oxygen. Another mechanism of brain cell

necrosis may involve excitotoxicity, for example inappropriate activation of NMDA receptors. Membrane depolarization leads to influx of calcium that can activate the hydrolytic enzymes and quenching of mitochondria <sup>164</sup>. Cells may die due to lack of energy necessary to maintain the membrane potential <sup>164</sup>. Morphologically, a cell undergoing necrosis exhibits cytoplasmic, mitochondrial, and nuclear swelling as water moves into the cell along osmotic gradients. The cell membranes rupture spilling cellular and organelle chemical contents into the surrounding tissue. Pro-inflammatory signals are emitted from necrotic cells inciting the entry of lymphocytes and polymorphonuclear cells into the area of injury with the potential for attendant secondary injury as these inflammatory cells engulf necrotic debris and release cytotoxic compounds. In the brain, infiltrating neutrophils and reactive microglia/macrophages following ICH can release proteolytic and oxidizing agents, and attack cells with bound complement, a plasma protein that adheres to damaged cells to kill the target cells.

Programmed cell death, which is more commonly known as apoptosis, is an inter-related collection of pathways and mechanisms utilized to eliminate excess or unwanted cells <sup>162, 165</sup>. During development the nervous system is sculpted by neuronal cell death. Apoptosis plays an important role to remove the excess neurons or unwanted cells in the brain to ensure the proper and precise synaptic connection <sup>162, 165</sup>. Neurons may die prematurely during adult life when subjected to acute or chronic neurotoxic condition <sup>162</sup>. Apoptosis involves single cells and results in cell shrinkage and apoptotic body formation, with subsequent phagocytosis by adjacent normal cells (Table 1-1) <sup>97, 162, 165</sup>. Apoptosis of brain cells plays a critical role in brain injury, which may cause neurological impairment. Apoptosis has been demonstrated in various animal models of

Table 1-1. Morphological Features of Cell Death

APOPTOSIS	NECROSIS	AUTOPHAGY
Programmed	Uncoordinated	Programmed
Individual cells	Groups of cells	Groups of cells
Caspase activation	Energy failure	Lysosomal enzymes
Cell shrinkage	Swelling, lysis	Cell shrinkage
Membrane blebbing	Membrane breakage	Autophagic vacuoles
Nuclear condensation	Karyolysis, pyknosis	Nuclear collapse
No inflammation	Macrophage Invasion	?
ATP dependant	Energy independent	ATP dependant
Delayed	Immediate	Delayed

ICH<sup>37-40, 54, 166, 167</sup> and there is evidence of ICH induced apoptosis in human brain<sup>168</sup>.

### 1.7.2 Apoptotic cell death pathway

Apoptotic cell death is a complex process, which depends upon the outcome of many signalling pathways before the terminal apoptotic pathway is completed. A caspase-dependent pathway is a common pathway involving caspases to cause the cell apoptosis. The 14 members of caspases are closely involved in the apoptotic process of the cell. In addition, caspases can be categorized as apoptotic initiators, executioners, and inflammatory mediators based on their specific role in the apoptotic process<sup>169</sup>. To date, two of the best-characterized caspase-mediated pathways are the intrinsic and extrinsic pathways.

### 1.7.3 Intrinsic caspase-dependent pathway

This pathway is activated by apoptotic stimuli such as hypoxic stress, growth factor withdrawal, or irradiation, inducing the emergence of mitochondrial membrane permeability (MMP). This change in permeability facilitates the release of cytochrome *c* from the mitochondria into the cytosol. Cytochrome *c* associates with Apaf-1 to activate caspase-9. The activated caspase-9 can cleave and activate caspase-3. Then the activated caspase-3 instigates the execution of the cell death pathway<sup>97</sup>.

### 1.7.4 Extrinsic caspase-dependent pathway<sup>97</sup>

This pathway is triggered by the activation of death receptors such as the ligation of FasL to Fas or of TNF to TNFR1. The activated death receptors activate caspase-8,

which can elicit the apoptotic pathway via two directions. First, it can cleave and activate caspase executioner caspase-3, -6, and -7 resulting in the terminal stages of the apoptotic pathway<sup>170, 171</sup>. Second, activated caspase-8 can activate Bid, which translocates to the mitochondria and stimulates Bax and Bak. In concert, Bax and Bak alter the mitochondrial membrane permeability, resulting in the release of cytochrome *c* into the cytoplasm. Cytochrome *c* triggers the intrinsic pathway to complete the apoptotic process<sup>97</sup>.

#### 1.7.5 Caspase-independent pathways<sup>97</sup>

Apoptosis inducing factor (AIF) is localized in the inter-membrane space of the mitochondria. Like cytochrome *c*, it can be released into the cytosol when the MMP is compromised. Once released, AIF translocates into the nucleus and induces cellular apoptosis<sup>172-174</sup>. In addition, the cathepsins, the calpains, and the granzymes have been implicated in caspase-independent apoptotic pathways.

Cathepsins are proteases that reside in the lysosome and have the capacity to degrade extracellular matrices, like collagen, fibronectin, laminin, and proteoglycans<sup>175</sup>. Cathepsins appears to play a role in apoptosis<sup>176</sup>.

Like caspases, calpains are a family of cytoplasmic neutral cysteine proteases<sup>177</sup>. The most ubiquitous calpains are calpain I and calpain II, which can be triggered by calcium influx and oxidative stress. They act on substrates including cytoskeletal proteins, kinases and phosphatases, membrane receptors and transporters, and steroid receptors<sup>178</sup>. Calpains are implicated in apoptosis based on two types of observations: (1)

the activation of calpains during cell death <sup>179</sup>; and (2) the inhibition of apoptosis in the presence of calpain inhibitors <sup>180, 181</sup>.

Granzymes, a family of serine proteases, can induce apoptosis via two mechanisms. One mechanism involves the stimulation of cell surface death receptors (e.g. TNF $\alpha$  receptor and Fas), such as Fas to achieve cell death following the extrinsic pathways. The second mechanism involves the transfer of the contents of the effector cell cytoplasmic granules into the target cell <sup>180</sup>. When perforins that form pores on the membrane are present, this enables the entry of granzyme B, which can cause DNA fragmentation and cell death <sup>97</sup>.

Leukocytes in the brain following ICH can release harmful substances such as proteolytic and oxidizing agents as well as cytokines, which can damage or kill the cells through caspase-dependent or independent pathways. Cytotoxic T lymphocytes (CTLs) and NK cells express CD95 ligand (CD95L or FasL), which binds to CD95 (Fas) on target cells to induce apoptosis. Activated CTLs and NK cells bind to target cells that express appropriate peptide/MHC class I complexes and costimulatory molecules, then they release perforin and deliver granzymes to induce apoptosis <sup>182</sup>.

It should be noted that there is a high degree of cross-talk between the caspase-dependent pathways. These proteases have a propensity to direct apoptotic pathways via activation of initiator or executioner caspases <sup>97</sup>.

#### 1.7.6 Bcl-2 family

The Bcl-2 family proteins are important regulators involved in the regulation of apoptotic cell death, consisting of anti-apoptotic and pro-apoptotic members. The anti-

apoptotic members of this family, such as Bcl-2, Bcl-XL, McL-1, and Bcl-W, prevent apoptosis either by sequestering proforms of caspases or by preventing the release of cytochrome c and AIF from mitochondria into the cytoplasm. In contrast, pro-apoptotic members of this family, such as Bax, Bak, Bok, Bcl-XS, Bad, and Bid, trigger the release of caspases and also by inducing the release of cytochrome c and AIF from mitochondria into the cytoplasm through mitochondrial permeability transition pore, thereby leading to caspase activation<sup>97, 183, 184</sup>.

#### 1.7.7 BNIP3-mediated neuronal cell death pathway

BNIP3, a pro-apoptotic member of the Bcl-2 family in mitochondria without a functional BH3 domain, induces cell death by acting on mitochondrial permeability transition pores in the absence of cytochrome c release and caspase activation<sup>185</sup>. BNIP3 may be an important participant in apoptotic and necrotic processes after brain ischemia. In brain ischemia, BNIP3-positive granules were seen in the nucleus at 1 and 2 days, and these neurons were damaged at 3 and 7 days<sup>186</sup>.

What happens to the apoptotic cells and how are they removed? Ingestion by phagocytes is the fate of most cells that undergo apoptosis<sup>187</sup>. In the early stages of apoptosis, changes occur at the cell surface and plasma membrane. Translocation of phosphatidylserine (PS) from inner side to the outer layer is one of the membrane alterations. It is an “eat me” signal for the macrophage to remove the apoptotic cell<sup>138, 187</sup>. Another class of surface changes that has been implicated in apoptotic cell removal is alteration of membrane carbohydrates<sup>138, 187</sup>.

### 1.7.8 Cell death detection methods

With increased understanding of the cell death, a number of methods have been developed for its detection based on different events.

TUNEL (terminal deoxynucleotidyl transferase (TdT)-mediated deoxyuridine triphosphate (dUTP)-biotin nick end labeling) was used to identify cells with damaged DNA to show cell death<sup>38-40, 54</sup>. It is important to know that TUNEL positive cells include necrotic and apoptotic cells which can be distinguished by the morphological appearance. TUNEL-positive nuclei with chromatin condensation and fragmented nuclei are considered as probable apoptotic cells. TUNEL positive cells with diffuse light brown labeling of nucleus and cytoplasm are considered as probable necrotic cells<sup>188</sup>. In situ nick translation (ISNT) technique with staining of DNA fragmentation and apoptotic bodies is similar to TUNEL staining.

Fluoro-Jade is an anionic fluorescein derivative useful for the histological staining of neurons undergoing degeneration. Fluoro-Jade staining is an easy way to quantifying dying neurons because the signal-to-noise ratio is high<sup>189, 190</sup>.

Hematoxylin and eosin (H&E) staining can identify the dying neurons as those with eosinophilic cytoplasm and pyknotic nuclei with loss of chromatin structure<sup>38-40, 54</sup>.

Apoptosis is characterized by a fragmentation of the genomic DNA. These DNA fragments have a length of about 180 base pairs or multiples thereof (360, 540, 720, ...), the characteristic DNA-length of a nucleosome (DNA-histone-complex). Endonucleases selectively cleave DNA at sites located between nucleosomal units (linker DNA). In agarose gel electrophoresis these DNA fragments are resolved to a distinctive ladder pattern.

Electron microscopy can directly find the apoptotic cells by looking for the condensed apoptotic bodies.

Caspase(s) assay by using immunohistochemistry and western blot detects the apoptotic related caspases proteins such as caspase-6, -7, -8, -9, -3.

Annexin V, a calcium-dependent phospholipid binding protein, has a high affinity for PS<sup>191</sup>, which is translocated from the inner side to the outer layer of the membrane apoptosis<sup>138, 187</sup>. Thus Annexin V has provided a suitable marker for detecting apoptotic cells. However, this test may only be used in cell culture for detecting apoptosis and is not suitable in situ in histopathologic sections, because when the tissue is cut, the PS would be exposed.

#### 1.7.9 Brain cell death following ICH in humans

Neuronal cell death after ICH and/or traumatic brain injury with blood in the brain has been ascribed to cellular necrosis that occurs not only at the impact site but also as a result of secondary brain insults such as intracranial hypertension, hypoxia or disturbances of microcirculation. In recent years it has been demonstrated that secondary neuronal loss may also be due to apoptosis.

There are few studies specifically regarding the cell death following ICH and little is known about cell death in the premature human brain after hemorrhage. Contused brain tissue from adult humans has been studied more frequently<sup>113, 114</sup>.

Clinical studies show that evidence of TUNEL positive cells in a retrospective histological analysis was present in surgical specimens obtained from 10 of 12 ICH patients<sup>168</sup>. The TUNEL-positive cells were observed within 1 day, 2 days, and 5 days in

the penumbra region after the onset of symptoms. The authors concluded that brain cell apoptosis represents a prominent form of cell death associated with ICH in humans <sup>168</sup>. However, this study has many shortcomings. For instance, the number of patients in the study group is small and the exact site of the biopsies was not recorded. Most importantly, only TUNEL staining was used to document apoptosis; TUNEL staining detects DNA fragments in apoptotic cells and necrotic cells <sup>38-40, 54</sup>. Therefore, other techniques should be used to confirm these findings.

In traumatic ICH, neuronal apoptosis has been investigated in paraffin-embedded brain tissue from 103 individuals who had sustained traumatic brain injury by use of the in situ nick translation (ISNT) technique with staining of DNA fragmentation. The authors claimed that apoptotic neuronal cells could be detected in a cortical contusion with a wound age of 45 minutes at the earliest and in the majority of the cases with post infliction intervals up to 2 weeks, numerous ISNT-positive cells were found adjacent to the traumatically injured area. The neuronal apoptosis peaks at about 1 day and persists for at least 22 weeks after traumatic brain injury <sup>192</sup>.

Thirty-one specimens of brain tissue removed during emergency craniotomy for evacuation of cerebral contusions with mass effect were examined. TUNEL positive cells were noted in eight patients. Bax expression was detected in all patients, whereas bcl-2 expression was noted in six patients. The apoptosis occurs in patients after traumatic brain injury and may contribute to the secondary injury processes <sup>193</sup>.

#### 1.7.10 Brain cell death following ICH in animal models

In addition to mass effect of the hematoma following ICH, the hematoma could release toxic substance such as thrombin, ROS, MMPs, and inflammatory cytokines, which can induce pathological changes in its vicinity, including neuronal and glial cell death, vasogenic edema, and breakdown of the blood-brain barrier<sup>39-41, 53, 54, 194, 195</sup>. Apoptosis has been observed in other central nervous system injuries, including epilepsy and cerebral ischemia<sup>97</sup>, and there is growing evidence from animal experiments suggesting that cell death in the penumbra region may involve apoptosis<sup>39, 40, 53, 54, 166, 167, 194, 196</sup>.

Exposure of primary cortical neurons to hemoglobin induced a dose- and time-dependent neurotoxicity. Caspase-9-like and caspase-3-like activities increased<sup>196</sup>. The free radical scavenger U83836E significantly reduced hemoglobin-induced neuronal death<sup>196</sup>. The activation of caspase cascades and pathways of oxidative stress may predominate in hemoglobin neurotoxicity in vitro<sup>196</sup>.

Brain cell death is mediated in part by apoptotic mechanisms following ICH in rats<sup>194</sup>. Double staining suggested that these TUNEL-positive cells with morphologies suggestive of apoptosis were mostly neurons and astrocytes<sup>194</sup>. The TUNEL-positive cells appeared at 6 hours in the ICH model and were present for more than 2 weeks after ICH, peaking at 3 days<sup>167</sup>. Brain cell loss after ICH is associated with activation of caspase-3<sup>167</sup>. The activation of caspase-3 precedes that of DNA fragmentation, peaking at 1 day after ICH. Caspase-3 was localized in the TUNEL positive cells. Intracerebral thrombin injection elicited DNA fragmentation similar to injection of blood<sup>167</sup>. Double-labeling studies demonstrated that both neurons and astrocytes surrounding the clot were TUNEL-positive. This claim may be incorrect because TUNEL labeling was found in the

cytoplasm but not the nucleus (it might have been a staining artifact)<sup>167</sup>. Cytochrome c increased at 24 hours and 3 days after ICH, and returned toward baseline by day 7. At 24 hours, stereology in the peri-ICH region showed decreased density in the region where cytochrome c immunoreactivity was the highest<sup>197</sup>.

Nuclear factor-kappaB (NF-kB) contributes to cell death after ICH in rats<sup>166</sup>. NF-kB is a ubiquitous transcription factor that, when activated, translocates to the nucleus, binds to DNA, and promotes transcription of many target genes. In an ICH model by double blood injection in rats, NF-kB in the 4-day group revealed a 1.8- to 2.5-fold increase compared control. NF-kB activation colocalized to cells containing fragmented DNA measured by TUNEL<sup>166</sup>. Neuronal, but not microglial, accumulation of extravasated serum proteins after intracerebral hemolysate exposure is accompanied by cytochrome c release and DNA fragmentation<sup>198</sup>. In an oxidant model of ICH, neuronal accumulation of extravasated serum proteins was associated with cytochrome c release, DNA fragmentation, and cell death. Stress protein induction in adjacent regions suggested that vasogenic edema might have exacerbated cellular dysfunction and cell death after ICH<sup>198</sup>.

In a rabbit ICH model, a large proportion of cells trapped within the matrix of the hematoma were either shrunken dark cells or swollen. In the TUNEL-stained sections, a high burden of apoptotic-like cells, the type of which is not known, was observed in the matrix of the hematoma but not in the perihematoma regions<sup>199</sup>.

#### 1.7.11 Proteolytic enzymes involved in cell death following ICH

Some of the adverse effects of blood have been attributed to proteolytic enzymes involved in blood clot formation and lysis such as proteolytic activity of thrombin and plasmin<sup>38</sup>. Thrombin promotes blood clotting by cleaving fibrinogen into fibrin. Plasmin digests fibrin in blood clots. Following ICH, prothrombin<sup>91</sup> and plasminogen<sup>88, 89</sup> in the blood, which are the precursors of thrombin and plasmin, enter the brain substance. Brain is also a minor source of thrombin and plasmin<sup>200-202</sup>. In vitro, thrombin can impair neurite outgrowth<sup>203</sup>, induce apoptosis<sup>204</sup>, and cause morphological changes of cultured astrocytes<sup>205</sup>, neurite retraction in cultured neurons<sup>206</sup>. In vivo, intracerebral injections of thrombin and plasmin can cause brain edema<sup>207-209</sup>, inflammation, brain cell necrosis and apoptosis<sup>38</sup>.

Matrix metalloproteinases (MMPs) and tissue plasminogen activator (tPA) induce cell death<sup>38</sup>. Matrix metalloproteinases are a family of proteolytic enzymes with relative specificity for components of the extracellular matrix. Following brain injury MMPs are produced by infiltrating inflammatory cells, microglia, and astroglia<sup>85</sup>. Plasmin can promote the activity of MMPs<sup>86, 87</sup>. MMPs can directly damage brain cells and cause cell death by processing of death molecules (e.g. FasL). MMP may also disrupt myelin and perpetuate inflammation<sup>86, 87</sup>. Tissue plasminogen activator, a fibrinolytic serine protease, is routinely given by intravenous administration for the treatment of ischemic stroke. It can mediate microglial activation and modulates neuronal survival<sup>210</sup>. The hematoma persists in tPA-deficient (tPA(-/-)) mice but is drastically reduced in size in wild-type mice at 1-3 weeks after autologous blood injection<sup>210</sup>.

The detrimental effects of MMPs, especially MMP-9, have gained much attention since it was observed that their expression is elevated in ICH<sup>157</sup>. t-PA treatment elevated

the levels of MMP-9 after ischemia <sup>211</sup>, there are growing concerns about the cell damage that is attributed to the elevated level of MMP-9. In concert, these two proteinases may cause brain hemorrhage by dissolving the extracellular matrix of the micro-vessels surrounding the injury as well as preventing the natural healing process of damaged blood vessels. t-PA-induced hemorrhage volumes were reduced significantly in the presence of an MMP inhibitor BB-94 <sup>212</sup>. The activated MMP-9 can induce neuronal cell death via apoptosis <sup>213</sup>.

#### 1.7.12 Treatment of ICH with pharmacological agents

There are no studies using agents which inhibit cell death in humans with ICH. However, experimental animals seem to benefit by reduction of cell death accompanied by reduction of inflammation following ICH. Several drugs have been studied in rats with collagenase-induced ICH, because this model is most consistent. Free radicals may contribute to cell death and brain injury in ICH. The free radical trapping agent disodium 4-[(tert-butylimino)methyl]benzene-1,3-disulfonate N-oxide (NXY-059) administered following ICH in rat significantly reduced the neutrophil infiltrate and the number of TUNEL-positive cells observed adjacent to the hematoma at 48 h, and it significantly decreased neurological impairment on days 1, 3, 7, 14, and 21 <sup>214</sup>. Systemic FK-506 (tacrolimus), a potent immunosuppressant, reduced neutrophil infiltration and cell death around the hematoma <sup>156</sup>. The neurological deficit induced by the ICH was significantly decreased from 3 to 21 days post-ICH by treatment with FK-506 <sup>156</sup>. However, FK-506 can be directly neuroprotective independent of inflammation. Minocycline, a tetracycline derivative that crosses the BBB, significantly reduced neutrophil and macrophage

infiltration, microglia activation, and cell death. Neurobehavioral outcomes were also significantly improved <sup>157</sup>. Reducing brain TNF-alpha expression by using ORF4-PE (a TNF $\alpha$  antisense oligodeoxynucleotide) directly into rat striatum is neuroprotective <sup>130</sup>. It decreased levels of TNF $\alpha$  mRNA and protein in brain tissue surrounding the hematoma. Brain cell death labelled by TUNEL was significantly reduced in animals receiving ORF4-PE compared to the saline-treated ICH group. ORF4-PE treatment improved neurobehavioral deficits observed from 24 hours to 28 days after ICH <sup>130</sup>. Intracerebral infusion of a second-generation ciliary neurotrophic factor (CNTF) (AXOKINE®) reduced neuronal loss in rat striatum following experimental intracerebral hemorrhage <sup>215</sup>. Counts of medium-sized striatal neurons adjacent to the hematoma 8 weeks revealed a slight but statistically significant benefit following AXOKINE treatment <sup>215</sup>. Neuronal and glial cell death in the striatum begins at 1 day and continues for at least 3 weeks after ICH <sup>215</sup>. Rare TUNEL-positive cells exhibited a weak cytoplasmic signal for the neuronal marker NSE <sup>215</sup>. The density of TUNEL-positive cells at 24 and 48 hours after ICH was significantly reduced by treatment with the broad-spectrum caspase inhibitor, zVADfmk <sup>194</sup>. Macrophage/microglial inhibitory factor (MIF), a tuftsin fragment 1-3, significantly reduced brain injury volume and the neurobehavioral deficits were improved. Endogenous tPA assists in the clearance of ICH, presumably by affecting microglial activation, and MIF could be a valuable neuroprotective agent for the treatment of ICH <sup>210</sup>. Tauroursodeoxycholic acid (TUDCA), an endogenous bile acid, reduces apoptosis and protects against neurological injury after ICH in rats <sup>216</sup>. TUDCA reduced lesion volumes and decreased apoptosis adjacent to hematoma, which was associated with a similar inhibition of caspase activity. TUDCA treatment increased expression of certain

antiapoptotic Bcl-2 family members which can inhibit cytochrome c release from mitochondria <sup>217, 218</sup>. NF-kB activity is decreased after TUDCA treatment. Neurobehavioral deficits, which improved with TUDCA treatment, are possibly related to the reduction of apoptotic cells in the brain of treated animals.

Aspiration of the hematoma after collagenase-induced ICH slightly improved acute functional outcome and reduced neuronal loss from the striatum <sup>219</sup>.

The transplantation of fetal forebrain tissue into the hematoma site of rats with ICH showed there were no statistically significant differences in histology and behavioral tests of rat with ICH compared to control <sup>220</sup>.

#### 1.7.13 Brain cell death following the ICH in immature brain

PVH/IVH can occur in premature infants of 24 - 30 weeks gestation and is associated with poor developmental outcome <sup>15</sup>. Following periventricular blood injection into brains of neonatal mice, TUNEL positive cells were evident by 8 hours, their quantity was maximal at 7 days, and then persisted up to 28 days <sup>37</sup>.

#### 1.7.14 Summary and conclusions of brain cell death

Previous studies indicate that brain cell death occurs in and around hematomas following ICH. Far less information is available for ICH than for ischemic stroke or trauma, with which there may be overlap and similarities. Brain cell death seems to be more severe after ICH than after ischemic stroke. In ICH, inflammation accompanies cell death. The more severe inflammation, the greater cell death occurs. Infiltration of leukocytes, activation of microglia, and production of cytokines may contribute to brain

cell death. Neutrophils and microglia / macrophages seem more likely to produce free radicals and cause brain cell necrosis. Therefore, inhibition of inflammation may reduce the cell death following ICH. Experimental blockade of inflammation and inhibition of caspases provide evidence that ICH-induced brain cell death may be amenable to treatment with anti-inflammatory and anti-apoptotic agents. More work is needed to define the role of brain cell death before embarking on pharmacological anti-inflammatory and anti-apoptotic therapy in human ICH.

### 1.8 Proteolytic enzymes in brain development

Neurons and glia can produce thrombin and thrombin receptors <sup>203</sup>, which are most abundant in the newborn rodent brain <sup>221</sup>. Plasminogen, tPA and uPA are produced by brain cells in neonatal and adult rodents <sup>202</sup>. tPA and uPA cleave plasminogen to plasmin. In the mouse brain, uPA and its receptor are maximally expressed by neurons at 8-10 days <sup>222</sup>. MMPs are also produced in the developing brain <sup>223</sup>. Endogenous proteolytic enzymes play a role in cell migration <sup>223</sup>, vascular growth <sup>224</sup>, synaptogenesis, and myelination <sup>225</sup> in the developing brain.

Following ICH additional proteolytic enzymes enter into the brain substance from the blood or are produced by the damaged brain. In vitro, thrombin induces apoptosis <sup>204</sup>, causes morphological changes of astrocytes <sup>205</sup>, and neurite retraction in cultured neurons <sup>203, 206</sup> likely through protease activated receptors-2 (PAR-2) <sup>226, 227</sup>. In vivo, injected thrombin and plasmin cause brain edema <sup>208, 209</sup>, inflammation, brain necrosis and apoptosis <sup>38</sup>. Endogenous tPA seems to potentiate neuronal degeneration through enhanced NMDA receptor-mediated signalling after focal cerebral ischemia<sup>228</sup>. MMPs

are produced by infiltrating inflammatory cells, microglia, and astroglia following brain injury<sup>85</sup>. Plasmin can promote the activity of MMPs<sup>86, 87</sup>. MMPs can directly damage brain cells, cause cell death by processing death molecules, disrupting myelin, and perpetuating inflammation<sup>86, 87</sup>. Endogenous inhibitors of proteolytic enzymes, including neuroserpin<sup>229</sup>, plasminogen activator inhibitors (PAI) 1 and 2<sup>222</sup>, protease nexin-1 (PN-1)<sup>230</sup>,  $\alpha$ 2-macroglobulin<sup>231, 232</sup>, and the tissue inhibitors of metalloproteinases (TIMPs)<sup>233</sup> are present in developing brain. Their quantities are likely insufficient for inhibition of high concentrations of proteolytic enzymes released following ICH. Potentially the proteolytic enzyme activity associated with ICH might interfere with normal brain development.

#### 1.9 Cell migration from germinal matrix

In premature infants at 24-30 weeks gestation the germinal matrix around the ventricles consists of pluripotential cells that gives rise largely to precursors of oligodendrocytes to produce myelin, and astrocytes to support maturation of neurons that have already migrated<sup>15</sup>. In the newborn mouse and rat, the periventricular germinal cells generate similar cells that migrate into various parts of the ipsilateral cerebral hemisphere<sup>234-236</sup>. Hypoxic ischemic damage to 7-day old rat brain, in which the germinal matrix has largely involuted, reduces the quantity of oligodendrocyte precursors<sup>237</sup>. In immature brain the germinal matrix may be directly injured by PVH, therefore the migration of glial precursors involved in the myelin formation and neuron development might be affected in PVH.

### 1.10 Brain injury in the developing brain in ICH and other brain injury

Neonatal brain hemorrhage has been largely overlooked. Newborn dogs have been used to study physiologic factors that predispose to hemorrhage<sup>69</sup>. Traumatic injury in young animals has been studied as a model of child abuse<sup>76, 238</sup>. Premature infant brains with hemorrhage in germinal matrix have reduced proliferating cell populations<sup>239</sup>. In a PVH/IVH model of 1-day old mice, whose brains are at a developmental stage similar to that in 24-25 week gestation in humans<sup>240</sup>, cell proliferation was greatly suppressed in germinal matrix. Cell death increased in the damaged brain and germinal matrix after PVH/IVH<sup>240</sup>. Those data indicated that extravasated blood might play an important role in brain damage following PVH/IVH through suppression of cell proliferation. The cytokines IL-1, IL-6, and TNF- $\alpha$  have been found associated with prenatal intrauterine infection (IUI), preterm birth, neonatal infections, and neonatal brain damage. Maternal IUI appears to increase the risk of preterm delivery, which in turn is associated with an increased risk of IVH, neonatal white matter damage, and subsequent cerebral palsy. Interrupting the cytokine cascade might prevent later disability in premature infants<sup>241</sup>.

Focal brain ischemia with reperfusion triggers acute inflammatory responses including neutrophils, lymphocyte, and microglia/macrophages in P7 rats<sup>242</sup>. In mouse brain, microglia are markedly increased during mouse development in the first postnatal week after birth, but may also related to pathological conditions of the brain<sup>243, 244</sup>. This suggested that activation of immune status affects the injury to the immature brain. Exposure to uterine infection is an independent risk factor for the development of cerebral palsy<sup>245</sup>.

### 1.11 Age-dependent brain response following brain injury

Age-dependent brain responses have been seen in a variety of brain injuries. A focal cortical impact study in piglets showed that the amount of hemisphere injured differed significantly among ages, with the 5-day old piglets sustaining smaller lesions than 1 or 4 months old piglets <sup>238</sup>. There is an age-dependent behavioral recovery following brain damage by removal of cortical tissue. In rat this is associated with poor behavioral recovery in newborn and adult rats and moderately good recovery in 10-day old rats, which suggests that there is a stage of development with optimal adaption to brain damage and subsequent brain reorganization <sup>246, 247</sup>.

Following focal ischemic brain injury there is an age-dependent reduction in the infarct volume in mice lacking the inducible nitric oxide synthase (iNOS-null). The size of the infarct produced by occlusion of the middle cerebral artery (MCA) is larger in 4 to 6-month old than in 1 to 2-month old mice. However, the reduction in infarct volume was greatest at 1 to 2 months old mice <sup>248</sup>. A single intracerebroventricular (ICV) injection of brain-derived neurotrophic factor (BDNF) showed neuroprotection against neonatal hypoxic-ischemic brain injury in 7-day old rats but not in 2-day old rats <sup>249</sup>.

In hypoxic-ischemic brain injuries the area of infarction in 2-week-old rat was reduced by pretreatment with dexamethasone, whereas in 1-month-old rats it was ineffective <sup>250</sup>. Apoptotic cell death following cerebral hypoxia-ischemia occurs more frequently in immature than older rats, possible because the immature brain retains a part of developmental programmed cell death that is readily activated following hypoxia-ischemia <sup>251</sup>.

Although the effects of ICH have been described for adult animal models, few have investigated these effects in the newborn or have characterized such effects as a function of age using a single model of injury. Gene expression in rat brain following blood injection varies with age. The 7-day-old mouse brain exhibits a more rapid and intense inflammatory response to stimuli by intracerebral injections of endotoxin in neonatal mouse brain than the adult brain<sup>252</sup>.

Age-dependent differences in brain injury response might explain certain unique clinical syndromes seen in infants and young children and would determine whether specific therapies might be effective or even counterproductive at different ages. Head trauma is also accompanied by bleeding into the brain. Prognosis following brain injury appears to be worst in children under 4 years of age<sup>253</sup>. In fact, brain damage in the very young is associated with a worse outcome than in older children<sup>254</sup>. Differences in pathways leading to brain damage may be relevant to designing therapies appropriate for patients of different ages.

### 1.12 Summary

ICH is a common occurrence in adults with hypertension and in prematurely born infants. Several mechanisms are involved in ICH-related brain damage. These include mechanical destruction of brain tissue, compromised cerebral blood flow<sup>2</sup>, cerebral edema, release of proteolytic enzymes, inflammation, and cell death. The mechanisms of ICH-related brain injury have been studied extensively in adult animals<sup>255</sup>, but neonatal hemorrhage has been largely ignored. Therefore, the general hypotheses and specific goals of present study are as follows.

### 1.13 General hypotheses

1.13.1. There are age-dependent responses following ICH in the rodent brain.

1.13.2. Uncontrolled proteolytic activity and inflammation contribute to the poor outcome following ICH in the rodent brain.

### 1.14 Specific goals

1.14.1 To describe the evolution of inflammation and cell death following intracerebral blood injection in adult rats.

1.14.2 To compare the evolution of inflammation and cell death in different models of adult rat brain hemorrhage, specifically autologous blood injection, collagenase injection and pial vessel disruption.

1.14.3 To investigate the relationship between blood fractions and brain cell death in intracortical hemorrhage in adult rats.

1.14.4 To investigate acute brain damage after injections of thrombin and plasmin into adult rat striatum.

1.14.5 To establish a model of periventricular / intraventricular hemorrhage and to investigate brain inflammation and damage in neonatal mouse cerebrum.

1.14.6 To determine the effect of age on the evolution of inflammation and cell death in mouse brain following injections of whole blood, thrombin, and plasminogen.

1.14.7 To determine the effect of immune pre-activation on brain inflammation and cell death by using LPS, Conavalin A, and Poly I:C in 3 ages of mouse following ICH.

1.14.8 To investigate whether inhibition of thrombin or plasmin improves the neurological outcome in neonatal mice following PVH.

NOTE: Five of these experiments have been published already and the remaining three have been submitted to journals for review at the time of writing. The journal citation (or planned for submission) is included on the front sheet of each chapter.

## CHAPTER 2 SPECIFIC EXPERIMENTS

### Chapter 2-1

Intracerebral injection of autologous whole blood in rats: time course of inflammation and cell death.

Mengzhou Xue

Marc R. Del Bigio

Neurosci Lett. 2000;283(3):230-232.

## ABSTRACT

Intracerebral hemorrhage is associated with stroke and head trauma. The purpose of this study was to study brain inflammation and cell death in adult rats 1 hour to 4 weeks after injection of blood into the striatum. TUNEL positive dying cells were evident 4 hours to 4 weeks post-hemorrhage. Neutrophil infiltration was brief and peaked at 48 hours. CD8a immunoreactive lymphocytes, possibly natural killer cells, became apparent at 48 hours and persisted for 1 week. Microglial reaction was evident at 4 hours and persisted for 4 weeks. We conclude that extravascular blood causes a mixed inflammatory cell reaction in brains that is maximal from 48-72 hours following hemorrhage. This is associated with death of brain cells over a prolonged period of at least 4 weeks.

## KEYWORDS

brain hemorrhage, inflammation, neutrophil, TUNEL, lymphocyte, microglia

Intracerebral hemorrhage (ICH) can be a consequence of hypertensive bleeding, rupture of cerebral vascular malformation, amyloid angiopathy, or trauma. Hematomas remain a significant management problem because the blood seems to have adverse effects beyond its space occupying effect<sup>256</sup>. Brain edema associated with ICH has been studied experimentally following infusion of autologous whole blood and after collagenase-induced hemorrhage<sup>41, 62</sup>. Ischemia in the surrounding tissue and toxicity of thrombin and / or hemoglobin might be involved in brain damage<sup>2, 42, 93</sup>. Neutrophil inflammation is considerable in the vicinity of collagenase-induced intracerebral hematoma<sup>52</sup>. Neutrophils release a variety of cytokines, such as tumor necrosis factor alpha (TNF- $\alpha$ ), interleukin 6 (IL-6) and interferon gamma (IFN- $\gamma$ ), which might play an important role in ischemic and traumatic brain damage<sup>79</sup>. Although the autologous whole blood injection model is one that might have relevance to the clinical situation, there are no reports concerning the subsequent inflammatory cell infiltration. Therefore, the purpose of this study was to investigate the temporal relationship between autologous intracerebral hemorrhage and brain inflammation and cell death.

All experimental procedures were done in accordance with guidelines of the Canadian Council on Animal Care. Protocols were approved by the local experimental ethics committee. Twenty-five young adult male Sprague-Dawley rats weighing 175 to 250 grams were used. Each rat was anesthetized with pentobarbital (50 mg/kg IP) and placed in a stereotactic frame. A midline scalp incision was made and a hole was drilled in the skull (3 mm lateral to midline, 0.02 mm anterior to coronal suture). Autologous whole blood was collected by placing the tail tip in warm water for 5 minutes, cleansing

the skin with 70% alcohol, cutting the tail tip with a razor blade, and drawing 50  $\mu$ l of freely dripping blood into a sterile syringe. A 25-gauge needle was attached, the syringe was secured in the frame, and the needle was quickly introduced into the striatum 5.5 mm below the skull surface. Blood was injected over 5 minutes, the needle was left in place for 3 minutes, then removed slowly. The bone hole was sealed with bone wax, the scalp wound was sutured, and the animal was placed in a cage with free access to food and water. To control for the process of injection, additional rats received injections of 50  $\mu$ l sterile 0.9% saline solution into the same site.

One hour, 4h, 24h, 48h, 72h, 1 week, or 4 weeks after the injection, rats were reanesthetized and perfused through the heart with 300 ml ice cold 4% paraformaldehyde in 0.1 mol/L phosphate-buffer saline (PBS). Rats with saline injection were killed at 48 hours. The brain was removed and kept in the same fixative then cut coronally approximately 2 mm on either side of the needle entry site. Brain slices were embedded in paraffin. Sections (6  $\mu$ m) were cut, and each 30<sup>th</sup> section from the rostral to the caudal portion of the residual hematoma was stained with hematoxylin and eosin (H-E). At the level of maximal brain damage a variety of histological and immunohistochemical staining procedures were performed. Chloracetate esterase reaction was used to stain neutrophil cytoplasm bright red<sup>257</sup>. To demonstrate lymphocyte subpopulations, sections were dewaxed, hydrated, quenched with 0.3 % H<sub>2</sub>O<sub>2</sub>, blocked with 10 % normal serum, incubated with anti-CD8a monoclonal antibody (diluted 1/400, PharMingen) at 4°C overnight, washed, incubated with biotinylated goat anti-mouse IgG (1/300) for 1 hour at room temperature, washed, incubated with peroxidase-streptavidin, and colored with diaminobenzidine. Control sections were processed with omission of the primary

antibody. Biotinylated Ricinus communis agglutinin-1 (RCA-1) lectin (Sigma) binding was used to demonstrate reactive microglial cells by incubation for 1 hour at room temperature followed by peroxidase-streptavidin and diaminobenzidine. Dying cells were demonstrated by TUNEL (terminal deoxynucleotidyl transferase (TdT)-mediated deoxyuridine triphosphate (dUTP)-biotin nick end labeling) using the *Apoptag in situ* kit (Intergen) as recommended by the manufacturer. Sections were counterstained with methyl green. Negative control sections were treated similarly but incubated in the absence of TdT enzyme, dUTP-digoxigenin, or anti-digoxigenin antibody. TUNEL-positive nuclei with chromatin condensation and fragmented nuclei were considered as probable apoptotic cells. TUNEL positive cells with diffuse light brown labeling of nucleus and cytoplasm were considered as probable necrotic cells<sup>188</sup>.

Using an ocular graticule and 250 x ocular magnification neutrophils, TUNEL positive dying cells, RCA-1 labeled cells and CD8a immunoreactive cells were counted in four fields (each area 250 x 250  $\mu\text{m}$ ) immediately adjacent to, but not including, the needle insertion and injection site, which was defined by the presence of erythrocytes. Areas with large blood vessels were avoided. A "camera lucida" drawing was made of the coronal slice with maximal hemorrhage. Areas of hematoma, defined by blood collections and tissue rarefaction, were traced onto a sheet of paper. Computerized planimetry was used to measure the traced areas.

All data are expressed as mean  $\pm$  standard deviation of mean. Data were analyzed by ANOVA with Bonferroni-Dunn post hoc intergroup comparisons or Student's t test using StatView 5 software (SAS Institute Inc.).

All rats tolerated the surgical procedure well and there was no surgical mortality. Residual hematoma was consistently located in the striatum with focal extension into adjacent white matter in 5/21 rats. In rats with blood injection, damaged brain surrounding the hematoma appeared pale. Microscopically, blood appeared as single or multiple contiguous collections of blood cells surrounding the needle tract. After 24 hours, degenerating erythrocytes and fragmented nuclear debris were seen. In intact brain tissue surrounding the hematoma, neutrophils were adherent to vessel walls or passing through capillaries and small veins. TUNEL positive dying cells with a necrotic appearance were present within the hematoma as early as 1 hour after blood injection. TUNEL positive dying cells, with a nucleus-only stained apoptotic appearance, were evident in the intact striatum surrounding the hematoma beginning at 4 hours. Cells that exhibited membrane immunoreactivity for CD8a were small with minimal cytoplasm and round nuclei. We believe these to be natural killer lymphocytes and not monocyte / macrophages<sup>258</sup>.

Quantitative analysis of cell death and inflammation in intact striatal tissue surrounding the hematoma is shown in Table 2-1-1. TUNEL positive dying cells were observed beginning at 4 hours, maximal at 72 hours, and persisting until 4 weeks. Neutrophils were present in the tissue, maximally at 48 h and were nearly gone by 72 hours. CD8a immunoreactive cells became apparent at 48 hours and persisted until 1 week. RCA-1 labeled microglia were evident beginning at 4 hours, were maximal at 48-72 hours, and persisted until 4 weeks. At 48 hours, inflammatory and dying cells were significantly more abundant following whole blood injection than saline injection. The

size of the hematoma appeared to be constant for at least 72 hours and perhaps 1 week but by 4 weeks was considerably reduced in size.

Intracerebral hemorrhage causes brain damage by multiple mechanisms. Direct tissue destruction by the hemorrhagic event and dissection of blood along tissue planes occurs immediately. This is followed by development of edema and the potential for ischemic damage due to raised intracranial pressure or distortion of microvasculature <sup>2</sup>. Delayed damage could result through a variety of mechanisms including local ischemia, release of toxins by blood breakdown products, thrombin release, or leukocyte infiltration <sup>4, 52, 92, 259</sup>.

This study demonstrates that injection of a small quantity of whole blood into the cerebral striatum of rats is associated with cell death, inflammatory cell infiltration, and microglial reaction. The tissue distortion was minimal and therefore mechanisms other than the local space-occupying effect and ischemia are presumed to contribute. Blood injections produce larger lesions and more inflammation than inert material injection into the brain <sup>256, 260</sup>. We have shown that collagenase-induced hematoma in rats is associated with considerable inflammation <sup>52</sup>, and that injection of blood causes a greater degree of neuronal death and inflammation after 48 hours than injection of mineral oil, saline, or plasma <sup>40</sup>. Blood clot formation is considered to contribute to early peri-hematoma edema development <sup>41</sup>. Cellular damage in the tissue adjacent to autologous whole blood injection sites might be due to chemical toxicity generated by the degrading hematoma itself <sup>42</sup>, by exogenous inflammatory cells including neutrophils that release harmful oxygen radicals <sup>261</sup> and cytokines including tumor necrosis factor alpha (TNF- $\alpha$ ) and interleukin 6 (IL-6), by natural killer cells that can release interferon gamma (IFN- $\gamma$ )

which is potentially toxic to neurons and oligodendrocytes<sup>262</sup>, by plasma proteins such as thrombin<sup>93</sup>, or by the endogenous inflammatory response of microglia<sup>263</sup>. Our data demonstrated that cell death was commonplace from 24 hours to 4 weeks and peaked 72 h after blood injection. We have previously shown that the most of dying cells are glial<sup>40</sup> but that there is significant neuronal loss in the penumbra surrounding the hematoma<sup>219</sup>. Whether the inflammation following intracerebral hemorrhage contributes directly to neuronal loss or if the two cellular processes are simply coexistent phenomena remains to be proved. Data from experimental ischemia models suggest that inflammation does contribute directly to brain injury<sup>264</sup>. If so, anti-inflammatory therapy during the first week might be useful following brain hemorrhage.

Table 2-1-1. Striatal inflammation and cell death following injection of autologous whole blood.

Time after blood injection	Hematoma size (mm <sup>2</sup> )	TUNEL positive cells	Neutrophils	CD8a positive cells	microglia/macrophages
1h (n=3)	4.6 ± 1.1	0.0 ± 0.0	0.0 ± 0.0	0.0 ± 0.0	0.0 ± 0.0
4h (n=3)	4.4 ± 1.0	3.0 ± 0.0	0.0 ± 0.0	0.0 ± 0.0	9.3 ± 7.0
24h (n=3)	3.1 ± 1.3	12.3 ± 1.5	1.3 ± 1.5	0.0 ± 0.0	13.3 ± 8.0
48h (n=3)	5.0 ± 3.8	18.7 ± 10.8 *	34.7 ± 13.6 *	41.7 ± 6.0 *	106.0 ± 1.0 *
48h saline control (n=4)	0.2 ± 0.1 #	2.5 ± 3.0 #	6.8 ± 3.6 **	3.8 ± 0.5 **	32.8 ± 6.4 **
72h (n=3)	6.9 ± 4.3	49.0 ± 2.6 *	5.0 ± 1.0	23.7 ± 11.1 *	97.3 ± 19.7 *
1w (n=3)	3.8 ± 1.7	17.7 ± 9.3	0.0 ± 0.0	4.7 ± 2.1	9.7 ± 5.5
4w (n=3)	1.5 ± 0.3	7.7 ± 7.2	0.0 ± 0.0	0.0 ± 0.0	14.3 ± 4.5

All data are expressed as mean ± SD. Cell counts are expressed as the number of cells per four 250 x 250 µm areas.

\* p<0.0003 vs. 1h and 4h times after blood injection (ANOVA)

# p<0.05, \*\* p<0.01 vs. 48 hours blood injection (Student's t test)

## Chapter 2-2

Comparison of brain cell death and inflammatory reaction in three models of intracerebral hemorrhage in adult rats

Mengzhou Xue, MD

Marc R. Del Bigio, MD, PhD, FRCPC

J. Stroke Cerebrovasc. Dis. 2003;12: 152-159.

ABSTRACT: Intracerebral hemorrhage is associated with stroke and head trauma. Different experimental models are used, but it is unclear to what extent the tissue responses are comparable. The purpose of this study was to compare the temporal responses to brain hemorrhages created by injection of autologous whole blood, collagenase digestion of blood vessels, and avulsion of cerebral blood vessels. Adult rats were subjected to intracerebral hemorrhage. Rats were perfusion fixed with paraformaldehyde 1 hour to 28 days later. Hematoxylin & eosin, Fluoro-Jade, immunohistochemical, and TUNEL staining were used to allow quantification of damaged and dying neurons, neutrophils, CD8 $\alpha$  immunoreactive lymphocytes, and RCA-1 positive microglia/macrophages, adjacent to the hemorrhagic lesion. In all models eosinophilic neurons peaked at 2-3 days. TUNEL positive cells were observed maximal at 2 days in blood injection model, 3 days in vessel avulsion model, 1-7 days in collagenase injection model, and were evident in small quantities in 21-28 days in 3 models. Neutrophils appeared briefly from 1-3 days in all models but they were substantially lower in the cortical vessel avulsion model, perhaps owing to the devitalized nature of the tissue. Influx of CD8 $\alpha$  immunoreactive lymphocytes was maximal at 2-3 days in autologous injection model, 3-7 days in other 2 models, and persisted for 21-28 days in all models. The microglial/ macrophage reaction peaked at 2-3 days in the blood injection model and at 3-7 days in other 2 models, and persisted for weeks in all groups. These results suggest that different models of intracerebral hemorrhage are associated with similar temporal patterns of cell death and inflammation. However, the relative magnitude of these changes differs.

Keywords: intracerebral hemorrhage, neutrophils, microglia, cell death

## Introduction

Intracerebral hemorrhage (ICH) can be a consequence of hypertension, bleeding into an ischemic infarct, rupture of abnormal blood vessels, or trauma. Hematomas remain a significant management problem because the blood itself seems to have adverse effects beyond its space occupying effect<sup>259</sup>. The development of therapies relies on the use of animal models. Several experimental models of ICH have been described including autologous whole blood injection<sup>38, 40, 44, 46, 57, 140, 265</sup> and bacterial collagenase injection, which disrupts the basal lamina of cerebral capillaries and causes bleeding into the brain tissue<sup>52, 63, 215</sup>. Another simple but infrequently used model of cortical injury involves stripping of the cortical surface blood vessels, wherein avulsion of the veins creates cortical hemorrhages<sup>266, 267</sup>. Brain cell death, inflammatory cell infiltration, and microglial reaction accompany stroke and brain trauma<sup>143, 264, 268</sup>. The purpose of this study was to investigate the similarities and differences of these three ICH models with regard to brain cell death and inflammatory cell infiltration. Furthermore, we sought to assess advantages of different methods for assessing cell death including TUNEL, eosinophilic neurons, and Fluoro-Jade staining.

## Materials and methods

### Animal preparation

All experimental procedures were done in accordance with guidelines of the Canadian Council on Animal Care. Protocols were approved by the local experimental ethics committee.

### Autologous whole blood induced ICH

Twenty-five young adult male Sprague-Dawley rats weighing 175 to 250 grams were used. Each rat was anesthetized with pentobarbital (50 mg/kg IP) and placed in a stereotactic frame. A midline scalp incision was made and a hole was drilled in the skull (3 mm lateral to midline, 0.02 mm anterior to coronal suture). Autologous whole blood (50  $\mu$ l) was collected in a sterile syringe by placing the tail in warm water for 5 minutes, cleaning the skin with 70% alcohol, and cutting the tail tip. A 25-gauge needle was attached and quickly introduced into the striatum 5.5 mm below the surface of the skull. Blood was injected over 5 minutes; the needle was left in the place for 3 minutes, and then removed slowly. The bone hole was sealed with bone wax, the scalp was sutured, and the animal was placed in a cage with free access to food and water.

### Collagenase induced ICH

Thirty-one young adult male Sprague-Dawley rats weighing 250-300 grams were used to induce intracerebral hemorrhage by collagenase as previously described<sup>52</sup>. Rats were anesthetized with pentobarbital (50 mg/kg, IP) and placed in a stereotactic frame (David Kopf Inst.). Through a 30 gauge needle placed in the caudatoputamen (3 mm lateral to midline, 0.2 mm anterior to bregma, 6 mm depth) 0.7  $\mu$ l of sterile saline containing 0.14 U collagenase (Type IV, Sigma Chemical Co., St. Louis) was injected over 5 minutes. Core temperature was monitored and maintained (37°C) throughout the procedure using a tympanic membrane thermocouple probe and a thermostatically controlled water blanket. Bone was sealed with bone wax, the scalp was sutured, and rats were placed in a box with free access to food and water.

### Cortical blood vessel avulsion

Twenty-six young adult male Sprague-Dawley rats weighing 175 to 250 grams were used. Rats were anesthetized with pentobarbital (50 mg/kg IP) and placed in a stereotactic frame. Under aseptic conditions, the scalp was incised along the midline. A rectangular craniotomy 3 mm wide and 5 mm long was created in the right hemiskull, 1 mm behind the bregma and 1 mm lateral to the midline. The exposed cortical vasculature was avulsed by gently pulling away the leptomeninges and surface blood vessels with a sterile needle (23 gauge) bent at the tip. Hemostasis was achieved by gentle tamponade with cotton-tipped applicators. The scalp wound was sutured, and the animal was placed alone in a clean cage with free access to food and water.

#### Histological examination

Rats were reanesthetized and perfused through the heart with 300 ml ice cold 4 % paraformaldehyde in 0.1 mol/L phosphate buffered saline (PBS), 1 and 4 hour(s), 1, 2, 3, 7 day(s), 28 days after whole blood injection into striatum, 1 and 4 hour(s), 1, 2, 3, 7 day(s) and 21 days after collagenase injection into the striatum, and 1 and 8 hour(s), 1, 2, 3, 7 day(s) and 28 days after cortical vessel avulsion. The brain was removed and stored in the same fixative for 1 - 10 days. Fixed brains were cut coronally approximately 2-4 mm on either side of the lesion center, which were identifiable on the brain surface. Brain slices were dehydrated and embedded in paraffin. Sections (6  $\mu$ m) were cut, and each 30<sup>th</sup> section from the rostral to the caudal portion of the damage area was stained with hematoxylin and eosin (H&E). Near the lesion center, where the brain damage was maximal, a variety of histological and immunohistochemical stains were performed.

#### Immunohistochemistry and histochemistry

To demonstrate lymphocyte infiltrates, sections were dewaxed and rehydrated, washed with distilled water, quenched with 0.3 % H<sub>2</sub>O<sub>2</sub>, blocked with 10 % normal goat serum, and incubated with anti-CD8 $\alpha$  monoclonal antibody (diluted 1/400, PharMingen International, Canada) at 4°C overnight. This detects cytotoxic T cells and natural killer (NK) cells <sup>258</sup>. Slides were then washed with Triton PBS, incubated in biotinylated goat anti-mouse IgG (1/300) for 1 hour at room temperature, washed, incubated with streptavidin-peroxidase (1/400) for 30 minutes at room temperature, colored with diaminobenzidine - H<sub>2</sub>O<sub>2</sub> solution, washed and coverslipped. Control sections were processed with omission of the primary antibody.

Histochemistry with Ricinus communis agglutinin lectin (RCA-1) labeling was used to demonstrate reactive microglial cells and macrophages <sup>269</sup>. Sections were dewaxed and rehydrated, washed with distilled water, quenched with 0.3% H<sub>2</sub>O<sub>2</sub>, blocked with 10 % normal sheep serum, and incubated with biotinylated lectin (diluted 1/2000, Vector Laboratories, Inc., Burlingame, U.S.A.) at room temperature for 1 hour. Slides were then washed with Triton PBS, incubated with streptavidin-peroxidase (1/400) for 1 hour at room temperature, colored with diaminobenzidine - H<sub>2</sub>O<sub>2</sub> solution, washed and coverslipped. Control sections were processed with omission of the biotinylated lectin.

#### TUNEL

TUNEL (terminal deoxynucleotidyl transferase (TdT)-mediated deoxyuridine triphosphate (dUTP)-biotin nick end labeling) was used to identify cells with damaged DNA, most of which are dying cells. Paraffin embedded sections were dewaxed and rehydrated, then incubated in 20  $\mu$ l/ml proteinase K for 15 minutes. TUNEL was accomplished using *Apoptag in situ* kit (Intergen; Purchase, NY, USA). After immersion

in equilibration buffer for 10 minutes, sections were incubated with TdT and dUTP-digoxigenin in a humidified chamber at 37°C for 1 hour and then incubated in the stop/wash buffer at 37°C for 30 minutes. Sections were washed with PBS before incubation in anti-digoxigenin-peroxidase solution (1/500 in PBS) for 30 minutes at room temperature, and colored with diaminobenzidine - H<sub>2</sub>O<sub>2</sub> solution. Sections were counterstained with methyl green. Negative control sections were treated similarly but incubated in the absence of TdT enzyme or dUTP-digoxigenin. TUNEL-positive nuclei with chromatin condensation and fragmented nuclei were considered as probable apoptotic cells. TUNEL positive cells with diffuse light brown labeling of nucleus and cytoplasm were considered as probable necrotic cells<sup>188</sup>. Together they were considered to be dying cells.

#### Fluoro-Jade staining

Sections were stained with Fluoro-Jade<sup>189, 190, 270</sup> by incubating sections in 0.06% potassium permanganate for 15 min while gently shaking on a rotating platform. Then 0.001% Fluoro-Jade (Histo-Chem Inc.; Jefferson, AR) staining solution was applied for 30 minutes, following by PBS wash and coverslip application.

#### Cell counts and determination of damage area

The coronal level with maximal damage was identified. A "camera lucida" drawing was used to trace the brain damage area, which was defined by the presence of blood, tissue rarefaction, or necrosis. Computerized planimetry was used to measure the traced areas. Using an ocular reticule and 250 x ocular magnification (objective magnification x 20) pyknotic or eosinophilic dying neurons, Fluoro-Jade positive neurons, TUNEL positive dying cells, extravascular neutrophils (identified on H&E

sections by characteristic nuclear morphology), CD8 $\alpha$  immunoreactive cells, and RCA-1 binding cells were counted in 4 fields (each area 250 x 250  $\mu$ m) immediately adjacent to the needle injection/damage site as previous described<sup>38-40</sup>. Areas with large blood vessels were avoided. Counts were made near the edge of the lesion because the necrotic cores were devoid of viable cells.

### Statistics

All data are expressed as mean  $\pm$  SEM. Data were analyzed to ensure normal distribution and then intergroup comparisons to compare temporal changes were made by ANOVA followed by Scheffé test using StatView 5.01 software (SAS Institute; Cary NC). The differences were considered significantly different when  $p < 0.05$ . To compare the quantity of dying neurons on H&E and Fluoro-Jade staining, paired t-test was performed at each time point. We did not directly compare the different lesion types because the experiments were not run concurrently.

### Results

All rats tolerated the surgical procedure well and there was no surgical mortality. In all groups, damaged brain surrounding the hematoma appeared pale on H&E stain due to edema and /or necrosis. Following autologous whole blood injection the irregular hematoma core was located in striatum (Fig. 2-2-1a), although there was extension into adjacent white matter in approximately 25 % rats. Following collagenase injection the hematoma core was more spherical; it was consistently located in striatum and did not extend into adjacent white matter (Fig. 2-2-1b). Following cortical vessel avulsion, damage appeared across the entire cortical thickness (Fig. 2-2-1c) and extended to the

callosal white matter in approximately 20% rats. The microscopic changes were essentially similar in all three models with the exception that the cortical vessel avulsion lesion had more necrosis and less hemorrhage. Acutely, autologous whole blood injection, collagenase injection, and cortical vessel avulsion lesions were characterized by single or multiple contiguous collections of blood cells, swollen glial cells, and damaged neurons with shrunken angular somata and nuclei. By 1 day and thereafter neurons with shrunken nuclei and hypereosinophilic cytoplasm were evident within and surrounding the lesions. After 1 day, pale-staining degenerating erythrocytes and fragmented nuclear debris were seen. In intact brain tissue surrounding the lesions neutrophils (Fig. 2-2-2a) were adherent to vessel walls, or passing through walls of capillaries and small veins. Most TUNEL positive nuclei in the damage area or penumbra were small and likely represent glial or inflammatory cells (Fig. 2-2-2c). Cells immunoreactive for CD8 $\alpha$  were small and round with round nuclei (Fig. 2-2-2d). The lesion sizes were roughly constant until ~3 days after which time they appeared smaller as blood was phagocytosed (data not shown).

Quantitative data are shown in Fig. 2-2-3. The number of dying neurons at the edge (i.e. in the penumbra) of the lesion core, identified by cytoplasmic pyknosis or eosinophilia, peaked at 2 days in all forms of injury. Pyknotic neurons were more prevalent at the earliest time points following brain damage in all groups. Pyknotic neurons with shrunken angular somata and nuclei were evident in the injured area at 1 and 8 hour(s). By 1 day and thereafter hypereosinophilic neurons with shrunken nuclei surrounded the edematous infarct (Fig. 2-2-2a). Dying neurons remained common at 7 days and persisted in small quantities 21-28 days in all groups (Fig. 2-2-3). There was no

significant difference between the quantity of eosinophilic neurons and Fluoro-Jade stained neurons (Fig. 2-2-2b) ( $p= 0.56$ , paired t test) except 1 hour in all groups, and 7 days in collagenase injection model. Fluoro-Jade did not detect pyknotic neurons, which are presumed to represent the earliest form of injury at 1 hour. For individual animals, at time points 1 hour to 1 day, there was no significant correlation between Fluoro-Jade and H&E detectable damaged neurons ( $r = 0$  to  $0.3$ ,  $p> 0.5$ ). On days 2-7 the two values correlated better ( $r = 0.6$  to  $0.83$ ,  $p=0.23$ ). TUNEL positive dying cells were observed beginning at 4 hours, maximal at 2 days in autologous blood injection group, 3 days in vessel avulsion group, 1-7 days in collagenase injection group, and persisted until 4 weeks in brain tissue surrounding the hematoma in all 3 groups. The temporal pattern and quantity of TUNEL positive cells were similar in all three models. The quantity of TUNEL positive cells differed significantly from the quantity Fluoro-Jade and eosinophilic neurons at all time points except 2 days ( $p< 0.0001$  paired t test).

Neutrophils were present in the striatal or cortical tissue surrounding the hematoma, starting at 1 day, peaking at 2 days, and were nearly gone by 3 days in all three models. Collagenase injection was associated with the most neutrophils while the cortical vessel avulsion was associated with the fewest neutrophils. CD8 $\alpha$  immunoreactive T lymphocytes (Fig. 2-2-2d, 2-2-3) were maximal at 2-3 days in autologous blood injection group, 3-7 days in vessel avulsion and collagenase injection groups and, unlike neutrophils, were still abundant at 7 days. They persisted for 21-28 days. In all groups, RCA-1 labeling of microglia/macrophages (Fig. 2-2-2e) appeared by 4 hours, was maximal at 2-3 days in autologous blood injection group, 3-7 days in vessel avulsion group and collagenase injection group, and persisted for weeks. By 2 days and

more prominently by 7 days the core of the lesion exhibited an accumulation of macrophages. The quantity of microglia following collagenase injection was greater than in the other two groups.

## Discussion

Intracerebral hemorrhage causes brain damage through multiple mechanisms. Direct tissue destruction by the hemorrhagic event and dissection of blood along tissue planes occurs immediately. This is followed by development of edema and secondary ischemic damage due to raised intracranial pressure and distortion of the microvasculature. Delayed damage could result through a variety of mechanisms including local ischemia, release of toxins by blood breakdown products, thrombin release, or inflammatory cell action<sup>4, 38, 52, 92, 208, 259</sup>.

This study demonstrates that brain hemorrhage in rats created by injection of autologous whole blood or collagenase, or by avulsion of cerebral blood vessels is associated with similar temporal patterns of cell death, inflammatory cell infiltration, and microglial reaction. Cortical vessel avulsion causes ischemic infarction and hemorrhage; the hemorrhage is probably a consequence of deep vein avulsion. Cortical vessel avulsion is therefore not a pure ischemic stroke model as has been previously implied<sup>266, 271</sup>, rather it is a model of mixed ischemia and hemorrhage more similar to a cortical laceration than an ischemic infarct. The neutrophil infiltration in this model was less than that following autologous blood or collagenase injections into either the cortex or striatum<sup>40</sup>. A possible reason is that neutrophils cannot reach the damaged area because the vasculature has been severely disrupted. However, this is unlikely considering that the quantity of lymphocytes

is roughly the same. Another possible reason is that chemokine production differs. In the collagenase lesion, cell death and inflammation began earlier in comparison to the other models. A possible reason could be that collagenase activity causes direct and rapid cell injury in addition to creating a hematoma. In this regard, the model differs from the human situation and models using autologous blood injections.

Neutrophil infiltration into brain tissue surrounding the hematoma is substantial by 2 days. Clotting blood and damaged brain tissue liberate chemotactic factors, including thrombin <sup>272</sup>, that prompt the movement of neutrophils from blood into intact brain and toward the hematoma <sup>273, 274</sup>. Many neutrophils invade intracerebral hematoma and surrounding tissue after contusion or ICH in rats after collagenase injection <sup>1, 63</sup>. The fact that inflammation is more intense and prolonged in rats with collagenase injections suggests that the collagenase may be acting as a potentiator of chemoattractant agents <sup>52</sup>. There is considerable interest in the possibility that activated neutrophils can cause secondary tissue injury and contribute to edema formation through the release of reactive oxygen species and a variety of proteases <sup>275, 276</sup>. Depletion of circulating neutrophils reduces brain injury after middle cerebral artery occlusion <sup>277</sup>. However, some authors have recently suggested that the evidence for a harmful effect of neutrophils is weak <sup>278</sup>. The rapid decrease in neutrophils occurs because they die within 1-2 days of extravasation.

Cell death was commonplace from 1 to 28 days and peaked 1 to 3 days after hemorrhagic injury. It was clear, however, that the quantity of TUNEL positive cells did not match that of the dying neurons defined by eosinophilia on H&E staining or Fluoro-Jade staining. There are several reasons for the disparity. TUNEL positive cells might

understate the magnitude of cell death because they persist only for several hours<sup>279</sup> while eosinophilic neurons can persist for days or weeks<sup>280</sup>. Furthermore, because TUNEL positive cells include neurons, glia, and inflammatory cells, the quantity does not necessarily reflect the final neurological injury<sup>281</sup>. Following autologous blood injection into brain we found that most TUNEL positive cells are not neurons<sup>215</sup>. We consider a claim by others that most dying cells in this model of brain hemorrhage are neurons to be incorrect. This report shows TUNEL label in the cytoplasm but not in the nucleus, which might be a staining artifact<sup>167</sup>. Nevertheless, the use of TUNEL at appropriate post-lesion times with additional markers to confirm the type of dying cell can provide a gauge of the magnitude of cell death for purposes of comparison. We observed no differences in the quantity of dying neurons shown with the Fluoro-Jade staining and the eosinophilic neurons shown with H&E staining. It is likely that they represent the same population of damaged neurons<sup>189, 190</sup>. It should be noted that Fluoro-Jade did not detect damaged neurons at the earliest time points when pyknosis is evident. At this stage the pyknotic neurons might represent “dark neurons” which can potentially either revert to normal or go on to die<sup>282</sup>. Fluoro-Jade staining, however, is an easy way for quantifying dying neurons because the signal-to-noise ratio is high.

This comparative study has some shortcomings. The time course of three groups under study is not identical because the experiments were not done concurrently. Furthermore, the anatomical regions affected were not the same; two models focused on the striatum and one on the cerebral cortex. We have previously done autologous blood injections in the cortex and found them to be complicated by subarachnoid hemorrhage

<sup>40</sup>. Regardless, the similarities and differences between the three models of ICH are apparent.

In summary, brain cell death and inflammatory cell infiltration following intracerebral hemorrhage in rats continues for several weeks after autologous whole blood injection, avulsion of cerebral blood vessels, and collagenase injection. The three models of ICH have similar temporal pattern of cell death and inflammation. Autologous whole blood injection is most similar to human ICH. Cortical vessel avulsion by pial stripping causes a mixed form of injury with non-perfusion ischemia and hemorrhage. The brain damage caused by collagenase injection is most consistent from an anatomical perspective but is most artificial from a biological perspective. The model of ICH should be chosen carefully to address parameters one is interested in studying.

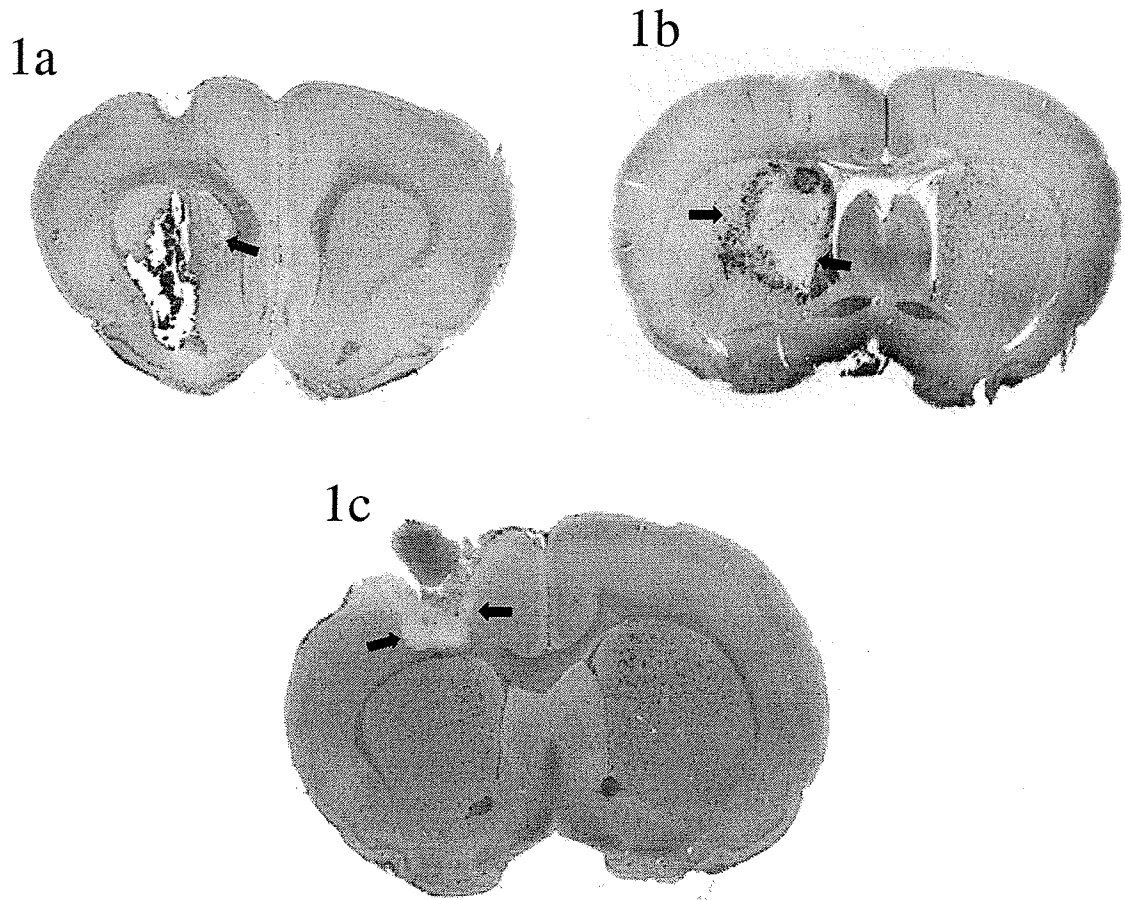


Figure 2-2-1. Photomicrographs showing brain lesions in rat cerebrum 48 hours after injection of 50  $\mu$ L autologous whole blood (Fig. 2-2-1a), and collagenase (Fig. 2-2-1b) or avulsion of cortical surface blood vessels (Fig. 2-2-1c). Collections of erythrocytes are seen as red areas. After blood injection, the edematous damaged striatum (arrows) extends well beyond blood collections. After collagenase injection, hematoma (arrows) is limited to the striatum. After vessel avulsion, the cortical tissue is partially necrotic and has fallen away during processing. The edematous tissue along the margin of the hematoma is evident (arrows), and there is blood on the brain surface.

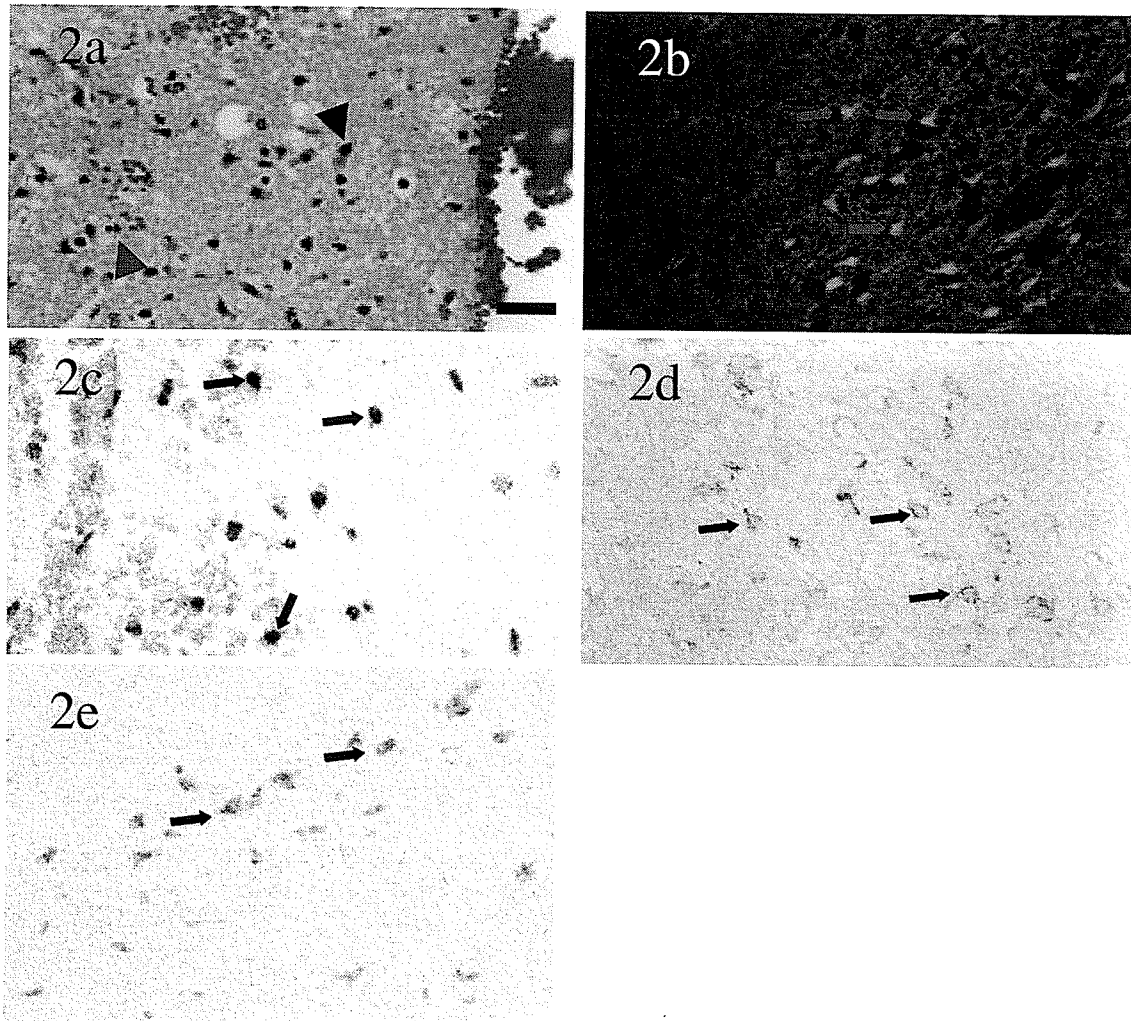


Figure 2-2-2. Photomicrographs of representative histopathologic features studied after ICH. H&E staining (Fig. 2-2-2a) shows neutrophils (blue arrow) and eosinophilic neurons (black arrow) in striatum. Fluoro-Jade staining (Fig. 2-2-2b) shows dying neurons (red arrow) in cerebral cortex. TUNEL (Fig. 2-2-2c) shows dying cells (arrow) in striatum. CD8a immunostaining (Fig. 2-2-2d) shows membrane localized immunoreactivity of T lymphocytes (arrow) in striatum. RCA-1 lectin staining (Fig. 2-2-2e) shows reactive microglial cells (arrow) in lesions. Bar = 5  $\mu$ m.

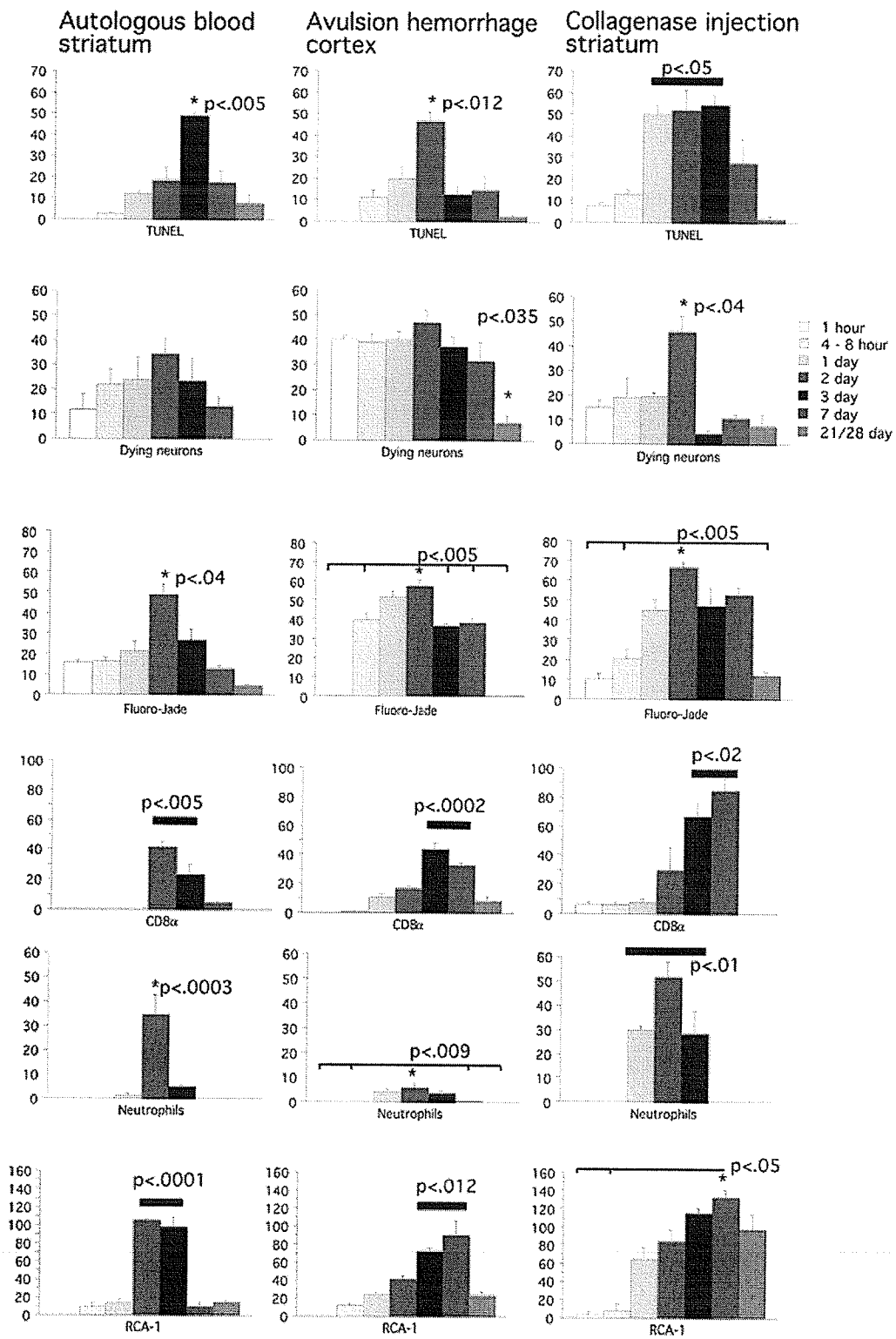


Figure 2-2-3. Quantitative comparison of TUNEL positive cells, dying neurons evident on H&E staining and Fluoro-Jade staining, CD8 $\alpha$  immunoreactive lymphocytes, neutrophils, and microglia/macrophages in the three different models of intracerebral hemorrhage in rat brain. \*: time points > all others. Bar: multiple points > others. Thick bar: all under bar > others

CHAPTER 2-3

Intracortical hemorrhage injury in rats: relationship between blood fractions and brain cell death.

Mengzhou Xue, MD

Marc R. Del Bigio, MD, PhD, FRCPC

Stroke. 2000;31(7):1721-1727.

## ABSTRACT

**Background and purpose:** Intracerebral hemorrhage is associated with stroke and head trauma. The purposes of this study were to investigate the effect of intracortical injections of autologous whole blood and blood components on inflammatory cell infiltration and brain cell death and to determine if non-hemorrhagic lesions differ in these respects.

**Methods:** Eighty-one adult rats were subjected to intracortical injections of autologous whole blood, or allogeneic plasma, erythrocytes, leukocytes, "activated" leukocytes, and serum. Injections of saline or mineral oil were controls. Blood injections were compared to cortical freeze injury and pial devascularization. Rats were perfusion fixed forty-eight hours after injection or lesioning. Eosinophilic neurons, TUNEL positive cells, brain damage area, infiltrating neutrophils and CD8a immunoreactive lymphocytes were quantified.

**Results:** Damage area, dying cells, and inflammatory infiltrate were significantly greater following autologous whole blood, leukocyte, and "activated" leukocyte injections than injection of other fractions.

**Conclusions:** These results suggest that extravasated whole blood causes a greater degree of cortical cell death and inflammation than ischemic lesions of similar size. Leukocytes "activated" by systemic illness might exacerbate the injury. Secondary hemorrhagic phenomena suggest that the harmful effect is directed toward both brain cells and the vasculature. Further studies are required to delineate the mechanism(s).

**KEYWORDS:** Hematoma, inflammation, neutrophil, TUNEL, lymphocyte

## INTRODUCTION

Intracortical hemorrhage can be a consequence of bleeding into an ischemic infarct, rupture of vascular malformation, amyloid angiopathy, or trauma<sup>1</sup>. Although hematomas in the cortex are amenable to surgical therapy<sup>283</sup>, they remain a significant management problem perhaps because the blood itself has adverse effects beyond its space occupying effect. Several animal models of intracerebral hemorrhage have been developed<sup>57, 63, 140, 265</sup> and experiments indicate that space-occupying effect, brain edema, ischemia, and neurotoxicity might all be involved in the brain damage that follows hemorrhage<sup>42, 93, 139, 284, 285</sup>. Ischemia may be induced by direct mechanical compression from the hematoma and / or vasoconstrictor substances in blood<sup>286</sup>. Neutrophilic inflammation is considerable in the vicinity of cerebral hematoma<sup>52</sup>. Neutrophils release a variety of cytokines, such as tumor necrosis factor alpha (TNF- $\alpha$ ), interleukin 6 (IL-6) and interferon gamma (IFN- $\gamma$ ), which might play an important role in ischemic and traumatic brain damage<sup>79, 127, 129</sup>. Work from one group suggested that thrombin and erythrocyte degradation products are responsible for edema production<sup>41, 42, 92, 93</sup>.

An understanding of evolution of brain injury after intracortical hemorrhage is important to determine the strategy of treatment. Therefore, the purpose of this study was to investigate the early effects of autologous whole blood, and compare its effect to that of separated blood components following intracortical injection. We hypothesized that cellular components of blood would cause greater cortical cell death and inflammation than soluble blood proteins. We have chosen a survival period of 48 hours because we have observed that inflammation and the frequency of dying cells both peak 48-72 hours after intracerebral injections of autologous blood<sup>39</sup> and after pial devascularization

(unpublished data). To test the secondary hypothesis that hemorrhagic brain injury causes more inflammation than non-hemorrhagic injury, we compared the damage caused by blood product injections to that caused by cortical freeze injury<sup>287-289</sup> and pial devascularization<sup>267, 290, 291</sup>.

## MATERIALS AND METHODS

### Animal preparation

All experimental procedures were done in accordance with guidelines of the Canadian Council on Animal Care. The local experimental ethics committee approved protocols. Eighty-seven young adult male Sprague-Dawley rats weighing between 175 to 250 grams were used. Ten groups of five to eight rats each (see Table 1) were used for injections of blood fractions, saline, or mineral oil. Because the blood components, which were derived from donor rats and prepared fresh, had limited stability *ex vivo*, randomization of the experiment was only partial with saline and mineral oil controls randomly included among batched recipient animals. Cortical freezing and pial devascularization experiments were done later, therefore these animals were not randomized among the blood fraction recipients.

### Intracortical hemorrhage model

For cortical injection each rat was anesthetized with pentobarbital (50 mg/kg IP) and placed in a stereotactic frame. Under aseptic conditions a midline scalp incision was made, a hole was drilled in the skull (3 mm lateral to midline, and 0.02 mm anterior to

coronal suture), a 100  $\mu$ l syringe was secured to the frame, and a 25-gauge needle was introduced into the deep cerebral cortex 2.5 mm below the surface of the skull. Pilot experiments wherein blood was injected to these coordinates showed that there was minimal extension into white matter or the subarachnoid compartment after short survival. Each rat received a 50  $\mu$ l injection of either normal saline, plasma, serum, erythrocytes, leukocytes, "activated" leukocytes, autologous whole blood, or mineral oil over 5 minutes. Mineral oil was chosen as additional inert control because it has greater viscosity than saline and was expected to better mimic the minimal space occupying effect of the infused blood. After infusion, the needle was left in place for 3 minutes and then removed slowly. The bone hole was sealed with bone wax, the scalp wound was sutured, and the animal was placed in a clean cage with free access to food and water. Invasive physiological monitoring was not used because it significantly increased the anesthesia time.

#### Whole blood and blood component separation

Autologous whole blood was obtained from anesthetized rats by placing the tail end in 40° C water for 30 seconds followed by cleansing with 70% alcohol and cutting the tail approximately 10 mm from tail tip. Freely dripping whole blood (50  $\mu$ l) was collected in a sterile syringe, which was then affixed to the stereotactic frame, and immediately injected into the cerebral cortex. To obtain allogeneic blood components, two donor rats were anesthetized with pentobarbital and 5 ml blood was removed from the heart. Fresh blood was put in CPD anti-coagulation-preservative<sup>292</sup>, gently mixed in a sterile plastic tube, and centrifuged at 2200 G for 20 minutes. Plasma appeared in the

upper layer, leukocytes and platelets formed a thin intermediate layer, and concentrated erythrocytes were in the lower layer<sup>292</sup>. To further concentrate the leukocytes, plasma was removed and the leukocytes were put in a 2 mm diameter sterile glass tube and centrifuged at 2200 G for 20 minutes. These were stored in a sterile vial for up to 2 hours prior to injection. To obtain autologous serum, rats were anesthetized and 0.5 ml whole blood was collected from tail in a sterile vial as described above. After 1 hour at room temperature, the blood coagulated. Serum was separated after clot retraction and stored up to 3 hours prior to injection.

To obtain allogeneic "activated" leukocytes, cardiac blood was obtained from two rats 24 hours after intracortical injection of autologous blood, which had been performed as described above. The rationale for this approach is that acute subarachnoid and intracerebral hemorrhages cause acute elevations in circulating leukocytes, especially neutrophils<sup>293-295</sup>.

#### Freeze and pial devascularization lesions

We observed that injections of autologous whole blood were frequently associated with lesions much larger than the area directly infused with blood. To test the secondary hypothesis that hemorrhagic brain injury causes more inflammation than non-hemorrhagic injury we attempted to create relatively non-hemorrhagic lesions of similar size in a similar dorsal cortical location. For induction of cortical freeze lesion rats were anesthetized with pentobarbital and placed in a stereotactic frame. The scalp was incised along the midline. A copper rod (end diameter 2 mm) cooled to -170°C in liquid nitrogen was applied to the skull surface for 4 minutes (3 mm lateral to midline, 0.02 mm anterior

to coronal suture). The scalp wound was sutured, and the animal was placed in a clean cage with free access to food and water. To study the early histological changes, rats were killed 4, 8, and 24 hours (n=2 each) after freezing in addition to the 48 hour survival period used for comparison to blood injections.

For pial devascularization, rats were anesthetized and placed in a stereotactic frame. The scalp was incised along the midline. A rectangle 3 mm wide and 5 mm long was delineated in the right hemiskull, the rostral margin 1 mm anterior to the bregma and the medial margin 1 mm lateral to the midline. The bone was removed carefully by enlarging a drill hole with rongeurs. Cortical blood vessels were interrupted by gently pulling the pia/arachnoid away with a needle (23 gauge) bent at the tip<sup>296</sup>. Hemostasis was achieved by gentle tamponade with cotton tipped applicators. The bone hole was covered with surrounding soft tissue, the scalp wound was sutured, and the animal was placed in a clean cage with free access to food and water. Rats were killed 4, 8, 24 (n=2 each), and 48 hours (n=4) after pial devascularization.

#### Histological examination

Forty eight hours after intracortical injection or lesioning, rats were anesthetized and perfused through the heart with 300 ml ice cold 4% paraformaldehyde in 0.1 mol/L phosphate-buffered saline (PBS). The brain was removed and stored in the same fixative for up to 10 days. Fixed brains were cut coronally approximately 2 mm on either side of the needle entry site, which was identifiable on the brain surface. Brain slices were dehydrated and embedded in paraffin. Sections (6  $\mu\text{m}$ ) were cut, and each 30<sup>th</sup> section from the rostral to the caudal portion of the residual hematoma cavity was stained with

hematoxylin and eosin (H&E) stain. At the level of the needle site with maximal brain damage area, a variety of histological and immunohistochemical stains were performed. Chloracetate esterase staining was used to assess neutrophils. Sections were dewaxed and hydrated, washed with distilled water, and incubated for 60 minutes in 4 % sodium nitrite, 4% new fuchsine, and 1 % esterase substrate solution (naphthol AS-D chloracetate dissolved in N-N dimethyl formamide) in phosphate buffer at pH 7.4. Slides were washed with distilled water, counterstained with Mayer's hematoxylin for 3 minutes, dehydrated, cleared and mounted. Neutrophilic granulocyte cytoplasm was stained bright red. Immunohistochemical localization of CD8a was performed <sup>258</sup>. Sections were dewaxed and hydrated, washed with distilled water, quenched with 0.3 % H<sub>2</sub>O<sub>2</sub>, blocked with 10 % normal serum, and incubated with anti-rat CD8a monoclonal antibody (clone G28 diluted 1/400; PharMingen International, Canada) at 4°C overnight. Slides were then washed with Triton PBS, incubated in biotinylated goat anti-mouse IgG (1/300) 1 hour at room temperature, washed, incubated with peroxidase-HRP (1/400) for 30 min at room temperature, colored with diaminobenzidine- H<sub>2</sub>O<sub>2</sub> solution, washed and coverslipped. Control sections were processed with omission of the primary antibody. TUNEL (terminal deoxynucleotidyl transferase (TdT)-mediated deoxyuridine triphosphate (dUTP)-biotin nick end labeling) was used to identify dying cells. Paraffin embedded sections were dewaxed and hydrated, then incubated in 20 µl/ml proteinase K for 15 minutes. TUNEL was accomplished using *Apoptag in situ* kit (Intergen; Purchase NY). After immersion in equilibration buffer for 10 minutes, sections were incubated with TdT and dUTP-digoxigenin in a humidified chamber at 37° C for 1 hour and then incubated in the stop/wash buffer at 37° C for 30 minutes. Sections were washed with PBS before

incubation in anti-digoxigenin-peroxidase solution (1/500 in PBS) for 30 minutes at room temperature, and colored with diaminobenzidine-  $H_2O_2$  solution. Sections were counterstained with methyl green. Negative control sections were treated similarly but incubated in the absence of TdT enzyme, dUTP-digoxigenin, or anti-digoxigenin antibody. TUNEL positive nuclei with chromatin condensation and fragmented nuclei were considered as probable apoptotic cells. TUNEL positive cells with diffuse light brown labeling of nucleus and cytoplasm were considered as probable necrotic cells<sup>188</sup>.

#### Determination of damaged brain area

The area of brain damage on the H&E stained coronal slice at the level of the needle injection site was defined by the presence of blood collections, tissue rarefaction due to edema, and dying cells around the injection sites. Computerized planimetry was used to measure the damage area on "camera lucida" drawings of the brain section.

#### Cell counts

Although the observer was technically blinded to the nature of the injection, because of some obvious differences (for example between whole blood and saline injections) blinding in an absolute sense was not possible. Using an ocular graticule and 250 x ocular magnification (objective magnification 20x), eosinophilic neurons, neutrophils, CD8a immunoreactive cells, and TUNEL positive dying cells were counted in four randomly selected fields (each area 250 x 250  $\mu m$ ) adjacent to but not including the needle insertion/injection site, which was defined by the presence of erythrocytes in all cases (see Figure 2-3-1). Areas with large blood vessels were avoided. In brains with

large areas of damage following autologous blood injection, similar counts were made at the edge of the lesion, distant from the injection site. Cortical freeze and pial devascularization lesions were assessed in four randomly selected areas at the periphery of the lesions.

#### Data analysis

All data are expressed as mean  $\pm$  standard deviation of mean. Data were analyzed using StatView 5 software (SAS Institute Inc.; Cary NC). ANOVA with Bonferroni-Dunn test was used for intergroup comparisons. Fisher's *r* to *z* test was used for correlations.

#### RESULTS

All rats tolerated the surgical procedures well and there was no surgical mortality. Residual hematoma in the cerebral cortex around the needle site was apparent at 48 hours. A small quantity of blood was in the adjacent white matter of 7 rats. Some rats in the whole blood and in both leukocyte injection groups exhibited additional blood in the subarachnoid space (4/8 whole blood, 2/8 leukocyte, and 3/6 "activated" leukocyte recipients). This extension was associated with areas of hemorrhagic and edematous brain damage far beyond (up to 2 mm) the site of injection. Because such extension was never seen following injection of saline, mineral oil, plasma, or serum, and because pilot experiments showed that 50  $\mu$ l of blood remained confined to the cortex in the immediate term, this suggests that a secondary hemorrhagic phenomenon, and not a simple surgical complication, had occurred.

Microscopically, whole blood injections appeared as single or multiple contiguous collections of blood cells in a column surrounding the needle tract. Leukocyte injections appeared as smaller collections of intact neutrophils and fragmented leukocytes with nuclear debris. Small collections of blood cells around the needle insertion site were seen in all other groups. In the vicinity of all lesions, neutrophils were seen adherent to blood vessel walls or passing out of capillaries and venules into the neuropil. Eosinophilic neurons, TUNEL positive cells with nuclear labeling presumed to indicate apoptosis, and TUNEL positive cells with cytoplasmic labeling presumed to indicate necrosis<sup>188</sup> were detected in cortical damage areas. Cells that exhibited membrane immunoreactivity for CD8a were small with minimal cytoplasm and round nuclei. Based upon the morphology of the cells and the known specificity of the antibody<sup>258</sup>, we believe these to be natural killer (NK) cells and / or activated cytotoxic T lymphocytes. Neutrophils were also noted in the subarachnoid compartment adjacent to the needle entry sites and at sites of subarachnoid hemorrhage.

Quantitative analysis showed that the total area of cortical damage was significantly larger following injection of 50 µl of whole blood or “activated” leukocytes than other blood fractions (Table 2-3-1), particularly when there was associated subarachnoid hemorrhage. At the microscopic level, eosinophilic neurons, TUNEL positive dying cells, neutrophils, and CD8a immunoreactive lymphocytes adjacent to the injection site were significantly more abundant following whole blood, leukocyte, and “activated” leukocyte injections than the other groups (Table 2-3-1). For the population as a whole, the quantities of dying cells and inflammatory cells were all intercorrelated ( $r = 0.556$  to  $0.795$ ,  $p < 0.0001$ ). The total damage area correlated poorly with TUNEL

positive cells and eosinophilic neurons per unit area in microscopic fields ( $r = .412$  and  $.544$  respectively,  $p < 0.001$ ) and not with the inflammation. Comparison of microscopic changes between the core and edge of hemorrhagic lesions that had enlarged beyond the site of whole blood injection showed that the quantity of dying cells and inflammatory cells was approximately half at the periphery.

To test the secondary hypothesis that hemorrhagic brain lesions are associated with more inflammation than non-hemorrhagic lesions we compared the lesions that had enlarged following whole blood injections to freeze lesions and pial devascularizing lesions in the dorsal cortex (Figure 2-3-2 and Table 2-3-2). Our goal was to create lesions of similar size in the same location, but we did not entirely succeed in this respect. Pial devascularization lesions exhibited a mixture of edematous and hemorrhagic brain at 8 hours as previously documented <sup>267</sup>. By 48 hours the core was necrotic and damage extended laterally to the margins of the craniectomy and deep to the white matter. Freeze lesions were pale on gross inspection and only microscopic petechiae were noted 8 hours after freezing. By 48 hours the majority of cells in the central region were necrotic with no basophilic staining of the nuclei. The surrounding viable brain was rarefied due to edema. The core of all large lesions exhibited advanced necrosis with only vague cell outlines apparent, absence of chromatin staining, minimal inflammation, and only very rare TUNEL positive cells. The margins of these lesions was edematous and exhibited both dying cells and inflammation. At the microscopic level lesions associated with blood injections exhibited more inflammation and cell death than the partially hemorrhagic devascularizing lesion and the relatively non-hemorrhagic freeze lesions (Table 2-3-2).

## DISCUSSION

Intracerebral hemorrhage causes brain damage through multiple mechanisms. Direct tissue destruction by the hemorrhagic event with dissection of blood along tissue planes occurs immediately. This is followed by development of edema and possibly ischemic damage due to raised intracranial pressure and distortion or vasospasm in the microvasculature. Delayed damage could result through a variety of mechanisms including local ischemia, release of toxins by blood breakdown products, thrombin release, or leukocyte infiltration<sup>42, 52, 259, 297</sup>. This study demonstrates that injection of a small quantity of whole blood into the cerebral cortex of rats is associated with cell death and inflammatory cell infiltration at 48 hours. In a prior experiment we have shown that this time represents the peak for both processes<sup>39</sup>. The tissue distortion was minimal and therefore mechanisms other than ischemia due to distortion are presumed to play a role. Plasma or serum alone and concentrated erythrocytes had negligible effect. Concentrated leukocytes had a mild adverse effect, whereas "activated" leukocytes had a strong adverse effect. Two issues need to be discussed. First, what is the nature of the early response to the released blood products? Second, what is the reason that some blood components are more harmful than others? One could argue that the experiment should have been conducted by injecting 50  $\mu$ l whole blood, ~20  $\mu$ l erythrocytes, ~25  $\mu$ l plasma, and ~2  $\mu$ l leukocytes to account for the true relative volumes of these blood fractions. We were, however, concerned that this would be confounded by different volumes of dispersion. Had this been done, the effect of erythrocytes and plasma, which were not significantly different than saline control, would have been even less. The effect of the leukocytes might be exaggerated in the experimental protocol that was used.

Following injection of the blood we observed cell death, inflammatory cell infiltration, and in some cases distant hemorrhagic / ischemic damage. In the immediate vicinity of the injection site, neuronal death was characterized by DNA damage and cytoplasmic hypereosinophilia. Although it is likely that the two features represent cells at different stages of death or those dying by different mechanisms (i.e. apoptosis or necrosis), our data do not add anything to explain the mechanism of delayed neuronal cell death, a subject of heated debate <sup>298-300</sup>. Reactive neuronal expression of heat shock protein (HSP72) and / or loss of MAP2 immunoreactivity indicative of proteolysis and impending death has been documented within 5 hours after intracerebral hemorrhage in humans. Increased astroglial expression of glial fibrillary acidic protein (GFAP) and metallothionin occurs within 18 - 48 hours <sup>116</sup>.

Inflammation is an obvious response to the injections. Although one might argue that the neutrophils had been injected and had not entered by diaporesis, we attempted to count cells only beyond the margin of the primary injection site. Substantial margination of leukocytes along blood vessel lumens supports the idea that they subsequently enter the brain tissue. Chemotaxis of these neutrophils and lymphocytes, and later of monocytes, is mediated by  $\alpha$ - and  $\beta$ -chemokines and complement <sup>301, 302</sup>. In rat brain injury experiments, intense neutrophilic infiltrate has been previously documented around collagenase-induced hematomas <sup>52, 63</sup>, contusions <sup>303, 304</sup>, and ischemic sites <sup>305</sup> beginning at 6 - 12 hours and peaking at 48 - 72 hours. In human brains, neutrophil infiltration is apparent 5 - 72 hours after hemorrhage or contusion <sup>1, 113-116</sup>. The present experimental comparison of hemorrhagic and non-hemorrhagic lesions suggests that something in, or a process initiated by, extravasated blood promotes chemotaxis. Neutrophils can release

potentially harmful factors such as oxygen radicals <sup>261</sup> or cytokines including tumor necrosis factor alpha (TNF- $\alpha$ ), interleukin 6 (IL-6) and interferon gamma (IFN- $\gamma$ ), which seem to play a role in brain damage <sup>79, 129</sup>. Neutrophils can also exacerbate brain injury by obstructing microvessels, which then causes local ischemia <sup>306</sup>. Many experimental studies have documented infiltration of natural killer (NK) cells into injured brain <sup>301, 307, 308</sup>. One study of brain contusions in rats showed that NK and T cell infiltration was more prevalent than neutrophilic infiltrate <sup>144</sup>. We also observed a significant number of CD8a immunoreactive cells, which could be either NK cells and / or activated cytotoxic T lymphocytes <sup>258</sup>, that could be directly injurious or indirectly so through release of IFN- $\gamma$ .

We observed that the injection of whole blood or the leukocyte fraction caused injury while injection of erythrocytes, plasma, and serum had minimal effects. However, it is conceivable that specific blood / plasma fractions exert damage at different times. Other investigators showed that cerebral edema develops only 3 days after erythrocyte injection and they suggested that hemoglobin released from lysed erythrocytes is toxic to brain <sup>42</sup>. Toxic effect of hemoglobin on neurons has been demonstrated in vitro <sup>94</sup>. In this study neither plasma nor serum caused more damage than saline injection. Thrombin, which is a component of plasma, has been shown to cause brain edema and seizures following intracerebral injection <sup>3, 93, 297</sup>. There are several possible explanations for the discrepancy. The thrombin effect might be mediated only by very large doses and is therefore relatively less important in vivo. Thrombin might for some reason be inactivated during processing of the plasma. Finally the "pharmacodynamics" might be altered because a blood clot allows slow focal release whereas plasma injection would diffuse rapidly leading to lower regional concentrations.

The leukocyte fraction, and in particular "activated" leukocytes, caused greater injury than other blood fractions. When one interprets the intensity of the leukocyte-mediated response, one must keep in mind that leukocytes occupy less than 1% of the volume of whole blood. Therefore the leukocyte injection groups received a dose equivalent to 5 ml of whole blood<sup>309</sup>. Regardless, "activated" cells appear to be more harmful, perhaps through production of more of the deleterious mediators mentioned above. This might help to explain the observation that fever during the first 3 days after intracerebral hemorrhage is an independent predictor of poor prognosis in patients<sup>310</sup>. To further study the role of leukocytes in this model one could inject microwave-killed cells whose proteins are inactivated, lysed cells, and supernatant from cultured cells in resting or active states. This would help to determine whether the noxious agents are actively or passively released. It is also important to recognize that activated platelets, which we did not study directly, are included in the leukocyte fraction. Platelets can release serotonin and platelet-derived growth factor, which are capable of increasing vascular permeability and causing vasoconstriction<sup>311</sup>.

Finally, we must try to explain why injection of some blood fractions was associated with enlargement of the lesions well beyond the limits of the injected substance. Several results suggest that mechanisms other than mass effect are involved in the contribution of blood to perihematoma edema formation, because blood produces larger lesions than would be expected from its space occupying effects alone<sup>256</sup>. This might be explained by a secondary effect of the injected substances on the vasculature through agents that promote vasospasm and / or increased vascular permeability<sup>312</sup>. Whole blood has greater adverse effects on cerebral blood flow than hemoglobin or

albumin when injected into the subarachnoid compartment, presumably because of vasoconstrictive agents<sup>313</sup>. It is because of these larger lesions that we also used control injuries of freeze lesion, which creates ischemia and coagulative necrosis<sup>287</sup>, and pial devascularization, which has been promoted as a model of ischemia<sup>290</sup>. Our goal was to create large non-hemorrhagic lesions that could be compared to the lesions caused by blood injections. The freeze lesion was reasonably successful in this regard, having caused only minimal hemorrhage but considerable release of plasma<sup>314</sup>. At the margin it was associated with considerably fewer dying cells and neutrophils than the whole blood injection. The devascularization injury was associated with deep hemorrhage that was likely a consequence of deep vein avulsion. This mixed hemorrhagic / ischemic lesion was associated with more dying and inflammatory cells than the freeze lesion but fewer than the whole blood injection.

In conclusion, extravascular whole blood, and perhaps the leukocyte fraction in particular, appears to play an important role in cortical damage. The magnitude of delayed cell death and inflammation is greater than that following non-hemorrhagic injury. Although coexistent, we cannot state that inflammation is necessarily a cause of neural cell injury. The precise molecular and chemical mechanisms remain to be determined, but are likely multiple and include secondary ischemia, inflammatory cell products, and iron-mediated effects.

Table 2-3-1. Cortical injury and inflammation following injection of whole blood or blood fractions.

Lesion	Total damage area (mm <sup>2</sup> )	Eosinophilic neurons / 0.25 mm <sup>2</sup>	TUNEL positive cells / 0.25 mm <sup>2</sup>	Neutrophils / 0.25 mm <sup>2</sup>	CD8a positive cells / 0.25 mm <sup>2</sup>
Saline (n=7)	0.1 ± 0.1	5.1 ± 3.0	1.3 ± 1.1	3.4 ± 1.6	2.4 ± 3.8
Whole blood (n=8)	2.8 ± 2.5 *	69.5 ± 40.2 *	25.3 ± 23.3 *	50.6 ± 45.9 *	36.5 ± 10.3 *
Erythrocytes (n=8)	0.3 ± 0.1	6.5 ± 6.7	4.4 ± 3.3	5.0 ± 1.9	12.6 ± 8.1
Leukocytes (n=8)	0.3 ± 0.2	41.1 ± 20.0 *	74.8 ± 40.9 *	50.5 ± 12.3 *	20.0 ± 15.1 *
“Activated” leukocytes (n=6)	5.9 ± 2.9 *	37.5 ± 4.7 *	55.4 ± 1.8 *	26.8 ± 5.1 *	18.5 ± 7.6 *
Plasma (n=8)	0.2 ± 0.1	4.9 ± 3.0	5.6 ± 2.3	3.3 ± 1.6	4.5 ± 2.6
Serum (n=6)	0.2 ± 0.2	8.8 ± 4.2	4.5 ± 5.3	3.8 ± 2.8	7.3 ± 8.4
Mineral oil (n=5)	0.2 ± 0.1	6.6 ± 4.3	3.2 ± 3.1	3.6 ± 3.4	3.2 ± 2.3

All data are expressed as mean ± SD. Cell counts are expressed as the number of cells per four 250x250 µm areas (i.e. 0.25 mm<sup>2</sup>).

\*: p<0.004 versus saline, plasma, serum, erythrocyte, and mineral oil groups (ANOVA with Bonferroni-Dunn intergroup comparisons)

Table 2-3-2. Cortical injury and inflammation in large lesions following injection of whole blood compared to freeze lesion and pial devascularization.

Lesion	Total damage area (mm <sup>2</sup> )	Eosinophilic neurons / 0.25 mm <sup>2</sup>	TUNEL positive cells / 0.25 mm <sup>2</sup>	Neutrophils / 0.25 mm <sup>2</sup>	CD8a positive cells / 0.25 mm <sup>2</sup>
Whole blood (n=4)	5.0 ± 1.0	106.3 ± 18.7	81.8 ± 44.8	71.0 ± 11.3	38.0 ± 5.3
Devascularizing lesion (n=4)	6.4 ± 0.8	44.5 ± 7.1 #	45.0 ± 7.8	6.0 ± 3.4 **	11.3 ± 2.9 **
Freeze lesion (n=7)	1.6 ± 0.3 *	13.7 ± 5.0 #	22.0 ± 11.4 @	4.3 ± 4.0 **	21.9 ± 4.8 **

All data are expressed as mean ± SD. Cell counts are expressed as the number of cells per four 250x250 μm areas (i.e. 0.25 mm<sup>2</sup>).

\* p<0.0001 significantly less than whole blood and devascularizing lesions

# p<0.002 all are significantly different from each other

@ p=0.003 significantly less than whole blood

\*\* p<0.0001 significantly less than whole blood

(ANOVA with Bonferroni-Dunn intergroup comparisons; note that the same conclusions are reached when the lesions are compared to the entire whole blood injection group)

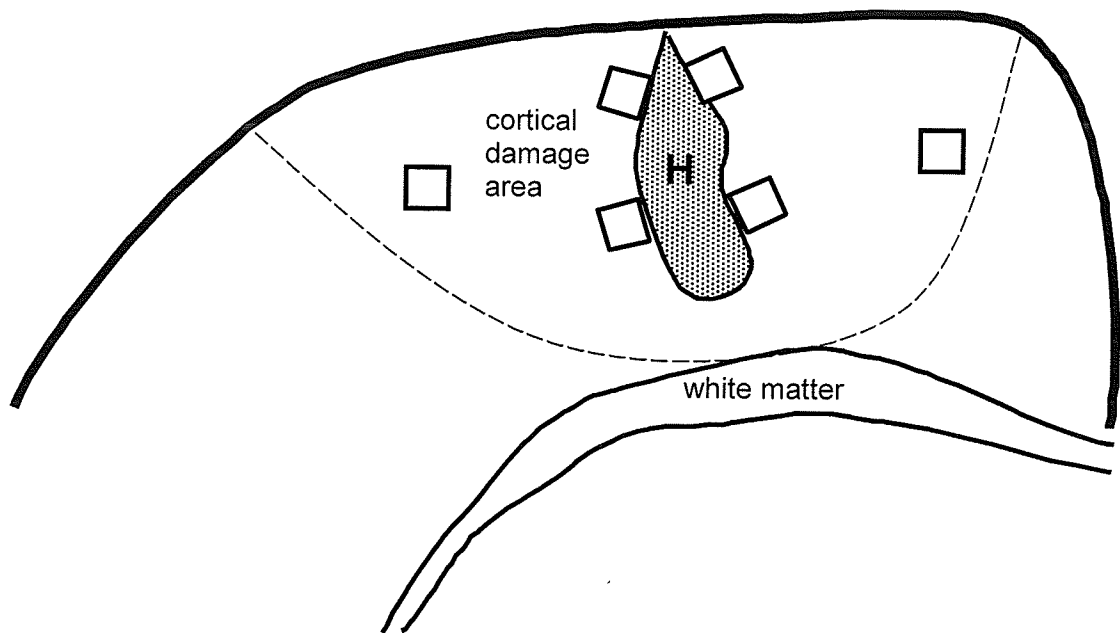


Figure 2-3-1. Diagram of coronal section of rat cerebrum to illustrate areas used for cell counts (□) relative to injected blood (H indicates hematoma) and margins of large lesions (dotted line).

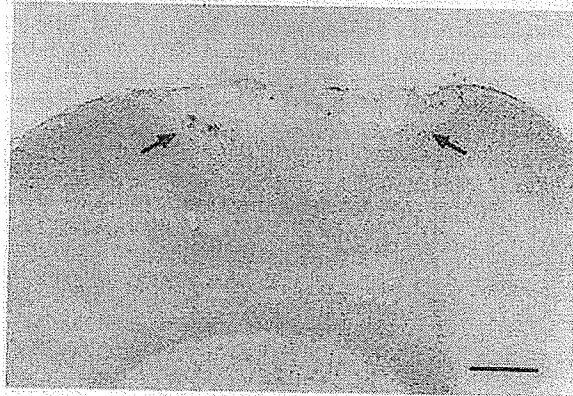
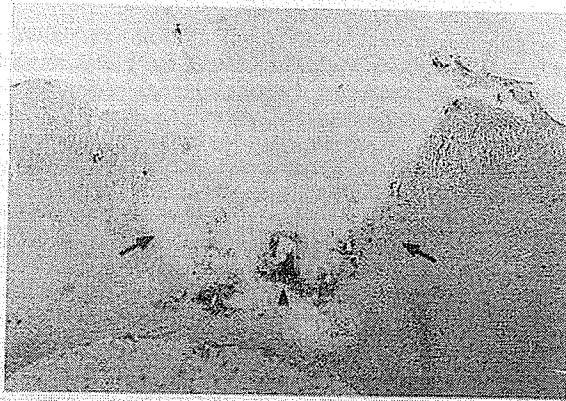
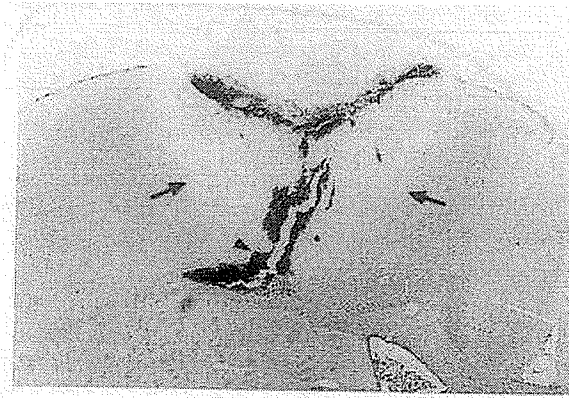


Figure 2-3-2. Photomicrographs showing cortical lesions in rat cerebrum 48 hours after injection of 50  $\mu$ l blood into the cortex (top), pial devascularization (middle), and freeze injury (bottom). Collections of erythrocytes are seen as dark areas. Following blood injection the edematous area of cortical injury (pale region defined by arrows) extends well beyond blood collections along the needle tract (arrowhead). There is some blood in the white matter and subarachnoid compartment. Following pial devascularization the cortical tissue is partially necrotic and has fallen away during processing. The edematous tissue along the edge is evident (arrows) and there is some blood in the depth (arrowhead), presumably due to bleeding from disrupted veins. The freeze lesion, defined by necrotic and edematous tissue (arrows), is less hemorrhagic and more superficial than the other lesions. Bar = 1 mm.

Chapter 2-4

Acute tissue damage after injections of thrombin and plasmin into rat striatum.

Mengzhou Xue, MD

Marc R. Del Bigio, MD, PhD, FRCPC

Stroke. 2001;32(9):2164-2169.

## ABSTRACT

**Background and purpose:** Extravasation of blood is associated with intracerebral hemorrhage and head trauma. The mechanism of brain cell injury associated with hemorrhage differs from that due to pure ischemia. The purpose of this study was to investigate the acute changes following intracerebral injections of proteins that are involved in blood clotting and clot lysis.

**Methods:** Sixty-eight adult rats were subjected to stereotactic intrastriatal injections of normal saline (5  $\mu$ l), low (2.5 U/5  $\mu$ l) and high dose (25 U/5  $\mu$ l) thrombin, low (0.1  $\mu$ g/5  $\mu$ l) and high dose (1  $\mu$ g/5  $\mu$ l) tissue plasminogen activator, low (0.05 U/5  $\mu$ l) and high dose (0.5 U/5  $\mu$ l) plasminogen, low (0.335 U/5  $\mu$ l) and high dose (3.35 U/5  $\mu$ l) plasmin. Forty-eight hours later rats were perfusion fixed. Brain damage area, eosinophilic neurons, TUNEL positive cells, infiltrating neutrophils, CD8a immunoreactive leukocytes, and reactive microglia were quantified.

**Results:** Damage area in striatum, dying cells, inflammatory cells, and microglial reaction were significantly greater following the high dose plasminogen, plasmin and thrombin injections. tPA injections were associated with mild inflammation.

**Conclusions:** These results suggested that thrombin and plasmin are harmful to brain cells in vivo. Although the doses required to cause damage are relatively great in consideration of the plasma content of these proteins, their pathological effect might be enhanced through synergism with other mechanisms.

**KEYWORDS:** blood coagulation, cerebral hemorrhage, leukocytes, microglia, proteolysis

## INTRODUCTION

Intracerebral hemorrhage can be a consequence of hypertension, bleeding into an ischemic infarct, rupture of abnormal blood vessels, or trauma. Hematomas remain a significant management problem because the blood itself seems to have adverse effects beyond its space occupying effect <sup>259</sup>. Some of the adverse effects of blood have been attributed to proteolytic enzymes involved in blood clot formation and lysis. Thrombin, which activates the formation of fibrin, causes morphological changes of cultured astrocytes <sup>205</sup>, neurite retraction in cultured neurons <sup>206</sup>, and causes edema when injected into brain <sup>315</sup>. Plasminogen is converted into plasmin by tissue plasminogen activator (tPA), which is produced by brain endothelia <sup>316</sup>. Plasmin serves to lyse blood clots through the digestion of fibrin. Plasmin also causes considerable edema when injected into brain <sup>209</sup>. tPA can potentiate brain damage caused by thrombin and that which follows middle cerebral artery occlusion in rats <sup>317, 318</sup>. However, injection of tPA to aid evacuation of intracerebral hematoma is not associated with adverse affects <sup>319</sup>. The consequences of thrombin, plasminogen, and tPA injections into brain are not well documented, in particular to what extent they resemble those caused by intracerebral hemorrhage. Nishino and coworkers infused thrombin or plasmin into rat striatum for 7 days and studied the histopathological changes after that time. Plasmin caused hemorrhage, and therefore they did not study the animals histologically. At sites of thrombin infusions neutrophils, macrophages, reactive astrocytes, and new blood vessels were observed <sup>84, 320</sup>. The purpose of this study was to investigate the acute inflammation and cell death that follow intracerebral injections of thrombin, tPA, plasmin, and plasminogen. Our previous experiments showed that cell death and inflammatory cell

infiltration peak 2-3 days after injection of autologous whole blood in to the rat brain, therefore we chose a survival period of 2 days<sup>39,40</sup>.

## MATERIALS AND METHODS

### Animal preparation

All experimental procedures were done in accordance with guidelines of the Canadian Council on Animal Care. Protocols were approved by the local experimental ethics committee. Sixty-eight young adult male Sprague-Dawley rats weighing 175 to 250 grams were used. Rats were anesthetized with pentobarbital (50 mg/kg IP) and placed in a stereotactic frame. The animals were draped but core temperature was not monitored or regulated during the 15-minute procedure. Following midline scalp incision, a hole was drilled through the skull, and a 27 gauge needle attached to a 10  $\mu$ l Hamilton microsyringe was inserted into the striatum (3 mm lateral to midline, 0.02 mm anterior to coronal suture, depth 5.5 mm below the surface of the skull). To allow clotting of any induced bleeding the needle was left in place for 5 minutes before beginning the infusion (5  $\mu$ l over 5 minutes). After infusion, the needle was left in the place for 3 more minutes then removed slowly. The bone hole was sealed with bone wax, the scalp wound was sutured, and the animal was placed in a warm cage with free access to food and water. Nine groups of six to eight rats each were used. Infusion solutions were prepared and passed through a 0.22  $\mu$ m filter. Rats received injection of saline, low dose (2.5 U/5  $\mu$ l) and high dose (25 U/5  $\mu$ l) thrombin (from bovine plasma; T-6634, Sigma Chemical Company, St. Louis MO), low dose (0.1  $\mu$ g/5  $\mu$ l) and high dose (1  $\mu$ g/5  $\mu$ l) tPA (from

human melanoma cell line; T-7776, Sigma), low dose (0.05 U/5  $\mu$ l) and high dose (0.5 U/5  $\mu$ l) plasminogen (from bovine plasma; P-9156, Sigma), or low dose (0.335 U/5  $\mu$ l) and high dose (3.35 U/5  $\mu$ l) plasmin (from porcine plasma; P-8644, Sigma) (see Table 2-4-1). Our original intent had been to inject equivalent unit activity doses of plasmin and plasminogen, but for technical reasons and financial constraints this did not occur. The proteins were not tested for the presence of endotoxin because of the known capacity for serine proteinases to yield false positive results (see E-TOXATE<sup>®</sup> technical bulletin No. 210; Sigma).

#### Histological examination

Forty-eight hours after injections rats were reanesthetized and perfused through the heart with 300 ml ice cold 4 % paraformaldehyde in 0.1 mol/L phosphate buffered saline (PBS). The brain was removed and stored in the same fixative for 1 - 7 days. Fixed brains were cut coronally approximately 2 mm on either side of the needle entry site, which was identifiable on the brain surface. Brain slices were dehydrated and embedded in paraffin. Sections (6  $\mu$ m) were cut, and each 30<sup>th</sup> section from the rostral to the caudal portion of the damage area was stained with hematoxylin and eosin (H&E). At the coronal level of the needle entry site, where the brain damage was maximal, a variety of histological and immunohistochemical stains were performed.

To demonstrate mononuclear leukocyte infiltrate, sections were dewaxed and rehydrated, washed with distilled water, quenched with 0.3 % H<sub>2</sub>O<sub>2</sub>, blocked with 10 % normal goat serum, and incubated with anti-CD8a monoclonal antibody (diluted 1/400, PharMingen International, Canada) at 4°C overnight. This detects cytotoxic T cells and

natural killer (NK) cells <sup>258</sup>. Slides were then washed with Triton PBS, incubated in biotinylated goat anti-mouse IgG (1/300) for 1 hour at room temperature, washed, incubated with streptavidin-peroxidase (1/400) for 30 minutes at room temperature, colored with diaminobenzidine - H<sub>2</sub>O<sub>2</sub> solution, washed and coverslipped. Control sections were processed with omission of the primary antibody. Histochemistry with Ricinus communis agglutinin lectin (RCA-1) labeling was used to demonstrate reactive microglial cells <sup>269</sup>. Sections were dewaxed and rehydrated, washed with distilled water, quenched with 0.3% H<sub>2</sub>O<sub>2</sub>, blocked with 10 % normal sheep serum, and incubated with biotinylated lectin (diluted 1/2000, Vector Laboratories, Inc., Burlingame, U.S.A.) at room temperature for 1 hour. Slides were then washed with Triton PBS, incubated with streptavidin-peroxidase (1/400) for 1 hour at room temperature, colored with diaminobenzidine - H<sub>2</sub>O<sub>2</sub> solution, washed and coverslipped. Control sections were processed with omission of the biotinylated lectin. TUNEL (terminal deoxynucleotidyl transferase (TdT)-mediated deoxyuridine triphosphate (dUTP)-biotin nick end labeling) was used to identify cells with damaged DNA, most of which are dying cells. Paraffin embedded sections were dewaxed and rehydrated, then incubated in 20 µl/ml proteinase K for 15 minutes. TUNEL was accomplished using *Apoptag in situ* kit (Intergen; Purchase, NY, USA). After immersion in equilibration buffer for 10 minutes, sections were incubated with TdT and dUTP-digoxigenin in a humidified chamber at 37°C for 1 hour and then incubated in the stop/wash buffer at 37°C for 30 minutes. Sections were washed with PBS before incubation in anti-digoxigenin-peroxidase solution (1/500 in PBS) for 30 minutes at room temperature, and colored with diaminobenzidine - H<sub>2</sub>O<sub>2</sub> solution. Sections were counterstained with methyl green. Negative control sections were

treated similarly but incubated in the absence of TdT enzyme or dUTP-digoxigenin. TUNEL-positive nuclei with chromatin condensation and fragmented nuclei were considered as probable apoptotic cells. TUNEL positive cells with diffuse light brown labeling of nucleus and cytoplasm were considered as probable necrotic cells <sup>188</sup>. Together they were considered to be dying cells.

#### Cell counts and determination of damage area

A “camera lucida” drawing was used to assess the overall brain morphology on the coronal slice with maximal striatum damage, which was defined by the presence of blood, tissue rarefaction, or necrosis at the injection sites. Computerized planimetry was used to measure the traced areas. Using an ocular graticule and 250 x ocular magnification (objective magnification x 20), eosinophilic dying neurons, TUNEL positive dying cells, neutrophils, CD8a immunoreactive cells, and RCA-1 binding cells were counted in 4 fields (each area 250 x 250  $\mu\text{m}$ ) immediately adjacent to the needle injection/damage site which was defined by the presence of erythrocytes or necrosis (Figure 2-4-1). Areas with large blood vessels were avoided. In brains with large areas of necrosis, counts were made near the edge of the lesion because the necrotic cores were devoid of viable cells. All data are expressed as mean  $\pm$  SEM. Data were analyzed to ensure normal distribution and then intergroup comparisons were made by ANOVA followed by Fisher’s protected least significant difference (PLSD) post hoc test using StatView 5.01 software (SAS Institute; Cary NC). The differences were considered significantly different when  $p < 0.05$ . Additional power calculations were made manually using published tables <sup>321</sup>.

## RESULTS

All rats tolerated the surgical procedure well and there was no surgical mortality. Microscopically, brains with saline injection, all low dose injections, and tPA high dose injections exhibited small collections of blood and negligible edema extending up to 50 $\mu$ m on either side of the needle tract (Figure 2-4-2). High dose injections of thrombin, plasmin, and plasminogen resulted in columns of necrosis characterized by lysis of all cell types and absence of nuclear staining extending up to 2 mm on either side of the needle tract (Figure 2-4-2). In a minority of these the necrotic core was hemorrhagic up to 200  $\mu$ m from the needle tract. Scattered karyorrhectic nuclei, eosinophilic or pyknotic neurons and TUNEL positive cells were identifiable up to 2 mm from the edge of necrotic lesion. Neutrophils were adherent to vessel walls or passing through the capillaries and venules. Neutrophils and CD8a immunoreactive leukocytes were rarely present within the necrotic tissue except at the periphery. They were found in the surrounding intact edematous striatum as well as occasionally in nearby white matter (Figure 2-4-3). Reactive microglia with ramified processes and swollen bodies were present in the parenchyma and around blood vessels.

Quantitative data are shown in Figure 2-4-4. Damage area in striatum, dying cells and inflammation in adjacent non-necrotic tissue were significantly greater following high dose thrombin, plasminogen, and plasmin injections compared to other groups. These destructive and reactive changes were roughly proportionate to the total area of injury although despite the absence of significant necrosis following the low dose

thrombin injection, there were more dying neurons and neutrophils in the penumbra. Neutrophil infiltration and microglial reaction were mildly but significantly elevated following injection of all substances.

## DISCUSSION

Intracerebral hemorrhage causes brain damage through multiple mechanisms <sup>259</sup>. Direct tissue destruction by the hemorrhagic event and dissection of blood along tissue planes occurs immediately. This is followed by development of edema and secondary ischemic damage due to raised intracranial pressure and distortion of the microvasculature. The enzymes involved in blood clotting and clot lysis are potentially toxic in the first day following hemorrhage <sup>92</sup>. Delayed damage also occurs through release of toxins by blood breakdown products <sup>42</sup>. This study demonstrated that injection of thrombin, plasminogen, and plasmin into the striatum of rats is associated with dose dependent tissue necrosis, cell death, and inflammation at 48 hours. The focal necrosis associated with enzyme injections was rapid and most likely due to a direct effect of these agents on the neuropil or the vasculature. Inflammation, including influx of neutrophils and lymphocytes as well as reaction by microglia, was generally proportionate to the total area of damage and not to the quantity of foreign protein injected. It was also similar in magnitude to that seen following infusions of autologous whole blood <sup>39, 40</sup>. Therefore, with the exception of tPA-associated changes the inflammation is likely stimulated by the damage and not directly by the infusate (or by small quantities of contaminants in the infusate such as endotoxin <sup>322</sup>). The inflammation

may contribute to secondary injury in the penumbra region surrounding the hematoma <sup>39</sup>,  
52, 130, 155

In blood, thrombin is produced by proteolytic cleavage of the plasma protein prothrombin. Thrombin converts fibrinogen into fibrin, which is ultimately involved in formation of a blood clot. Brain and spinal cord tissues including neurons and endothelia have a large number of thrombin receptors (also known as protease-activated receptor, PAR-1) as well as the related PAR-2 <sup>221, 226, 323, 324</sup>. These can be activated by low concentrations of trypsin, thrombin, and plasmin <sup>227</sup>. The brain itself appears to be capable of producing small quantities of prothrombin <sup>200, 325</sup>. Through these receptors, whose precise role in normal signaling is unclear, thrombin causes retraction of cell processes of cultured neurons <sup>206</sup> and is toxic to neurons in brain slices in a dose-dependent manner <sup>326</sup>. When injected into the brain, thrombin can cause brain edema <sup>297, 315</sup>. The edema-inducing effect of thrombin can be inhibited by several thrombin inhibitors <sup>93, 297, 315, 327</sup>, thrombin preconditioning <sup>208</sup>, or heparin <sup>41</sup>. Plasminogen is a plasma protein that is converted into plasmin by tissue plasminogen activators. They are produced by brain endothelia as well as by some neurons <sup>316</sup>. Plasmin can digest fibrin to allow lysis of blood clots. When injected into brain, plasmin also causes considerable edema <sup>317</sup>, potentially through an effect on the blood brain barrier <sup>207</sup>.

Brain necrosis and cell death caused by injection of high dose thrombin and plasmin are likely due to direct proteolytic activity. We suggest this because the tissue necrosis was rapid and involved all cell elements, even those without known thrombin receptors. Thrombin, plasmin, and tPA are all trypsin-like serine proteinases of the tissue kallikrein family. Their active sites have similar substrate specificity although their

affinity varies, being modified by additional binding sites<sup>328-331</sup>. At lower doses thrombin also causes apoptosis of neurons and astrocytes in culture, apparently through surface receptors that are activated by proteolytic cleavage at a specific site<sup>332, 333</sup>. Because the receptors are proteolytic substrates, experiments with antagonists would not help determine whether thrombin and plasmin are acting in a selective or indiscriminant manner. More detailed investigation of the dose-response relationship would. Although it is conceivable that thrombin or plasmin can induce endothelin synthesis and subsequent vasospasm and ischemia<sup>334-336</sup>, vasoconstriction following thrombin injection has been previously excluded<sup>297</sup>. Thrombin, tPA, and plasminogen are normally present in brain at low concentrations, especially during development and during reactive changes. In addition to action through the PAR receptors, plasmin is known to degrade a range of extracellular matrix proteins and to activate matrix metalloproteinases, which can also digest matrix proteins<sup>328, 337</sup>. In high doses their proteolytic activity likely exceeds that which can be controlled by endogenous regulatory proteins (e.g.  $\alpha$ 2 macroglobulin, protease nexin-1, plasminogen activator inhibitors, etc) and proteolysis continues unchecked<sup>230, 338-340</sup>. Plasminogen activator inhibitor-1 (PAI-1), the major regulator of plasminogen activation, exists in brain only in very small quantities<sup>341</sup>, although it can be upregulated following experimental stroke<sup>342</sup>. PAI-1 deficient mice exhibit larger infarcts following middle cerebral artery occlusion<sup>343</sup>. It has also been shown that mice deficient in tPA, in which plasmin is not activated, are less susceptible to neuronal injury following brain ischemia<sup>318</sup> or excitotoxin injection<sup>344</sup>.

The plasma proteins we injected, with the exception of tPA, caused dose-dependent brain injury. We must point out several caveats to the experiment. First,

expressed in terms of the whole blood volume that would contain that quantity (see Table 1), it seems obvious that the toxic doses could only be delivered in unrealistically large blood volumes relative to the brain size. Furthermore, plasma infusions alone are not overtly toxic<sup>40, 345</sup>. However, one cannot exclude the possibility that a large hematoma in a large brain would allow diffusion of toxic quantities into the surrounding tissue, at least at the microscopic level. Second, there were considerable differences in the apparent potency of the different proteins. Although, the high dose plasminogen and the low dose plasmin were roughly equivalent in terms of nominal enzyme activity, the effect of plasminogen was much greater. We speculate that some plasmin activity is lost when it is purified in the post-activated form. In contrast, the plasminogen is activated in situ. Third, the relative potency of thrombin delivered in a hematoma would appear to be greater than that of plasminogen (compare high dose thrombin to low dose plasminogen, which are contained in roughly the same amount of blood). However, we must consider for several reasons that this type of comparison is naive. The true quantity of thrombin delivered is not accurately known because it can adsorb to glass and plastic. Furthermore, the actual activity of thrombin at a particular site can be very difficult to predict because it is self-amplifying and because it is rapidly inactivated by binding to fibrin<sup>329, 331</sup>. Fourth, tPA injections appeared to cause mild inflammation, perhaps a non-specific effect of foreign protein, but minimal cell death. This was previously observed by Figueroa and coworkers<sup>317</sup> and may be because tPA injected alone lacks sufficient substrate to be toxic. In neither experiment, however, was the tPA tested independently to prove activity prior to injection. It is clear that tPA potentiates various forms of brain injury<sup>317</sup>. Fifth, with only two doses, we cannot know that the maximal adverse effect would not be

achievable at a much lower dose. Therefore we have not determined the dose-response relationship necessary to speculate accurately on the mechanism of injury. Finally, we cannot exclude the possibility that mild hypothermia was protective in the low dose situation, magnifying the apparent difference between low and high doses.

In summary, the results demonstrate that injections of thrombin, plasminogen, or plasmin into rat striatum are associated with necrosis, cell death, and inflammation in a dose dependent manner. Because of the rapid evolution, the most likely mechanism of action is uncontrolled proteolytic digestion of neurons, glia, and vascular cells. Peripheral to the necrotic core, cell death might be mediated by indiscriminate proteolysis, selective cleavage of protease activated receptors<sup>226</sup>, or by inflammation, which might be induced by general mediators of tissue injury or perhaps directly by thrombin<sup>346</sup>. Although the toxic doses are seemingly high when injected individually, we cannot exclude the likelihood that applied together, as in the case of intracerebral hemorrhage, they can act synergistically along with other plasma proteins not studied here. The plasma enzymes thrombin and plasmin might play an important role in the brain injury that follows intracerebral hemorrhage, and therefore represent potential targets for therapeutic intervention.

Table 2-4-1. Striatum damage area, cell injury and inflammatory cell infiltration following injection of enzymes involved in blood clotting and clot lysis.

Injection (in 5 $\mu$ l)	Number of rats	Blood volume equivalent ( $\mu$ l) <sup>a</sup>
Saline	8	--
tPA low (0.1 $\mu$ g)	6	35
tPA high (1.0 $\mu$ g)	6	350
Plasminogen low (0.05U)	8	110
Plasminogen high (0.5U)	8	1100
Plasmin low (0.335U)	8	750
Plasmin high (3.35U)	8	7500
Thrombin low (2.5U)	8	15
Thrombin high (25U)	8	150

<sup>a</sup>: Crude approximation - see references <sup>347, 348</sup>

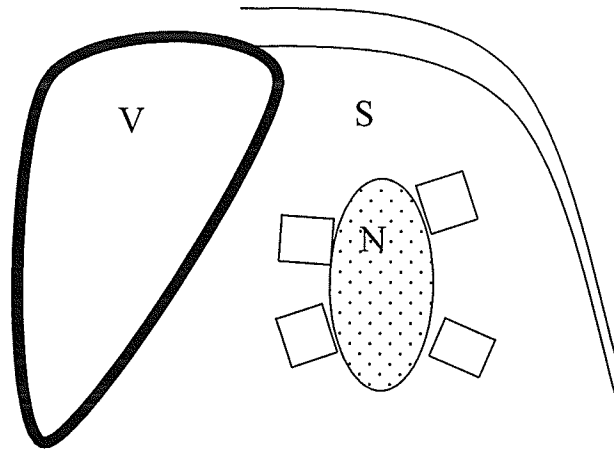
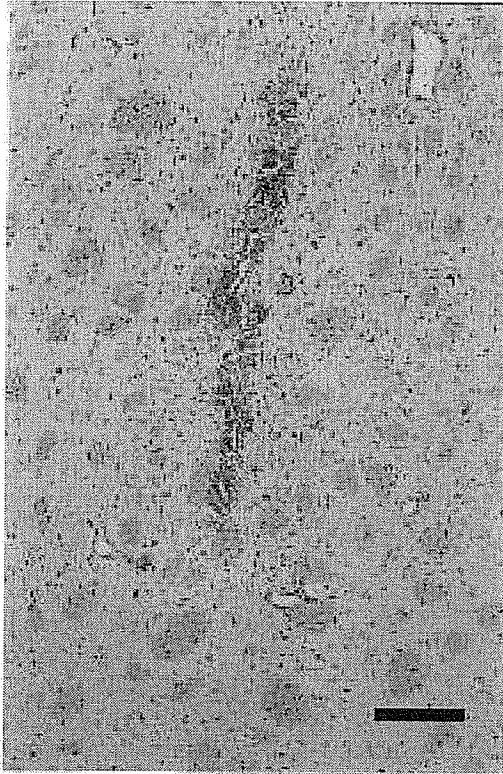


Figure 2-4-1. Schematic diagram of coronal section through rat striatum (S), bounded medially by the lateral ventricle (V) and superiorly by the external capsule, illustrating areas in which cells were counted (squares) surrounding the area of damage at the injection site.

Saline



Thrombin

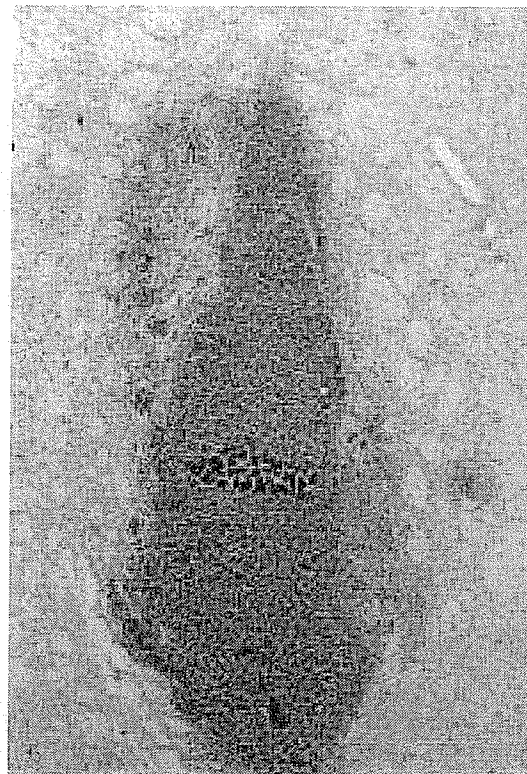


Figure 2-4-2. Photomicrographs showing striatal damage 48 hours after saline or high dose thrombin injection. Insertion of the needle resulted in a narrow column of extravasated blood due to microvascular injury. Injection of 25 units thrombin (and similarly 0.5 units plasminogen) resulted in a necrotic lesion characterized by necrotic and edematous tissue in which cells stain weakly. (Hematoxylin and eosin stain) Bar = 100  $\mu$ m for both images.

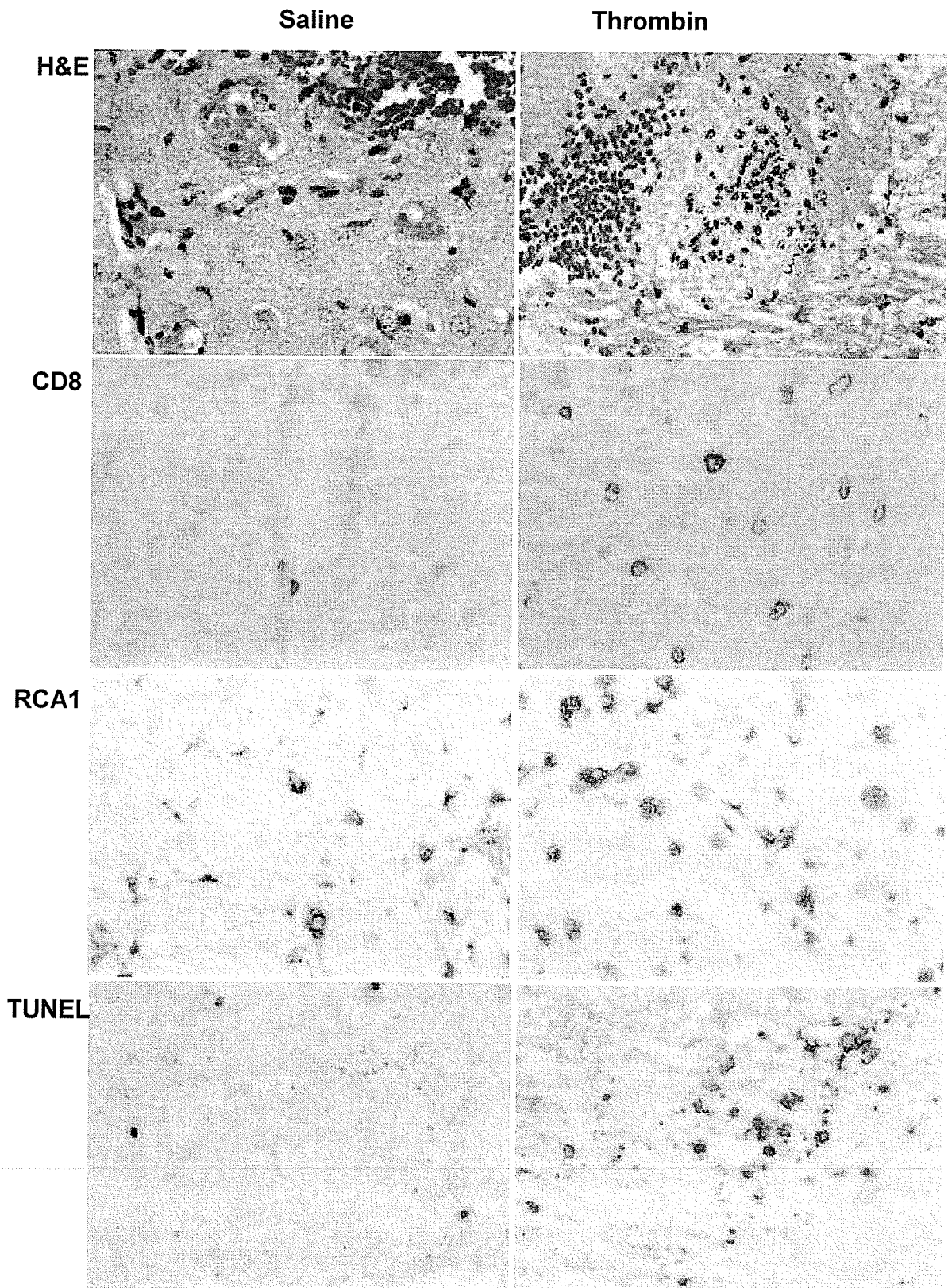


Figure 2-4-3. Photomicrographs showing comparable areas of striatum adjacent to the injection site following administration of saline or high dose thrombin. Neutrophils (arrows on H&E stained sections), cytotoxic lymphocytes (immunohistochemical detection of CD8 antigen on cell membranes), reactive microglia and early macrophages (lectin histochemical detection with RCA1), and dying cells (TUNEL detection of fragmented DNA) are all more abundant following injection of proteolytic enzymes. (All micrographs were photographed at 250x slide magnification, scanned and color balanced using Adobe Photoshop 5.0) Bar = 20  $\mu$ m.

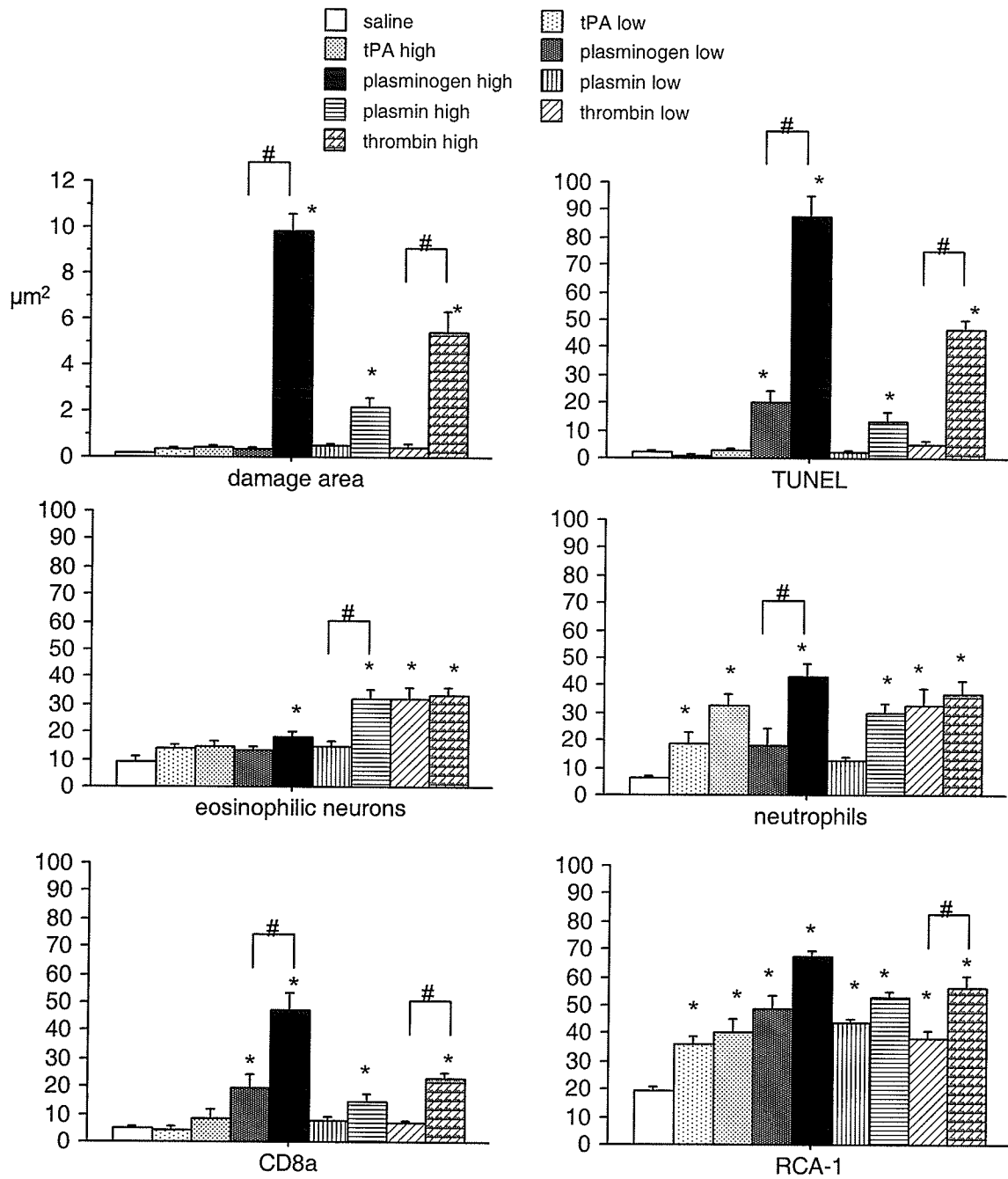


Figure 2-4-4. Bar graphs showing relative tissue damage area (in  $\mu\text{m}^2$ ) and quantity of TUNEL positive dying cells, eosinophilic dying neurons, neutrophils, CD8 immunoreactive lymphocytes, and RCA-1 lectin binding reactive microglia and macrophages. All data are expressed as mean  $\pm$  SEM. Cell counts are expressed as the number of cells per four 250x250  $\mu\text{m}$  areas.

\*  $p < 0.05$  versus saline control group.

#  $p < 0.05$  high dose versus low dose

(ANOVA followed by Fisher's PLSD post hoc test)

NOTE: Using the mean differences for values that were minimally different (e.g. CD8a for low dose plasminogen) the actual power of the test is calculated at  $\sim 50\%$  ( $d = 1.142$ ;  $k$ , the total number of groups, = 9;  $f$ , for intermediate pattern of variability, = .368). To achieve a power of 80% with  $\alpha = 0.05$ , group sizes of 14-15 would have been required

321

Chapter 2-5

Periventricular / intraventricular hemorrhage in neonatal mouse cerebrum.

Mengzhou Xue, MD

Janani Balasubramaniam, MSc

Richard J. Buist, PhD

James Peeling, PhD

Marc R. Del Bigio, MD, PhD, FRCPC

Journal of Neuropathology and Experimental Neurology. 2003;62: 1154–1165.

(The Ki67 staining and quantification in this project was done by Ms. Janani Balasubramaniam. The magnetic resonance imaging was done by Dr. R. Buist with direction by Dr. J. Peeling.)

## Abstract

Periventricular/intraventricular hemorrhage (PVH/IVH) into brain can occur in premature infants and is associated with poor developmental outcome. The purpose of this study was to develop and characterize a model of PVH/IVH in newborn mouse. We hypothesized that periventricular germinal matrix would exhibit reduced cell proliferation. PVH/IVH was induced in 1-day old mice by injection of autologous blood into the periventricular tissue. Magnetic resonance images (MRI) were obtained from 15 minutes to 14 days later. Mice were killed 4 hours to 28 days later. Cell proliferation, dying cells, astrocyte and microglial reactions, neutrophils, and lymphocytes were quantified. Histological studies showed that MRI accurately localizes the hematoma but overestimates the size of the hematoma. The hematoma, located in the striatum and germinal tissue, always extended into the lateral ventricles. Cell proliferation, measured by Ki67 immunoreactivity, was suppressed bilaterally in germinal matrix and beyond from 8 hours to 7 days. Increased cell death was observed in the ipsilateral striatum and germinal matrix 1 and 2 day(s) after PVH/IVH. Astrocyte and microglia reaction peaked at 2 days and persisted up to 28 days. Inflammatory response was minimal. Extravasated blood might play an important role in brain damage following PVH/IVH through suppression of cell proliferation.

Keywords: cell death, cell proliferation, inflammation, immunohistochemistry, Ki67, MRI, PVH/IVH

## INTRODUCTION

Periventricular/intraventricular hemorrhage (PVH/IVH) is defined as hemorrhage originating primarily from subependymal germinal matrix (GM) with extension into the ventricles. It occurs most commonly in premature infants 24 - 30 weeks gestation<sup>15</sup>. The pathogenesis of PVH/IVH is multifactorial and consists of a combination of varying arterial and venous blood flow<sup>15, 69, 349</sup>, coagulation disturbances<sup>350, 351</sup>, veins with fragile walls in the germinal matrix<sup>15</sup>, and excessive fibrinolytic activity in the immature brain tissue<sup>349</sup>. Perinatal brain damage is among the most prevalent and costly forms of neurologic disability<sup>352, 353</sup>. PVH/IVH can be associated with hemiplegic cerebral palsy<sup>354</sup>, mental retardation<sup>355</sup>, and hydrocephalus<sup>15, 353</sup>. Hemorrhage causes brain damage through direct tissue destruction, followed by secondary damage to cells through proteolytic activity of enzymes involved in blood clot formation and lysis, inflammation and cytokine production, edema, and hemoglobin released from lysed erythrocytes<sup>38, 40, 42</sup>. Some of these mechanisms have been studied experimentally in adult brains. However, unlike damage due to hypoxia-ischemia which has been studied extensively<sup>255</sup>, neonatal brain hemorrhage has been largely ignored<sup>69</sup>.

The periventricular GM consists of pluripotential cells that give rise largely to cerebral neurons before 20 weeks gestation in humans and later to precursors of oligodendrocytes and astrocytes<sup>15</sup>. In humans the GM involutes by about 34-38 weeks gestation. In the mouse and rat, periventricular germinal cells generate neurons prior to birth and glial cell precursors during the week after birth<sup>234, 235, 356</sup>. Experimental studies have shown that plasticity is not very effective in the newborn rodent brain, likely because normal developmental processes are interrupted<sup>246</sup>. Hypoxic ischemic damage to

7-day rat brain, in which the GM has largely involuted, reduces the quantity of oligodendrocyte precursors <sup>237</sup>. In humans we have observed that hemorrhage is associated with suppression of germinal cells in cell cycle (Figure 2-5-1). Because reduced brain cell production could have important consequences, our goal was to develop and characterize a novel animal model of PVH/IVH in which we could test the hypotheses that GM cell proliferation is reduced after PVH/IVH. We used 1 - 2 day(s) old mice based upon the state of the subependymal zone/ganglionic eminence, which is roughly comparable to that in 24 - 26 week gestational age human brains <sup>357, 358</sup>. Magnetic resonance imaging (MRI) was used to standardize the hematoma for successive time point analyses of the mouse brain following PVH/IVH.

## MATERIALS AND METHODS

### Animal model

All experimental procedures were done in accordance with guidelines of the Canadian Council on Animal Care. Protocols were approved by the local experimental ethics committee. A total of one hundred and eighteen newborn (24-36 hours) CD-1 mice weighing 1.42 - 1.95 grams were used. The mice were anesthetized with 1.5 - 2 % halothane in a 70:30 mixture of N<sub>2</sub>O:O<sub>2</sub>. Autologous whole blood (15 µL) was collected in a sterile syringe by placing the tail in warm water for 1 minute, cleaning the skin with 70% alcohol, and cutting the tail tip. Because the mice could not be secured in a stereotaxic frame, the injections of blood were done freehand with the needle inserted percutaneously. A 27-gauge needle was attached to the syringe and quickly introduced

into the right periventricular region of the newborn mouse (1 mm lateral, 0.5 mm behind the right eye, 3 mm deep to the scalp surface). A shield around the needle stabilized it against the scalp and ensued correct depth of penetration. Blood (15  $\mu$ L) was injected over 1 minute; the needle was left in the place for 10 - 20 seconds, and then removed slowly. Mice were returned to the mother after the 3-minute procedure. Sham controls consisted of 12 newborn CD-1 mice into which 15  $\mu$ L sterile saline was injected. Because needle insertion alone also can cause hemorrhage, 25 intact mice were also used as controls following halothane anesthesia only. Physiological monitoring was not possible. To compare the extent of blood spread, five additional adult CD-1 mice (weight 20 - 25 grams) underwent autologous whole blood (50  $\mu$ L) injection. The method was similar except the head was affixed in a stereotaxic frame.

#### Magnetic Resonance Imaging

Proton magnetic resonance imaging (MRI) was carried out using a Bruker Biospec/3 MR scanner equipped with a 21 cm bore magnet operating at a field of 7 Tesla. The MR probe used was a custom-built quadrature volume coil (length 3.0 cm, inside diameter 2.0 cm)<sup>359</sup>. The mouse pups were anesthetized with 1.5 - 2 % halothane in a 70:30 mixture of N<sub>2</sub>O:O<sub>2</sub> and maintained normothermic by blowing warm air over the animal holder. Scout MR scans were taken with a magnetization transfer prepared TurboFLASH (MT-FLASH) sequence with a TR of 3.7 ms, TE of 2.3 ms, field of view of 4.0 x 4.0 cm<sup>2</sup>, slice thickness of 1.0 mm, and matrix size of 128 x 128 pixels. Applying a 2 second continuous-wave RF pulse at an offset of 12000 Hz and strength of 25 mT effected the magnetization transfer. High-resolution scans were taken with a standard

multi-slice spin-echo sequence using TR's in the range of 800 - 2500 ms, TE's of either 7.2, 60, or 120 ms, field of view of 3.0 x 3.0 cm<sup>2</sup>, slice thickness of 1.0 mm, and matrix size of 256 x 256. Our predominant interest was to observe the signal loss due to the injected blood. This was dramatic even at very short TE (7.2 ms). We found that the T1-weighting produced by the short TR was far less than the T2-contrast produced by the paramagnetic relaxation effect. Therefore, the short TR was chosen for most scans to reduce the overall scan time. Mice were only used for subsequent histological analysis if MRI showed a standard hematoma size and location.

The volume of the acute hematoma observed by MRI and histology was compared. For this we used 13 mice, 4 of which were imaged twice at 15 - 30 minutes and 4 hours. Four had MRI and histology compared at 15 - 30 minutes, and 9 were compared at 4 hours. On MR images, the area of signal alteration was traced and measured by computerized planimetry. The total volume proportion was calculated based on 1 mm slice thickness. Histological sections every 200 µm encompassed the entire hematoma site. Camera lucida tracing was used to measure the blood collections on each slice (including intraventricular blood and parenchymal hematoma). The total volume of extravasated blood was then calculated.

#### Histologic evaluation

Mice were reanesthetized 4, 8 hours, 1, 2, 7, and 28 day(s) (4 - 5 mice were used for each time point) after blood injection into brain, or 8 hours, 1, 2, 7 day(s) (3 - 4 mice were used for each time point) after saline injection. They were perfused through the heart with 5 to 20 ml ice cold 4 % paraformaldehyde in 0.1 mol/L phosphate buffered

saline (PBS). The brain was removed and stored in the same fixative for 1 - 10 day(s). Fixed brains were cut coronally to surround the injection sites, and slices were dehydrated and embedded in paraffin. Sections (6  $\mu\text{m}$ ) were cut serially for the whole brain, and each 10<sup>th</sup> section was stained with hematoxylin and eosin (H&E). Near the lesion center, where the brain damage was maximal, and a variety of histological and immunohistochemical stains were performed (see below).

We wanted to investigate the inflammation that occurs after PVH/IVH, but the relevant antigens cannot be detected reliably on paraffin sections. Therefore, additional mice were reanesthetized at 2, 4, 7, 14, and 28 day(s) (4 - 5 mice were used for each time point) after blood injection into brain, perfused through the heart with 5 to 20 ml ice cold 0.15 mol/L phosphate buffered saline (PBS), following by 5 to 20 ml ice cold 10% sucrose in 0.1 mol/L phosphate buffer (PB). The brain and spleen were removed and stored in 10% sucrose in 0.1 mol/L PB with 0.02 % sodium azide for 3 - 8 days. Brains were cut coronally approximately 3 - 4 mm on either side of the lesion center. Frozen sections (14  $\mu\text{m}$ ) were cut serially through the anterior half of the cerebrum. Selected levels were stained with H&E. Near the lesion center, a variety of immunolabeling procedures were performed using anti-CD3, anti-CD3 $\epsilon$ , anti-CD4, anti-CD8, anti-Gr-1 antibodies to detect the lymphocyte and neutrophil infiltration (see Table 2-5-1). Anti-CD3 $\epsilon$  antibody was used to detect lymphocytes in the frozen brain tissues by labeling the T cell receptor associated CD3 complex, which is expressed on thymocytes and mature T lymphocytes of all mouse strains<sup>360</sup>. Frozen sections were fixed in  $-20^{\circ}\text{C}$  acetone, washed, blocked with 10% donkey serum, and incubated with biotin-conjugated hamster anti mouse CD3 $\epsilon$  monoclonal antibody (diluted 1/300 in 1% BSA, Pharmingen Canada)

at 4°C overnight. Slides were then washed, incubated in streptavidin-peroxidase HRP (1/400), washed, colored with diaminobenzidine - H<sub>2</sub>O<sub>2</sub> solution, washed and coverslipped. Purified rat anti-mouse CD3, anti-mouse CD4, anti-mouse CD8 (Ly-2), anti-mouse Ly-6G (Gr-1) antibodies were used to detect the lymphocyte and neutrophils infiltration on frozen brain sections by immunofluorescence. Frozen sections were fixed in -20° C acetone, washed, blocked with 10% donkey serum, and incubated with rat anti mouse monoclonal antibodies (all antibodies from Pharmingen Canada, diluted 1/100 for anti-CD8 and anti-CD3, 1/300 for anti-CD4, 1/500 for anti-Gr-1 in 1% BSA) at 4°C overnight. Slides were then washed and incubated in mouse anti rat Cy3, coverslipped with mounting media for fluorescence microscopy (Kirkegaard & Perry Laboratories Gaithersburg, Maryland, USA) and observed by fluorescence microscopy. For all antibodies procedures negative control sections were processed with omission of the primary antibody. Positive controls were pieces of spleen tissue embedded adjacent to the brain.

Ricinus communis agglutinin lectin (RCA-1) labeling was used to demonstrate reactive microglial cells <sup>269</sup>. Paraffin sections were dewaxed and rehydrated, washed, quenched with 0.3 % H<sub>2</sub>O<sub>2</sub>, blocked with 10 % normal sheep serum, and incubated with biotinylated lectin (diluted 1/2000, Vector Laboratories, Inc., Burlingame, U.S.A.). Slides were then washed, incubated with streptavidin-peroxidase (1/400), colored with diaminobenzidine - H<sub>2</sub>O<sub>2</sub> solution, washed and coverslipped. Control sections were processed with omission of the biotinylated lectin.

Anti-GFAP (glial fibrillary acidic protein) antibody was used to evaluate astrocyte reaction. Paraffin sections were dewaxed, rehydrated, quenched with 0.3 % H<sub>2</sub>O<sub>2</sub>,

blocked with 10 % normal goat serum, and incubated with rabbit anti-cow GFAP polyclonal antibody (diluted 1/1000, Dako) at 4°C overnight. Slides were then washed, incubated with biotinylated goat anti-rabbit IgG (1/300), streptavidin-peroxidase (1/400), and colored with diaminobenzidine - H<sub>2</sub>O<sub>2</sub> solution. Control sections were processed with omission of the primary antibody.

#### Detection of proliferating cells and dying cells

Cell proliferation status in the brain was assessed with an antibody that recognizes nuclear Ki67 antigen, which is expressed from late G1 to M phase of the cell cycle<sup>361</sup>. Bisbenzimidide (2-(4-ethoxyphenyl)-5-(4-methyl-1-piperazinyl)-2,5-bi-1H-benzimidazole trihydrochloride; Hoechst 33342, Sigma) counterstaining was used to show all nuclei. Paraffin sections were dewaxed and rehydrated. Slides were microwaved in 0.6 M citric acid buffer for 15 minutes and were cooled in 0.1M PBS for 20 minutes. Slides were blocked with 10 % normal donkey serum and incubated with rabbit anti-Ki67 polyclonal antibody (Novocastra, U.K, diluted 1/500) at 4°C overnight. Slides were then washed, incubated with Cy3 donkey anti-rabbit IgG (1/500), and coverslipped. Negative controls were processed without the primary antibody.

TUNEL (terminal deoxynucleotidyl transferase (TdT)-mediated deoxyuridine triphosphate (dUTP)-biotin nick end labeling) was used to identify dying cells with damaged DNA. Paraffin embedded sections were dewaxed and rehydrated, then incubated in 20 µL/ml proteinase K for 15 minutes. TUNEL was accomplished using *Apoptag in situ* kit (Intergen; Purchase, NY, USA). After immersion in equilibration buffer for 10 minutes, sections were incubated with TdT and dUTP-digoxigenin in a

humidified chamber and then incubated in the stop/wash buffer. Sections were washed before incubation in anti-digoxigenin-peroxidase solution (1/500 in PBS), and colored with diaminobenzidine - H<sub>2</sub>O<sub>2</sub> solution. Sections were counterstained with methyl green. Negative control sections were treated similarly but incubated in the absence of TdT enzyme or dUTP-digoxigenin.

Sections of brain were stained with Fluoro-Jade to show dying neurons<sup>189, 190</sup> by incubating sections in 0.06% potassium permanganate for 15 minutes while gently shaking on a rotating platform. Then 0.001% Fluoro-Jade (Histo-Chem Inc.; Jefferson, AR) staining solution was applied for 30 minutes, following by PBS washing, drying in air, and coverslip application.

#### Determination of hematoma size and cell counts

The coronal levels with damage were identified. A "camera lucida" drawing was used to trace the damaged areas, defined by the presence of blood, tissue rarefaction, or necrosis. Computerized planimetry was used to measure the traced areas. Using an ocular reticule and 400x ocular magnification, TUNEL positive dying cells, extravascular neutrophils identified on H&E sections by characteristic nuclear morphology, and RCA-1 labeled cells were counted in 4 fields (each area 540  $\mu$ m x 540  $\mu$ m) immediately adjacent to the damage site including striatum and GM as previous described<sup>39</sup>. Areas with large blood vessels were avoided. The GFAP positive cells were assessed semiquantitatively by using four grades (0, no positive cells; 1, rare positive cells; 2, moderate number positive cells; and 3, many positive cells). The proportion of cells in cycle was calculated by dividing the number of Ki67 immunoreactive nuclei by the total number of nuclei

stained with bisbenzimidazole. These proportions were determined in germinal matrix (three areas comprised of four 540  $\mu\text{m}$  x 540  $\mu\text{m}$  field each, objective 40x magnification). Cells were also counted in striatum (S), white matter (W), and cerebral cortex (superficial and deep cortex) in 2 fields each (each 1.08  $\mu\text{m}$  x 1.08  $\mu\text{m}$ , objective 20x magnification). All counts were made by an observer blinded to the time after injection. For acute experiments the presence of blood precluded blinding between groups.

### Statistics

All data are expressed as mean  $\pm$  SEM. Data were analyzed to ensure normal distribution. Intergroup comparisons were made by ANOVA followed by Fisher least square difference test. The differences were considered significantly different when  $p < 0.05$ . Non-parametric data (i.e. GFAP) were assessed using Kruskal-Wallis test. We used StatView 5.01 software (SAS Institute; Cary NC).

## RESULTS

### MRI of PVH/IVH in newborn mice

All mice tolerated the injection of 15- $\mu\text{L}$  blood into the periventricular tissue well and there was no surgical mortality. On T2-weighted MR images, blood appeared dark (Figure 2-5-2 A-D) due to the large susceptibility effect of paramagnetic hemoglobin products. The blood appeared to spread widely and rapidly following injection into the periventricular region. In the majority of mice blood entered the lateral ventricles. Bright regions surrounding the ventricles on T2-weighted images are likely due to susceptibility artifact. This was confirmed by switching the read and phase encoding gradients in

imaging studies carried out 1-day post PVH/IVH (data not shown). When the read gradient was directed left-right (L-R) and phase-encoding anterior-posterior (A-P), the bright artifact appeared to the right and left of the hematoma; when the read gradient was A-P and phase encoding gradient L-R, the artifact appeared A-P. The hematomas resolved rapidly, significantly decreasing in size by 1 day (Figure 2-5-2 E, F). Mild ipsilateral (or sometimes bilateral) ventricle enlargement was apparent at 2 weeks (Figure 2-5-2 G, H). Saline injection was associated with only very small foci of blood accumulation (Figure 2-5-2 I). MR images after injection of 50  $\mu$ L blood into medial striatum of adult mouse brain had a similar appearance to those obtained following acute PVH/IVH in neonates but was associated with less spread into tissue (Figure 2-5-2 J). As in newborns, by 1 day the site of blood injection was hardly apparent (not shown).

We quantified and compared the hematoma volume on MRI and histological sections immediately (15-30 minutes) and 4 hours following the blood injection into newborn mouse brain (Figure 2-5-3). On MRI there was a significant decrease in size of the hematoma by 4 hours. On histological examination there was no significant difference in size at the 2 time points. In comparison to MRI, histological preparations showed that blood was in a much more confined region of the periventricular tissue. Although the ventricles were filled with blood they were only minimally expended. Therefore MRI overestimates the size of the hematoma, but reliably documents the location and allows in vivo documentation of a standard hematoma size. All mice used for quantitative analyses had a similar MR appearance initially.

Histological features of PVH/IVH in neonatal mice

Examination of the normal mouse brain at 1-2 days age, the time at which blood would be injected, showed that the large elongated cells of the pseudostratified ventricular zone occupied a ~50 $\mu$ m thick layer. The smaller, rounder subventricular zone cells over the caudatoputamen (the ganglionic eminence) were packed in a dense layer up to 300 $\mu$ m thick. Rare mitotic figures could be identified along the ventricle wall and many more were in the subventricular zone. Scattered apoptotic bodies were present in the subventricular zone. The germinal tissue of the ganglionic eminence was largely gone by 7 days and absent by 28 days, confirming prior observations that the mouse lateral ventricular wall resembles that of adults by 15 days<sup>362</sup>. A few ciliated ependymal cells were apparent along the roof of the ventricle by 3 days and many were present along the lateral wall by 7-9 days. Their appearance coincided with involution of the ventricular and subventricular zones. Long processes of radial glial cells were apparent on the GFAP immunostained sections<sup>363</sup> extending into the white matter at the roof of the ventricle and into the caudatoputamen along the wall of the ventricle at 2 days. Far fewer cells with long processes were evident at 7 days. During this involution period many apoptotic bodies were present.

Qualitative and quantitative assessments of brain changes following blood injection were studied in the germinal matrix of the ganglionic eminence, the caudatoputamen, the white matter at the roof of the lateral ventricle, and the dorsal cerebral cortex (Figure 2-5-4). From hours to 2 days after blood injection, damaged brain surrounding the hematoma appeared pale on hematoxylin and eosin (H&E) stain due to edema. The irregular hematoma was located in striatum and GM with extension into the ventricles (Figure 2-5-5 A-C). Acutely, hematomas were characterized by single or

multiple contiguous collections of blood cells, and blood cells mixed with GM cells. These collections were often continuous with intraventricular blood collections because ventricular zone was split. It was difficult to assess ependyma in the blood-filled ventricles. At 1 day scattered neurons with hypereosinophilic cytoplasm were evident within the damaged striatum. After 1 day, pale-staining degenerating erythrocytes and fragmented nuclear debris were seen. By 7 days no blood or edema could be identified in the tissue. The hematoma site was difficult to find with the exception of scattered hemosiderin-containing macrophages. The ventricles were slightly enlarged at 28 days.

#### Cell proliferation and cell death

Counts of proliferating cells were made in several regions of brain adjacent to and distant from the site of the hematoma (Figure 2-5-4). In normal brain, large proportions of cells were Ki67 positive (Figures 2-5-5 D-G) in the GM and white matter from 8 hours to 28 days. Fewer proliferating cells were identified in the striatum and cortex. In comparison to intact and saline-injected controls we observed that the proportion of proliferating cells in the GM significantly decreased 8 hours, 2 and 7 days (but not 1 day) post PVH/IVH bilaterally (Figure 2-5-6). In the white matter (corpus callosum and external capsule), decreased cell proliferation was observed bilaterally from 8 hours to 7 days following PVH/IVH. The cerebral cortex showed a significant decrease in cell proliferation bilaterally 1 - 2 day(s) post PVH/IVH. The striatum did not show significant change in cell proliferation at any time point.

TUNEL positive dying cells (Figures 2-5-5 H-J) were infrequent in the normal control tissue and contralateral to the hematoma. Ipsilateral to the hematoma more

TUNEL positive dying cells were observed in the striatum and GM 1 and 2 day(s) after PVH/IVH (Figure 2-5-7). Rare, scattered Fluoro-Jade-stained dying neurons, corresponding to hypereosinophilic neurons, were observed in the striatum 1 - 2 day(s) after PVH/IVH and thereafter (data not shown). Cells that stained weakly with Fluoro-Jade were evident in the striatum, cortex of ipsilateral and contralateral hemisphere, and septum, but these were not obviously dying cells.

In normal brains, astrocytes were immunoreactive for GFAP around blood vessels in the striatum and cerebral cortex, and also among axons in the white matter (Figure 2-5-5 K-M), beginning at 7 days. Radial glia were immunoreactive for GFAP 2-7 days. Following PVH/IVH slightly hypertrophic astrocytes were evident at 2 days. Semiquantitative assessment (Figure 2-5-7) showed that the astrocyte reaction was maximal 2 - 7 days after PVH/IVH in the ipsilateral striatum, 2 - 28 days in the ipsilateral white matter, 7 - 28 days in contralateral white matter. We could not determine specifically whether radial glia cells were disrupted except at the site of the hematoma.

### Inflammation

RCA-1 labeling of microglia (Figures 2-5-5 N-P) was not evident in normal brain. By 8 hours after PVH/IVH some reactive microglia with narrow cell bodies and branched processes were evident. Their quantity was maximal at 2 - 7 days and had decreased by 28 days (Figure 2-5-7). By 7 days there were round macrophages adjacent to the hematoma. Neutrophils, evident with H&E stain and Gr1 immunostaining, were present in the brain tissue surrounding the hematoma in very small quantities only at 1 - 2 days (1.6 ? 1.5 and 2.4 ? 1.8 respectively, per count region). Immunolabeling with anti-CD3,

CD3ε, CD4, and CD8 antibodies showed only very few scattered lymphocytes in the vicinity of the hematoma, 2 - 7 days after blood injection (not shown).

## DISCUSSION

Animal models are needed to study the pathogenesis of brain damage after PVH/IVH. Intraventricular hemorrhage has been induced using glycerol to create intracranial hypotension in prematurely born rabbits (27 - 30 days gestation)<sup>70</sup>. Injection of blood into newborn dog brains has been used to study the effect of acute ventricular distension on the surrounding blood flow patterns<sup>73</sup>. Dog models have played an important role in understanding the physiologic factors that predispose to PVH/IVH<sup>69</sup>. A mouse model of neonatal hypoxia develops superficial foci of bleeding unlike those seen in humans<sup>74</sup>. These studies have been concerned with the physiologic processes and structural features that allow PVH/IVH but not the tissue reactions. In this study, we developed a novel model of PVH/IVH in newborn mouse by injection of autologous whole blood into periventricular tissue including GM and striatum. All mice exhibited extension of the hematoma into the ventricles. Therefore, this model corresponds to grade III / IV PVH/IVH as defined by imaging studies in premature infants<sup>364</sup>. This model provides an opportunity to study mechanisms of cellular injury after PVH/IVH.

Histological examination showed that MRI was capable of accurately localizing the hematoma to the periventricular region and the ventricle. MRI allows us to ascertain the size and site of the acute hematoma regardless of the subsequent survival period. There are few studies of human infants with PVH/IVH using MRI. T2-weighted fast spin echo MRI is more sensitive than ultrasound for detecting small sites of hemorrhage<sup>365</sup>.

<sup>366</sup>. The MRI features we observed in mice are similar. However, MRI consistently showed a larger hematoma volume than the histological preparation. This suggests that hypointensity in the MR image is due to diffusing hemoglobin from lysed cells and/or the large susceptibility effect of paramagnetic hemoglobin. Sequential studies after PVH/IVH showed rapid dispersion of the blood. Blood in the ventricles is probably washed away by cerebrospinal fluid (CSF). The loosely organized newborn brain might also allow rapid removal of hemoglobin degradation products. MRI showed that the ventricles enlarged slightly weeks after PVH/IVH. This is similar to the hydrocephalus that develops after PVH/IVH in prematurely born infants <sup>367</sup>. However, we never observed progression to severe ventricle and head enlargement. When enlargement was unilateral we believe that it is related to mild tissue atrophy.

This study demonstrates that injection of a small quantity of whole blood into the brain of neonatal mice is associated with widespread reduction of cell proliferation, local increase in cell death, diffuse astroglial reaction, and negligible inflammation except for microglial activation. Dying cells, demonstrated by TUNEL and Fluoro-Jade, significantly increased in quantity in the damaged striatum, peaking 2 days following the blood injection. Cell death is expected after brain injury. However, the most impressive finding was that the proportion of proliferating cells decreased ipsilateral and contralateral to the PVH/IVH in the periventricular GM and in white matter. In the newborn rodent, the periventricular germinal region gives rise to glial precursors that migrate into various parts of the ipsilateral cerebral hemisphere <sup>234, 235, 356</sup>.

Decreased proliferation was observed as early as 8 hours following IVH/PVH. Thus the mechanism of proliferation suppression is likely a direct effect of some

mediator from blood or damaged cells and not, for example through immune cell mediators; the effects of immune activation would probably not be seen until later times after most brain injuries. We expect that the decrease in cell proliferation can be due to one of or a combination of the following mechanisms. The hematoma may cause mechanical destruction including tearing of cell processes and fragile blood vessels in GM. Cerebral blood flow or venous outflow may be compromised locally <sup>2</sup> in turn leading to ischemic damage <sup>15, 368</sup>. Extravasation of blood components, clotting blood, and damaged brain tissue may liberate neurotoxic factors including thrombin, plasminogen, hemoglobin, glutamate, and agents from inflammatory cells <sup>38, 41, 93, 196, 259, 273</sup>. These agents could spread through ventricular CSF or edematous white matter. High serum concentrations can suppress neuronal proliferation in chick neuroblast cultures <sup>369</sup>. Neurotransmitters released in response to injury, such as glutamate and gamma-aminobutyrate (GABA), have also been shown to suppress cell proliferation <sup>370, 371</sup>. Together, these mechanical, ischemic, and potentially neurotoxic components constitute a complex insult after PVH/IVH. Because our TUNEL study showed no increase in cell death in the contralateral germinal tissue, it is likely that the factors involved in mediating cell death are different from those that suppress proliferation. Cell proliferation was not significantly decreased at 24 hours. This could be an experimental artifact or there could be a population of cells (e.g. astrocytes or microglia) that begin to proliferate at this time. In the absence of pulse labeling studies with a thymidine analogue, we cannot be certain about this. Longer term suppression could be mediated by other agents produced later e.g. cytokines <sup>372</sup>. PVH/IVH can result in enlargement of the lateral ventricles that might

compress the adjacent brain tissue causing further damage. This did not seem to be a factor in this experiment.

Our data show that inflammatory cell infiltration has a similar temporal pattern to that in adult rat brain following blood injection<sup>39</sup>. However, the number of infiltrating neutrophils and lymphocytes is much lower. Possible reasons are that the chemokines are diluted and washed quickly from the highly hydrated newborn brain<sup>373</sup>, that there is an interspecies difference, or that cellular production of chemokines might differ<sup>374</sup>. These data suggest that leukocytes probably play a minor role in the brain damage following the PVH/IVH. Microglial reaction, evident beginning at 2 days, persisted up to 28 days, similar to the temporal pattern in adult rats<sup>39</sup>.

This study has several potential shortcomings. Newborn mice are very small and they could not be secured in a stereotactic frame. Therefore, the method of freehand blood injection could cause variable brain damage. We used MRI to be sure that blood was indeed injected into the correct location and we only used mice with comparable hematomas. The small size of the brain dictates that diffusible toxic agent(s) have effects in anatomic regions different from those in human brain. For example, a given protein that diffuses 5 mm in both mouse and human brain would produce bilateral effects in mice but only "focal" effects in humans. We do not know whether the route of toxic agent spread is through tissue or CSF. The absence of an intact ependymal layer at the age when blood is injected could allow toxic agents to spread directly from CSF into germinal tissue. We did not attempt to determine conclusively whether the suppression of mitotic activity occurs in the ventricular zone or the subventricular zone, although subjectively both would seem to be affected. This is of potential significance because

they give rise to different cell types. Nor did we assess whether there was an effect on the differentiation of radial glia, which can act as stem cells as well as migration guides <sup>362</sup>. RC2 immunohistochemistry might help address this issue. Finally, cell proliferation was measured indirectly by assessing immunoreactivity for Ki67, which is expressed from late G1 to M phase of the cell cycle and correlates well with thymidine analogue uptake by proliferating cells <sup>375, 376</sup>. The loss of expression does not prove that too few cells were generated because generally a surplus of cells is produced. Perhaps the residual proliferative activity was sufficient to produce the necessary cells.

In conclusion, extravasated blood may play an important role in brain damage following PVH/IVH through suppression of cell proliferation in the GM. This is potentially important because MRI studies on humans show that premature birth or periventricular hemorrhage is associated with reduced white matter volume <sup>377</sup>. If GM suppression is associated with impaired development of glial precursors it could explain some aspects of the final (sometimes subtle) brain damage following premature birth. The precise molecular and chemical mechanisms remain to be determined but probably are multiple. Complete understanding of the mechanisms of damage associated with PVH/IVH should direct us to new treatment strategies.

Table 2-5-1. Summary of immunohistochemical and histochemical staining used.

Antibody / Histochemical method	Specificity	Dilution	Source
Hamster anti mouse CD3ε monoclonal (biotin-conjugated)	T lymphocytes	1/300	Pharmingen
Rat anti-mouse CD3	T lymphocytes	1/100	Pharmingen
Rat anti-mouse CD4	Helper T cells	1/300	Pharmingen
Rat anti-mouse CD8 (Ly-2)	Cytotoxic T cells	1/100	Pharmingen
Rat anti-mouse Ly-6G (Gr-1)	Neutrophils	1/500	Pharmingen
Rabbit anti-cow GFAP	Astrocytes	1/1000	Dako
Rabbit anti-Ki67	Proliferating cells	1/500	Novocastra
Ricinus communis agglutinin lectin (RCA-1) (biotin-conjugated)	Microglia	1/2000	Sigma
TUNEL	Dying cells	-	Intergen
Fluoro-Jade	Dying neurons	-	Histo-Chem Inc

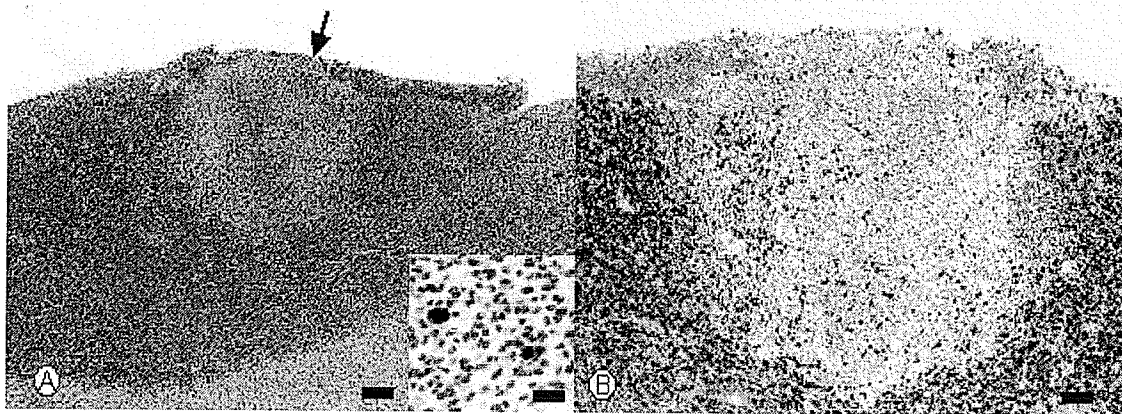


Figure 2-5-1. (A) Photomicrograph showing periventricular germinal tissue (ganglionic eminence) of a human fetus (~ 24 weeks gestational age) a few days after a small periventricular hemorrhage. There is a circular area of decreased cellularity along the ventricle wall (arrow) (hematoxylin and eosin stain) (Bar = 100 $\mu$ m). This was shown to be the site of hemorrhage by the presence of hemosiderin-containing macrophages (inset, Perl's stain for iron) (Bar = 25 $\mu$ m). (B) Immunohistochemical labeling of an adjacent section with anti-Ki67 antibody demonstrates that the damaged area has a greatly reduced proportion of proliferating cells (brown nuclei) (Bar = 50 $\mu$ m).

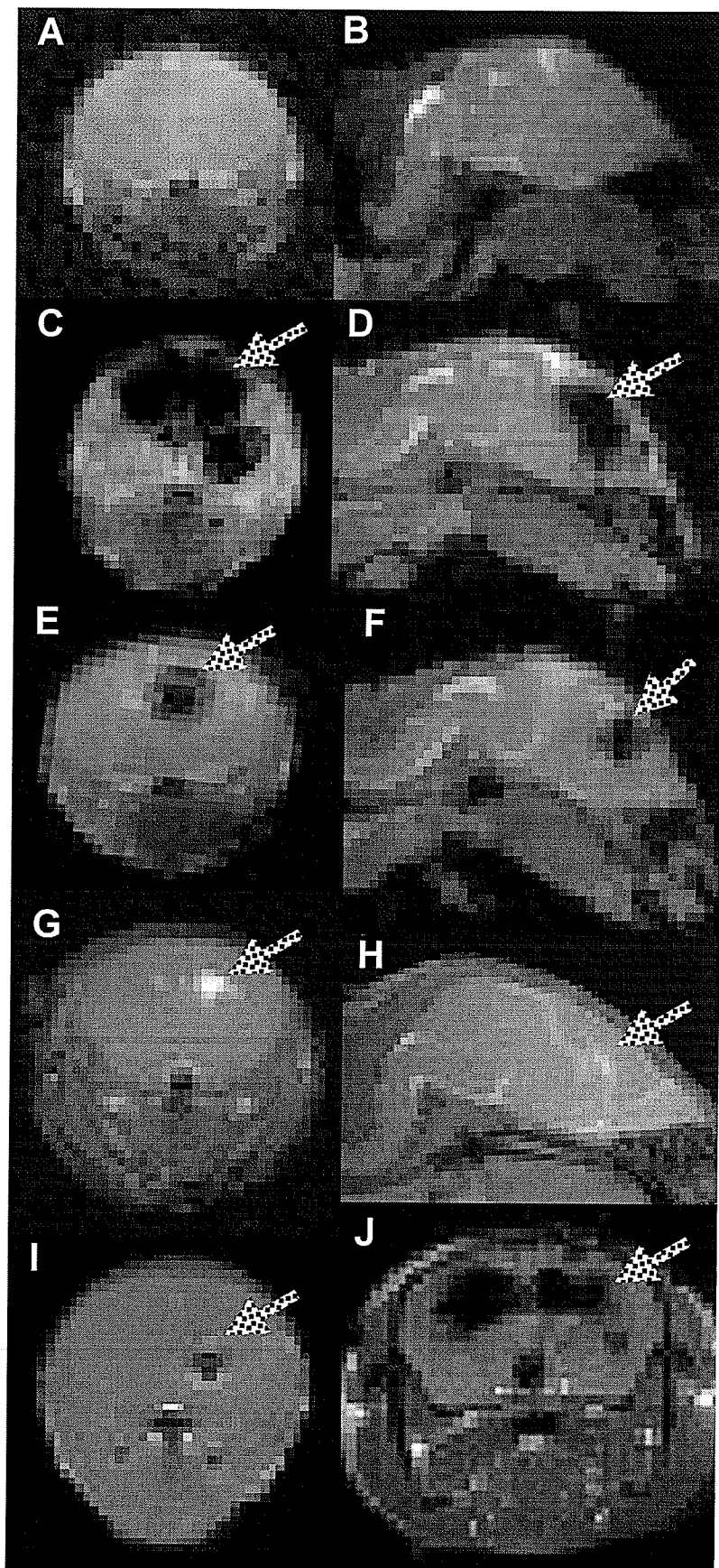


Figure 2-5-2. T2-weighted MR (MT-FLASH) showing coronal (A, C, E, G, I, J) and sagittal images (B, D, F, H) of mouse brain. Normal 1-day mouse brain is shown in A and B. One hour following blood injection (15  $\mu$ L), the hematoma in the striatum (arrow) and ventricles appears dark (C, D). A similar but less extensive change is seen in adult mouse brain 1 hour after injection of 50- $\mu$ L blood (J). One hour after saline (15  $\mu$ L) injection (I) into 1-day mouse brain, a small blood collection due to the needle damage is evident (arrow). The injected hematomas resolve rapidly as shown by a significant decrease in size by 1 day (E, F) (arrow). By 2 weeks only a small fluid-filled cavity and / or slightly enlarged ipsilateral ventricle (bright area, arrow) is evident (G, H).

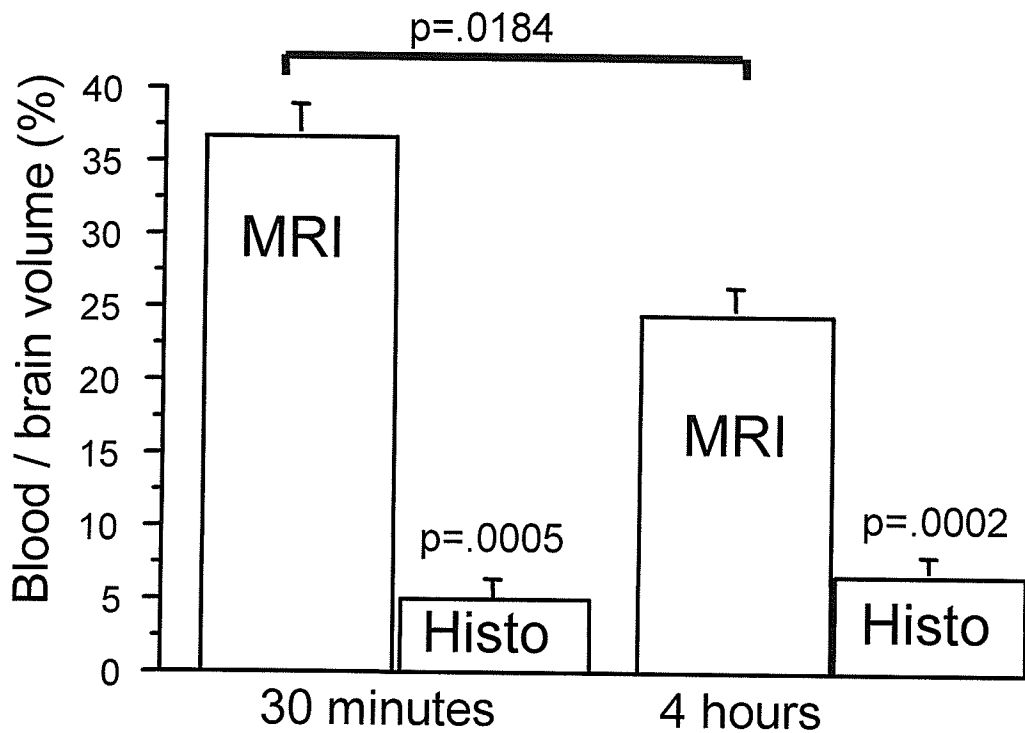


Figure 2-5-3. Proportionate hematoma size on MR images and histological sections 30 minutes and 4 hours following blood injection into newborn mouse brain. On sequentially imaged mice there was a significant difference in the apparent size of the blood collection between the two time points (paired t test,  $p < 0.02$ ). MR images consistently displayed an apparent hematoma size that was significantly larger than the true hematoma size evident on the histological sections (paired t test,  $p < 0.0001$ ).

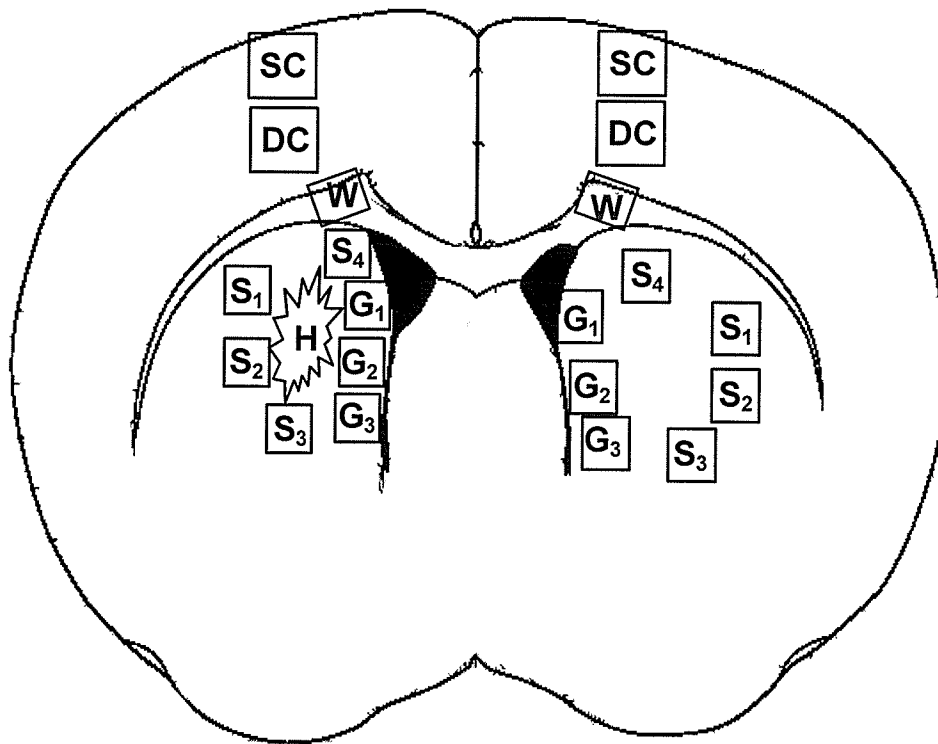


Figure 2-5-4. Schematic diagram of mouse brain showing areas in which cells were counted following blood injection. For quantification of proliferating cells, Ki67 immunolabeled nuclei and bisbenzimidazole-stained nuclei were counted in the periventricular germinal matrix (G1, G2, and G3), striatum (S1, S2, S3, and S4) adjacent to the hematoma (H), white matter (W), deep cerebral cortex (DC) and superficial cerebral cortex (SC). GFAP immunoreactivity, an indicator of reactive astrogliosis, was assessed semiquantitatively in the same regions. To evaluate cell death and inflammation, TUNEL positive cells, neutrophils, and RCA-1 labeled microglia were counted in striatum (S1, S2, S3, and S4) adjacent to the hematoma (H). All assessments were made bilaterally.

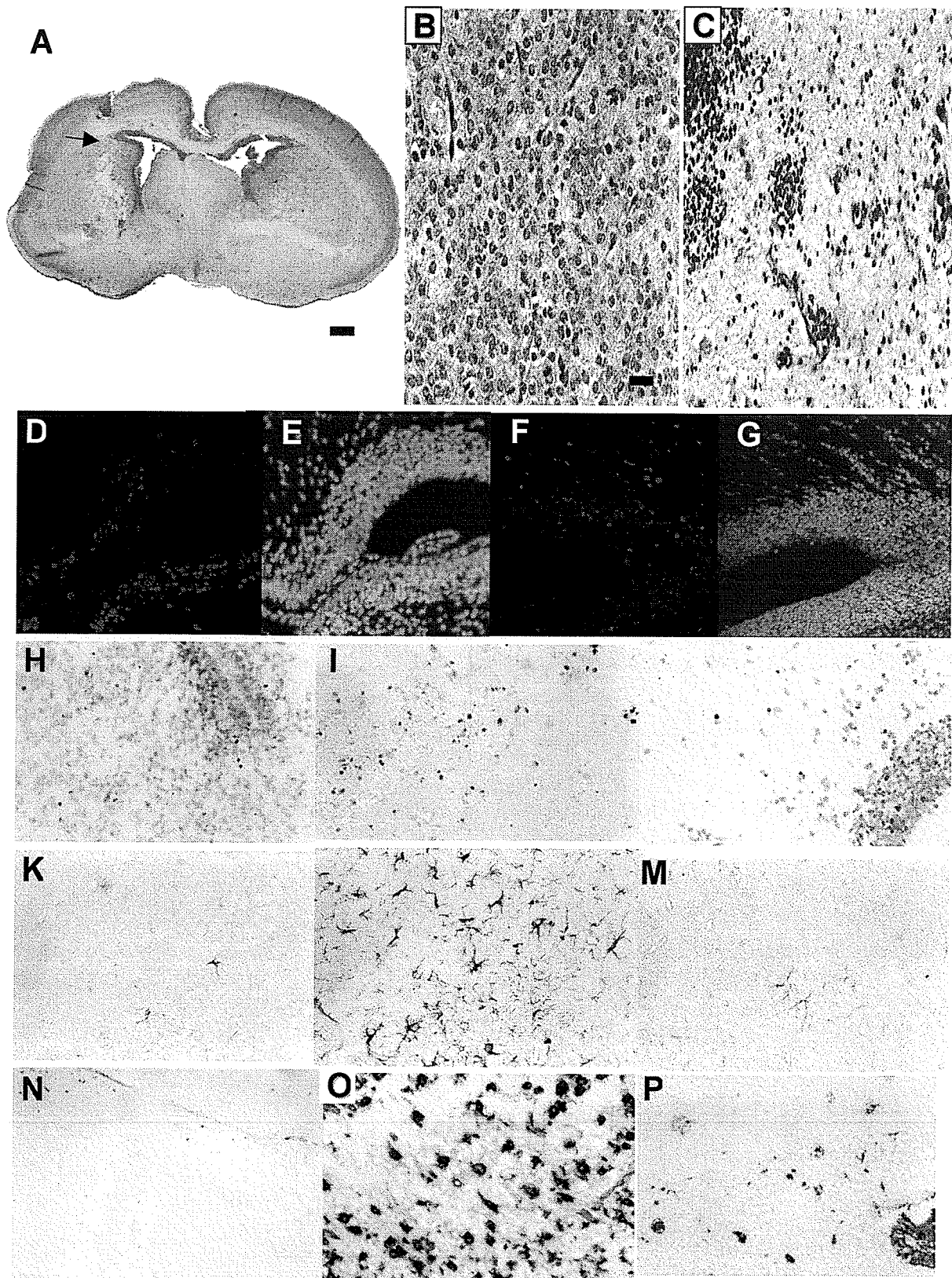


Figure 2-5-5. Photomicrographs of histopathologic features following blood injection into newborn mouse brain. (A) Low magnification photomicrograph of mouse brain coronal section (hematoxylin and eosin stain) at the site of blood injected into the striatum adjacent to the periventricular germinal matrix (arrow). The lateral ventricles are enlarged bilaterally and contain a small quantity of blood 4 hours after injection (Bar = 0.5 mm). (B) Intact newborn medial striatum exhibits tightly packed immature neurons (Bar = 25  $\mu$ m for B-P). (C) Damaged striatum adjacent to hematoma 2 days after PVH/IVH exhibits fewer neurons, small collections of erythrocytes, and mild pallor due to edema. (D) Ki67 immunolabeling with Cy3 detection shows abundant proliferating cells (bright red) in the normal germinal matrix at the angle of the lateral ventricle. (F) Far fewer cells are seen in the age-matched brain, 1 day after blood injection. (E & G) Bisbenzimidazole stained nuclei of same fields respectively. TUNEL showing rare dying cells (brown) in normal newborn striatum (H), in striatum adjacent to hematoma (I), and in contralateral striatum (J) 2 days after PVH/IVH. GFAP immunolabeling shows scattered stellate astrocytes in normal brain (K), an increased quantity and size of astrocytes adjacent to the hematoma (L) 2 days after blood injection, and few labeled cells in striatum contralateral to the hematoma (M). RCA-1 lectin staining shows a negligible number of microglial cells in normal striatum (N), an abundance of round macrophages and plump activated microglia adjacent to the hematoma (O) 2 days after blood injection, mild activation of cells in striatum contralateral to the hematoma (P).

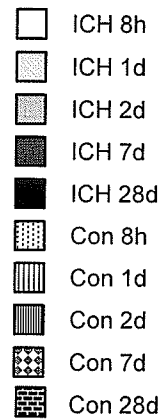
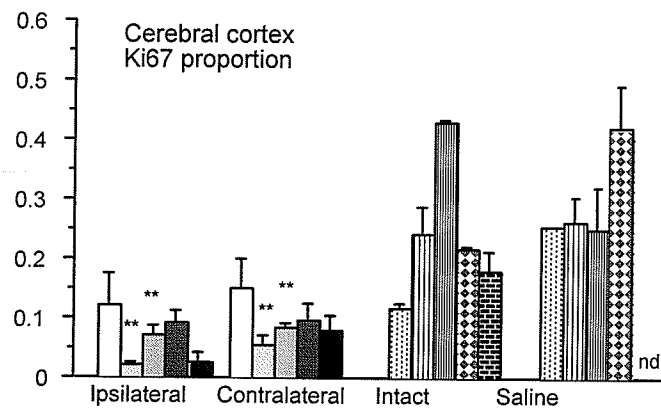
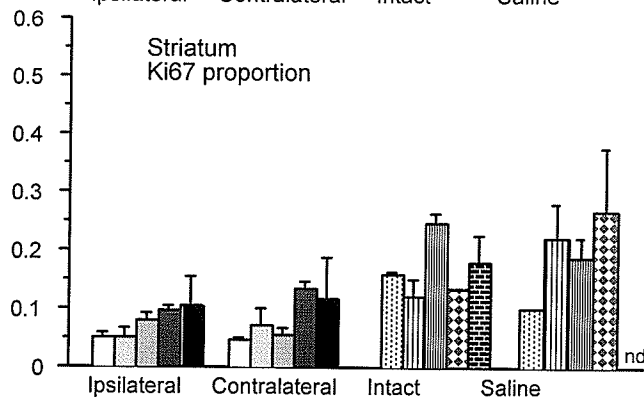
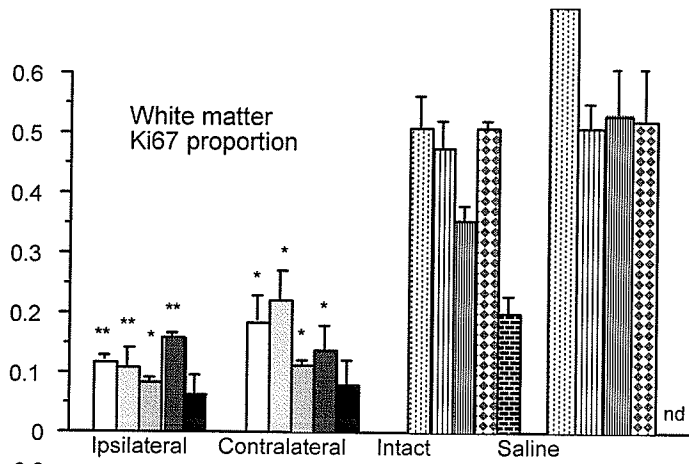
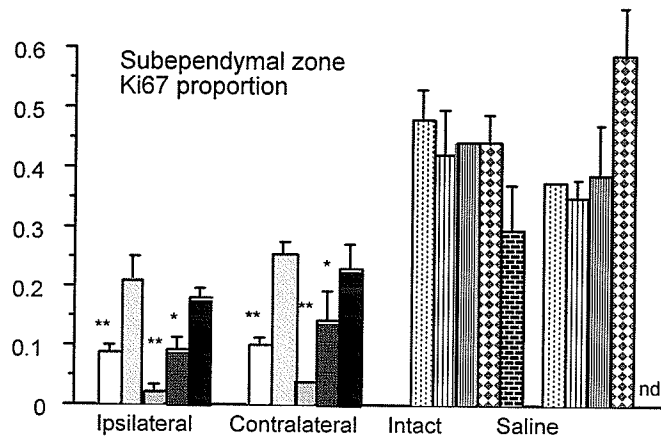


Figure 2-5-6. Bar graphs showing the proportion of proliferating cells (calculated by the number of Ki67 immunoreactive nuclei / total bisbenzimidazole stained nuclei) in various regions of mouse brain (see Figure 2-5-4) at sequential times after blood injection. In intact control mice the highest proportions were observed in germinal matrix (subependymal zone). The quantities were negligible by 28 days age, by which time the germinal matrix periventricular white matter had involuted. There was no change following injection of saline. Following injection of blood the proportion of proliferating cells decreased in the ipsilateral (and to a lesser degree in the contralateral) germinal matrix and white matter from 8 hours to 7 days. There was a moderate decrease in the immature cerebral cortex bilaterally, and no change in the striatum. (nd = no data). \* $p < 0.05$ ; \*\* $p < 0.01$  ANOVA. (On legend ICH = intracerebral hemorrhage, Con = control)

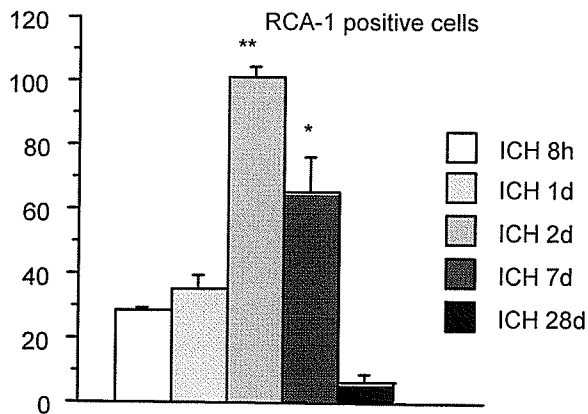
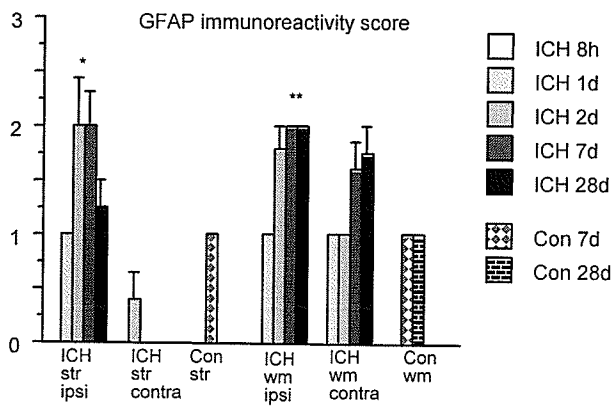
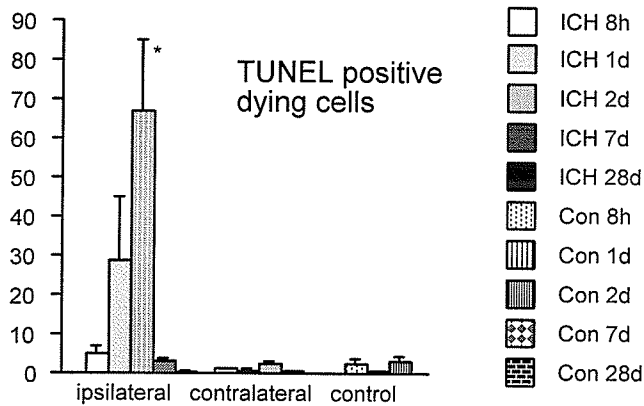


Figure 2-5-7. Bar graphs comparing cell death (upper panel), GFAP immunoreactivity in reactive astrocytes (middle panel), and RCA-1 lectin detection of reactive microglia (lower panel) in control (Con) brains and mouse brains after blood injection (ICH). Rare dying cells were apparent in control brains up to 3 days age (shown as 2 days post-hemorrhage). The number of dying cells was greater adjacent to the hematoma 1-2 days after blood injection, but there was no change in the contralateral striatum ( $p < 0.05$  ANOVA). GFAP immunoreactivity in astrocytes was negligible in intact control striatum (str) and white matter (wm) prior to 7 days (8 days age). It was increased significantly in the ipsilateral (ipsi) striatum and white matter and slightly in the contralateral (contra) white matter 2-7 and 7-28 days respectively after blood injection. (\* $p < 0.05$ ; \*\* $p < 0.01$ , Kruskal-Wallis). The quantity of reactive microglia and macrophages binding RCA-1 lectin was negligible in normal brains at all ages (not shown) and was increased 2 - 7 days following the blood injection. (\* $p < 0.05$ ; \*\* $p < 0.01$  ANOVA). (On legend ICH = intracerebral hemorrhage, Con = control)

## Chapter 2-6

Neonatal mouse brain is more severely damaged than mature brain by injections of blood, thrombin, and plasminogen

Mengzhou Xue, MD

Marc R. Del Bigio, MD, PhD, FRCPC

(Submitted to Brain Pathology July 2004).

## Abstract

The mechanism of brain cell injury associated with intracerebral hemorrhage may be in part related to proteolytic enzymes in blood, some of which are also functional in the developing brain. We hypothesized that there is an age-dependent brain response following intracerebral injection of blood, thrombin, and plasminogen. Mice at three ages (neonatal, 10-day old, and adult) received autologous blood (15, 25, 50  $\mu$ l respectively), thrombin (3, 5, 10 units respectively), plasminogen (0.03, 0.05, 0.1 units respectively) (the doses expected in same volume blood), or saline injection into lateral striatum. Forty-eight hours later mice were perfusion fixed with paraformaldehyde. Hematoxylin and eosin, lectin histochemistry, Fluoro-Jade, and TUNEL staining were used to quantify the volume of damage, as well as neutrophils, microglia, and cell death at the edge of the hemorrhagic lesion. Damage volume, dying neurons, neutrophils, and microglial reaction were significantly greater following injections of blood, plasminogen, and thrombin compared to saline injection in all 3 ages. Plasminogen and thrombin associated brain damage was greatest in neonatal mice and, in that group, greater than the damage caused by whole blood. These results suggest that the neonatal brain is relatively more sensitive to proteolytic plasma enzymes than blood.

## Introduction

Intracerebral hemorrhage (ICH) is a consequence of hypertension, bleeding into an ischemic infarct, rupture of abnormal blood vessels, or trauma. A significant proportion of premature births are also accompanied by bleeding into the brain<sup>27</sup>. The incidence of periventricular/intraventricular hemorrhage (PVH/IVH) increases progressively with decreasing gestational age, e.g. from 1.6% at 38-43 weeks up to 50.0% at 24-30 weeks of gestation<sup>27</sup>. Following ICH, prothrombin<sup>91</sup> and plasminogen<sup>88, 89</sup> in the blood, which are the precursors of thrombin and plasmin, enter the brain substance. Neurons and glia are capable of expressing thrombin receptors<sup>203</sup>, which are most abundant in the neonatal rodent brain<sup>221</sup>. In vitro, thrombin induces apoptosis<sup>204</sup>, causes morphological changes of astrocytes<sup>205</sup>, and causes neurite retraction in cultured neurons<sup>203, 206</sup> likely through protease activated receptors (PARs)<sup>226, 227</sup>. In vivo, injected thrombin causes brain edema<sup>208</sup> perhaps by lysis of vascular basement membrane<sup>315, 317</sup>, inflammation, brain necrosis and apoptosis<sup>38</sup>. Plasmin is produced when plasminogen is cleaved by tissue type (tPA) or urokinase type plasminogen activators (uPA)<sup>316</sup>. In mouse brain, uPA and its receptor are maximally expressed by neurons at 8-10 days<sup>222</sup>. Injected plasmin also causes considerable brain edema<sup>209</sup>, inflammation, and brain cell death<sup>38</sup>. Following brain injury endogenous tPA seems to potentiate neuronal degeneration<sup>228</sup>. Endogenous brain thrombin and plasmin<sup>200-202</sup> are implicated in migration of immature neurons, synaptogenesis, and formation of myelin. Endogenous inhibitors of plasmin and thrombin, including neuroserpin<sup>229</sup>, plasminogen activator inhibitors (PAI) 1 and 2<sup>222</sup>,  $\alpha$ 2-macroglobulin<sup>231, 232</sup>, and protease nexin-1 (PN-1)<sup>378</sup>, are present in developing brain in at generally higher concentrations than mature brain.

We have observed that gene expression in the rat brain following blood injection varies with age (unpublished data). We hypothesized that brain damage related to plasmin and thrombin will be greater in young brains than mature brains. To test the hypothesis we assessed the brain damage and inflammation following intracerebral injections of autologous blood and plasma enzymes in 3 ages of mice. Our previous data in adult rats showed that inflammatory cell infiltration and cell death peak 2-3 days after injection of autologous whole blood into the brain, therefore we chose a survival period of 48 hours<sup>39, 40, 54</sup>. Neonatal (1 - 2 day(s) old) mice have a maturational state of the subependymal zone/ganglionic eminence roughly comparable to 24 - 26 week gestational age human brains<sup>357, 358</sup>. Ten-day old mice are roughly comparable to neonatal human brains. Adult mice (7 weeks) are roughly comparable to young adult human brains<sup>379</sup>.

## Materials and methods

### Experimental group design

All experimental procedures were done in accordance with guidelines of the Canadian Council on Animal Care. Protocols were approved by the local experimental ethics committee. Seventy-four CD-1 mice (Charles River Canada, St. Constant, Quebec) at three ages (neonatal 24-48 hours weighing 1.42 - 1.95 grams; 10 day old weighing 5-7 grams; adult weighing 22-26.5 grams) were used in this study. Young mice were housed with their mothers in litters of ten. Each group consisted of 6 mice (no more than two to three mice from a given litter). There were 12 groups (3 ages with 4 treatments) (Table 2-6-1): saline injection as control, autologous blood injection, thrombin injection, and plasminogen injection.

## Animal model

Neonatal mice were anesthetized by cooling on an ice bed. Ten-day old and adult mice were anesthetized by intraperitoneal injection with ketamine / xylazine (9.0/0.5 mg/kg). Autologous blood was collected in a sterile syringe by placing the tail in warm water for 1 minute, cleaning the skin with 70% alcohol, and cutting 2 mm off the tail tip as previous described<sup>37, 39, 40</sup>. Because the neonatal and 10-day old mice could not be secured in a stereotaxic frame, the brain injections were done by freehand with the needle inserted percutaneously. In 10-day old and adult mice, a midline scalp incision was made. A 27-gauge needle was attached to the syringe and quickly introduced into the right striatum of the mouse brain with a custom-made guide to help stabilize the needle and guide it to the correct depth (in neonatal mice 1.5 mm lateral to midline, 0.5 mm posterior to the outer canthus of the right eye, 2.5 mm deep to the skull surface; in 10 day old mice 2 mm lateral to midline, 1.0 mm posterior to the outer canthus of the right eye, 3.0 mm deep to the skull surface; in adult mice 2.0 mm lateral to midline, 1.5 mm posterior to the outer canthus of the right eye, 3.5 mm deep to the skull surface). The sites of injection were more lateral than those used in our PVH/IVH models<sup>37</sup> because we wanted to avoid blood escape into the lateral ventricles. The volume of injected blood was 15  $\mu$ l in neonatal, 25  $\mu$ l in 10-day old, 50  $\mu$ l in adult mice. Saline, thrombin, and plasminogen solutions were of the same volumes respectively. We chose these volumes so that the hematoma was of similar proportion to the total brain size at all ages. We based our calculation on prior studies that showed the brain weights are approximately 150 mg in neonatal mice, 250 mg in 10-day mice, and 420 mg in adult mice<sup>380, 381</sup>. Thrombin (from

bovine plasma; T-6634, Sigma Chemical Company) (3, 5, 10 units in 3 ages respectively) and plasminogen (from bovine plasma; P-9156, Sigma) (0.03, 0.05, 0.1 units in 3 ages respectively) were administered in doses estimated to be in the equivalent blood volume (Table 2-6-1). We chose plasminogen rather than plasmin because a previous study showed that plasmin potency seemed to be reduced<sup>38</sup>. We calculated the units of thrombin and plasminogen in whole blood based on the following assumptions: plasma volume is ~ 60% total blood volume, each ml plasma contains 260 to 360 units of prothrombin, and 200 µg (1.95 units) plasminogen<sup>347, 348, 382</sup>. Agents were injected over 1 minute; the needle was left in the place for 30 seconds, and then removed slowly. The scalp (in 10-day old and adult mice) was sutured. Physiological monitoring was not practical due to the small size of the mice. All mice were returned to the cages after the procedure, which took approximately 3-5 minutes. Adult mice were placed in a cage (in groups 4-5) with free access to food and water. The syringes were loaded and supplied blindly with thrombin, plasminogen, and saline.

#### Histological evaluation

Mice were overdosed with ketamine / xylazine at 48 hours after injection into brain and perfused through the heart with ice cold 4% paraformaldehyde in 0.1 mol/L phosphate buffered saline (PBS). The brain was removed and stored in the same fixative for 1 - 10 day(s). Fixed brains were cut coronally to surround the injection sites, and the slices were dehydrated and embedded in paraffin. Sections (6 µm) were cut serially through the whole slice, and each 10<sup>th</sup> section was stained with hematoxylin and eosin (H&E). Near the lesion center, where the brain damage was maximal, a variety of

histological and histochemical stains were performed on adjacent sections and the same regions were compared on these sections.

### Histochemistry

Ricinus communis agglutinin lectin (RCA-1) labeling was used to demonstrate reactive microglial cells<sup>269</sup>. Paraffin sections were dewaxed and rehydrated, washed, quenched with 0.3 % H<sub>2</sub>O<sub>2</sub>, blocked with 10 % normal sheep serum, and incubated with biotinylated lectin (diluted 1/2000, Vector Laboratories, Inc., Burlingame, U.S.A.). Slides were then washed, incubated with streptavidin-peroxidase (1/400, Dako Corporation, Carpinteria, CA, USA), colored with diaminobenzidine - H<sub>2</sub>O<sub>2</sub> solution, washed and coverslipped. Control sections were processed with omission of the biotinylated lectin.

### TUNEL

TUNEL (terminal deoxynucleotidyl transferase (TdT)-mediated deoxyuridine triphosphate (dUTP)-biotin nick end labeling) was used to identify dying cells with damaged DNA. Paraffin embedded sections were dewaxed and rehydrated, then incubated in 20 µL/ml proteinase K for 15 minutes. TUNEL was accomplished using *Apoptag in situ* kit (Intergen; Purchase, NY, USA). After immersion in equilibration buffer for 10 minutes, sections were incubated with TdT and dUTP-digoxigenin in a humidified chamber and then incubated in the stop/wash buffer. Sections were washed before incubation in anti-digoxigenin-peroxidase solution (1/500 in PBS), and colored with diaminobenzidine - H<sub>2</sub>O<sub>2</sub> solution. Sections were counterstained with methyl green.

Negative control sections were treated similarly but incubated in the absence of TdT enzyme or dUTP-digoxigenin.

#### Fluoro-Jade staining

Sections of brain were stained with Fluoro-Jade to show dying neurons<sup>189</sup> by incubating sections in 0.06% potassium permanganate for 15 minutes while gently shaking. Then 0.001% Fluoro-Jade (Histo-Chem Inc.; Jefferson, AR) staining solution was applied for 30 minutes, followed by PBS wash, drying in air, and coverslip application.

#### Determination of damaged brain volume

Using H&E stained sections of all affected levels, a "camera lucida" was used to trace the brain damage area, which was defined by the presence of blood, tissue rarefaction, or necrosis. Computerized planimetry was used to measure the cross sectional areas of damage and of brain. The volumes of damaged brain were calculated by adding the areas of damage on all levels multiplied by the distance between sections.

#### Cell counts

Using an ocular reticule and 400x magnification (objective magnification x 40), Fluoro-Jade positive neurons, TUNEL positive dying cells, extravascular neutrophils (identified on H&E sections by characteristic nuclear morphology), and RCA-1 binding cells were counted in 4 fields (each area 540  $\mu\text{m}$  x 540  $\mu\text{m}$ ) immediately adjacent to the needle injection/damage site as previous described (Figure 2-6-1)<sup>38-40, 54</sup>. Areas with

large blood vessels were avoided. Counts were made near the edge of the lesion because the necrotic cores were devoid of viable cells. The cell count and damaged brain areas were blindly measured or calculated by an experienced junior author to minimize the observation bias.

### Statistical Analysis

All data are expressed as mean  $\pm$  SEM. Data were analyzed to ensure normal distribution. The initial test was 2-way analysis of variance (ANOVA) using age and treatment as independent variables. Intergroup comparisons within a given age and between ages were made using Scheffé test. The differences were considered significant when  $p < 0.05$ . We used StatView 5.01 software (SAS Institute; Cary NC).

### Results

Most mice tolerated the surgical procedure well. There were no overt neurological deficits on casual observation. No seizures were observed. There were 2 deaths among 10-day old mice, possibly related to anesthesia, immediately after injection of whole blood and plasminogen (1 each). Following saline injection, only a small area of damaged brain could be seen (Figure 2-6-2A). Brains with saline injection exhibited small collections of blood and negligible edema around the needle tract in the striatum. Following autologous blood injection the irregular hematoma characterized by the presence of edema, blood debris, and necrosis (Figure 2-6-3), was located in striatum (Figure 2-6-2B).

Following injections of plasminogen and thrombin, the volume of damaged brain was large, especially in the neonatal mouse, where hemorrhagic infarction consistently extended into adjacent white matter and cerebral cortex (Figure 2-6-2C, 2-6-2D). Microscopically, brain surrounding the damaged area appeared pale on H&E stain due to edema. Neutrophils were rarely present within the necrotic tissue except at the periphery. Reactive microglia/macrophages with ramified processes and swollen bodies were present in the parenchyma adjacent to the damaged brain tissues and around blood vessels. Fluoro-Jade staining highlighted the dying neurons. TUNEL positive dying cells were also present (Figure 2-6-3).

Age and treatment had significant effects on TUNEL positive cells (ANOVA  $F(\text{age}) = 42.800$ ,  $df = 2$ ,  $p < 0.0001$ ;  $F(\text{treatment}) = 9.599$ ,  $df = 3$ ,  $p < 0.0001$ ;  $F(\text{interaction}) = 5.718$ ,  $df = 6$ ,  $p < 0.0003$ ), on dying neurons (ANOVA  $F(\text{age}) = 145.375$ ,  $df = 2$ ,  $p < 0.0001$ ;  $F(\text{treatment}) = 71.984$ ,  $df = 3$ ,  $p < 0.0001$ ;  $F(\text{interaction}) = 53.798$ ,  $df = 6$ ,  $p < 0.0001$ ), and on neutrophils (ANOVA  $F(\text{age}) = 52.295$ ,  $df = 2$ ,  $p < 0.0001$ ;  $F(\text{treatment}) = 43.682$ ,  $df = 3$ ,  $p < 0.0001$ ;  $F(\text{interaction}) = 22.530$ ,  $df = 6$ ,  $p < 0.0001$ ). RCA-1 labeling was influenced by treatment ( $F = 13.620$ ,  $df = 13.620$ ,  $p < 0.0001$ ) but not age ( $F = 1.009$ ,  $df = 1.009$ ,  $p = 0.375$ ) and there was no interaction effect ( $F = 0.614$ ,  $df = 6$ ,  $p = 0.717$ ). Total brain damaged volume and damaged area on the most severely affected level were highly correlated ( $r = 0.897$ ,  $p < 0.0001$ ). Damaged area (ANOVA,  $F(\text{treatment}) = 7.658$ ,  $df = 3$ ,  $p < 0.0005$ ;  $F(\text{age}) = 6.605$ ,  $df = 2$ ,  $p < 0.005$ , respectively) and damaged volume (ANOVA,  $F(\text{treatment}) = 7.099$ ,  $df = 3$ ,  $p < 0.0008$ ;  $F(\text{age}) = 8.895$ ,  $df = 2$ ,  $p < 0.0008$ , respectively) were influenced by treatment and age and there were no interaction effects (ANOVA,  $F(\text{area}) = 2.036$ ,  $df = 6$ ,  $p = 0.0877$ ,  $F(\text{volume}) = 1.356$ ,  $df = 6$ ,  $p = 0.2602$ ,

respectively). The proportionate damage was used because the doses were adjusted in proportion to the brain size. There was a significant interaction effect between age and treatment (ANOVA,  $F(\text{treatment}) = 9.557$ ,  $df = 3$ ,  $p = 0.0001$ ;  $F(\text{age}) = 16.288$ ,  $df = 2$ ,  $P < 0.0001$ ;  $F(\text{interaction}) = 5.843$ ,  $p = 0.0003$ ) indicating that the immature brain is relatively more sensitive to the blood and enzyme injections. Intergroup comparisons showed that brain damage volumes, as well as dying cells and inflammation in adjacent non-necrotic striatum were significantly greater following whole blood, thrombin, and plasminogen injections compared to saline injection (Figures 2-6-4, 2-6-6). These destructive and reactive changes were roughly proportionate to the total volume of injury. Only small volumes of damaged brain were presented in brains that received saline injection (Figure 2-6-4). Injections of blood and plasma enzymes caused proportionally larger volumes of damage in neonatal mice than in 10-day old and adult mice. TUNEL positive dying cells were infrequently seen in striatum of the normal control brain in neonatal group and never in the older mice. No Fluoro-Jade positive dying neurons were apparent in normal brains (Figure 2-6-3). The quantities of TUNEL positive cells and dying neurons were greater following the injections of blood, plasminogen, and thrombin compared to saline control injection (Figure 2-6-5). TUNEL positive cells were significantly more abundant after plasminogen injection compared to blood injection in the neonatal group. The quantity of dying neurons was significantly greater after plasminogen and thrombin injection compared to blood injection in the neonatal group. In contrast, dying neurons were significant fewer following plasminogen and thrombin injection compared to blood injection in 10 days and adult mouse groups. Neutrophils and microglia/macrophages were more abundant adjacent to damaged brain 48 hours

after blood, plasminogen, and thrombin injection compared to saline control group in all 3 age groups. In the neonatal group, the neutrophils and microglia / macrophages were significantly greater after plasminogen injection compared to blood injection (Figure 2-6-6).

## Discussion

Intracerebral hemorrhage causes brain damage through multiple mechanisms <sup>259</sup>. Direct tissue destruction by the hemorrhagic event and dissection of blood along tissue planes occurs immediately. This is followed by development of edema and secondary brain damage due to raised intracranial pressure and distortion of the microvasculature. The enzymes involved in blood clotting and clot lysis are potentially toxic in the first day following ICH <sup>92</sup>. Delayed damage could result through a variety of mechanisms including local ischemia, release of toxins by blood breakdown products, proteolytic enzymes, or inflammatory cell action which including cytokines, chemokines, and leukocytes <sup>38, 42, 53, 54, 259</sup>. Blood clot and damaged brain cells after blood injection liberate chemotactic factors, including thrombin <sup>272</sup>, that prompt the movement of leukocytes from the blood into the insulted brain <sup>273</sup>. It is possible that the activated leukocytes can cause secondary brain damage through the release of cytokines, reactive oxygen species, nitric oxide, matrix metalloproteinases (MMPs), and other proteases <sup>275, 276</sup>.

In this study, the sites of intracerebral injection were more lateral than those we used in a previously reported PVH/IVH model <sup>37</sup> because we wanted to avoid blood entry into the lateral ventricles. Consequently we observed more inflammation and more parenchymal damage. This may be because the toxic substances were not washed away

by cerebrospinal fluid. The main finding in this experiment was that injections of blood, thrombin, and plasminogen caused relatively more brain damage in neonatal mouse brain than in 10-day old or adult mouse brain. Furthermore, the neonatal mouse brain is relatively more sensitive to serine proteases involved in blood clotting than to whole blood. Thrombin converts fibrinogen into fibrin, which causes the blood to clot. Plasmin digests fibrin to allow lysis of blood clots. Thrombin receptors, PAR-1 and PAR-2 are located on neurons and endothelia of brain<sup>221, 226, 323, 324</sup>. These receptors can be activated by low concentrations of thrombin<sup>227</sup>. Through these receptors, thrombin causes retraction of cell processes of cultured neurons<sup>206</sup> and is toxic to neurons in brain slices in a dose-dependent manner<sup>326</sup>. Thrombin and plasmin can induce endothelin synthesis and subsequent vasospasm and ischemia<sup>334-336</sup>. Why is the brain damage more severe in neonatal mice? The possible reasons include a) immature cells in neonatal brain might be more sensitive to blood borne agents including thrombin and plasminogen; b) toxic substances associated with the hematoma might diffuse more broadly in neonatal brain due to its higher water content; c) the neonatal brain vasculature might be more fragile because the stroma is incomplete<sup>15</sup>. Thrombin and plasminogen are normally present in the brain at low concentrations<sup>203</sup>, especially during development and during reactive changes<sup>221</sup>. It has also been shown that adult mice deficient in tPA, in which plasmin is less activated, are less susceptible to neuronal injury following brain ischemia<sup>318</sup> or excitotoxin injection<sup>344</sup>. In addition to dissolving fibrin, plasmin is known to directly degrade a range of extracellular matrix proteins of vascular basal lamina as well as elastin and to activate MMPs, which can also digest matrix proteins<sup>328, 337</sup>. Damage to immature vessel walls might explain the widespread hemorrhagic infarct in the middle cerebral

artery distribution of neonatal brain following thrombin and plasmin injections. PAI-1, the major regulator of plasminogen activation exists in brain only in very small quantities<sup>341</sup>, although they tend to be more highly expressed in the young brain, perhaps to control proteolysis involved in development<sup>222, 229, 231, 232, 378</sup>. The endogenous inhibitors of proteolytic enzymes can also be upregulated following experimental brain damage<sup>342</sup>. However, they probably are insufficient and cannot respond quickly to deal with the large amounts of plasmin and thrombin released following hemorrhage.

Although the quantity of TUNEL positive cells and dying neurons defined by Fluoro-Jade staining were similar, they might not reflect the same cell populations. TUNEL positive cells might understate the magnitude of cell death because they persist only for several hours<sup>279</sup> while dying neurons can persist for days or weeks<sup>280</sup>. Furthermore, TUNEL positive cells include neurons, glia, and inflammatory cells, therefore, the quantity does not necessarily reflect the final neurological injury<sup>281</sup>. Following autologous blood injection into adult rat brain we found that most TUNEL positive cells are not neurons<sup>215</sup>.

There were several shortcomings in this experiment. First, we have no way of determining whether the proteolytic activity is representative of what actually occurs following hemorrhage. We injected plasminogen instead of plasmin because some plasmin activity seems to be lost when it is purified in the post-activated form; the plasminogen is presumed to be activated *in situ*<sup>38</sup>. Furthermore, the activity of thrombin at a particular site can be very difficult to predict because it is self-amplifying as well as rapidly inactivated by binding to fibrin<sup>329, 331</sup>. Second, the plasminogen and thrombin that we used were bovine proteins and we cannot exclude the contribution of an immune

response to foreign proteins. Third, the neonatal and young mice are very small. Therefore, the method of freehand blood injection could cause variable brain damage. Histological examination revealed that the injections were not entirely consistent in terms of depth. Nevertheless, our histological assessments were in similar striatal areas and therefore the quantification is likely valid. Fourth, we did not assess long-term outcomes to determine if the response in older animals is delayed<sup>38</sup>, although based on our prior work we think that is unlikely. Fifth, ketamine, which we used as an anesthetic in the older animals, is a potentially neuroprotective glutamate antagonist<sup>383</sup>. In the future we might use other types of anesthesia, such as halothane or isoflurane. Sixth, the water-contained in neonatal mouse brain is much higher than in the old mice. This could have affected the age-related results because the toxic substance in the hematoma easily spread.

In summary, the results demonstrate that injections of blood, thrombin, and plasminogen into mouse brain are associated with cell death and inflammation in an age dependent manner. There is no age effect on microglia /macrophages. The neonatal brain could be most susceptible because the blood vessels are more fragile, or because it has higher levels of PARs on immature cells, or because the immature cells are more susceptible to proteolytic damage independent of specific receptors. Due to the rapid evolution, the likely mechanism of damage is uncontrolled proteolytic digestion of neurons, glia, and vascular cells. This observation complements Kolb's findings that the neonatal rat brain recovers less than juvenile or adult brains following cortical aspiration<sup>246, 384, 385</sup>. Thrombin and plasmin in the blood might play an important role in premature

neonatal brain injury that follows brain hemorrhage, and therefore represent potential targets for therapeutic intervention.

Table 2-6-1. Experimental intracerebral injections into CD1 mouse brains.

	Saline	Blood	Thrombin	Plasminogen
Neonatal mouse	15 $\mu$ l (n = 6)	15 $\mu$ l (n = 6)	3 units in 15 $\mu$ l (n = 6)	0.03 units in 15 $\mu$ l (n = 6)
10-day old mouse	25 $\mu$ l (n = 6)	25 $\mu$ l (n = 6)	5 units in 25 $\mu$ l (n = 6)	0.05 units in 25 $\mu$ l (n = 6)
Adult mouse	50 $\mu$ l (n = 6)	50 $\mu$ l (n = 6)	10 units in 50 $\mu$ l (n = 6)	0.1 units in 50 $\mu$ l (n = 6)

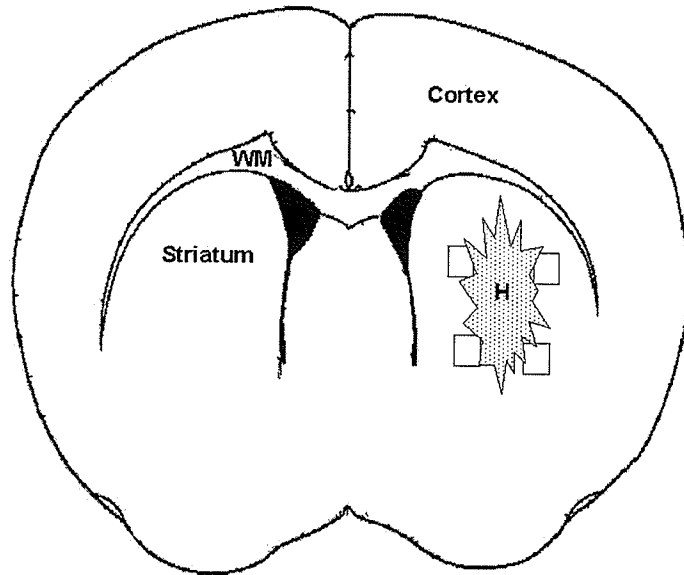


Figure 2-6-1. Schematic diagram of mouse brain in coronal section showing the cerebral cortex, striatum, and white matter (WM). The hematoma (H) represents the site where the whole blood, thrombin, and plasminogen were injected. Neutrophils, RCA-1 labelled microglia/macrophages, TUNEL positive cells, and Fluoro-Jade stained neurons were counted in striatum adjacent to the injection site (squares).

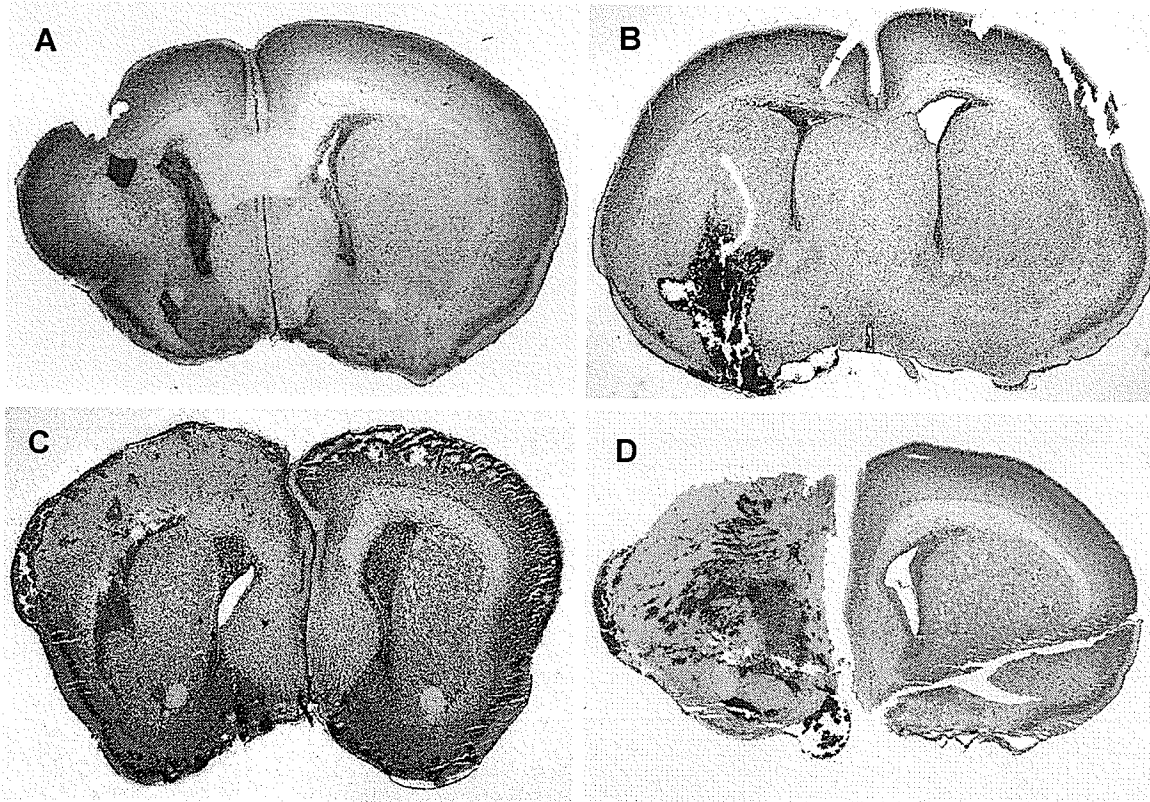


Figure 2-6-2. Low magnification photomicrographs of neonatal mouse brain coronal sections 48 hours after injection of 15  $\mu$ l of saline (2A), autologous whole blood (2B), plasminogen (2C), and thrombin (2D). After saline injection, there is small quantity of blood in the striatum. Blood injection is associated with a localized hematoma. After plasminogen and thrombin injection, the damage areas are large; hemorrhagic infarcts extend to the white matter and cerebral cortex.

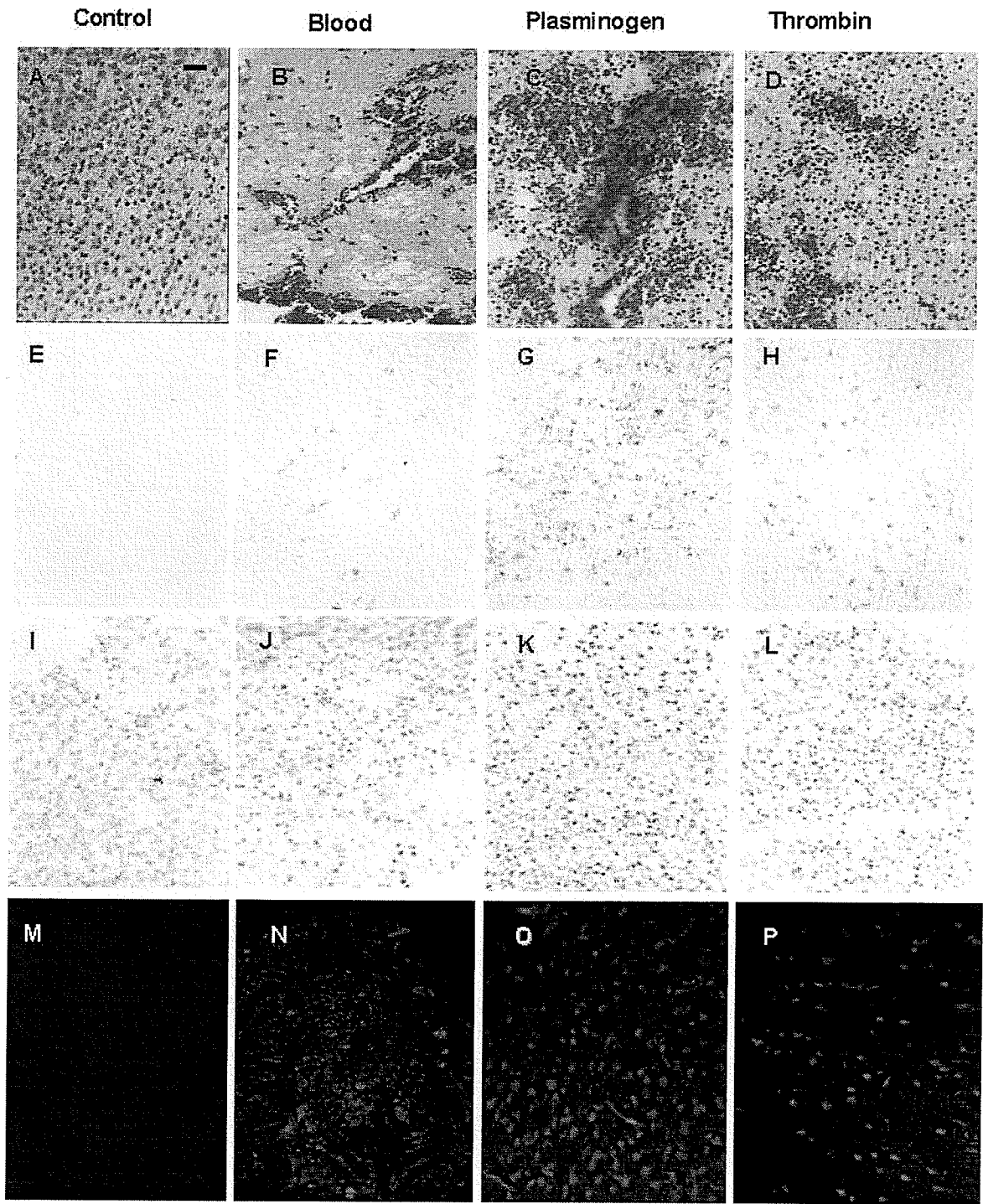


Figure 2-6-3. Photomicrographs showing histopathologic features 48 hours following injections into neonatal mouse brain. Intact neonatal medial striatum exhibits tightly packed immature neurons (A). Damaged striatum after blood (B), plasminogen (C), and thrombin (D) injection exhibits fewer neurons, collections of erythrocytes, and pallor due to edema. RCA-1 lectin staining demonstrates negligible microglial cells in intact striatum (E), mild accumulation of activated microglia / macrophages in striatum after blood injection (F), and more substantial collections associated with plasminogen (G) and thrombin (H) injection. TUNEL demonstrates rare dying cells (brown) in intact neonatal striatum (I), and many dying cells in striatum after blood (J), plasminogen (K), and thrombin (L) injection. Fluoro-Jade shows no dying neurons in normal brain (M), and an increased quantity of dying neurons adjacent to the blood (N), plasminogen (O), and thrombin (K) injection sites. Bar = 50  $\mu$ m.

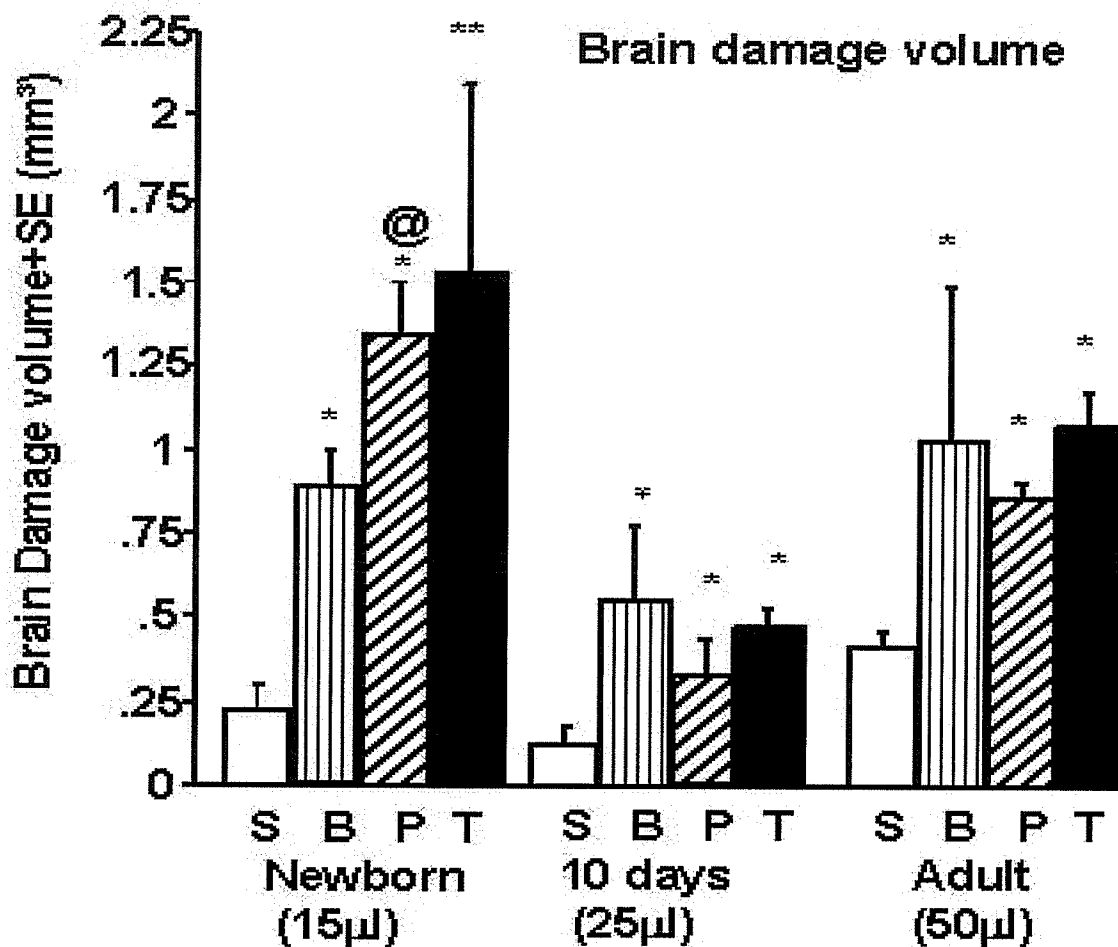


Figure 2-6-4. Bar graphs showing the brain damage volume in mouse brains 48 hours following saline, blood, plasminogen, and thrombin injections. There is a significantly larger volume of brain damage following the injection of plasminogen in newborn mice compared to 10-day old and adult mice (@ $p < 0.001$ , ANOVA using age as independent variable). The volumes of damaged brain were greater after blood, plasminogen, and thrombin injection compared to saline control in all 3 ages. (\* $p < 0.05$ ; \*\* $p < 0.01$ , ANOVA with Scheffé post hoc intergroup comparisons). Abbreviations: S = saline, B = blood, P = plasminogen, T = thrombin.

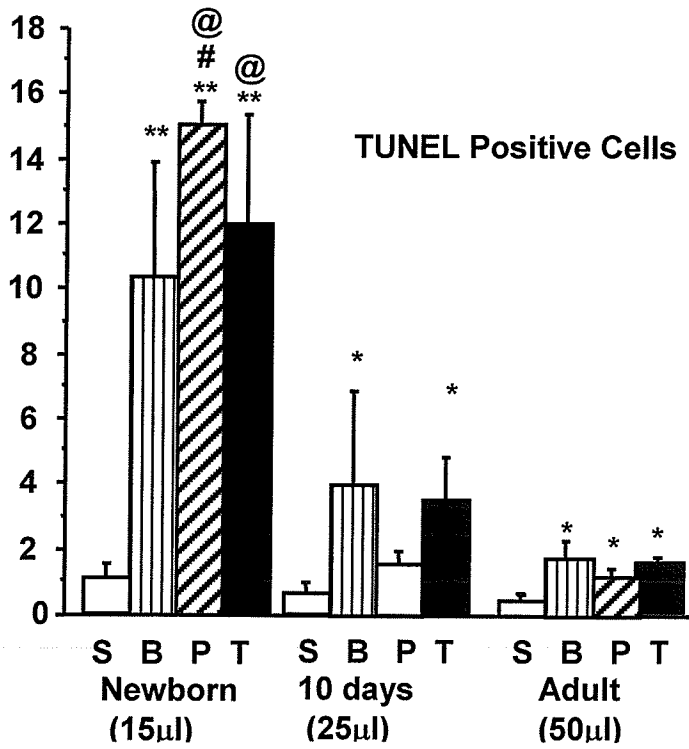
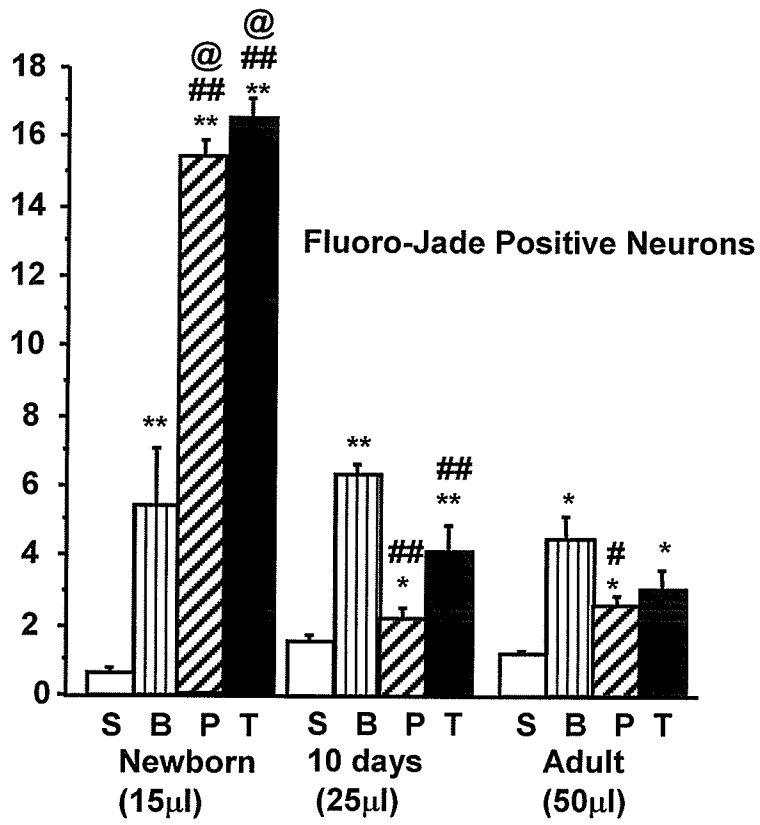


Figure 2-6-5. Bar graphs showing dying neurons (per 4 x 540 x 540  $\mu\text{m}^2$  area) detected by Fluoro-Jade staining (upper panel) and cell death detected by TUNEL (lower panel), in mouse striatum 48 hours after saline, blood, plasminogen, and thrombin injections. There is a significantly larger number of dying neurons and TUNEL positive cells following the injection of plasminogen and thrombin in newborn mice compared to 10-day old and adult mice (@ $p < 0.001$ , 2-way ANOVA using age as independent variable). The number of dying neurons and TUNEL positive cells were greater adjacent to the blood, plasminogen, and thrombin injection sites compared to saline control (\* $p < 0.05$ ; \*\* $p < 0.01$ , \*, \*\* compared to saline, ANOVA with Scheffé post hoc intergroup comparisons). Dying neurons were significantly more abundant after plasminogen and thrombin injections compared to blood injection in the neonatal group, whereas there were significantly fewer dying neurons after plasminogen and thrombin injection compared to blood injection in 10-day old and adult mice (# $p < 0.05$ ; ## $p < 0.01$ , #, ## compared to blood, ANOVA with Scheffé post hoc intergroup comparisons). The number of TUNEL positive cells exhibited a similar pattern of differences. Abbreviations: S = saline, B = blood, P = plasminogen, T = thrombin.

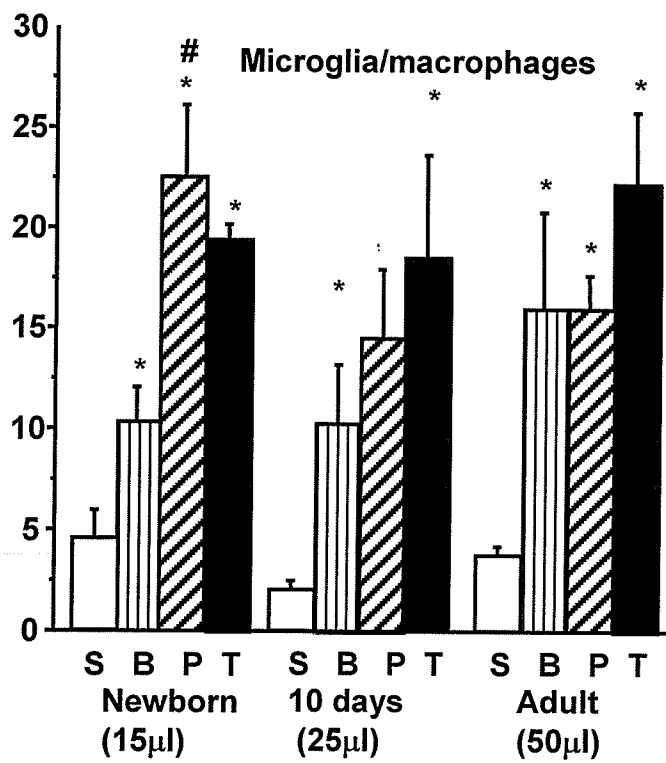
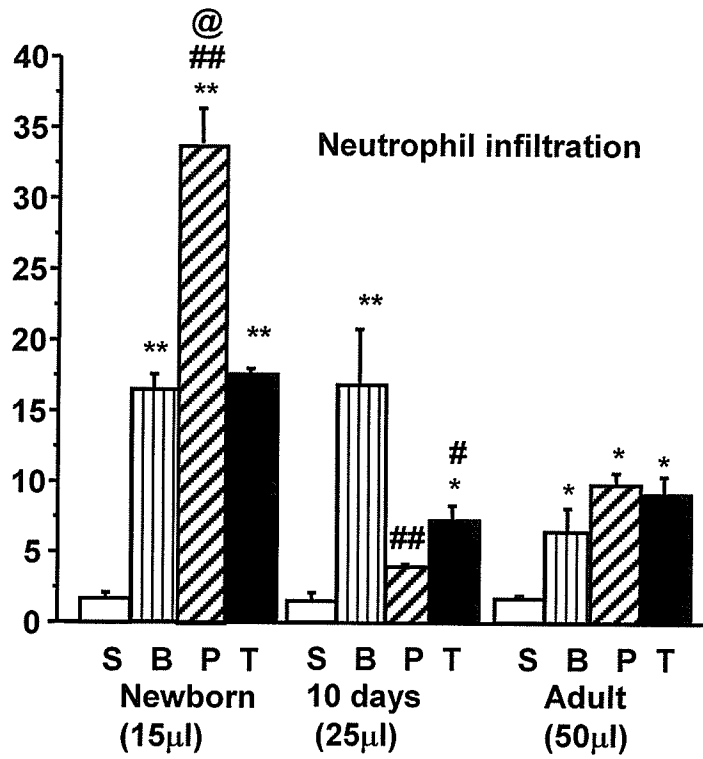


Figure 2-6-6. Bar graphs showing neutrophil infiltration (per  $4 \times 540 \times 540 \mu\text{m}^2$  area, upper panel) and microglia/macrophages reaction (lower panel) in mouse striatum 48 hours after injections. Rare inflammatory cells were apparent in saline control brains. There is a significantly larger number of neutrophils with the injection of plasminogen in newborn mice compared to 10-day old and adult mice (@ $p < 0.001$ , 2-way ANOVA using age as independent variable). There is no difference in number of microglia/macrophages in the 3 ages. The number of neutrophils and microglia/macrophages were greater adjacent to the blood, plasminogen, and thrombin injection sites ( $*p < 0.05$ ;  $**p < 0.01$ , \*, \*\* compared to saline, ANOVA with Scheffé post hoc intergroup comparisons). The number of neutrophils was significantly greater after plasminogen injection compared to blood injection in the neonatal group. The number of neutrophils was significantly lower after plasminogen and thrombin injection compared to blood injection in the 10-day old group ( $\#p < 0.05$ ;  $\#\#p < 0.01$ , #,  $\#\#$  compared to blood, ANOVA with Scheffé post hoc intergroup comparisons). Abbreviations: S = saline, B = blood, P = plasminogen, T = thrombin.

Chapter 2-7

Immune preactivation exacerbates hemorrhagic brain injury in immature mouse brain.

Mengzhou Xue, MD

Marc R. Del Bigio, MD, PhD, FRCPC

(Submitted to Stroke June 2004).

## Abstract

**Background and Purpose:** Premature infants with placental infection and adult stroke patients with fever have worse outcome following intracerebral hemorrhage (ICH). We hypothesized that immune pre-activation would aggravate brain injury in mouse brain following ICH.

**Methods:** The immune systems of 2-day, 10-day old and adult CD1 mice were stimulated by intraperitoneal injection of concanavalin A (ConA, 10 mg/kg), lipopolysaccharide (LPS, 1 mg/kg) or polyinosinic-polycytidilic acid (PolyI:C 4 mg/kg), with saline as a control, 12 hours prior to intracerebral injection of autologous blood (15, 25, 50  $\mu$ l respectively in the three ages,). In addition, adult interferon-gamma (IFN- $\gamma$ ) knockout and C57B/6 wild-type controls received intracerebral blood injections (50  $\mu$ l). Mice were perfusion fixed 48 hours later. The area of brain damage and the quantity of neutrophils, microglia/macrophages, and dying cells at the edge of the brain lesion were determined.

**Results:** LPS acutely reduced body temperature and suppressed circulating mononuclear leukocytes in adult mice. LPS significantly increased the brain damage and inflammation in neonatal mice following ICH. PolyI:C significantly increased inflammation and neuronal death in 10-day old mice. ConA significantly increased neutrophils in neonatal and 10-day old mice and cell death in neonatal mice. IFN- $\gamma$  knockout mice exhibited significantly fewer neutrophils and dying cells in the brain.

**Conclusions:** These data suggest that immune pre-activation aggravates hemorrhagic brain injury in mouse. IFN- $\gamma$  might play a role following brain inflammation in ICH.

**KEYWORDS:** cerebral hemorrhage, infection, interferon gamma, prematurity

Intracerebral hemorrhage (ICH) may be associated with hypertension, coagulopathy, brain trauma, or premature birth. The magnitude of inflammation is greater in hemorrhagic brain lesions than in non-hemorrhagic brain lesions <sup>40</sup>. Systemic illness including maternal/placental and fetal infection can predispose to neurological injury in the premature infant <sup>386</sup>. Fever following ICH in adults is associated with poor outcome <sup>310</sup>. Systemic stimulation with lipopolysaccharide (LPS, endotoxin), a constituent of gram-negative bacteria, provides a strong stimulus for leukocytes, brain endothelium and microglia <sup>387</sup>. It induces production of cytokines, adhesion molecules, and chemoattractants <sup>388</sup>. Polyinosinic-polycytidilic acid (polyI:C) enhances the peripheral activity of natural killer (NK) cells, increases IFN- $\gamma$  production and promotes lymphocyte adhesion to endothelium <sup>389</sup>. IFN- $\gamma$  is a pleotropic cytokine released by T-lymphocytes and NK cells. It also plays a role in brain inflammatory responses <sup>390</sup>. Concanavalin A (ConA) promotes polyclonal activation of T cells <sup>391</sup>.

We hypothesized that immune pre-activation would aggravate brain damage in mouse brain following experimental hemorrhage at various ages. We used 2-day old mice in which the maturational state of the subependymal zone/ganglionic eminence is comparable to 24-26 week gestational age human brains <sup>358</sup>, 10-day old mice that are comparable to newborn human brains <sup>379</sup>, and young adult mice. Furthermore, we investigated experimental brain hemorrhage in IFN- $\gamma$  knockout mice. Our previous experiments showed that inflammatory cell infiltration and cell death peak 2-3 days after injection of autologous blood into the rat brain, therefore we chose a survival period of 2 days for our analyses <sup>54</sup>.

## Materials and methods

### Animal preparation

All experimental procedures were done in accordance with guidelines of the Canadian Council on Animal Care. Protocols were approved by the local experimental ethics committee. One hundred and eight CD1 mice of mixed gender (Charles River Canada, St. Constant, Quebec) (2-day, 10-day old, and 7-week adult) were used. An additional 9 female adult C57BL/6 wild-type mice and 9 IFN- $\gamma$  knockout mice were used (Jackson Laboratory, Bar Harbor, ME).

### Drug administration

Twelve hours prior to autologous blood injection into brain, ConA, (C-2010, Sigma, 10 mg/kg), LPS (*Escherichia coli* serotype 055:B5 lot L-2637, Sigma, Mississauga, ON, 1 mg/kg), and PolyI:C (INC Biomedicals, Aurora, OH 4 mg/kg) dissolved in pyrogen-free 0.9% sodium chloride solution were administered intraperitoneally in volumes of 7, 28, and 100 $\mu$ L/mouse (2-day, 10-day, and adult respectively). The doses of the immune stimulators were based on previous studies<sup>387, 389, 392, 393</sup>. Controls received an equal volume of vehicle. The agents were provided in coded syringes so that the experimenter was blinded.

### Intracerebral hemorrhage model

Two-day old mice were anesthetized by cooling, and 10-day old and adult mice were anesthetized by intraperitoneal ketamine/xylazine (9.0/0.5 mg/kg). Autologous blood was collected in a sterile syringe by placing the tail in warm water, cleansing the

skin with 70% alcohol, and cutting 2 mm off the tail tip<sup>37</sup>. Because the 2-day old and 10-day old mice could not be secured in a stereotaxic frame, injections were done freehand with the needle inserted percutaneously. In 10-day old and adult mice, a midline scalp incision was made. A 27-gauge needle was attached to the syringe and quickly introduced into the right striatum with a custom-made guide to help stabilize and guide the needle to the correct depth (in neonatal mice 1.5 mm lateral, 0.5 mm posterior to the outer canthus of the eye, 2.5 mm deep; in 10 day old mice 2 mm lateral, 1.0 mm posterior to the outer canthus of the eye, 3.0 mm deep; in adult mice 2.0 mm lateral, 1.5 mm posterior to the outer canthus of the eye, 3.5 mm deep). The sites of injection were more lateral than those used in our periventricular/intraventricular hemorrhage model<sup>37</sup> because we wanted to avoid blood escape into the lateral ventricles. The volume of injected blood was 15  $\mu$ l in neonatal, 25  $\mu$ l in 10-day old, 50  $\mu$ l in adult mice. These volumes are proportionate to the brain weight (approximately 150 mg in 2-day, 250 mg in 10-day, and 420 mg in adult mice<sup>381</sup>). Blood was injected over 1 minute and the needle was left in the place 30 seconds. The scalp of 10-day old and adult mice was sutured. The 2-day and 10-day old mice were housed with their mothers in litters of 10. Four to 5 adult mice were placed in a cage with free access to food and water. Each experimental group for histological studies consisted of 6 mice (2-3 mice from each litter).

#### Temperature measurement

An additional 36 mice (12 each age) received the same drug doses to assess the effect on body temperature. Rectal temperature monitoring was not safe in the young mice. Therefore in all ages temperature was measured with a thermocouple probe

(Anritherm, Anritsu Meter) placed in the axilla, acknowledging that this likely does not reflect brain temperature; we were more interested in the systemic effects of immune stimulators. Temperature was measured before the intraperitoneal injection and every 2 hours in for 8 hours (9 am to 5 pm) then every 4 hours for 24 hours. The ambient room temperature was 24°C

#### Blood samples

At the time of sacrifice 2 days after surgery, ~250µl cardiac blood from adult mice was placed in heparinized containers then subjected to complete blood count (Coulter blood cell counter in the hematology laboratory of the Winnipeg General Hospital). We could not get sufficient blood from the young mice.

#### Histological evaluation

Mice were overdosed with ketamine/xylazine 2 days after intracerebral blood injection and perfused through the heart with ice-cold 4 % paraformaldehyde in 0.1M PBS. Fixed brains were cut in the coronal plane surrounding the injection sites, dehydrated and embedded in paraffin. Sections (6 µm) were cut serially through the slice and each 20<sup>th</sup> section was stained with hematoxylin and eosin (H&E). Near the lesion center where the brain damage was maximal additional histological stains were performed <sup>37, 54</sup>. Briefly, to demonstrate reactive microglial cells <sup>269</sup> dewaxed and rehydrated sections were incubated with biotinylated Ricinus communis agglutinin lectin (RCA-1) (diluted 1/2000, Vector Laboratories, Inc., Burlingame, U.S.A.) followed by streptavidin-peroxidase (1/400, Dako Corporation, Carpinteria, CA, USA) and

diaminobenzidine - H<sub>2</sub>O<sub>2</sub> solution. Control sections were processed with omission of the lectin. Terminal deoxynucleotidyl transferase (TdT)-mediated deoxyuridine triphosphate (dUTP)-biotin nick end labeling (TUNEL) was used to identify dying cells with damaged DNA using *Apoptag in situ* kit (Intergen; Purchase, NY, USA). Negative control sections were incubated in the absence of TdT enzyme or dUTP-digoxigenin. Fluoro-Jade staining was used to show dying neurons<sup>189</sup> by incubating sections in 0.06% potassium permanganate followed by 0.001% Fluoro-Jade (Histo-Chem Inc.; Jefferson, AR). To evaluate astrocyte reaction in the IFN- $\gamma$  experiment dewaxed sections were incubated with rabbit anti-cow GFAP (glial fibrillary acidic protein) polyclonal antibody (diluted 1/1000, Dako) followed by biotinylated goat anti-rabbit IgG (1/300), streptavidin-peroxidase (1/400), and diaminobenzidine - H<sub>2</sub>O<sub>2</sub> solution. Control sections were processed without the primary antibody.

#### Assessment of brain damage

A "camera lucida" was used to draw the maximal area of brain damage, which was defined by the presence of blood, tissue rarefaction, or necrosis, and computerized planimetry was used to measure the area. Proportionate damage was calculated by dividing the damage area by cerebrum area. Using an ocular reticule and 400x ocular magnification, Fluoro-Jade positive neurons, TUNEL positive dying cells, neutrophils (identified on H&E sections by characteristic nuclear morphology), and RCA-1 binding cells were counted in 4 fields (each area 540 $\mu$ m x 540 $\mu$ m) immediately adjacent to the needle injection/damage site as previous described<sup>40, 54</sup>. Counts were made along the edge of the lesion because the necrotic cores were devoid of viable cells.

## Statistical Analysis

All quantitative data were determined by the junior author, who was blinded to the nature of the treatment. All data are expressed as mean  $\pm$  SEM. Data were analyzed to ensure normal distribution. The initial test was 2-way analysis of variance (ANOVA) using age and treatment as independent variables. Intergroup comparisons within a given age and between ages were made using Scheffé test. IFN- $\gamma$  knockout and wild-type adults were compared using unpaired t-test. The differences were considered significant when  $p < 0.05$ . We used StatView 5.01 software (SAS Institute; Cary NC).

## Results

During the 28-hour recording period, there was a gradual variation in body temperature of the control adult mice, a reflection of diurnal rhythm. Younger mice had lower and more stable temperatures, probably reflecting their susceptibility to ambient conditions (Figure 2-7-1). In adults, there was significant hypothermia at 6 hours after LPS, but not after ConA or PolyI:C. There was no significant change in temperature of 2-day and 10-day old mice (Figure 2-7-1). The quantities of total white blood cells and lymphocytes in adult mice were significantly lower after LPS. The quantity of monocytes was significantly lower after ConA (Figure 2-7-2). There was no significant change in hemoglobin, although hematocrit was significantly lower after ConA and LPS (not shown). There was no mortality following injections of immune stimulators or intracerebral blood. In all groups, damaged striatum surrounding the hematoma appeared pale and microscopically one could identify edema, blood debris, and necrosis.

Neutrophils were present at the periphery. Reactive microglia/macrophages were present in the parenchyma adjacent to the damaged brain and around blood vessels. Fluoro-Jade staining highlighted the dying neurons and TUNEL demonstrated all types of dying cells.

Age and treatment had significant effects on dying neurons (ANOVA,  $F(\text{age}) = 22.389$ ,  $df = 2$ ,  $p = 0.0001$ ;  $F(\text{treatment}) = 10.743$ ,  $df = 3$ ,  $p < 0.0001$ ;  $F(\text{interaction}) = 2.533$ ,  $df = 6$ ,  $p = 0.0349$ ), on proportionate damaged area (ANOVA  $F(\text{treatment}) = 3.586$ ,  $df = 3$ ,  $p = 0.0214$ ;  $F(\text{age}) = 9.640$ ,  $df = 2$ ,  $p = 0.0004$ ;  $F(\text{interaction}) = 2.259$ ,  $df = 6$ ,  $p = 0.0460$ ). TUNEL positive cells (ANOVA,  $F(\text{age}) = 8.047$ ,  $df = 2$ ,  $p = 0.0011$ ;  $F(\text{treatment}) = 11.095$ ,  $df = 3$ ,  $p < 0.0001$ ), neutrophils (ANOVA,  $F(\text{age}) = 10.934$ ,  $df = 2$ ,  $p = 0.0002$ ;  $F(\text{treatment}) = 11.246$ ,  $df = 3$ ,  $p < 0.0001$ ), and damaged area (ANOVA,  $F(\text{treatment}) = 3.250$ ,  $df = 3$ ,  $p = 0.0311$ ;  $F(\text{age}) = 7.289$ ,  $df = 2$ ,  $p = 0.0019$ ) and were influenced by treatment and age and there were no significant interaction effects (ANOVA,  $F(\text{TUNEL}) = 1.996$ ,  $df = 6$ ,  $p = 0.0878$ ;  $F(\text{neutrophil}) = 1.816$ ,  $df = 6$ ,  $p = 0.1192$ ;  $F(\text{area}) = 1.780$ ,  $df = 6$ ,  $p = 0.1266$ , respectively). RCA-1 labeling was influenced by treatment (ANOVA,  $F = 20.338$ ,  $df = 3$ ,  $p < 0.0001$ ) but not age ( $F = 1.578$ ,  $df = 2$ ,  $p = 0.2184$ ) and there was an interaction effect ( $F = 6.394$ ,  $df = 6$ ,  $p < 0.0001$ ).

In 2-day old mice, the absolute and proportionate brain damage areas due to blood injection were significantly increased after LPS stimulation and tended to increase after ConA. No difference was observed in the other ages (Figure 2-7-3). Neutrophil infiltration and microglia/macrophage reactions were greater after LPS and PolyI:C stimulation in the 2-day and 10-day old brains. In adults, ConA and LPS were associated with more microglial reaction (Figure 2-7-4). The number of dying cells detected by TUNEL was increased in 2-day old mice after Con A, LPS, and PolyI:C stimulation

(Figure 2-7-5). Dying neurons detected by Fluoro-Jade were significantly more abundant in the 2-day old brain after stimulation with LPS and in the 10-day old and adult mice brain after stimulation with PolyI:C (Figure 2-7-5).

In IFN- $\gamma$  knockout mice the number of infiltrating neutrophils and TUNEL positive dying cells adjacent to the hematoma were significantly fewer compared to C57BL/6 wild-type mice (Figure 2-7-6).

## Discussion

ICH causes brain damage through multiple mechanisms <sup>259</sup>. Delayed brain damage could result through a variety of mechanisms including inflammation <sup>38, 54</sup>. In this study, cellular damage and inflammation caused by blood injection into mouse brain were aggravated by immune pre-stimulation with LPS, ConA, and PolyI:C. The effect was especially strong in neonatal mice. LPS produced transient hypothermia, which has been shown to correlate with elevated plasma TNF $\alpha$  <sup>394</sup>. LPS also caused leukocytopenia, which is likely mediated by enhanced interaction between leukocytes and endothelium <sup>395</sup>. Stimulated inflammatory cells included in the hematoma and those infiltrating brain from blood could release oxygen free radicals, nitric oxide, endothelin-1, prostaglandin I<sub>2</sub> and H<sub>2</sub>, tumor necrosis factor alpha (TNF $\alpha$ ) and IFN- $\gamma$ , which are harmful to brain cells <sup>79</sup>. Systemic administration of cytokines interleukin (IL)-1 $\beta$ , IL-6, IL-9, and TNF- $\alpha$  exacerbate brain lesions in 5-day old mice following intracerebral injection of ibotenate <sup>396</sup>. We observed that IFN- $\gamma$  knockout mice had significantly reduced neutrophil infiltration and cell death compared to wild-type control mice following ICH. IFN- $\gamma$  can enhance the microbicidal activity of macrophages, activate cytotoxic T cells and NK

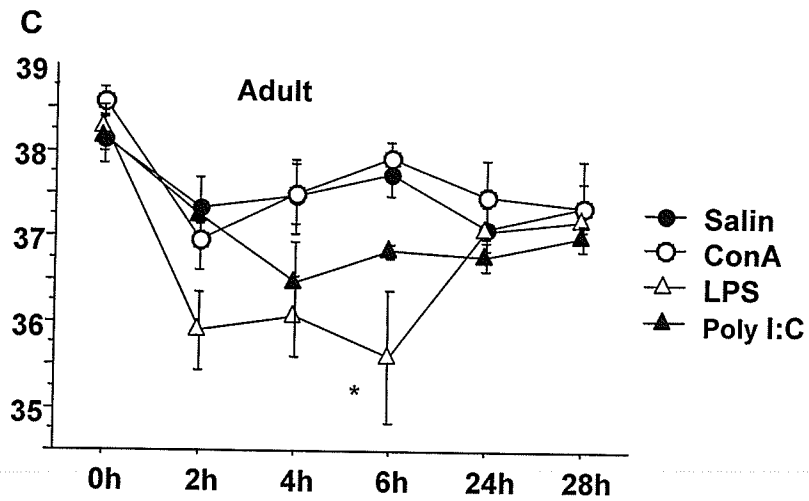
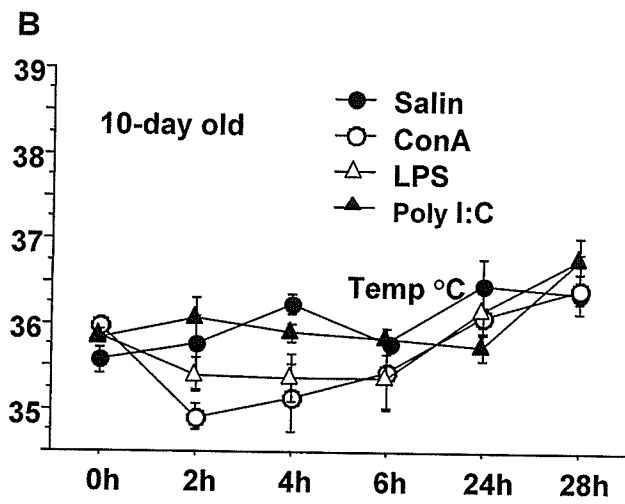
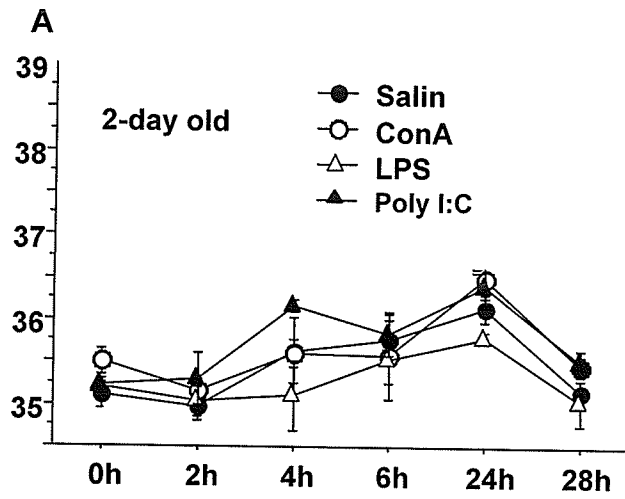
cells, and upregulate class I and II MHC antigen expression on a variety of cells <sup>397</sup>. In multiple sclerosis tissue, IFN- $\gamma$  has been detected at high levels on microglia and leukocytes <sup>398</sup>. These data suggest that IFN- $\gamma$  might contribute to secondary brain injury following ICH.

We showed that there was an age-dependent response following ICH after immune pre-stimulation. The age-dependent brain response has shown in other types of brain damage. We observed that hemorrhage and thrombin-associated brain damage is more severe in 2-day mice than in 10 day-old or adult mice (Xue and Del Bigio, unpublished data). Traumatic brain injury in neonatal pigs differs from that in older pigs <sup>238</sup>. Rats exposed to systemic LPS in infancy exhibit altered CNS-mediated inflammatory responses even as adults <sup>399</sup>. The mechanisms for the age-dependent brain injury are not clear. Immune prestimulation could affect microglia directly or it could alter the systemic inflammatory status, which in turn affects brain following damage. Nitric oxide synthase (iNOS) in the intestine is induced by LPS in 4-day old rats to a different extent than in 15-day rats; this may be a mediator of intestinal injury <sup>400</sup>. The intrapulmonary inflammatory response to LPS stimulation is minimal early in life and does not approach adult levels until approximately 4 weeks of age in rats <sup>401</sup>. However, neonatal mice are markedly more susceptible to LPS-induced lethality but more resistant to staphylococcal enterotoxin B than are adults; the response correlates with plasma TNF- $\alpha$  levels <sup>402</sup>. Clearly the age-related differences depend on the model system studied.

There are several potential shortcomings in the experiment. First, there is some variability in the lesion because of our inability to use a stereotaxic frame. However, this should not explain differences between the groups. Second, it is possible that the immune

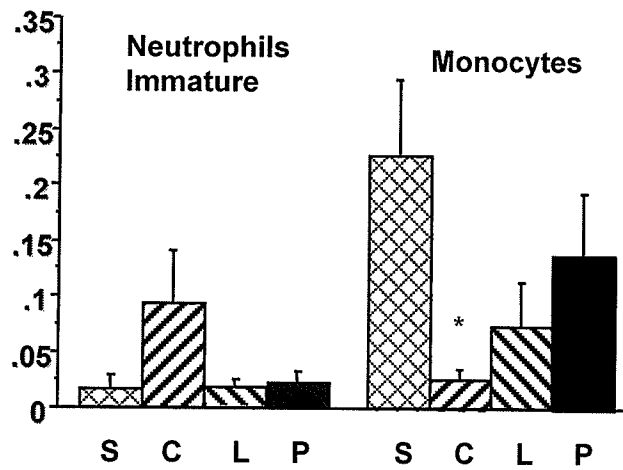
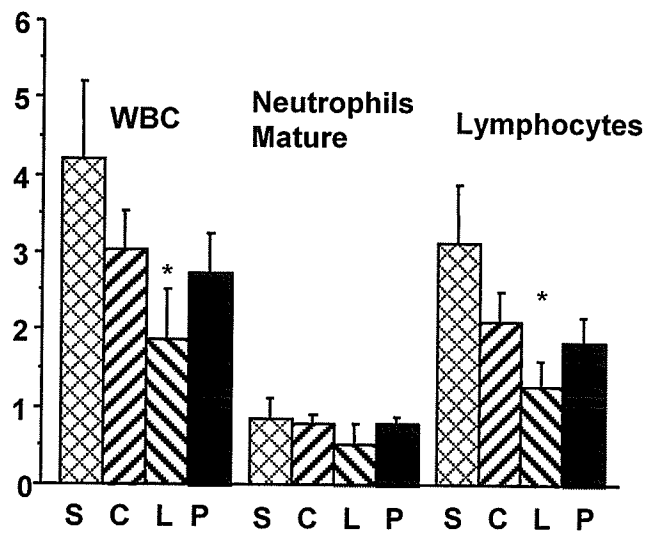
stimulators only alter the time course of injury; long-term survival studies are required to address this. Third, brain temperature might not be reflected in the axilla, nevertheless our measurements did demonstrate differences between the agents and the ages of mice. Fourth, we could not get enough cardiac blood from the 2-day and 10-day old mice to perform blood counts and differentiation and we did not determine circulating cytokine levels. This would require an additional experiment. Fifth, actual bacterial or viral infection of the animal might have a different effect, however our experiment demonstrates the principal effect. Finally, although there is an association between increased inflammation and increased damage, we cannot determine which is cause or effect.

In summary, our results demonstrate that brain damage and inflammation after injections of blood into mouse brain are aggravated after immune pre-stimulation, most obviously in 2-day old mice. We conclude that inflammation, including the cytokine IFN- $\gamma$ , might be an important factor in brain injury following ICH. We also conclude that the effects are age-specific. As has been previously suggested, these represent potential targets for therapeutic intervention.



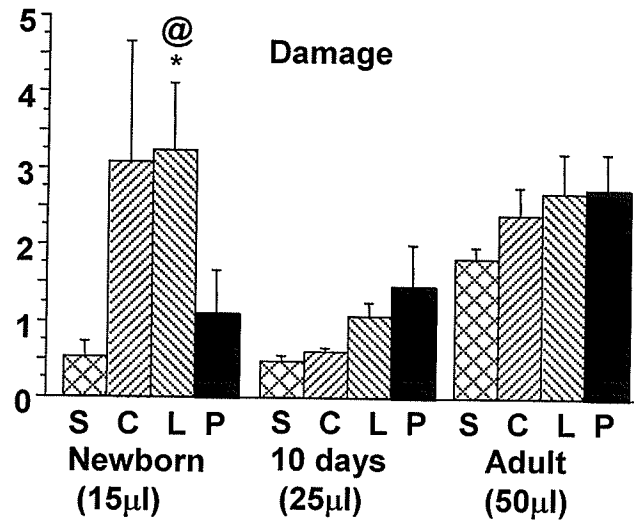
Y axis: temperature °C

Figure 2-7-1. Body temperature (mean $\pm$ SEM,) changes induced by i.p. injections of saline, ConA, LPS, and PolyI:C into mice at 2-day, 10-day, and adult age (n=3 each group). There was no significant change in temperature of the 2-day and 10-day old mice (A, B) compared to saline injection. In adult mice significant hypothermia occurred at 6 hours after LPS administration. Basal temperatures in 2-day and 10-day old are lower than in adult mice. (\*p<0.05 compared to saline; ANOVA and Scheffé test).

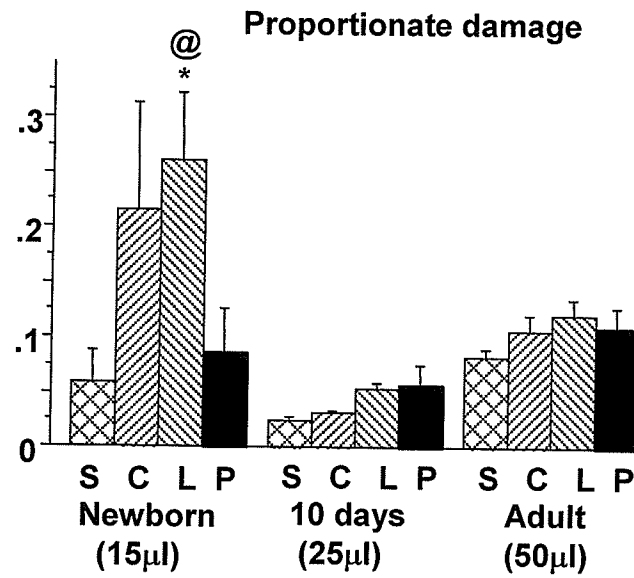


Y axis: thousand/mL

Figure 2-7-2. Bar graphs (mean±SEM) showing leukocyte counts and differential in the peripheral blood 48 hours following blood injection into brain after Con A, LPS, and PolyI:C prestimulation in adult mice (n=6 in each group). The numbers of white blood cells and lymphocytes were significantly lower after LPS stimulation compared to saline. There was no significant difference in mature and immature neutrophils. The number of monocytes was significantly lower after ConA stimulation compared to saline. (\*p<0.05 compared to saline; ANOVA and Scheffé test). Abbreviations: S: saline, C: concanavalin A, L: lipopolysaccharide, P: polyinosinic-polycytidilic acid.



Y axis: Damage area mm<sup>2</sup>



Y axis: Damage area/hemisphere area

Figure 2-7-3. Bar graphs showing the absolute brain damage areas (upper panel) and proportionate brain damage areas (lower panel) following ICH after saline, Con A, LPS, and PolyI:C stimulation in the mouse brain (n=6 in each group). The absolute brain damage area and proportionate brain damage area were greater following stimulation with LPS in the 2-day old mice compared to 10-day old and adult mice (@p<0.002, 2-way ANOVA using age as independent variable). Brain damage area was also significantly increased after LPS stimulation compared to saline injection in the 2-day old mice (\*p<0.05; ANOVA and Scheffé test). Abbreviations: S: saline, C: concanavalin A, L: lipopolysaccharide, P: polyinosinic-polycytidilic acid.

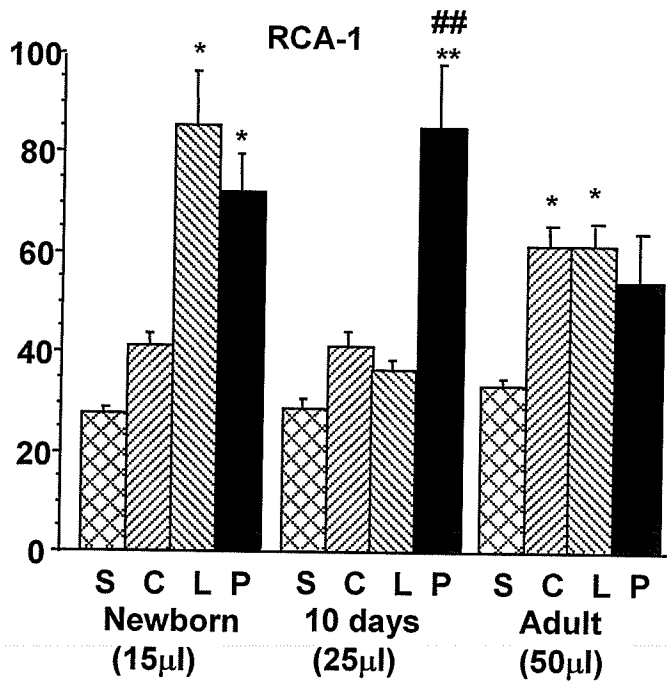
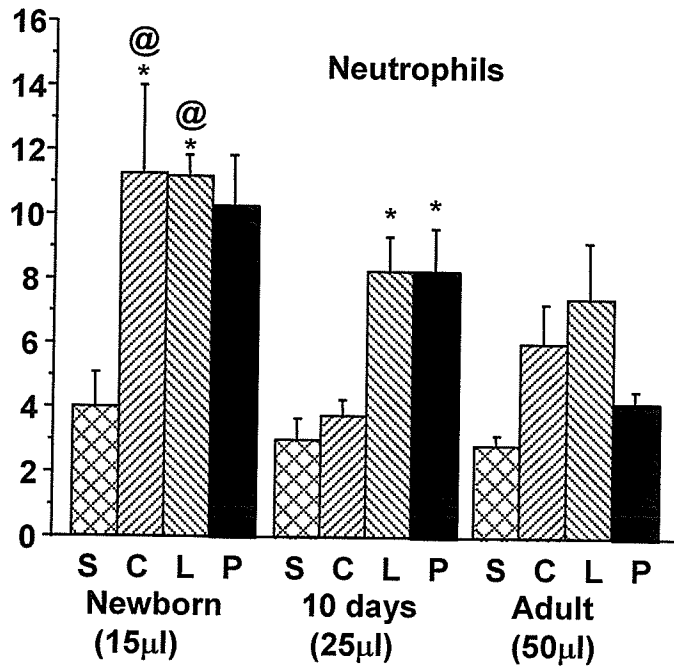


Figure 2-7-4. Bar graphs (mean±SEM) showing neutrophil infiltration (upper panel) and microglia/macrophage reaction (lower panel) in mouse striatum (per 4 x 540 x 540 μm<sup>2</sup> area) 48 hours following blood injection with saline, ConA, LPS, and PolyI:C stimulation. The number of neutrophils was increased following stimulation with ConA and LPS in 2-day old mice compared to 10-day old and adult mice (@p<0.002, 2-way ANOVA using age as independent variable). There was no age dependent difference in the number of microglia/macrophages. The number of neutrophils was significantly greater after ConA and LPS stimulation in the 2-day old mice and after LPS and PolyI:C stimulation in 10-day old mice compared to saline, but there was no significant difference in adult mice. The number of microglia / macrophages was significantly greater after LPS and PolyI:C stimulation in the 2-day old mice compared to saline and PolyI:C stimulation in 10-day old mice compared to saline and LPS as well as ConA and LPS stimulation in adult mice compared to saline. (\*p<0.05; \*\*p<0.01 compared to saline; ##p<0.01 compared to LPS, ANOVA and Scheffé test). Abbreviations see Figure 2.

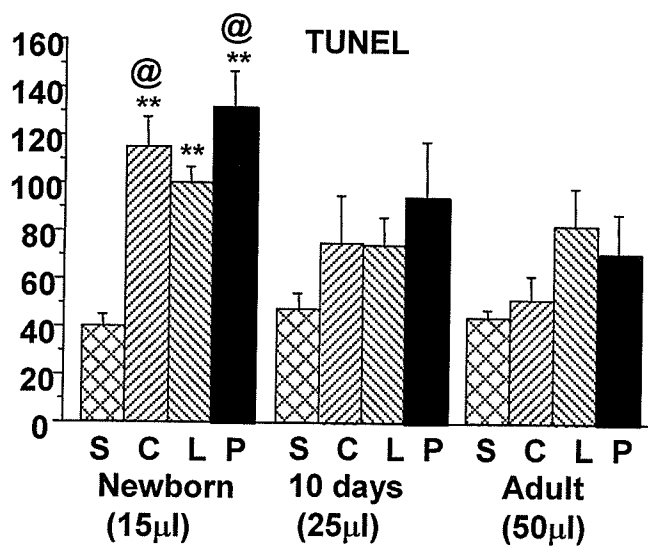
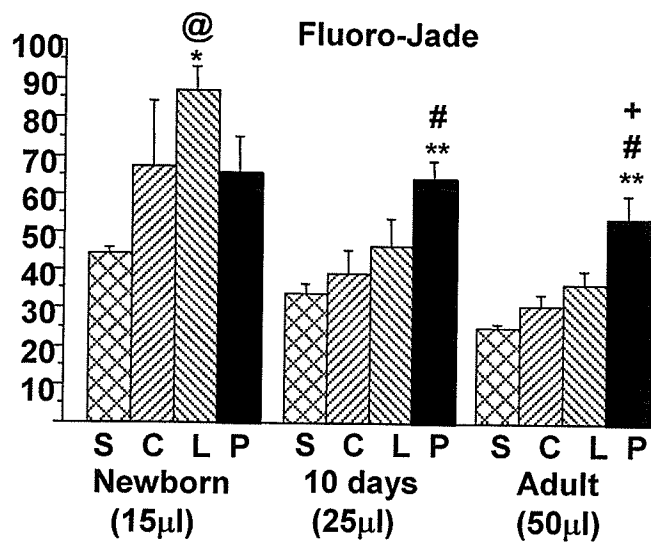


Figure 2-7-5. Bar graphs showing dying neurons (upper panel) and TUNEL positive cells (lower panel) (per  $4 \times 540 \times 540 \mu\text{m}^2$  area) following blood injection after saline, Con A, LPS, and PolyI:C stimulation. There were significant age-dependent differences in TUNEL positive cells following stimulation with ConA and PolyI:C and dying neurons following stimulation with LPS in the 2-day old mice compared to 10-day old and adult mice (@ $p < 0.002$ , 2-way ANOVA using age as independent variable). The number of TUNEL positive cells following stimulation with ConA, LPS, and PolyI:C and dying neurons following stimulation with LPS was significantly increased following blood injection in 2-day old mouse brain compared to saline injection. There was no significant change in TUNEL positive cells in the 10-day old and adult mouse brain. Dying neurons were significantly more abundant following blood injection with PolyI:C stimulation compared to saline and ConA in the 10-day old and adult mice, and compared to LPS in the adult mice. (\* $p < 0.05$ ; \*\* $p < 0.01$  compared to saline; #  $p < 0.05$  compared to ConA; +  $p < 0.05$  compared to LPS, ANOVA and Scheffé test). Abbreviations see Figure 2.

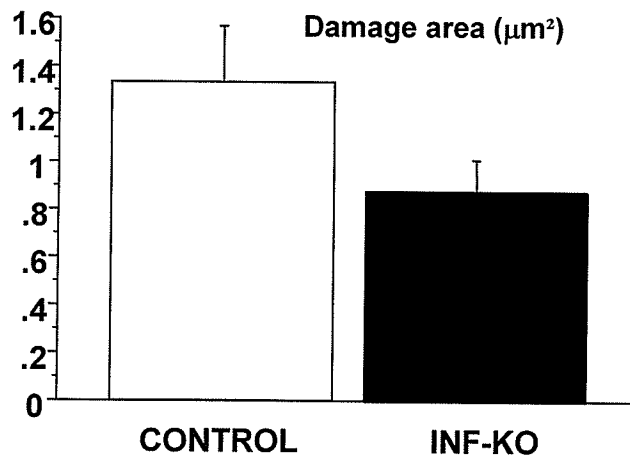
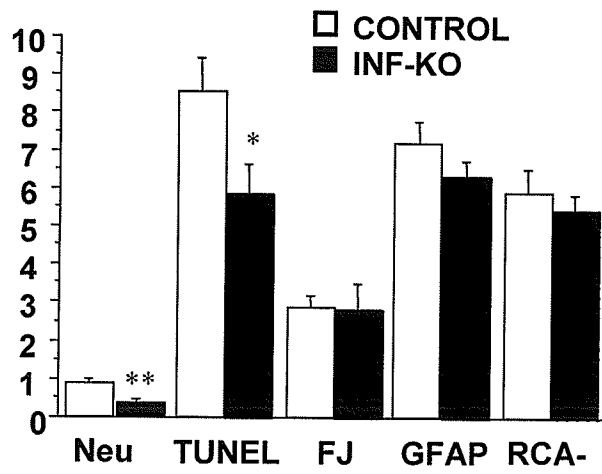


Figure 2-7-6. Bar graphs showing neutrophils (Neutr), TUNEL positive dying cells, dying neurons (FJ=Fluoro-Jade), reactive astrocytes (GFAP), and microglia/macrophages (RCA-1) (per 4 x 540 x 540  $\mu$ m area, upper panel) and brain damage area (lower panel) 48 hours following ICH in adult C57BL/6 wild-type and IFN- $\gamma$  knockout mice. The quantities of neutrophils and TUNEL positive cells were significantly decreased adjacent to the hematoma following blood injection in IFN- $\gamma$  knockout mice. (\* $p$ <0.05; \*\* $p$ <0.01 compared to wild-type mice. Unpaired Student t-tests).

Chapter 2-8

Inhibition of thrombin reduces brain damage following intracerebral blood injections in neonatal mice

Xue M, Balasubramaniam J, Parsons K, McIntyre I, Peeling J, Del Bigio MR.

(Submitted to J Neuropath Exp Neur, October 2004)

(The cell culture and enzyme overlay experiments described in this project were done by Ms. Janani Balasubramaniam. Ms. Kari Parsons assisted with the behavioral tests. Mr. Ian McIntyre assisted with the cell culture. The magnetic resonance imaging was directed by Dr. James Peeling.)

## Abstract

The mechanisms of brain injury following intracerebral hemorrhage (ICH) may include proteolytic activities, some of which are also functional in the developing brain. We hypothesized that activities of thrombin and plasmin (serine proteases) are responsible for damage following neonatal PVH and that inhibition of activity would reduce brain damage. Neonatal rat brain cells were cultured for colorimetric viability assay after treatment with blood, thrombin, or plasmin. Following in vivo injection of autologous blood, rat brain slices were tested with enzyme overlays using thrombin and plasmin fluorogenic substrates. Rats at 2 days of age received intracerebral injection of blood, thrombin, and plasminogen. Mice at 2- and 10-day ages received intracerebral injections of blood in combination with saline, hirudin,  $\alpha$ 2macroglobulin, or plasminogen activator inhibitor-1. After 2 days survival, hematoxylin & eosin, Fluoro-Jade, lectin histochemistry, and TUNEL staining were performed. Neonatal mice received low and high doses of hirudin mixed with blood, behavioral testing was conducted repeatedly, and histological studies were conducted at 10 weeks. Whole blood and thrombin, but not plasmin, decreased cultured brain cell viability. Enzyme overlays showed increased serine protease activity in a halo around the hematoma after blood injection. Thrombin and blood caused greater damage in neonatal rat brain than saline or plasminogen. Hirudin significantly reduced the inflammation, cell death, and brain damage 48 hours following PVH in 2-day old mice. Ten weeks after neonatal PVH, high dose hirudin reduced brain infarction. These results indicate that thrombin plays a role in neonatal brain damage following PVH.

## Introduction

A significant proportion of premature births is accompanied by periventricular hemorrhage (PVH) in the brain <sup>27</sup>. Some of the adverse effects of blood have been attributed to the proteolytic enzymes thrombin and plasmin <sup>38, 88, 89, 91</sup>, which are involved in blood clot formation and lysis respectively. The immature brain is also a minor source of thrombin and plasmin <sup>200-202</sup>. Proteolytic enzymes are active in the developing brain where they play a role in cell migration <sup>223</sup>, vascular growth <sup>224</sup>, synaptogenesis, and myelination <sup>225</sup>. In vitro, thrombin can impair neurite outgrowth <sup>203, 206</sup>, induce apoptosis <sup>204</sup>, and cause morphological changes in astrocytes <sup>205</sup>. Thrombin and plasmin cause brain edema, inflammation, and cell death when injected into adult rodent brain <sup>38, 207-209</sup>. Endogenous inhibitors of proteolytic enzymes, including neuroserpin <sup>229</sup>, plasminogen activator inhibitors (PAI) 1 and 2 <sup>222</sup>, protease nexin-1 (PN-1) <sup>230</sup>,  $\alpha$ 2-macroglobulin <sup>231, 232</sup>, and the tissue inhibitors of metalloproteinases (TIMPs) <sup>233</sup> are present in developing brain. Their quantities are likely insufficient to inhibit the high levels of proteolytic enzymes released following PVH.

Inhibition of thrombin with hirudin following blood injection into rat brain reduced brain edema <sup>93</sup> and brain cell death <sup>403</sup>. Blocking of protease activated receptor 1 (PAR-1) by knockout or intraventricular injection in wild-type mice of the PAR-1 antagonist BMS-200261, decreased brain damage following transient focal cerebral ischemia <sup>404</sup>. However, the neonatal brain has not been studied in vivo. We hypothesized that activities of the serine proteases thrombin and plasmin are responsible for brain damage following neonatal PVH and that inhibition would reduce brain damage and improve the neurological impairment following PVH in the neonatal rodents. The goals

of this study were to demonstrate toxicity on brain cells in vitro and in vivo, to demonstrate proteolytic activity in brain following PVH, and to investigate the role of inhibitors of proteolytic activities post PVH. The inhibitors we chose to study are hirudin, which is a thrombin inhibitor derived from leech saliva with proven efficacy in brain edema reduction <sup>93</sup>,  $\alpha$ 2-macroglobulin, which is a broad-spectrum inhibitor of serine proteases that is normally present in small quantities in developing brain and in plasma <sup>338</sup>, and PAI-1, which is produced in the brain and prevents activation of plasmin <sup>222</sup>. Previous studies showed that inflammation and cell death peak 2-3 days after injection of blood into the adult rat brain, therefore we chose a survival period of 2 days <sup>39, 40, 54</sup> for the initial screening. We used 2-day old mice because the maturational state of the subependymal zone/ganglionic eminence is roughly comparable to 24-26 week gestational age human brains, an age at which premature birth is associated with PVH.

## Materials and methods

### Animal preparation

All experimental procedures were done in accordance with guidelines of the Canadian Council on Animal Care. Protocols were approved by the local experimental ethics committee. One hundred and twenty eight CD1 mice (Charles River Canada, St. Constant, Quebec) of two ages (2-day old weighing 1.42-1.95 grams, 10-day old weighing 5-7 grams) were used. An additional 76 locally bred Sprague-Dawley rats were used for cell culture and enzyme overlay studies because the tissue dissections were more

reliable; additional histological studies were done in the acute stages to ensure that similar abnormalities occurred in rats and mice.

#### Brain cell culture

Twelve 2-day old Sprague-Dawley rat pups were sacrificed using CO<sub>2</sub> anesthesia and euthanasia by decapitation. Brains were removed and placed in a circulating bath of 4°C artificial cerebrospinal fluid containing (in mM) 124 NaCl, 25 NaHCO<sub>3</sub>, 3 KCl, 1.5 CaCl<sub>2</sub>, 1.0 MgSO<sub>4</sub>, 0.5 NaH<sub>2</sub>PO<sub>4</sub>, and 30 D-glucose equilibrated with 95% O<sub>2</sub> to 5% CO<sub>2</sub> (pH 7.4). Tissue lateral to the frontal ventricles including the ganglionic eminence and striatum was excised and minced in a sterile solution containing trypsin (5%) dissolved in a dissection medium supplemented with antibiotics (penicillin G, Streptomycin Gibco). Cells were counted using a Spotline hemocytometer and plated at a concentration of 50-100,000 cells/well into Corning 96-well tissue culture plates (Corning 3997) and culture dishes were stored in a humidified incubator and maintained at 37.5°C and at an ambient 5% CO<sub>2</sub> concentration. Cultures were fed twice weekly with Eagle's minimal essential medium (MEM, Gibco 82-0234), containing added 5% horse serum, glutamine (2mM) and supplemented with a solution containing T<sub>3</sub>, insulin, progesterone, putrescine dihydrochloride, corticosterone, human transferrin, BSA, and nerve growth factor<sup>405</sup>. The cultures were grown to confluency (7-10 days).

#### Assessment of cell viability after blood, thrombin and plasmin exposure

Blood was obtained from 4 healthy adult male Sprague-Dawley rats. Cultured brain cells were exposed to blood volumes of 10 µl, 25 µl, 50 µl, 100 µl, and 200 µl in

total culture medium volume of 400  $\mu$ l. We calculated the units of thrombin and plasminogen in whole blood based on the following assumptions: plasma volume is ~ 60% total blood volume, each ml plasma contains 260 to 360 units of prothrombin and 200  $\mu$ g (1.95 units) plasminogen<sup>347, 348, 382</sup>. The quantities of thrombin (from bovine plasma, T-6634, Sigma Chemical Company) and plasmin (from porcine plasma, P-8644, Sigma) calculated to be contained in blood volumes of 25 $\mu$ l (plasmin 0.0295 units and thrombin 6.5 units) and 100  $\mu$ l (plasmin 0.118 units and thrombin 26 units) were applied to cell cultures in 400 $\mu$ l wells. Cell viability in response to blood, thrombin, and plasmin was determined by using the MTT [3-(4,5-dimethyl-2-thiazolyl)-2,5-diphenyl-2H tetrazolium bromide] colorimetric assay. Twenty-four or 48 hours after application of blood or blood products, 100  $\mu$ l of MTT solution (1mg/ml, Sigma Chemical Co., St. Louis, MO) was added to each well. After 4 hours of incubation at 37°C, the reaction was terminated by removing the supernatant and adding 100  $\mu$ l of DMSO, followed by thorough mixing. The plates were read at 570 nm (absorption background = empty well + DMSO) on a plate reader (BioRad). Mean absorbance was calculated for control well and treatments. All tests were done in triplicate. For immunocytology, cultured cells in 12-well plates were labeled with rabbit anti-cow GFAP (1:1000, Dako, CA) or mouse anti-neurofilament 200 (1:40, Sigma) and incubated for 1 hour with Cy3- conjugated donkey anti-rabbit (1:500, Jackson ImmunoResearch laboratories, PA) or FITC- conjugated sheep anti-mouse (1:150, Jackson ImmunoResearch laboratories, PA) secondary antibodies.

#### Intracerebral injections

For the acute brain response study, 2-day old rats and mice were anesthetized by cooling on an ice bed. Ten-day old mice were anesthetized by intraperitoneal injection with ketamine/xylazine (9.0/0.5 mg/kg). Autologous blood was collected in a sterile syringe by placing the tail in warm water for 1 min, cleaning the skin with 70% alcohol, and cutting 2 mm off the tail tip as previous described<sup>37, 39, 40</sup>. Because the neonatal animals could not be secured in a stereotaxic frame, the brain injections were done freehand with the needle inserted percutaneously. In 10-day old mice, a midline scalp incision was made. After blood collection, a 28-gauge needle was attached to the syringe and quickly introduced into the right striatum of the mouse brain with a custom-made guide that helped to stabilize the needle and guide it to the correct depth (in 2-day old: 1.5 mm lateral to midline, 0.5 mm posterior to the outer canthus of the right eye, 2.5 mm deep to the skull surface; in 10 day old: 2 mm lateral to midline, 1.0 mm posterior to the outer canthus of the right eye, 3.0 mm deep to the skull surface). The volume of injected blood was 15  $\mu$ l in neonatal and 25  $\mu$ l in 10-day old mice. We chose these volumes so that the hematoma was of similar proportion to the total brain size at all ages. We based our calculation on prior studies that showed the brain weights in mice are approximately 150 mg in 2-day old, 250 mg in 10-day mice<sup>380, 381</sup>. The sites of injection were more lateral compared to the periventricular/intraventricular hemorrhage model previously described<sup>37</sup> because we wanted to study the reactions in brain parenchyma (not intraventricular hemorrhage) following PVH. Blood, in some cases combined with inhibitory agents (see below), was injected over 1 minute. Newborn rats received intrastriatal injections of saline (15 $\mu$ L, n=6), blood (15 $\mu$ L, n=8), thrombin (3.9U/15  $\mu$ L, from bovine plasma; T-6634, Sigma Chemical Company, n=8), or plasminogen (0.03

U/15  $\mu$ L, from bovine plasma; P-9156, Sigma, n=8). The needle was left in the place for 30 seconds, and then removed slowly. Then the opened scalp (10-day old) was sutured. Physiological monitoring was not practical because of the small size of the animals. All were returned to the cages with their mothers after the procedure.

For the long-term behavioral study two-day old mice were anesthetized with 1.5-2 % halothane in a 70:30 mixture of N<sub>2</sub>O:O<sub>2</sub>. Immediately after injection mice were examined with MRI, which allowed us to assess accuracy of the injection. There was no injection in intact control group. Nine intact 2-day old mice were used as control.

#### In vivo assessment of serine protease activity using enzyme overlay membranes

In a qualitative manner, proteolytic activity related to serine proteases was assessed using chromogenic substrates impregnated in enzyme overlay membranes applied to fresh brain slices. Rats were used because the larger brains were more practical for this experiment. At 0, 1, 6, 24, 48 hours after the injection of blood (at each time point, blood n=4 and controls n=2), rats were re-anesthetized and perfused with 0.1M phosphate-buffered saline (PBS) to flush the vasculature. The brains were quickly removed and sliced (1mm) in the coronal plane through the needle insertion site, and placed onto a glass microscope slide at room temperature. Overlay membranes impregnated with peptides conjugated to fluorogenic substrates (Thrombin: D-Pro-Phe-Arg, AFC 80; and Plasmin: D-Val-Phe-Arg, AFC 80 or D-Val-Leu-Lys, AFC 56; Enzyme Systems, Livermore, CA, USA) were used to assess proteolytic activity of both thrombin and plasmin. Membranes were cut into 1cm squares, soaked in 0.1M PBS with or without 5 units of hirudin, and marked with small hole to place directly over the

hematoma. The membrane was monitored by epifluorescence (FITC filter set) on an upright microscope (10X objective) and photographed at 5-minute intervals to document the time dependent release of substrate. Fresh human blood, pure thrombin (0.1  $\mu\text{g}/5 \mu\text{L}$  from bovine plasma; T-6634, Sigma Chemical Company), and plasmin (0.335 U/5  $\mu\text{L}$  from porcine plasma; P-8644, Sigma) were directly applied on both membranes to assess the specificity of thrombin and plasmin substrates impregnated on the membranes.

#### Intracerebral administration of drugs to mice

Five units (in 15  $\mu\text{l}$ ) or 9 units (in 25  $\mu\text{l}$ ) of hirudin (H-0393, Sigma Chemical Company), 50  $\mu\text{g}$  (in 15  $\mu\text{l}$ ) or 90  $\mu\text{g}$  (in 25  $\mu\text{l}$ ) of  $\alpha 2$ -macroglobulin (M-6159, Sigma Chemical Company), 5  $\mu\text{g}$  (in 15  $\mu\text{l}$ ) or 9  $\mu\text{g}$  (in 25  $\mu\text{l}$ ) of recombinant mouse PAI-1 (Technoclone GmbH A-1235, Vienna), or equal volumes of saline were preloaded and supplied blindly in syringes by the senior author without blood for the acute brain response study in the 2-day and 10-day old mice respectively (Table 2-8-1). The doses are based upon the amount theoretically needed to block all enzyme activity in equal volumes of blood<sup>347, 348, 382</sup>. For the blood injections, the solutions were provided in 5 or 10  $\mu\text{l}$  aliquots and combined with autologous blood obtained from the tail for injection into the striatum in 2-day and 10-day-old mouse brain (15 or 25  $\mu\text{l}$  respectively). For the behavioral study in 2-day old mice, the preloaded syringes with low dose hirudin (5 units, n=11), high dose hirudin (10 units, n=12), or saline (n=12) in 5  $\mu\text{l}$  were combined with 15  $\mu\text{l}$  blood from the tail.

## Magnetic Resonance Imaging (MRI)

MRI was used to assess the hematoma size and location in the neonatal mice as previously described<sup>37</sup>. Briefly, the mouse pups were anesthetized with 1.5-2 % halothane in a 70:30 mixture of N<sub>2</sub>O:O<sub>2</sub>. MRI was performed using a Bruker Biospec/3 MR scanner equipped with a 21cm bore magnet operating at a field of 7T (Karlsruhe, Germany) to obtain T2-weighted images of brain. Two-day old mice were imaged immediately after the injection and the size of the hematoma was assessed. Mice were only used for long-term behavioral tests and histological analysis if MRI showed a standard hematoma size and location.

## Evaluation of acute brain damage

Newborn rats were re-anesthetized at 24 or 48 hours after saline (n=3 at each time point), blood (n=4 at each time point), thrombin (n=4 at each time point), or plasminogen (n=4 at each time point) injections. Mice were re-anesthetized 48 hours after injections of blood or blood combined with hirudin,  $\alpha$ 2-macroglobulin, or PAI-1 (n=5 each). They were perfused through the heart with 5ml of ice-cold 4% paraformaldehyde in 0.1M PBS. The brains were removed, fixed and cut coronally to surround the injection sites. Slices were dehydrated and embedded in paraffin. Sections (6  $\mu$ m) were cut serially and each 20th section from the rostral to the caudal portion of the damage area was stained with hematoxylin and eosin (H&E). The coronal levels with damage were identified. In the rat brains, using characteristic cellular morphology, dying cells were counted in 3 fields (each area 540 $\mu$ m x 540 $\mu$ m, objective 40X magnification) of lateral cerebral cortex, white matter, and germinal matrix at three levels. Near the lesion center in the mouse

brains, where the brain damage was maximal, a variety of additional histological and immunohistochemical stains were performed as previously described<sup>37, 54</sup>. Briefly, histochemistry with Ricinus communis agglutinin lectin (RCA-1) labeling was used to demonstrate reactive microglial cells<sup>269</sup>. Paraffin sections were dewaxed and rehydrated, incubated with biotinylated lectin (diluted 1/2000, Vector Laboratories, Inc., Burlingame, U.S.A.) and incubated with streptavidin-peroxidase (1/400, Dako Corporation, Carpinteria, CA, USA), colored with diaminobenzidine - H<sub>2</sub>O<sub>2</sub> solution, washed and coverslipped. Control sections were processed with omission of the biotinylated lectin. Terminal deoxynucleotidyl transferase (TdT)-mediated deoxyuridine triphosphate (dUTP)-biotin nick end labeling (TUNEL) was used to identify dying cells with damaged DNA using *Apoptag in situ* kit (Intergen; Purchase, NY, USA). Negative control sections were treated similarly but incubated in the absence of TdT enzyme or dUTP-digoxigenin. Fluoro-Jade staining showed dying neurons<sup>189, 190</sup> by incubating sections in 0.06% potassium permanganate for 15 minutes. Then 0.001% Fluoro-Jade (Histo-Chem Inc.; Jefferson, AR) staining solution was applied for 30 minutes, following by PBS washing, drying in air, and coverslip application. On the coronal sections with brain damage a "camera lucida" drawing was used to document the area of brain damage, which was defined by the presence of blood, tissue rarefaction, or necrosis. Computerized planimetry was used to measure the areas of damaged brain. The proportion of brain damage was calculated as the area of damage divided by the area of the whole hemisphere. Using an ocular reticule and 400x ocular magnification (objective magnification x 40), Fluoro-Jade positive neurons, TUNEL positive dying cells, neutrophils (identified on H&E sections by characteristic nuclear morphology), and

RCA-1 binding cells were counted in 4 fields (each area 540  $\mu\text{m}$  x 540  $\mu\text{m}$ ) immediately adjacent to the needle injection/damage site as previously described<sup>38-40, 54</sup>. Counts were made near the edge of the lesion because the necrotic cores were devoid of viable cells.

#### Long-term behavioral testing (Table 2-8-2)

Mice were weighed twice weekly for 10 weeks. To study sensorimotor development, the tests include pivoting (forelimb movements involved in early ambulation), righting response (mice were placed on their backs and the time to righting was measured), and negative geotaxis (mice were placed on an 15° incline pointing downward and the time it took to face upward was recorded)<sup>406</sup>. The mice were housed with their mother until weaning on postnatal day 21. Then 3-4 same sex mice were housed cages without the mother. Grip strength was tested at 14, 16, 20, and 23 days of age by allowing the mice to grasp a 1.5 mm diameter wire with their forelimbs and measuring the hanging time for a maximum 2 minutes. A soft blanket was placed under the wire to catch any mice that fell.

Starting on the fifth week, the following behavioral tests were performed. 1) Cylinder exploration: forelimb placing during vertical exploration was analyzed by placing mice in a transparent cylinder (15 cm diameter and 30 cm height) for 2 minutes. Videotapes were analyzed and the frequency of left and right forepaw placement on the cylinder wall was counted. 2) Rotating cylinder: gait agility was assessed using a rotating cylinder with 7 cm diameter (Economex, Columbus Instruments) in two separate trials. First, endurance was assessed at a constant speed of 5 rpm for a maximum of 2 minutes. Second, the cylinder accelerated at a rate of 0.1 rpm every second for up to 2 minutes.

The time that the animals remained on the cylinder was recorded. 3) Beam walking: to assess motor coordination, mice were trained to walk along a 0.7 cm wide 50 mm long Plexiglas beam to a platform. The mice were videotaped from behind. The time taken to walk the beam and the frequency of hindlimb slips off the beam were recorded. Five trials were used for each test. 4) Swimming: a 20 cm deep, 65 cm long, 20 cm wide aquarium filled with 22°C water and containing a 12 cm diameter round platform 2 mm above of the water level at one end was used. The mice were videotaped from the side and below. The time to swim the length of the pool, the ease of climbing onto the platform, and the forepaw position during swimming were scored. Five trials were used for each test separated by a 30 second rest period.

#### Brain tissue evaluation 10 weeks after PVH

At the end of the 10-week behavioral testing period, the mice were given an overdose of pentobarbital, the vascular system was flushed by transcardiac perfusion with ice-cold 0.1M PBS, and the brains were removed quickly. The cerebral hemispheres were split down the midline. The left hemisphere was frozen in liquid nitrogen and stored at -80 °C (for ELISA). The right hemisphere was immersion fixed in 4 % buffered formalin, embedded in paraffin and cut in the coronal plane. Sections (6µm) were stained with H&E and solochrome cyanine for visualization of myelin. Brain damage was graded as follows: 0 (intact); 1 (mildly enlarged lateral ventricle, mild atrophy of striatum or external capsule, or dorsal cortex); 2 (moderately severe dorsal cortex atrophy, atrophy of lateral striatal white matter bundles); 3 (severe dorsal/lateral cortex atrophy, loss of corpus callosum and external capsule, atrophy of striatum).

## Enzyme-Linked Immunosorbent Assay (ELISA)

ELISA was used to measure the quantity of myelin basic protein (MBP). The left hemispheres were weighed and homogenized in RIPA buffer proportional to the weight of the brain samples. Following centrifugation at 15,000 x G for 30 min at 4° C the clarified supernatant was used to do protein assay. The wells of coated NUNC brand ELISA plates were coated with 100 µL/well of 1 µg/mL polyclonal rabbit anti-human myelin basic protein (DAKO, A0623) overnight at 5 °C. Washed plates were blocked with 100 µl/well of 5% skim milk powder in PBS for 1 hour at room temperature and washed with PBST (0.5% Triton in 1X PBS). To make the standard curve, 100 µl/well of myelin basic protein (bovine brain MBP, M1891, Sigma) standards were diluted (15 ng/mL, 50, 100, 200, 300, 400, and 500) on ice in PBST (0.5% Triton in 1X PBS). Samples at 25 and 50 µg/ml concentrations, 100 µl/well, were diluted on ice in PBST. Standards and samples on plates were incubated 1 hour at room temperature. Mouse anti-human monoclonal MBP antibody (US Biological, M9758-01) diluted to 1:500 in 5% skim milk/PBST was applied 100 µl/well for 1 hour at room temperature. Plates were washed with PBST. Alkaline phosphatase conjugated goat anti-mouse antibody (Cedarlane/Biocan, 115-055-146) diluted to 0.5 µg/mL in 5% skim milk/PBST was applied, 100 µL/well, for 1 hour at room temperature. Plates were washed with PBST. Phosphatase substrate (100 µL/well, Pierce, 37620) was applied in a dark place for 30 minutes at room temperature. The reaction was stopped with 50 µL/well of 2N NaOH and plates were read at 405 nm absorption with a microplate reader (Corona). Controls without antigen were measured to determine the background.

## Statistical Analysis

All data are expressed as mean  $\pm$  SEM. Unblinding was done only after all analysis was complete. Data were analyzed to ensure normal distribution. Intergroup comparisons were made by ANOVA followed by Fisher's protected least significant difference (PLSD), or nonparametric Kruskal-Wallis test as appropriate. The differences were considered significantly when  $p < 0.05$ . We used StatView 5.01 software (SAS Institute; Cary NC).

## Results

### Brain cell culture

Cultured cells were predominantly immunoreactive for GFAP, i.e. astrocytes, and approximately 5% of smaller cells were neurofilament positive neurons. Whole blood starting at 25% of the culture medium caused significant loss of viability ( $p < 0.05$ ; Figure 2-8-1). There was no neurofilament reactivity after the treatment. At low doses, thrombin or plasmin (equivalent to 6.25% blood) alone did not cause significant decrease in viability. Thrombin at high doses (equivalent to 25% blood) caused a significant decrease in cell viability (Figure 2-8-1). Plasmin had no effect at comparable doses (data not shown).

### Magnetic resonance imaging

MRI was used in 2-day old rats and mice to ensure accurate placement of the injection and comparable hematoma size. On T2-weighted MR images, twenty minutes following whole blood (15  $\mu$ L) injection, the hematoma in the striatum and ventricles appears dark (Figure 2-8-2) due to the large susceptibility effect of paramagnetic hemoglobin products.

#### Assessment serine protease activity using enzyme overlay membrane (EOM)

Membranes embedded with all substrates showed fluorescence within 2 minutes upon direct application of fresh human blood. When pure plasmin and thrombin were applied to corresponding membranes fluorescence was also observed. However, when the substrates were interchanged, fluorescence activity was still present. We concluded all substrates (Thrombin substrate: D-Pro-Phe-Arg , and Plasmin substrates D-Val-Phe-Arg and D-Val-Leu-Lys) could be cleaved by either plasmin or thrombin, despite the manufacturer's claim of specificity. Application of membranes to brain slices revealed no fluorescence directly over the hematoma (Figure 2-8-3). Increased serine protease activity was observed in brain tissue around hematoma extending to a distance of approximately of 300 $\mu$ m. Fluorescence appeared approximately 20 minutes after membrane application and the intensity increased to 90 minutes. Fluorescence intensity peaked after approximately 60-90 minutes. The reaction was most evident using slices from acutely injected brains, but some fluorescence developed even in brains 24 hours after blood injection. There was a qualitative reduction in serine protease activity following pre-incubation of membranes with hirudin (data not shown).

Cell death after injections of blood, thrombin, and plasminogen into neonatal rat striatum

Twenty-four hours after blood injection, a small hematoma could be seen in the rat striatum. In addition, 6 out of 8 rats exhibited hemorrhagic infarction in the lateral cerebral cortex in the distribution of the middle cerebral artery, remote from the needle insertion site and not necessarily contiguous with the hematoma. Similar changes were seen at 48h and following thrombin injection. Blood and thrombin injection resulted in significant increase in dying cells compared to saline and plasminogen (Figure 2-8-4).

Brain reaction 48 hours following injections of inhibitors with blood

All mice tolerated the surgical procedure well and there was no surgical mortality. Following injections of saline, thrombin,  $\alpha$ 2macroglobulin, and PAI-1 alone, there was a small area of brain damage surrounding the injection tracks. These appeared as a pale area on H&E stain due to edema. Brains that underwent injections of blood had large area of damage (Figure 2-8-5). Microscopically, the hematoma was identified by the presence of edema, blood debris, and necrosis within the brain striatum.

Age and treatment had significant effects on dying neurons (ANOVA,  $F(\text{age}) = 28.744$ ,  $df = 1$ ,  $p < 0.0001$ ;  $F(\text{treatment}) = 22.797$ ,  $df = 7$ ,  $p < 0.0001$ ;  $F(\text{interaction}) = 5.186$ ,  $df = 7$ ,  $p = 0.001$ ), on microglia/macrophages (ANOVA,  $F(\text{age}) = 100.696$ ,  $df = 1$ ,  $p < 0.0001$ ;  $F(\text{treatment}) = 30.005$ ,  $df = 7$ ,  $p < 0.0001$ ;  $F(\text{interaction}) = 6.538$ ,  $df = 7$ ,  $p < 0.0001$ ), on neutrophils (ANOVA  $F(\text{age}) = 36.683$ ,  $df = 1$ ,  $p < 0.0001$ ;  $F(\text{treatment}) = 5.927$ ,  $df = 7$ ,  $p < 0.0001$ ;  $F(\text{interaction}) = 3.347$ ,  $df = 7$ ,  $p = 0.0047$ ), and on proportionate damaged area (ANOVA  $F(\text{treatment}) = 3.992$ ,  $df = 7$ ,  $p = 0.0013$ ;  $F(\text{age}) = 4.664$ ,  $df = 1$ ,  $p = 0.00350$ ;  $F(\text{interaction}) = 3.913$ ,  $df = 7$ ,  $p = 0.0015$ ). TUNEL positive cells were

influenced by treatment (ANOVA,  $F = 22.096$ ,  $df = 7$ ,  $p < 0.0001$ ) but not age ( $F = 0.551$ ,  $df = 1$ ,  $p = 0.4608$ ) and there was an interaction effect ( $F = 8.561$ ,  $df = 7$ ,  $p < 0.0001$ ). Damaged areas were influenced by treatment (ANOVA,  $F = 9.749$ ,  $df = 7$ ,  $p < 0.0001$ ) but not age ( $F = 2.293$ ,  $df = 1$ ,  $p = 0.1355$ ) and there was an interaction effect ( $F = 8.463$ ,  $df = 7$ ,  $p < 0.0001$ ). Intergroup comparisons showed that brain inflammation adjacent to the injection was mildly increased by  $\alpha 2$ macroglobulin and PAI-1 but not hirudin (Figure 2-8-6). In comparison to saline with blood, hirudin with blood reduced neutrophil infiltrate, microglial activation, Fluoro-Jade dying neurons and TUNEL positive dying cells in both ages.  $\alpha 2$ macroglobulin and PAI-1 tended to be protective in 10-day old mice but not 2-day old mice (Figures 2-8-5, 2-8-6, 2-8--7).

#### Long term outcome following hirudin co-administration

All mice tolerated the surgical procedure well and there was no acute surgical mortality. There were three delayed deaths, one in each group for unknown reasons (necropsies were not obtained). There were no significant differences in body weight between the experimental and control groups (Figure 2-8-8). In the righting test at three days ( $p = 0.117$ , saline versus low dose hirudin) and negative geotaxis at 7 days ( $p = 0.092$  saline versus high dose hirudin), there was no significant difference (Figure 2-8-9). On the beam, mice with PVH exhibited significantly more slipping of the contralateral hind limb than normal mice ( $p < 0.05$ ), but there were no significant differences with hirudin treatments (Figure 2-8-10). There were no significant changes in any of the other tests including pivoting, cylinder exploration, rotating cylinder, and swimming (data not shown). Following sacrifice, a range of brain damage was observed. On gross inspection,

tissue loss was often obvious in the right hemisphere, while the left hemisphere appeared normal. The mildest form was focal dorsal cortical damage, which might be attributable to needle insertion. This ranged to complete infarction of the lateral and dorsal cerebral cortex in the distal middle cerebral artery distribution. Fewer mice treated with high dose hirudin exhibited large infarcts ( $p=0.259$ , Kruskal-Wallis test) (Figure 2-8-11). ELISA for the MBP content in the contralateral hemispheres showed no significant difference between groups (data not shown).

## Discussion

In the present study, viability of mixed striatal cell culture was reduced by addition of whole blood (25% of total medium volume) and by thrombin in a dose calculated to be in the same amount of blood. Plasmin administered at doses relative to the same blood volumes had no such effect. Enzyme overlays placed on brain slices with injected blood showed that there was a qualitative increase in serine protease activity around the hematoma immediately following injection of blood. The absence of activity directly over the hematoma could indicate that the enzyme activity is exhausted in the blood clot. Pre-incubation of the membranes with hirudin was associated with a subjective decrease in activity, suggesting that thrombin activity is at least partially responsible. Neonatal rats injected with blood or thrombin, but not plasminogen, exhibited large areas of damage. Brain damage area, dying cells, and inflammation in 2-day and 10-day old mice were significantly decreased at 48 hours when blood injections were combined with hirudin. The effect was less consistent with  $\alpha 2$ -macroglobulin and PAI-1, which have effects on plasmin. Therefore, we selected hirudin as the agent to

study long-term following intracerebral injection of blood into 2-day old mice. High dose hirudin reduced the brain infarction in 10 weeks after PVH. Together these observations suggest that thrombin from blood plasma plays a role in damage to the newborn brain following hemorrhage.

In blood, thrombin converts fibrinogen into fibrin during clotting. Neurons and glia produce thrombin and thrombin receptors, also known as protease activated receptors (PARs)<sup>203</sup>, especially in the newborn period when they play a role in development<sup>221</sup>. To date, four members of the PAR family have been identified. PAR-1, PAR-3, and PAR-4 are considered as thrombin receptors, while PAR-2 is activated by serine proteases other than thrombin, such as trypsin and tryptase<sup>407, 408</sup>. In culture, thrombin causes astrocytes to proliferate by acting through PAR-1<sup>84, 407</sup>, it impairs neurite outgrowth<sup>203</sup> and induces neuronal apoptosis<sup>204</sup> through PAR-2<sup>226, 227</sup>, and it causes microglia proliferate through PAR-4<sup>409</sup>. Thrombin and plasmin proteolytic activity after hemorrhage likely exceed the regulatory capacity of endogenous proteins such as  $\alpha$ 2macroglobulin, PAI-1, and PN-1. Thrombin and plasmin cause tissue necrosis and inflammation when injected into adult rat brain<sup>38</sup> and neonatal mouse brain in an age-dependent manner (M. Xue and M.R. Del Bigio, unpublished observations). The neonatal brain is relatively more sensitive to proteolytic plasma enzymes possibly because there are more PARs on immature cells, or perhaps because blood vessels are more fragile. Thrombin can act directly on cytoskeletal actin<sup>410</sup>. In addition, inflammation may contribute to secondary injury following ICH<sup>39, 52, 54</sup> and thrombin itself is chemotactic for neutrophils<sup>272</sup>.

Tissue type or urokinase type plasminogen activators (tPA and uPA) convert plasminogen in blood to plasmin, which digests fibrin in blood clots. Plasmin-mediated

activation of platelets occurs by cleavage of PAR-4<sup>411</sup>. Plasmin, tPA and uPA are also produced in small quantities by brain cells<sup>202</sup> where they play a role in cell migration, synaptogenesis, and formation of myelin. Plasmin may regulate PAR-2 signaling in brain endothelial cells under pathological conditions<sup>412</sup>. Plasmin is known to degrade a range of extracellular matrix proteins and to activate matrix metalloproteinases (MMPs), which also can digest matrix proteins<sup>328, 337</sup> and myelin. Following brain injury MMPs are produced by infiltrating inflammatory cells, microglia, and astroglia<sup>85</sup>. In this study plasmin seemed to play a minor role compared to thrombin in the damage of neonatal rat brains when injected directly at physiologically comparable doses (in terms of blood content), and in relation to the blockers that were tested in mouse brain. This is similar to other experiments we have done in which low doses (0.05U) caused minor damage and high doses of plasminogen (0.5U from the same supplier and same lot) caused severe brain damage in adult rats<sup>38</sup>. In a recent study, however, the same dose (0.03U) caused more extensive damage in neonatal mice (M. Xue and M.R. Del Bigio, see Chapter 2-6). We cannot offer a certain explanation – there may be interspecies differences.

Hirudin binds to thrombin in a one-to one molecular manner and can reduce brain inflammation and cell death by inhibition of thrombin. This may be beneficial to the brain following PVH. However, hirudin did not completely inhibit the damage even though we used equimolar concentrations for the amount of blood injected. This may be because more thrombin is produced by the injured brain<sup>203</sup> or because further bleeding occurs from broken blood vessels in the brain. Other factors such as leukocytes<sup>40</sup>, plasminogen<sup>38</sup>, and hemoglobin<sup>196</sup>, also play roles in the brain damage.  $\alpha$ 2-macroglobulin or PAI-1 also partially reduced brain inflammation and cell death,

suggesting that plasmin plays at least some role in brain damage. Previous experiments showed that PAI-1 deficient mice exhibit larger infarcts following middle cerebral artery occlusion<sup>343</sup>.

Other issues remain unresolved. More sophisticated cell culture, cell death assays, and immunostaining could help differentiate the kinetics of cell death, which may vary between different types of cells. Furthermore, additional blood component toxicity experiments should be done. We have no way of determining whether the proteolytic activity is truly representative of what occurs following PVH. Fresh human tissues are hard to obtain. We used plasminogen instead of plasmin because some plasmin activity is lost when it is purified in the post-activated form. Our prior studies did show brain damage in adult rats following injection of high dose (10 times of the some amount of the blood) of plasminogen<sup>38</sup>. Although the method of freehand blood injection could cause variable brain damage, through extensive experience and use of MR screening the results are quite reproducible.

In summary, our results demonstrate that blood and thrombin cause comparable levels of brain cell loss in vitro and in vivo. Hirudin can significantly reduce the acute brain damage following neonatal mouse PVH and high dose hirudin slightly reduced brain infarction in long-term study. Thrombin therefore represents a potential target for therapeutic intervention in neonatal brain hemorrhage. The mechanisms of thrombin toxicity, and specifically the reasons for neonatal susceptibility need to be explored more fully.

Table 2-8-1. Intracerebral injections of inhibitors of proteolytic activity with whole blood into CD1 mouse brain.

	2-day old (n = 5, each group)	10-day old (n = 5, each group)
Hirudin	5 U in 15 $\mu$ l saline	9 U in 25 $\mu$ l saline
$\alpha$ 2-macroglobulin	50 $\mu$ g in 15 $\mu$ l saline	90 $\mu$ g in 25 $\mu$ l saline
PAI-1	5 $\mu$ g in 15 $\mu$ l saline	9 $\mu$ g in 25 $\mu$ l saline
Saline	15 $\mu$ l	25 $\mu$ l
Hirudin + blood	5 U in 5 $\mu$ l saline + 15 $\mu$ l blood	9 U in 10 $\mu$ l saline + 25 $\mu$ l blood
$\alpha$ 2-macroglobulin + blood	50 $\mu$ g in 5 $\mu$ l saline + 15 $\mu$ l blood	90 $\mu$ g in 10 $\mu$ l saline + 25 $\mu$ l blood
PAI-1 + blood	5 $\mu$ g in 5 $\mu$ l saline + 15 $\mu$ l blood	9 $\mu$ g in 10 $\mu$ l saline + 25 $\mu$ l blood
Saline + blood	5 $\mu$ l saline + 15 $\mu$ l blood	10 $\mu$ l saline + 25 $\mu$ l blood

Table 2-8-2. Long-term study: Behavioral testing after inhibition of thrombin by hirudin and control in neonatal mice.

Age of testing	Behavioral test	Testing schedule
1 day to 10 weeks	Body weight	Twice a week first 5 weeks Once a week last 5 weeks
1 day to 2 weeks	Pivoting	Twice a week
3-10 days	Righting	Twice a week
3-10 days	Negative geotaxis	Twice a week
2-4 weeks	Wire hanging	Twice a week
5-7 weeks	Beam walking	Once a week
5-8 weeks	Cylinder exploration	Once a week
4,5,7 weeks	Rotating rod	Once a week
8-10 weeks	Swimming	Once a week

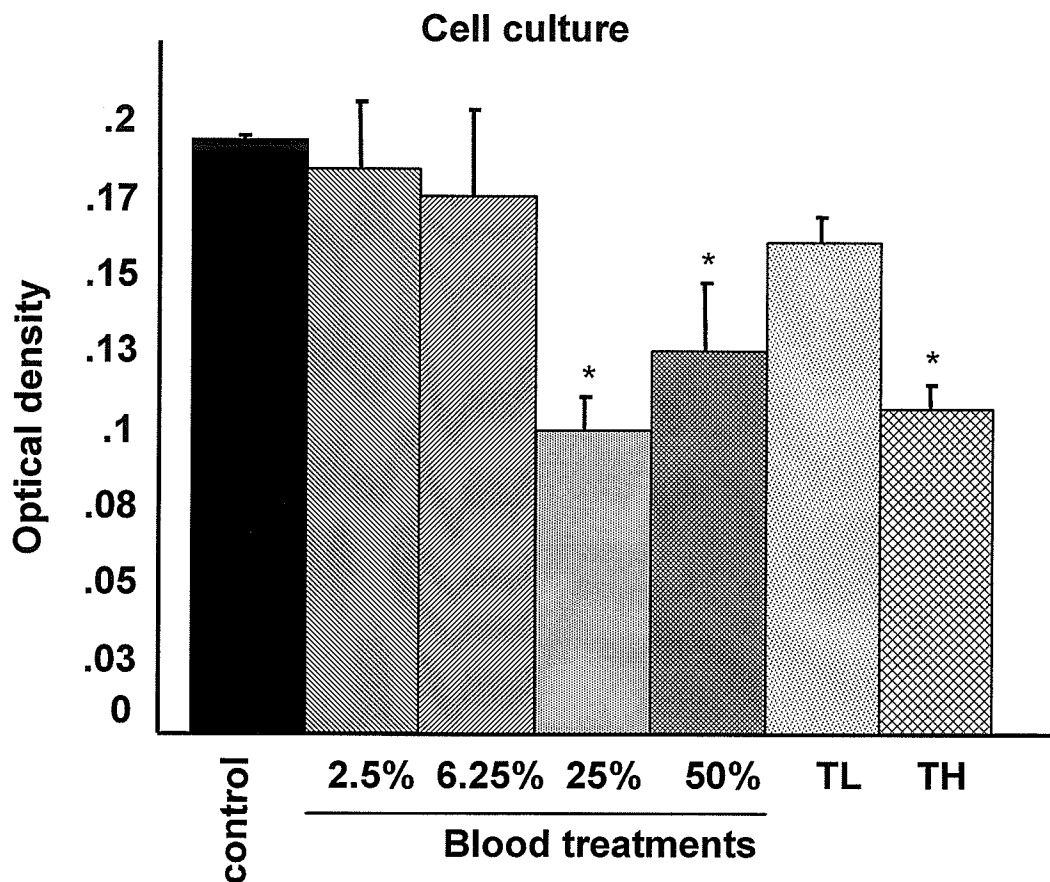


Figure 2-8-1. Viability of cultured rat brain cells 24 hours after exposure to whole blood or thrombin. For blood treatments, percentages indicate the proportion of blood in total of culture medium volume. Whole blood starting at 25% caused a significant decrease in viability. Thrombin at 6.5 units (TL), which is in a blood volume equivalent to 6.25% of the culture medium, did not cause a significant decrease in viability of cells. Thrombin at 26 units (TH) which is in a blood volume equivalent to 25% of the culture medium, caused significant loss in cell viability ( $p < 0.05$ , ANOVA and Fisher's PLSD).

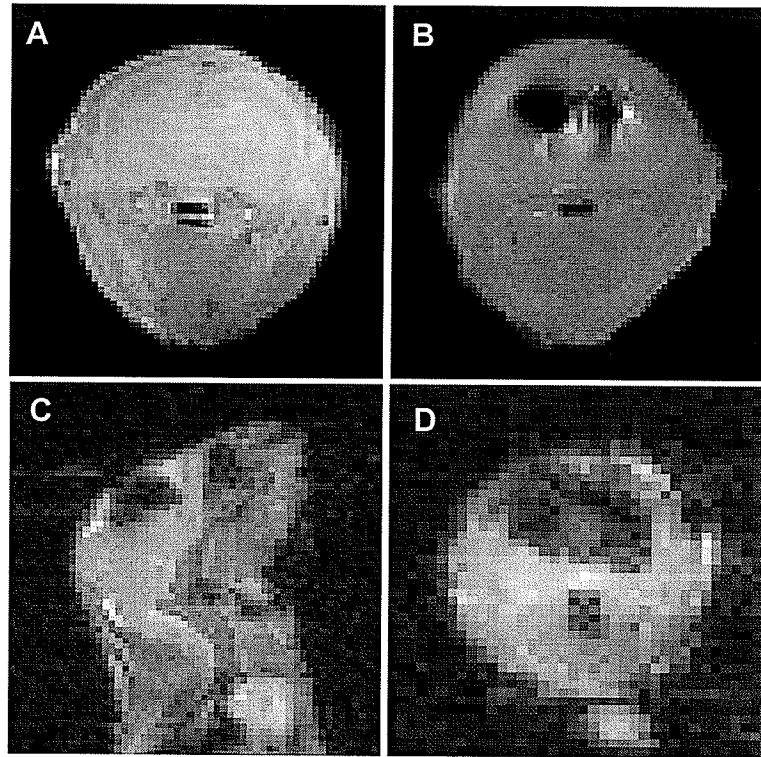


Figure 2-8-2. Magnetic resonance imaging of neonatal rodent brain. A. Coronal image of normal 2-day rat brain. B. Twenty minutes following blood (15  $\mu$ L) injection, the hematoma in rat striatum and ventricles appears dark. C and D. The appearance of the acute hematoma is similar in the striatum and ventricles in sagittal and coronal images of 2-day old mouse.

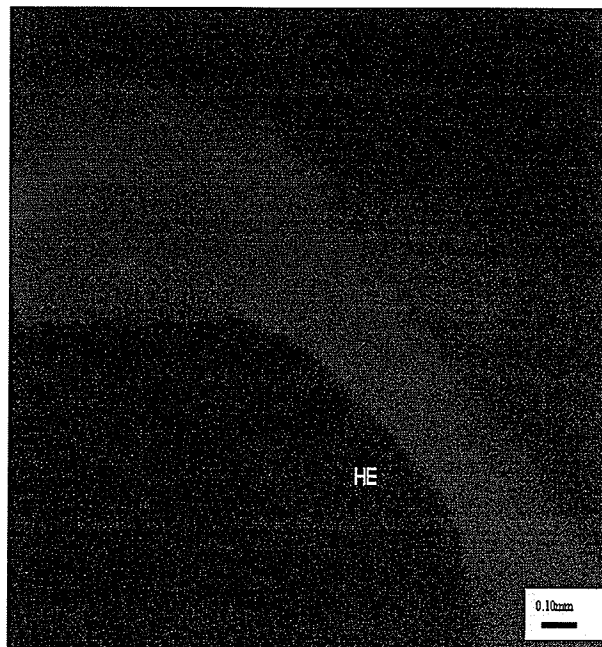


Figure 2-8-3. Serine protease activity following neonatal rat periventricular hemorrhage. An overlay membrane impregnated with D-Pro-Phe-Arg (“thrombin” substrate) exhibits a halo of fluorescence beginning at ~20 minutes (60 minutes is shown), indicating that there is increased serine protease activity for a limited distance around the hematoma (HE). Activity over the hematoma itself was very low.

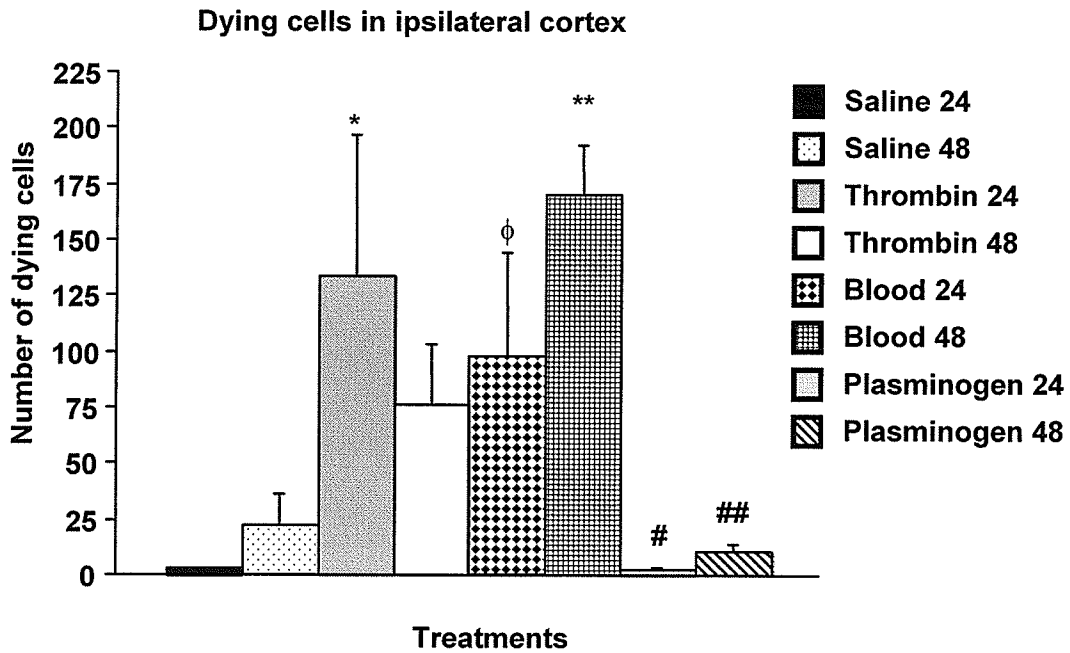


Figure 2-8-4. Dying cells in rat brain following injections of blood and thrombin. Bar graphs show the average number of dying cells (per 4x 540  $\mu$ m x 540  $\mu$ m area) in the lateral cortex of rat brain 24 and 48 hours following injection of saline, blood, thrombin, and plasminogen. (\*  $p < 0.01$ , saline 24 hours vs. thrombin 24 hours; \*\*  $p < 0.01$ , saline 48 hours vs. blood 48 hours; #  $p < 0.05$ , plasminogen 24 hours vs. thrombin 24 hours; ##  $p < 0.01$ , plasminogen 48 hour vs. blood 48 hours; phi  $p < 0.05$ , thrombin 48 hours vs. blood 48 hours). ANOVA and Fisher's PLSD were used.

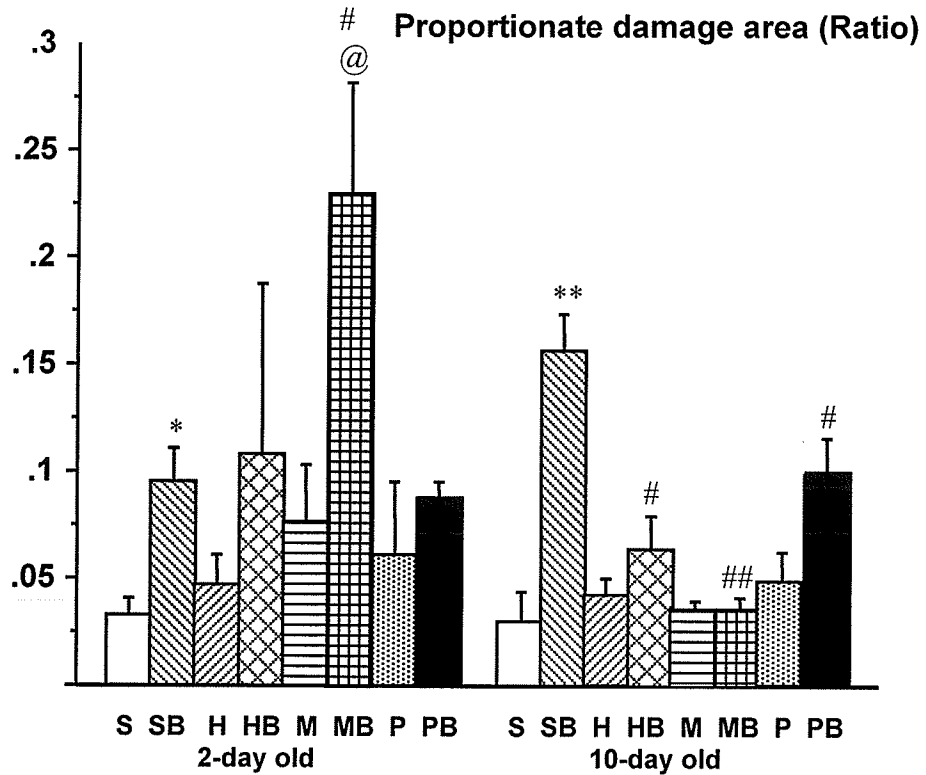
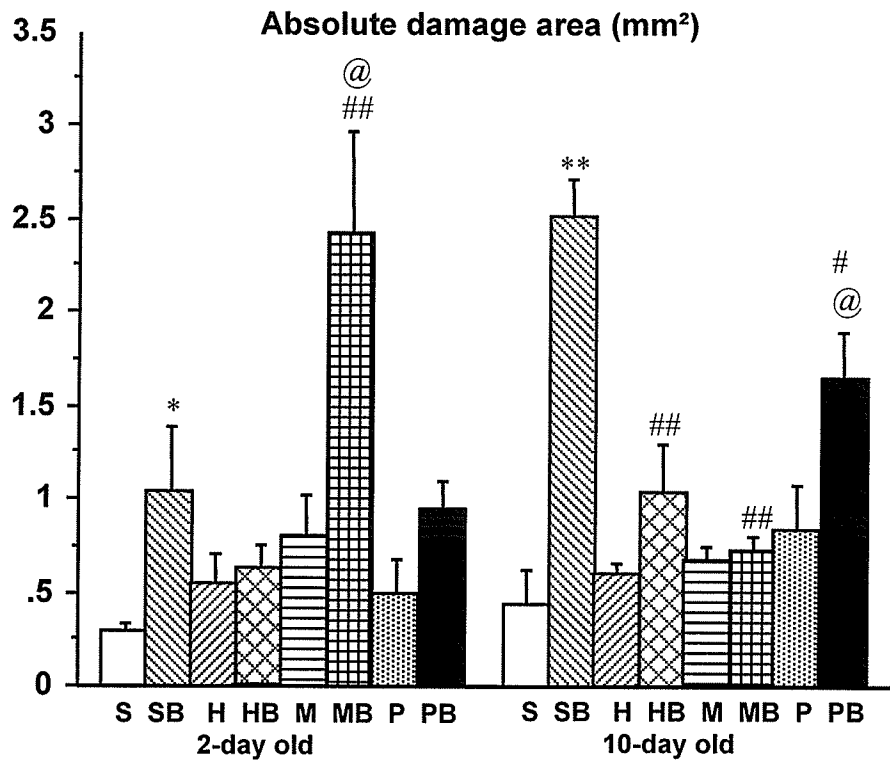


Figure 2-8-5. Acute mouse brain damage following injections of blood alone or with inhibitors. Bar graphs (mean  $\pm$  SE) show the absolute brain damage areas (upper panel) and proportionate brain damage areas (lower panel) 2 days following injections of agents alone or with blood into mouse brain. The absolute and proportionate brain damage areas were significantly increased following injections of blood with saline compared to saline injections in 2 and 10-day old mice. No significant changes could be seen following injections of hirudin,  $\alpha$ 2macroglobulin, and PAI-1 alone compared to saline injection. (\*:  $p < 0.05$ , \*\*:  $p < 0.01$  saline vs. saline with blood). Both indices of brain damage areas were significantly increased following injection of  $\alpha$ 2macroglobulin with blood in 2-day old compared with injection of saline with blood. Injection of blood with hirudin,  $\alpha$ 2macroglobulin, and PAI-1 significantly decreased the both indices of brain damage areas compared to saline with blood in 10-day old mice (#:  $p < 0.05$ , ##:  $p < 0.01$ , saline with blood vs. hirudin,  $\alpha$ 2macroglobulin, and PAI-1 with blood). Injections of hirudin with blood significantly reduced brain damage areas compared with injection of  $\alpha$ 2macroglobulin with blood in both ages and PAI-1 with blood in 10-day old mice (@:  $p < 0.05$ ; @@:  $p < 0.01$ , hirudin with blood vs.  $\alpha$ 2macroglobulin and PAI-1 with blood). (ANOVA and Fishers PLSD test). Abbreviations: S: saline, SB: saline and blood, H: hirudin, HB: hirudin and blood, M:  $\alpha$ 2macroglobulin, MB:  $\alpha$ 2macroglobulin and blood, P: PAI-1, PB: PAI-1 and blood.

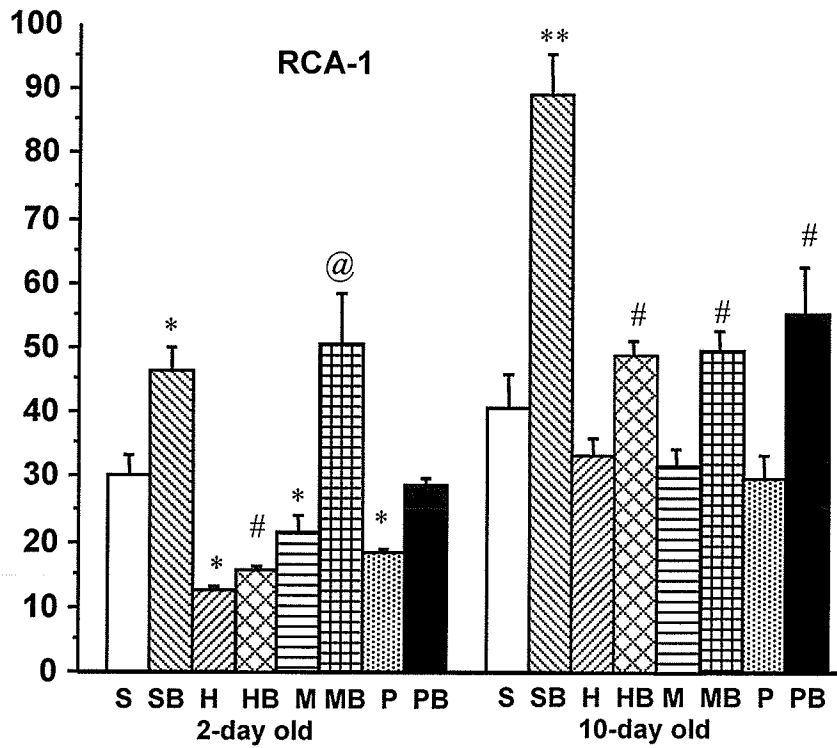
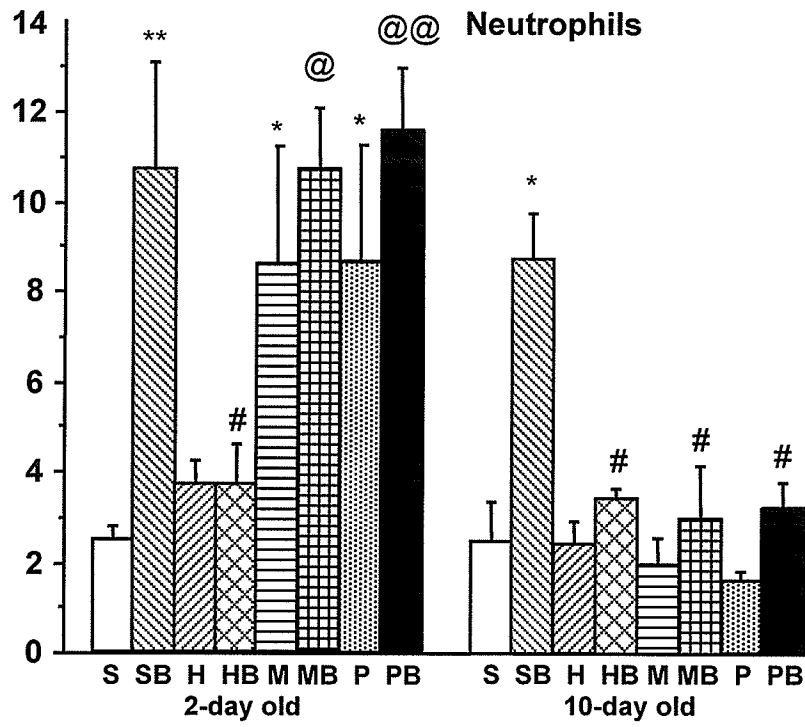


Figure 2-8-6. Acute mouse brain inflammation following injections of blood alone or with inhibitors. Bar graphs (mean  $\pm$  SE) show neutrophil infiltration (upper panel) and microglia / macrophages reaction (lower panel) 2 days following injections of agents with or without blood into mouse brain. Injection of  $\alpha$ 2macroglobulin and PAI-1 caused more neutrophil infiltration compared to saline alone in 2-day old mice. The number of neutrophils and microglia / macrophages was greater following injections of saline with blood compared to saline alone in both ages (\*:  $p < 0.05$ , \*\*:  $p < 0.01$ , saline vs.  $\alpha$ 2macroglobulin, PAI-1, and saline with blood). The number of neutrophils and microglia / macrophages was significantly reduced following injections of hirudin with blood in both ages. Injections of  $\alpha$ 2macroglobulin or PAI-1 with blood compared with saline with blood significantly reduced microglia / macrophages in 10-days old mice (#:  $p < 0.05$ , ##:  $p < 0.01$ , saline with blood vs. hirudin,  $\alpha$ 2macroglobulin, and PAI-1 with blood). Injections of hirudin with blood significantly reduced neutrophils and microglia/macrophages compared with injection of  $\alpha$ 2macroglobulin and PAI-1 with blood in 2-day old mice (@:  $p < 0.05$ ; @@:  $p < 0.01$ , hirudin with blood vs.  $\alpha$ 2macroglobulin and PAI-1 with blood). (ANOVA and Fishers PLSD test). Abbreviations: S: saline, SB: saline and blood, H: hirudin, HB: hirudin and blood, M:  $\alpha$ 2macroglobulin, MB:  $\alpha$ 2macroglobulin and blood, P: PAI-1, PB: PAI-1 and blood.

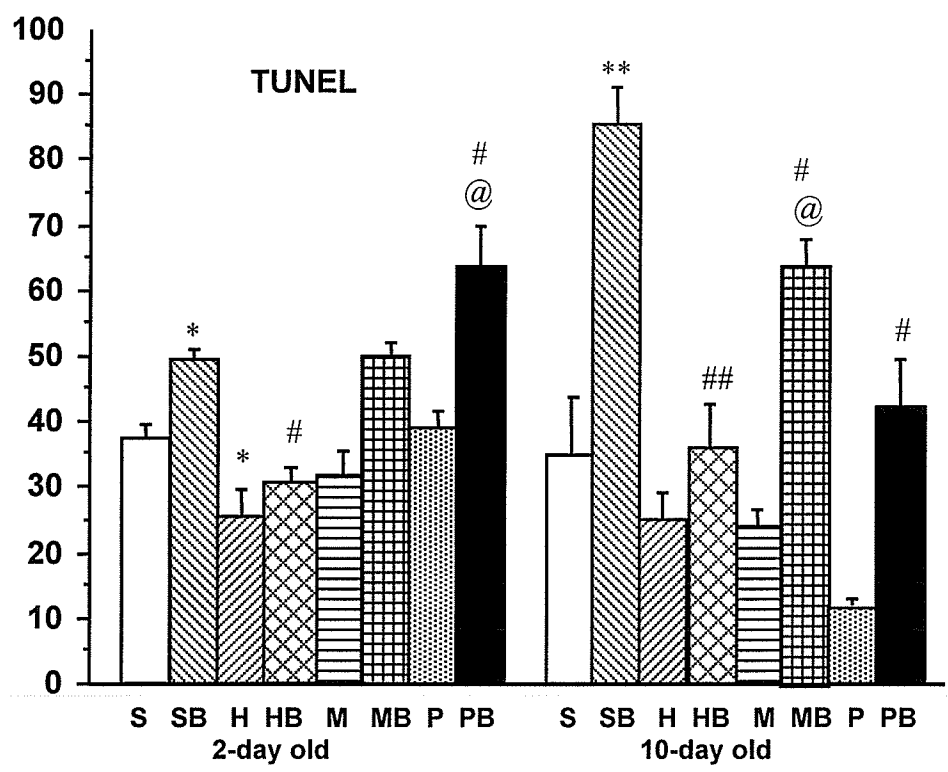
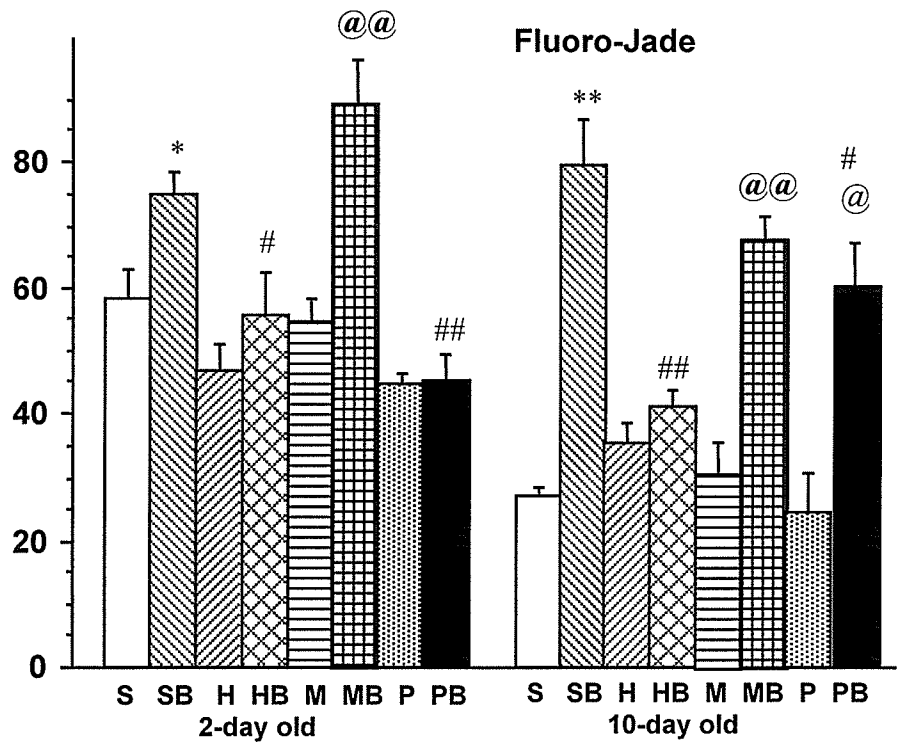


Figure 2-8-7. Acute mouse brain cell death following injections of blood alone or with inhibitors. Bar graphs (mean  $\pm$  SE) show neuron death (upper panel) detected by Fluoro-Jade staining and cell death detected by TUNEL (lower panel) 2 days following injections of agent alone or with blood into mouse brain. The number of dying neurons and TUNEL positive cells were greater following injections of saline with blood compared to saline injections. Injection of hirudin and PAI-1 caused less TUNEL positive cells compared to saline in both ages. (\*:  $p < 0.05$ , \*\*:  $p < 0.01$ , saline vs. hirudin, PAI-1 and saline with blood). The number of dying neurons and TUNEL positive cells were significantly reduced following injections of hirudin and PAI-1 with blood in both ages compared to saline with blood. Injection of  $\alpha 2$ macroglobulin with blood significantly increased the TUNEL positive cells compared to saline with blood in 10-day old mice (#:  $p < 0.05$ , ##:  $p < 0.01$ , saline with blood vs. hirudin,  $\alpha 2$ macroglobulin, and PAI-1 with blood). Injections of hirudin with blood significantly reduced cell death compared with injection of  $\alpha 2$ macroglobulin with blood in both ages (@:  $p < 0.05$ ; @@:  $p < 0.01$ , hirudin with blood vs.  $\alpha 2$ macroglobulin and PAI-1 with blood). (ANOVA and Fishers PLSD test). Abbreviations: S: saline, SB: saline and blood, H: hirudin, HB: hirudin and blood, M:  $\alpha 2$ macroglobulin, MB:  $\alpha 2$ macroglobulin and blood, P: PAI-1, PB: PAI-1 and blood.

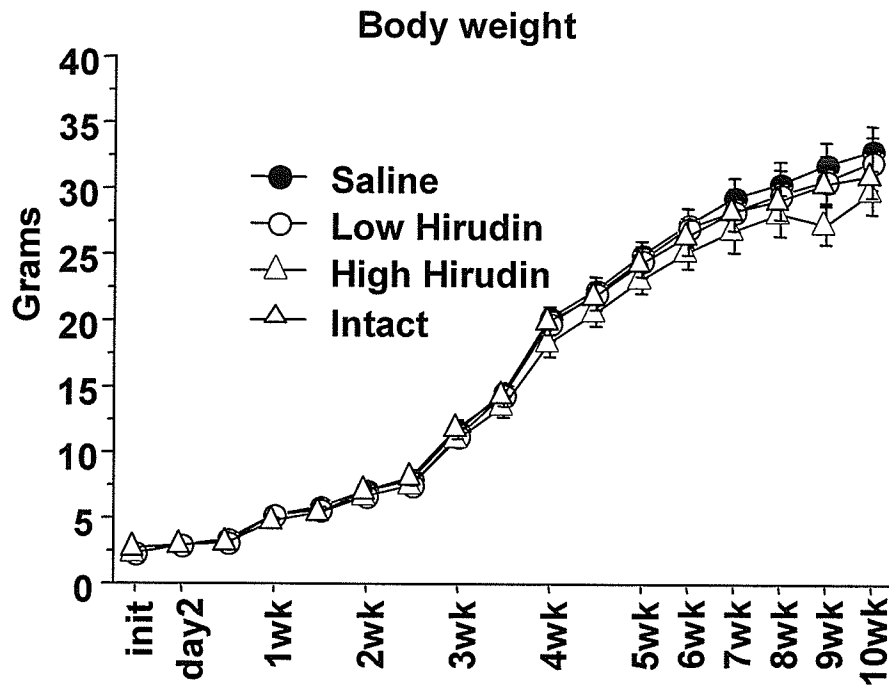
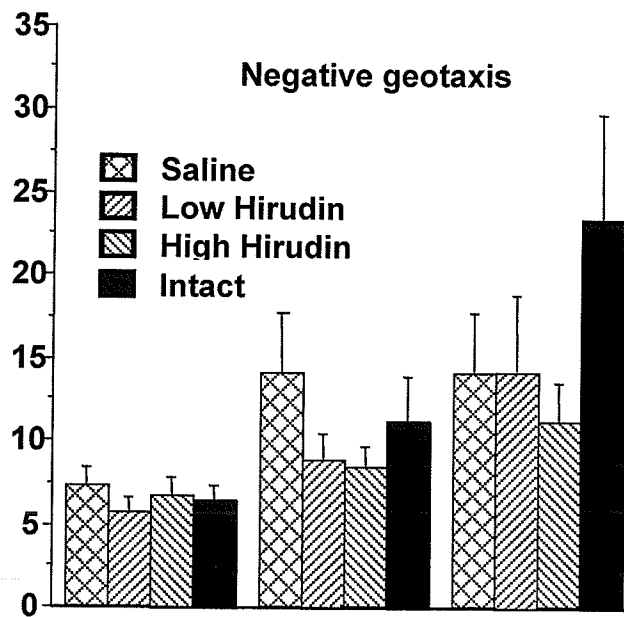
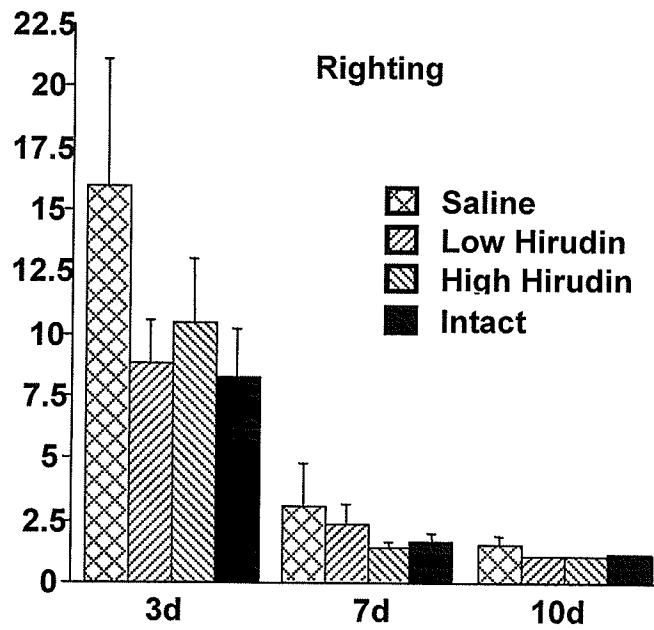


Figure 2-8-8. Body weight of mice that received intracerebral injections of blood alone or with hirudin. Line graph shows the body weight (mean  $\pm$  SE) of mice in intact controls as well as prior to injections (init) and following injections of blood with saline, low dose (5 U), or high dose hirudin (10 U) in 2-day old mouse brain. There was no significant difference in body weight between the four groups (ANOVA and post hoc Fishers PLSD test).



Y axis: Time (Seconds)

Figure 2-8-9. Behavior of mice that received intracerebral injections of blood alone or with hirudin in the neonatal period. Bar graphs (mean  $\pm$  SE) show the latency to righting (upper panel) and negative geotaxis (lower panel) at age 3 to 10 days in intact controls and 2 days following injections of blood with saline, low dose hirudin (5 U), or high dose hirudin (10 U). The righting latency decreased as the mice matured. There was no significant difference between groups ( $p=0.117$ , ANOVA and post hoc Fishers PLSD test). The negative geotaxis latency gradually increased from the 3 days to 10 days as the reflex to turn became suppressed. However, mice with PVH had persistence of the reflex. Hirudin had minor effect at 7 days ( $p=0.092$ ).

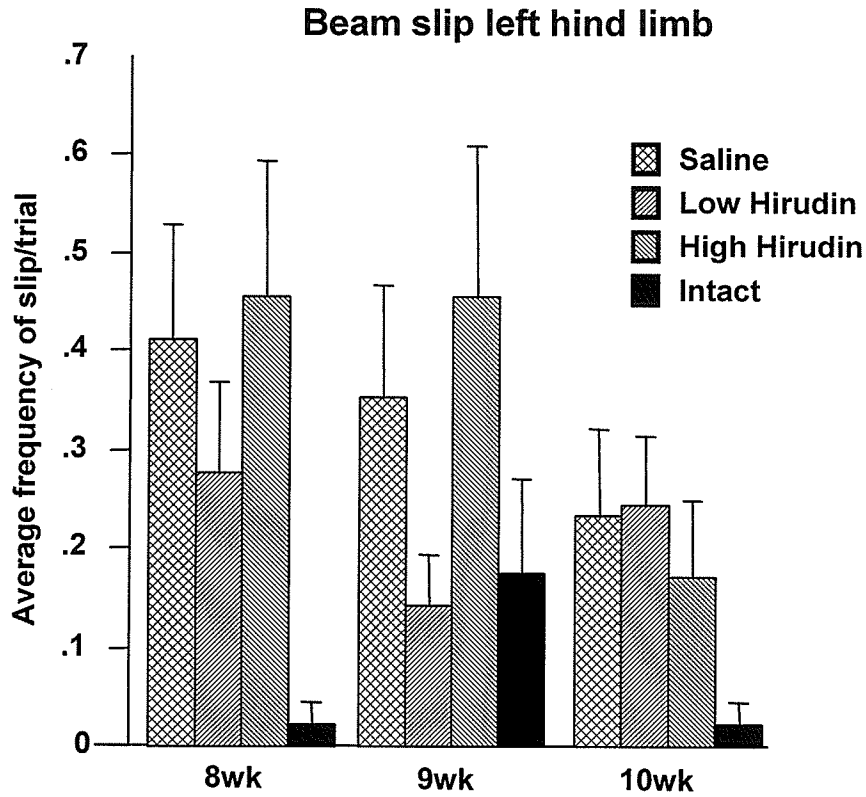


Figure 2-8-10. Beam walking by mice that received intracerebral injections of blood alone or with hirudin in the neonatal period. Bar graphs showing the left hind limb slips (mean  $\pm$  SE) during beam walking from 8 to 10 weeks in intact control and following injections of blood with saline, low dose (5U), or high dose hirudin (10 U) into 2-day old mouse brain. There was no significant difference in the groups with PVH although the test showed significant ( $p < 0.05$ ) impairment compared to intact mice (ANOVA and post hoc Fishers PLSD test).

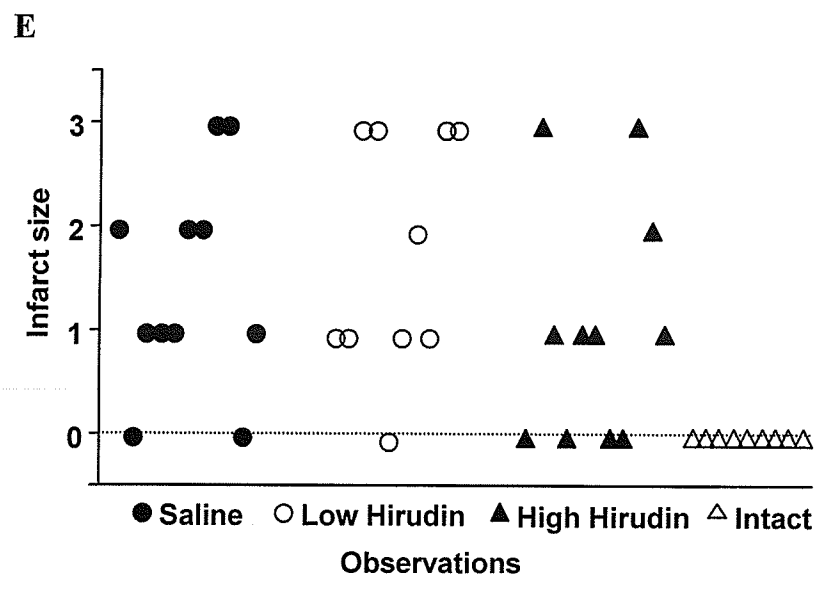
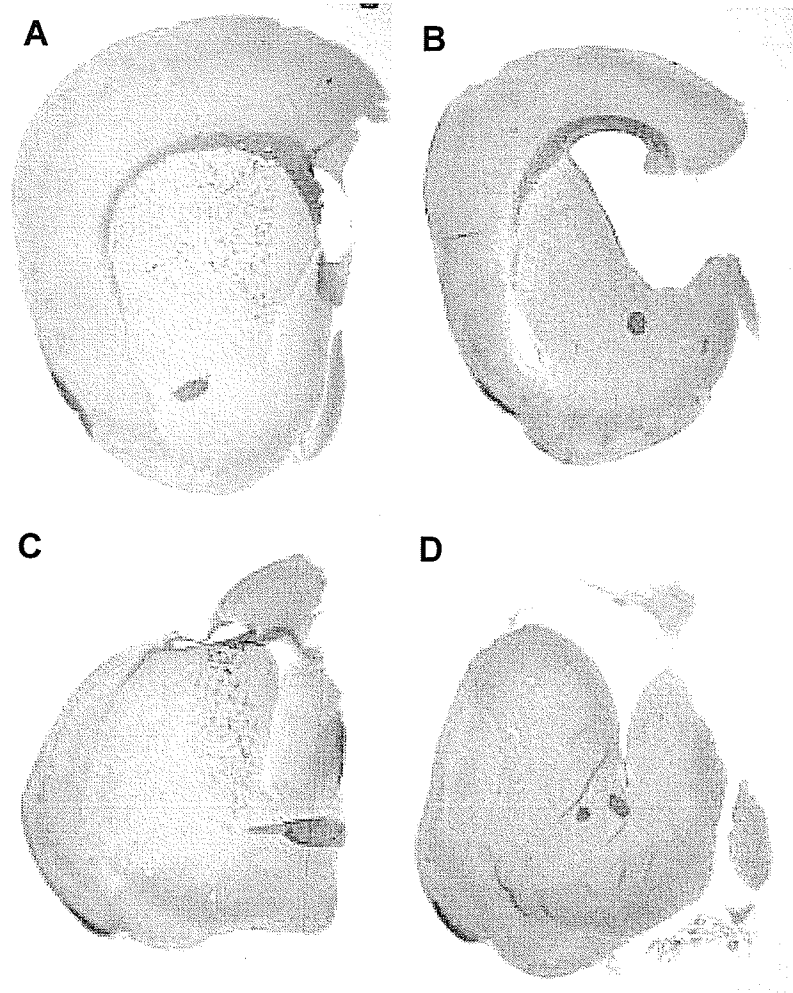


Figure 2-8-11. Chronic brain damage in mice that received intracerebral injections of blood alone or with hirudin in the neonatal period. Photographs of solochrome cyanine stained mouse brain hemispheres in coronal section illustrate the infarct grading. A is an intact normal half brain in 10-week old mouse. B shows grade 1 damage; mildly enlarged lateral ventricle with mild atrophy of striatum, external capsule, or dorsal cortex. C shows grade 2 damage; the dorsal cortex and white matter are destroyed and there is loss of lateral striatal white matter bundles. D shows grade 3 damage; the superior and lateral cortex and white matter are destroyed and the striatum is atrophic. Scattergram of the injury grades (E) shows that the high dose hirudin (10 U) slightly reduced the frequency of brain infarction following injection with blood compared to injection of saline with blood in mouse brain ( $p=0.259$ , Kruskal-Wallis test).

## CHAPTER 3 GENERAL DISCUSSION

The data described in this thesis provide new information regarding the pathophysiology of experimental ICH by correlating brain inflammation and cell death with blood fragments, proteolytic enzymes, type of animal model, and stage of brain maturation. Qualitative and quantitative data have revealed aspects of brain pathology not previously reported. ICH causes brain damage through multiple mechanisms<sup>259</sup>. Direct tissue destruction by the hemorrhagic event and dissection of blood along tissue planes occurs immediately. This is followed by development of edema and secondary brain damage due to raised intracranial pressure and distortion of the microvasculature<sup>2</sup>. Thrombin and plasmin are potentially toxic in the first day following ICH<sup>92</sup>. Delayed damage could result through a variety of mechanisms including local ischemia, release of toxins by blood breakdown products, release of proteolytic enzymes, or inflammation involving chemokines, cytokines, and leukocytes<sup>4, 38, 42, 52-54, 92, 259, 297</sup>. Blood clot and damaged brain after ICH liberate chemotactic factors, including thrombin<sup>272</sup>, that prompt the movement of leukocytes from the blood into insulted brain<sup>273</sup>. Activated leukocytes possibly can cause secondary brain damage through the release of cytokines, ROS, NO, MMPs, and other proteases<sup>275, 276</sup>.

### 3.1 Animal models play an important role in ICH research

Animal models of ICH are very important to understand the pathogenesis and to evaluate preventive or therapeutic strategies. ICH has been studied in several species

including mouse<sup>37</sup>, rat<sup>38-42</sup>, rabbit<sup>9, 43</sup>, cat<sup>44</sup>, pig<sup>45</sup>, and primate<sup>46</sup>. In the present study we compared inflammation and cell death in three commonly used models of ICH, and developed a novel model of PVH/IVH in neonatal mice to study the ICH in immature brain.

Brain cell death and inflammatory cell infiltration following ICH in rats continues for several weeks after autologous blood injection, avulsion of cerebral blood vessels, and collagenase injection. The three models are associated with similar temporal patterns of cell death and inflammation. Autologous blood injection is most similar to human ICH with the exception of needle insertion. Cortical vessel avulsion causes ischemic infarction and hemorrhage. It is therefore not a pure ischemic stroke model as has been previously implied<sup>266, 271</sup>, rather it is a model of mixed ischemia and hemorrhage more similar to a traumatic cortical laceration than an ischemic infarct. The brain damage caused by collagenase injection is most consistent from an anatomical perspective but is most artificial from a biological perspective. Cell death and inflammation begin earlier in comparison to the other models. Possibly the collagenase activity causes direct and rapid cell injury in addition to creating a hematoma. In this regard, the model differs from the human situation and models using autologous injections. The model of ICH should be chosen carefully to address parameters one is interested in studying.

PVH/IVH occurs most commonly in premature infants 24 - 30 weeks gestation<sup>15</sup>. Some models of IVH or PVH/IVH had been developed in rabbits<sup>70</sup> and dogs<sup>69, 73</sup>, but these studies have been concerned with the physiologic processes and structural features that allow PVH/IVH to occur, but not the tissue reactions. We developed a novel model of PVH/IVH in newborn mouse by injection of a small amount of autologous blood into

periventricular tissue including germinal matrix and striatum. Most mice exhibited extension of the hematoma into the ventricles. Therefore, this model corresponds to grade III / IV PVH/IVH as defined by imaging studies in premature human infants <sup>364</sup>. Sequential studies after PVH/IVH showed rapid dispersion of the blood, which is probably washed away by CSF. MRI showed that ventricles enlarged slightly weeks after PVH/IVH. This is similar to the hydrocephalus that develops after PVH/IVH in prematurely born infants <sup>367</sup>. This model provides an opportunity to study mechanisms of cellular injury after PVH/IVH.

### 3.2 Brain inflammation plays a role in brain injury following ICH

#### 3.2.1 Brain inflammation is significant following ICH

Inflammation is an obvious brain response following ICH and includes influx of neutrophils, CD8 lymphocytes (possibly CTL or NK cells), and microglia/macrophages as well as actions of cytokines and chemokines. We found that obvious inflammation occurred following infusions of blood, leukocytes, collagenase, thrombin, and plasminogen into rodent brain <sup>38-40</sup>. Similar brain reactions are seen following mechanical brain trauma in mice <sup>143</sup> and brain contusion in rats <sup>144</sup>. Chemotaxis of neutrophils and lymphocytes, and later of monocytes, is mediated by chemokines and complement <sup>301, 302</sup>. Neutrophils can release potentially harmful factors such as oxygen radicals <sup>261</sup> or cytokines including TNF- $\alpha$ , IL-6, and IFN- $\gamma$ , which seem to play a role in brain damage <sup>79, 129</sup>. Neutrophils can also exacerbate brain injury by obstructing microvessels, thereby causing local ischemia <sup>306</sup>. Many experimental studies have documented infiltration of

NK cells into injured brain <sup>301, 307, 308</sup>. Brain contusions in rats showed that NK and T cell infiltration was more prevalent than neutrophilic infiltrate <sup>144</sup>. We also observed a significant number of CD8 $\alpha$  lymphocytes that could be injurious directly or indirectly through release of IFN- $\gamma$ . CTLs and NK cells express CD95 ligand (CD95L or FasL) which binds to CD95 (Fas) on target cells to induce apoptosis. Alternatively activated CTLs release perforin and deliver granzymes to induce the target cell apoptosis.

### 3.2.2 Brain inflammation along with cell death is time-dependent following ICH

Chapter 2-1 demonstrates that injection of a small quantity of whole blood into the rat striatum is associated with cell death, inflammatory cell infiltration, and microglial/macrophage reaction that varies in a time-dependent manner. Cell death was commonplace from 24 hours to 4 weeks and peaked 72 h after blood injection. Neutrophil infiltration into brain surrounding the hematoma is substantial by 1 day, peaked at 2 days then rapidly decreased, possibly because neutrophils died within 1-2 days of extravasation. Intense neutrophilic infiltrate has been previously documented in brain contusions <sup>303, 304</sup>, and ischemic sites <sup>305</sup> beginning at 6 - 12 hours and peaking at 48 - 72 hours. In human brains, neutrophil infiltration is apparent 5 - 72 hours after ICH or contusion <sup>1, 113-116</sup>. In our comparison of three models of ICH we found that many neutrophils invade the hematoma and surrounding tissue after collagenase-induced ICH in rats <sup>63</sup>.

We observed that the injection of whole blood, concentrated leukocytes, and "activated" leukocytes into the cerebral cortex of rats is associated with cell death and inflammatory cell infiltration at 48 hours. Plasma or serum alone and concentrated

erythrocytes had negligible effect. Concentrated leukocytes had a mild adverse effect, whereas “activated” leukocytes had a strong adverse effect. We can not exclude the possibility that specific blood / plasma fractions exert damage at different times. Other investigators showed that cerebral edema develops 3 days after erythrocyte injection and they suggested that hemoglobin released from lysed erythrocytes is toxic to brain <sup>42</sup>. The toxic effect of hemoglobin on neurons has been demonstrated in vitro <sup>94</sup>. In our study neither plasma nor serum caused more damage than saline injection. However, thrombin has been shown to cause brain edema and seizures following intracerebral injection <sup>3, 93, 297</sup>. Possible explanations are that thrombin might be inactivated during processing of the plasma or that the “pharmacodynamics” might be altered because a blood clot allows slow focal release whereas plasma injection would diffuse rapidly leading to lower regional concentrations.

The concentrated leukocytes caused greater injury than other blood fractions. We have to mention that the leukocytes occupy less than 1% of the volume of whole blood. Therefore the leukocyte injection groups received a dose equivalent to 5 ml of whole blood <sup>309</sup>. Regardless, “activated” cells appear to be more harmful, perhaps through production of more of the deleterious mediators mentioned above. This might help to explain the observation that fever during the first 3 days after ICH is an independent predictor of poor prognosis in patients <sup>310</sup>. It is important to recognize that activated platelets, which we did not study directly, are included in the leukocyte fraction. Platelets can release serotonin and platelet-derived growth factor (PDGF), which are capable of increasing vascular permeability and causing vasoconstriction <sup>311</sup>.

Why was injection of some blood fractions associated with enlargement of the lesions well beyond the limits of the injected substance? Several results suggest that mechanisms other than mass effect are involved in the contribution of blood to perihematoma edema formation, because blood produces larger lesions than would be expected from its space occupying effects alone <sup>256</sup>. This might be explained by a secondary effect of the injected substances on the vasculature through agents, for example endothelin <sup>413</sup>, that can promote vasospasm and / or increased vascular permeability <sup>312</sup>. We created large non-hemorrhagic necrotic lesions by freezing that could be compared to the lesions caused by blood injections. The freeze lesion was reasonably successful in this regard, having caused only minimal hemorrhage but considerable release of plasma <sup>314</sup>. At the margin it was associated with considerably fewer dying cells and neutrophils than the whole blood injection. The devascularization injury was associated with deep hemorrhage.

The data from newborn mouse PVH/IVH showed that inflammatory cell infiltration and cell death had a similar temporal pattern as adult rat brain following blood injection <sup>39</sup>. However, the number of infiltrating neutrophils and lymphocytes was much lower. Possible reasons are that the chemokines are diluted and washed quickly from the highly hydrated newborn brain <sup>373</sup>, or that there may be an interspecies difference. The latter can be excluded because injection more laterally into the striatum caused inflammation similar to that in adults. This suggests that leukocytes probably play a minor role in the brain damage following the PVH/IVH. Dying cells, demonstrated by TUNEL and Fluoro-Jade, significantly increased in quantity in the damaged striatum, peaking 2 days following PVH/IVH.

### 3.2.3 Brain cell death accompanies inflammation following ICH

Brain cell death always accompanies brain inflammation, which might be a cause of cell death or be stimulated by the same factors. The quantity of TUNEL positive cells did not match that of the dying neurons defined by eosinophilia on H&E staining or Fluoro-Jade staining. There are several reasons for the disparity. TUNEL positive cells might understate the magnitude of cell death because they persist only for several hours<sup>279</sup> while dying neurons can persist for days or weeks<sup>280</sup>. Furthermore, TUNEL positive cells include neurons, glia, and inflammatory cells. Death of the latter does not necessarily reflect the final neurological injury<sup>281</sup>. Nevertheless, the use of TUNEL with additional markers to confirm the type of dying cell can provide a gauge of the magnitude of cell death. There are no differences in the quantity of dying neurons shown with the Fluoro-Jade staining and the eosinophilic neurons shown with H&E staining. It is likely they represent the same population of damaged neurons<sup>189</sup>. Fluoro-Jade staining is an easy way for quantifying dying neurons because the signal-to-noise ratio is high.

### 3.2.4 Immune preactivation exacerbates the brain damage following ICH

Our current data demonstrate that brain inflammation, cell death, and damage are aggravated following blood injection into mouse brain after immune pre-stimulation using LPS, ConA, and PolyI:C in mice of three ages, most obviously in 2-day old mice. Microglia become activated in response to injury, infection or inflammation<sup>414</sup>. The bacterial endotoxin LPS after intraperitoneal injection stimulates inflammatory cells to produce the pro-inflammatory factors that may have detrimental action on the brain.

Increased brain damage following blood injection after LPS pre-stimulation in neonatal mice might be caused by increased inflammation<sup>40</sup>. Inflammatory cells included in the hematoma, as well as those infiltrating from blood, could release free radicals and inflammatory cytokines<sup>141, 142</sup>, which are harmful to the brain cells<sup>79</sup>, and may cause cell death. Systemically administered cytokines IL-1 $\beta$ , IL-6, IL-9, or TNF- $\alpha$  exacerbate brain lesions in 5-day old mice following intracerebral injection of ibotenate<sup>396</sup>.

INF- $\gamma$  is mainly produced by leukocytes and activated microglia/macrophages. Adult INF- $\gamma$  knockout mice had significantly reduced neutrophil infiltration and cell death compared to wild-type mice following ICH. The immune effects of INF- $\gamma$  include the ability to enhance the microbicidal activity of macrophages, activation of CTL and NK cells, and upregulation of class I and II MHC antigen expression on a variety of cells<sup>397, 415</sup>. INF- $\gamma$  can enhance apoptosis through perforin/granzymes or Fas ligand mechanism. INF- $\gamma$  is elevated in unspecified brain cells of the ischemic hemispheres after brain ischemia in rats<sup>416</sup>. In MS tissue, INF- $\gamma$  has been detected at high levels on microglia and leukocytes<sup>398</sup>. The aberrant expression of INF- $\gamma$  within the CNS is thought to contribute to upregulation of genes such as class I and II MHC, ICAM-1, and others. These data indicate that INF- $\gamma$  might contribute to the secondary brain injury following ICH.

We conclude that inflammation, including the cytokine mediator INF- $\gamma$ , might be an important factor in brain injury following ICH. Whether the inflammation following ICH contributes directly to neuronal loss remains to be proved. If so, anti-inflammation represents potential targets for therapeutic intervention during the early stage following ICH.

### 3.3 Proteolytic enzymes are involved in the pathogenesis of brain damage following ICH

#### 3.3.1 Brain inflammation and damage caused by thrombin and plasmin are dose and age-dependent

Injection of thrombin and plasminogen into the striatum of rodents is associated with dose and age dependent brain damage, cell death, and inflammation at 48 hours. Culture of striatal cells showed that thrombin but not plasmin caused significant reduction in cell viability. The focal brain damage associated with enzyme injections was rapid and most likely due to a direct effect of these agents on the neuropil or the vasculature. It was similar in magnitude to that seen following intracerebral infusions of blood<sup>39,40</sup>.

Thrombin is produced by cleavage of prothrombin and it converts fibrinogen into fibrin, which is ultimately involved in formation of a blood clot. Neurons and glia produce thrombin and thrombin receptors<sup>203</sup>, especially in the newborn period<sup>221</sup>. Thrombin induces numerous responses through protease activated receptors (PARs). To date, four members of the PAR family have been identified. PAR-1, PAR-3, and PAR-4 are considered as thrombin receptors, while PAR-2 is activated by serine proteases other than thrombin, such as trypsin and mast cell tryptase<sup>407, 408</sup>. In culture, astrocytes proliferate in response to thrombin acting through PAR-1<sup>84, 407</sup>. In vitro, thrombin impairs neurite outgrowth<sup>203</sup> and induces apoptosis<sup>204</sup> likely through PAR-2<sup>226, 227</sup>. Microglia proliferate in response to thrombin through PAR-4<sup>409</sup>.

Plasminogen is produced by brain endothelia and some neurons<sup>316</sup> and converted into plasmin by tPA and uPA. Plasmin can digest fibrin to allow lysis of blood clots. Plasmin, tPA, and uPA play a role in migration, synaptogenesis, and formation of myelin. Plasmin-mediated activation of platelets occurs by cleavage of PAR-4<sup>411</sup>. Plasmin may regulate PAR-2 signalling under pathological conditions<sup>412</sup>. Thrombin and plasmin can induce endothelin synthesis and subsequent vasospasm and ischemia<sup>334-336</sup>. When injected into the brain, thrombin<sup>297, 315</sup> and plasmin<sup>317</sup> can cause brain edema. The edema induced by thrombin can be inhibited by thrombin inhibitors such as hirudin<sup>93, 297, 315, 327</sup>, argatroban<sup>417</sup>. The edema-induced by plasmin may be through an effect on the blood brain barrier<sup>207</sup>. Plasmin and thrombin cause tissue necrosis and inflammation when injected into rodent brain<sup>38</sup> (Chapter 2-6).

Brain cell death caused by injection of high dose thrombin and plasmin is likely due to direct proteolytic activity, because the tissue necrosis was rapid and involved all cell elements, even those without known thrombin receptors. Thrombin and plasmin are both trypsin-like serine proteinases and are normally present in brain at low concentrations, especially during development. Plasmin is known to degrade a range of extracellular matrix proteins and to activate MMPs, which can also digest matrix proteins<sup>328, 337</sup>. MMPs are a family of proteolytic enzymes with relative specificity for components of the extracellular matrix. Following brain injury MMPs are produced by infiltrating inflammatory cells, microglia, and astroglia<sup>85</sup>. Plasmin can promote the activity of MMPs<sup>86, 87</sup>. MMPs can directly damage brain cells, cause cell death by processing the death molecules, disrupt myelin, and perpetuate inflammation<sup>86, 87</sup>. The proteolytic activity of high doses of thrombin and plasmin likely exceeds what can be

controlled by endogenous inhibitors (e.g. PAI-1,  $\alpha$ 2 macroglobulin, PN-1) and proteolysis continues unchecked<sup>230, 338-340</sup>. PAI-1 exists in brain only in very small quantities<sup>341</sup>, although it can be upregulated following experimental stroke<sup>342</sup>. In tPA deficient mice, plasmin is not activated, and they are less susceptible to neuronal injury following brain ischemia<sup>318</sup>.

### 3.3.2 Hirudin reduces brain injury following ICH

Brain damage caused by ICH may be due to many mechanisms such as inflammation, thrombin, edema, as well as direct proteolytic activity. Acute histological evaluation showed that the brain damage area, dying cells, and inflammation in 2-day and 10-day old mice were significantly decreased following injections of hirudin with blood compared to injections of saline with blood. Hirudin, the most potent natural thrombin inhibitor, was originally isolated from the medicinal leech, *Hirudo medicinalis*. Hirudin binds to thrombin's fibrinogen-binding exosite to inhibit the thrombin activity directly. Injections of  $\alpha$ 2-macroglobulin or PAI-1 with blood were less effective. Previous studies showed that PAI-1 deficient mice exhibit larger infarcts following middle cerebral artery occlusion<sup>343</sup> suggesting that plasmin plays a role in the brain damage. In our long-term behavioural study, there was no significant improvement following injections of two doses of hirudin with blood. However the high dose hirudin slightly reduced the incidence of brain infarction. Although the precise mechanism of thrombin induced damage is not known, these data suggest that thrombin inhibitor might protect the brain following the ICH.

### 3.4 Brain responses are age-dependent following ICH

The current data showed that injections of blood, plasminogen, and thrombin are associated with cell death and inflammation in an age dependent manner. There is greater brain damage in 2-day old than in 10-day old or adult mouse brain. Furthermore, the 2-day old brain is relatively more sensitive to the serine proteases than to whole blood. Why is the brain damage more severe in neonatal mice? Possibly the neonatal brain could be more susceptible because the blood vessels are more fragile <sup>15</sup>, because it has higher levels of PARs on immature cells, because the immature cells are more susceptible to proteolytic damage independent of specific receptors, or because toxic substances associated with the hematoma might diffuse more quickly in neonatal brain due to its higher water content. Damage to immature vessel walls might explain the widespread hemorrhagic infarct in the neonatal cerebral cortex following thrombin and plasmin injections.

We showed that there was an age dependent brain response following ICH after immune pre-stimulation in which the brain damage was more severe in 2-day old mice than in 10-day old or adult mice (Chapter 2-6). There is a significant interaction between age and treatment by ANOVA analysis, which supports the conclusion that interaction to ICH is age-dependent. This observation complements Kolb's findings that the neonatal rat brain recovers less well than juvenile or adult brains following cortical aspiration <sup>246, 384, 385</sup>. The age-dependent brain response has also been shown in other types of brain damage, such as brain ischemia <sup>248</sup>, traumatic brain injury <sup>238</sup>, and age-dependent neuroprotection against neonatal hypoxic-ischemic brain injury <sup>249</sup>. The mechanisms for the age-dependent brain injury are not clear. The immune prestimulation could affect

microglia directly, or could alter the systemic inflammatory status, which in turn affects brain following damage. However, neonatal mice are markedly more susceptible to LPS-induced lethality but more resistant to staphylococcal enterotoxin B (SEB) than are adults, and this was correlated directly with plasma TNF- $\alpha$  levels<sup>402</sup>. Clearly the age-related differences depend on the model system studied.

### 3.5 Shortcomings of these experiments and alternate approaches

The injection of thrombin and plasminogen (Chapter 2-3, 2-6) caused dose-dependent brain injury. Several caveats must be noted. First, we have no way of determining whether the proteolytic activity is representative of what actually occurs following hemorrhage. We injected plasminogen instead of plasmin due to possibility that some plasmin activity is lost when it is purified in the post-activated form; the plasminogen is presumed to be activated *in situ*<sup>38</sup>. Furthermore, the actual activity of thrombin at a particular site can be very difficult to predict because it is self-amplifying and because it is rapidly inactivated by binding to fibrin<sup>329,331</sup>. Second, the plasminogen and thrombin that we used were bovine proteins and we cannot exclude the contribution of an immune response to foreign proteins. Third, we did not assess long-term outcomes to determine if the response in older animals is delayed<sup>38</sup>, although based on our prior work we think that is unlikely. Fourth, in the adult rats only two doses were used, we cannot know that the maximal adverse effect would not be achievable at a much lower dose. Therefore we have not determined the dose-response relationship necessary to speculate accurately on the mechanism of injury. Other non-rodent species need to be

studied to confirm these findings. Blocking experiments must be developed to ensure that all thrombin or plasmin activity is blocked selectively.

The comparative study (Chapter 2-3) showed the time course of three groups under study is not identical. However, the experiments were not done concurrently and were not originally designed for direct comparison. Furthermore, the anatomical regions affected were not the same; two models focused on the striatum and one on the cerebral cortex. We have previously done blood injections in the cortex and found them to be complicated by subarachnoid hemorrhage <sup>40</sup>. Regardless, the similarities and differences between the three models of ICH are apparent.

In the PVH/IVH study, neonatal mice are very small and they could not be secured in a stereotactic frame. Therefore, the method of freehand blood injection could cause variable brain damage. Histological examination revealed that the injections were not entirely consistent in terms of depth. We used MRI to be sure that blood was indeed injected into the correct location. The small size of the brain dictates that diffusible toxic agent(s) have effects in anatomic regions different from those in human brain. For example, a given protein that diffuses 5 mm in both mouse and human brain would produce bilateral effects in mice but only “focal” effects in humans. We do not know whether the route of toxic agent spread is through tissue or CSF. The absence of an intact ependymal layer at the age when blood is injected could allow toxic agents to spread from CSF into germinal tissue.

In the pre-activation of immune system study, we must consider the following. First, these are only short-term studies. It is possible that the immune stimulators only alter the time course of injury. A more complete dose response study is necessary.

Second, we could not measure the core and brain temperature, which might not be reflected in the axilla. A study using invasive monitoring should solve this question. Third, we could not get enough cardiac blood from the young mice to perform blood counts and differentiation. Furthermore, we did not test the circulating cytokine levels. This should be done with pooled blood studies. Fourth, actual bacterial or viral infection of the animal might have a different effect. Finally, although there is an association between increased inflammation and increased damage, we cannot determine which is cause and which is effect. Extensive experiments would be needed to clarify the cytokines involved and whether immune cells contribute to brain cell death. For example, the severe combined immune deficient (SCID) mice could be tested.

### 3.6 Conclusions

Extravascular blood causes a mixed inflammatory cell reaction in brains that is time dependent and maximal from 48-72 hours following hemorrhage. This is associated with death of brain cells over a prolonged period of at least 4 weeks. The contributing factors are leukocytes, which can be "activated" by systemic illness to exacerbate the injury, and thrombin as well as plasmin. The neonatal brain is relatively more sensitive to proteolytic enzymes than to blood possibly because the normal developmental processes rely on similar proteolytic activity. Extravasated blood might also play an important role in brain damage following PVH/IVH through suppression of cell proliferation. Different models of ICH are associated with similar temporal patterns of cell death and inflammation, but the magnitude of inflammation varies. This should be taken into consideration when choosing an experimental model. The precise molecular and

chemical mechanisms remain to be determined. They are likely multiple and include secondary ischemia, inflammation, and proteolytic enzymes. Complete understanding of the mechanisms of damage associated with PVH/IVH/ICH should direct the development of new treatment strategies.

## REFERENCES

1. Garcia JH, Ho KL, Caccamo DV. Intracerebral hemorrhage: pathology of selected topics. In: Caplan LR, ed. *Intracerebral Hemorrhage*. Boston: Butterworth-Heinemann, 1994:45-72
2. Kingman TA, Mendelow AD, Graham DI, Teasdale GM. Experimental intracerebral mass: time-related effects on local cerebral blood flow. *J. Neurosurg.* 1987;67:732-738
3. Lee KR, Drury I, Vitarbo E, Hoff JT. Seizures induced by intracerebral injection of thrombin: a model of intracerebral hemorrhage. *J. Neurosurg.* 1997;87:73-78
4. Rosenberg GA, Navratil M. Metalloproteinase inhibition blocks edema in intracerebral hemorrhage in the rat. *Neurology.* 1997;48:921-926
5. Mayo NE, Neville D, Kirkland S et al. Hospitalization and case-fatality rates for stroke in Canada from 1982 through 1991: the Canadian collaborative study group of stroke hospitalizations. *Stroke.* 1996;27:1215-1220
6. Dennis MS, Burn JP, Sandercock PA et al. Long-term survival after first-ever stroke: the Oxfordshire Community Stroke Project. *Stroke.* 1993;24:796-800
7. Giroud M, Gras P, Chadan N et al. Cerebral haemorrhage in a French prospective population study. *J. Neurol. Neurosurg. Psychiatr.* 1991;54:595-598
8. Broderick JP, Brott T, Tomsick T et al. The risk of subarachnoid and intracerebral hemorrhages in blacks as compared with whites. *N Engl J Med.* 1992;326:733-736
9. Kagan A, Harris BR, Winkelstein W, Jr. et al. Epidemiologic studies of coronary heart disease and stroke in Japanese men living in Japan, Hawaii and California:

- demographic, physical, dietary and biochemical characteristics. *J Chronic Dis.* 1974;27:345-364
10. Tomonaga M. Cerebral amyloid angiopathy in the elderly. *J Am Geriatr Soc.* 1981;29:151-157
  11. Hart RG, Boop BS, Anderson DC. Oral anticoagulants and intracranial hemorrhage. Facts and hypotheses. *Stroke.* 1995;26:1471-1477
  12. Bertram M, Bonsanto M, Hacke W, Schwab S. Managing the therapeutic dilemma: patients with spontaneous intracerebral hemorrhage and urgent need for anticoagulation. *J Neurol.* 2000;247:209-214
  13. Aygun N, Masaryk TJ. Diagnostic imaging for intracerebral hemorrhage. *Neurosurg Clin N Am.* 2002;13:313-334
  14. Woo D, Broderick JP. Spontaneous intracerebral hemorrhage: epidemiology and clinical presentation. *Neurosurg Clin N Am.* 2002;13:265-279
  15. Volpe JJ. *Neurology of the Newborn.* 4th Edition. Philadelphia: W.B. Saunders, 2001:912
  16. Jorgensen HS, Nakayama H, Raaschou HO, Olsen TS. Intracerebral hemorrhage versus infarction: stroke severity, risk factors, and prognosis. *Ann. Neurol.* 1995;38:45-50
  17. Broderick JP, Brott TG, Duldner JE et al. Volume of intracerebral hemorrhage: a powerful and easy-to-use predictor of 30-day mortality. *Stroke.* 1993;24:987-993
  18. Anderson CS, Chakera TMH, Stewart-Wynne EG, Jamrozik KD. Spectrum of primary intracerebral haemorrhage in Perth, Western Australia, 1989-90: incidence and outcome. *J. Neurol. Neurosurg. Psychiatr.* 1994;57:936-940

19. Qureshi AI, Tuhim S, Broderick JP et al. Spontaneous intracerebral hemorrhage. *N Engl J Med.* 2001;344:1450-1460
20. Lindsberg PJ, Roine RO. Hyperglycemia in acute stroke. *Stroke.* 2004;35:363-364
21. Saver JL. Surgery for primary intracerebral hemorrhage: Meta-analysis of CT-era studies. *Stroke.* 1998;29:1477
22. Fernandes HM, Gregson B, Siddique S, Mendelow AD. Surgery in intracerebral hemorrhage. The uncertainty continues. *Stroke.* 2000;31:2511-2516
23. Kelly PJ, Furie KL, Shafiqat S et al. Functional recovery following rehabilitation after hemorrhagic and ischemic stroke. *Arch Phys Med Rehabil.* 2003;84:968-972
24. Towbin A. Central nervous system damage in the human fetus and newborn infant. *Am. J. Dis. Child.* 1970;119:529-542
25. Wigglesworth JS, Pape KE. Pathophysiology of intracranial haemorrhage in the newborn. *J Perinat Med.* 1980;8:119-133
26. Ross G, Boatright S, Auld PA, Nass R. Specific cognitive abilities in 2-year-old children with subependymal and mild intraventricular hemorrhage. *Brain Cogn.* 1996;32:1-13
27. Berger R, Bender S, Sefkow S et al. Peri/intraventricular haemorrhage: a cranial ultrasound study on 5286 neonates. *Eur J Obstet Gynecol Reprod Biol.* 1997;75:191-203
28. Paneth N, Pinto-Martin J, Gardiner J et al. Incidence and timing of germinal matrix/intraventricular hemorrhage in low birth weight infants. *Am J Epidemiol.* 1993;137:1167-1176

29. Gleissner M, Jorch G, Avenarius S. Risk factors for intraventricular hemorrhage in a birth cohort of 3721 premature infants. *J Perinat Med.* 2000;28:104-110
30. Hesser U, Katz-Salamon M, Mortensson W et al. Diagnosis of intracranial lesions in very-low-birthweight infants by ultrasound: incidence and association with potential risk factors. *Acta Paediatr Suppl.* 1997;419:16-26
31. Dooling EC, Gilles FH. Intracranial hemorrhage: topography. In: Dooling EC, ed. *The Developing Human Brain. Growth and Epidemiologic Neuropathology.* Boston: John Wright Inc., 1983:193-203
32. Fedrick J, Butler NR. Certain causes of neonatal death. II. Intraventricular haemorrhage. *Biol Neonate.* 1970;15:257-290
33. Shalak L, Perlman JM. Hemorrhagic-ischemic cerebral injury in the preterm infant: current concepts. *Clin Perinatol.* 2002;29:745-763
34. Shankaran S. Hemorrhagic lesions of the central nervous system. In: Sunshine P, ed. *Fetal and Neonatal Brain Injury. Third Edition.* Cambridge, UK: Cambridge University Press, 2003:175-188
35. Whitelaw A. Intraventricular streptokinase after intraventricular hemorrhage in newborn infants. *Cochrane Database Syst Rev.* 2001:CD000498
36. Whitelaw A, Pople I, Cherian S et al. Phase 1 trial of prevention of hydrocephalus after intraventricular hemorrhage in newborn infants by drainage, irrigation, and fibrinolytic therapy. *Pediatrics.* 2003;111:759-765
37. Xue M, Balasubramaniam J, Buist R et al. Periventricular / intraventricular hemorrhage in neonatal mouse cerebrum. *J. Neuropathol. Exp. Neurol.* 2003;62:1154-1165

38. Xue M, Del Bigio MR. Acute tissue damage after injections of thrombin and plasmin into rat striatum. *Stroke*. 2001;32:2164-2169
39. Xue M, Del Bigio MR. Intracerebral injection of autologous whole blood in rats: time course of inflammation and cell death. *Neurosci. Lett*. 2000;283:230-232
40. Xue M, Del Bigio MR. Intracortical hemorrhage injury in rats: relationship between blood fractions and cell death. *Stroke*. 2000;31:1721-1727
41. Xi GH, Wagner KR, Keep RF et al. Role of blood clot formation on early edema development after experimental intracerebral hemorrhage. *Stroke*. 1998;29:2580-2585
42. Xi GH, Keep RF, Hoff JT. Erythrocytes and delayed brain edema formation following intracerebral hemorrhage in rats. *J. Neurosurg*. 1998;89:991-996
43. Kaufman HH, Pruessner JL, Bernstein DP et al. A rabbit model of intracerebral hematoma. *Acta Neuropathol*. 1985;65:318-321
44. Kobari M, Gotoh R, Tomita M et al. Bilateral hemispheric reduction of cerebral blood volume and blood flow immediately after experimental cerebral hemorrhage in cats. *Stroke*. 1988;19:991-996
45. Wagner KR, Xi GH, Hua Y et al. Ultra-early clot aspiration after lysis with tissue plasminogen activator in a porcine model of intracerebral hemorrhage: edema reduction and blood-brain barrier protection. *J. Neurosurg*. 1999;90:491-498
46. Bullock R, Brock-Utne J, van Dellen J, Blake G. Intracerebral hemorrhage in a primate model: effect on regional cerebral blood flow. *Surg. Neurol*. 1988;29:101-107

47. Sinar EJ, Mendelow AD, Graham DI, Teasdale GM. Experimental intracerebral hemorrhage: effects of a temporary mass lesion. *J. Neurosurg.* 1987;66:568-576
48. Kingman TA, Mendelow AD, Graham DI, Teasdale GM. Experimental intracerebral mass: description of model, intracranial pressure changes and neuropathology. *J. Neuropathol. Exp. Neurol.* 1988;47:128-137
49. Valdes EL, Lain AH, Calandre L et al. Time window for clinical effectiveness of mass evacuation in a rat balloon model mimicking an intraparenchymatous hematoma. *J. Neurol. Sci.* 2000;174:40-46
50. Nehls DG, Mendelow DA, Graham DI, Teasdale GM. Experimental intracerebral hemorrhage: early removal of a spontaneous mass lesion improves late outcome. *Neurosurgery.* 1990;27:674-682
51. Ichimi K, Kuchiwaki H, Inao S et al. Responses of cerebral blood flow regulation to activation of the primary somatosensory cortex during electrical stimulation of the forearm. *Acta Neurochir Suppl (Wien).* 1997;70:291-292
52. Del Bigio MR, Yan HJ, Buist R, Peeling J. Experimental intracerebral hemorrhage in rats. Magnetic resonance imaging and histopathological correlates. *Stroke.* 1996;27:2312-2320
53. Xue M, Balasubramaniam J, Del Bigio MR. Brain inflammation following intracerebral hemorrhage. *Current Neuropharmacology.* 2003;1:325-332
54. Xue M, Del Bigio MR. Comparison of brain cell death and inflammatory reaction in three models of intracerebral hemorrhage in adult rats. *J. Stroke Cerebrovasc. Dis.* 2003;12:152-159

55. Qureshi AI, Wilson DA, Hanley DF, Traystman RJ. No evidence for an ischemic penumbra in massive experimental intracerebral hemorrhage. *Neurology*. 1999;52:266-272
56. Andaluz N, Zuccarello M, Wagner KR. Experimental animal models of intracerebral hemorrhage. *Neurosurg Clin N Am*. 2002;13:385-393
57. Wagner KR, Xi GH, Hua Y et al. Lobar intracerebral hemorrhage model in pigs: rapid edema development in perihematoma white matter. *Stroke*. 1996;27:490-497
58. Wagner KR, Xi GH, Hua Y et al. Early metabolic alterations in edematous perihematoma brain regions following experimental intracerebral hemorrhage. *J Neurosurg*. 1998;88:1058-1065
59. Narayan RK, Narayan TM, Katz DA et al. Lysis of intracranial hematomas with urokinase in a rabbit model. *J Neurosurg*. 1985;62:580-586
60. Altieri DC. Interface between inflammation and coagulation. In: Ley K, ed. *Physiology of Inflammation*. New York: Oxford University Press, 2001:402-422
61. Hua Y, Xi GH, Keep RF, Hoff JT. Complement activation in the brain after experimental intracerebral hemorrhage. *J Neurosurg*. 2000;92:1016-1022
62. Rosenberg GA, Estrada E, Kelley RO, Kornfeld M. Bacterial collagenase disrupts extracellular matrix and opens blood-brain barrier in rat. *Neurosci. Lett*. 1993;160:117-119
63. Rosenberg GA, Mun-Bryce S, Wesley M, Kornfeld M. Collagenase-induced intracerebral hemorrhage in rats. *Stroke*. 1990;21:801-807

64. Rosenberg GA, Kornfeld M, Estrada E et al. TIMP-2 reduces proteolytic opening of blood-brain barrier by type IV collagenase. *Brain Res.* 1992;576:203-207
65. Rosenberg GA, Estrada EY. Atrial natriuretic peptide blocks hemorrhagic brain edema after 4-hour delay in rats. *Stroke.* 1995;26:874-877
66. Liard JF, Cowley AW, McCaa RE et al. Renin, aldosterone, body fluid volumes and the baroreceptor reflex in the development and reversal of Goldblatt hypertension in conscious dogs. *Circ. Res.* 1974;34:549-560
67. Zeng JS, Zhang YQ, Mo JW et al. Two-kidney, two clip renovascular hypertensive rats can be used as stroke-prone rats. *Stroke.* 1998;29:1708-1713
68. Okamoto K, Yamori Y, Nagaoka A. Establishment of the stroke-prone spontaneously hypertensive rat. *Circ. Res.* 1974;34/35 Suppl.:I-143 - I-153
69. Goddard-Finegold J. Experimental models of intraventricular hemorrhage. In: Wigglesworth JS, ed. *Perinatal Brain Lesions. Vol. 5.* Boston MA: Blackwell Scientific, 1989:115-133
70. Conner ES, Lorenzo AV, Welch K, Dorval B. The role of intracranial hypotension in neonatal intraventricular hemorrhage. *J Neurosurg.* 1983;58:204-209
71. Lorenzo AV, Welch K, Conner S. Spontaneous germinal matrix and intraventricular hemorrhage in prematurely born rabbits. *J Neurosurg.* 1982;56:404-410
72. Goddard J, Lewis RM, Armstrong DL, Zeller RS. Moderate, rapidly induced hypertension as a cause of intraventricular hemorrhage in the newborn beagle model. *J Pediatr.* 1980;96:1057-1060

73. Batton DG, Nardis EE. The effect of intraventricular blood on cerebral blood flow in newborn dogs. *Pediatr Res.* 1987;21:511-515
74. Yoshioka H, Iino S, Sato N et al. New model of hemorrhagic hypoxic-ischemic encephalopathy in newborn mice. *Pediatr Neurol.* 1989;5:221-225
75. Cherian SS, Love S, Silver IA et al. Posthemorrhagic ventricular dilation in the neonate: development and characterization of a rat model. *J Neuropathol Exp Neurol.* 2003;62:292-303
76. Smith SL, Andrus PK, Gleason DD, Hall ED. Infant rat model of the shaken baby syndrome: preliminary characterization and evidence for the role of free radicals in cortical hemorrhaging and progressive neuronal degeneration. *J Neurotrauma.* 1998;15:693-705
77. Morganti-Kossmann MC, Rancan M, Otto VI et al. Role of cerebral inflammation after traumatic brain injury: a revisited concept. *Shock.* 2001;16:165-177
78. Morganti-Kossmann MC, Rancan M, Stahel PF, Kossmann T. Inflammatory response in acute traumatic brain injury: a double-edged sword. *Curr Opin Crit Care.* 2002;8:101-105
79. Ghirnikar RS, Lee YL, Eng LF. Inflammation in traumatic brain injury: role of cytokines and chemokines. *Neurochem Res.* 1998;23:329-340
80. Leech RW, Kohlen P. Subependymal and intraventricular hemorrhages in the newborn. *Am J Pathol.* 1974;77:465-475
81. Towbin A. Cerebral intraventricular hemorrhage and subependymal matrix infarction in the fetus and premature newborn. *Am J Pathol.* 1968;52:121-140

82. Baron JC. Mapping the ischaemic penumbra with PET: Implications for acute stroke treatment. *Cerebrovasc. Dis.* 1999;9:193-201
83. Obrenovitch TP. The ischaemic penumbra: twenty years on. *Cerebrovasc. Brain Metabol. Rev.* 1995;7:297-323
84. Nishino A, Suzuki M, Ohtani H et al. Thrombin may contribute to the pathophysiology of central nervous system injury. *J. Neurotrauma.* 1993;10:167-179
85. Rosenberg GA. Matrix metalloproteinases in brain injury. *J. Neurotrauma.* 1995;12:833-842
86. Yong VW, Power C, Forsyth P, Edwards DR. Metalloproteinases in biology and pathology of the nervous system. *Nat Rev Neurosci.* 2001;2:502-511
87. Rosenberg GA. Matrix metalloproteinases in neuroinflammation. *Glia.* 2002;39:279-291
88. Pfefferkorn T, Wiessner C, Allegrini PR et al. Plasminogen activation in experimental permanent focal cerebral ischemia. *Brain Res.* 2000;882:19-25
89. Pfefferkorn T, Staufer B, Liebetrau M et al. Plasminogen activation in focal cerebral ischemia and reperfusion. *J. Cerebral Blood Flow Metab.* 2000;20:337-342
90. Van Beek J, Elward K, Gasque P. Activation of Complement in the Central Nervous System: Roles in Neurodegeneration and Neuroprotection. *Ann N Y Acad Sci.* 2003;992:56-71

91. Xi G, Reiser G, Keep RF. The role of thrombin and thrombin receptors in ischemic, hemorrhagic and traumatic brain injury: deleterious or protective? *J Neurochem.* 2003;84:3-9
92. Lee KR, Betz AL, Kim S et al. The role of the coagulation cascade in brain edema formation after intracerebral hemorrhage. *Acta Neurochir.* 1996;138:396-401
93. Lee KR, Colon GP, Betz AL et al. Edema from intracerebral hemorrhage: the role of thrombin. *J. Neurosurg.* 1996;84:91-96
94. Regan RF, Guo Y. Toxic effect of hemoglobin on spinal cord neurons in culture. *J. Neurotrauma.* 1998;15:645-653
95. Janeway CA, Travers P, Walport M, Shlomchik M. *Immunobiology.* 5th ed. New York and London: Garland Publishing, 2001:732
96. Irani DN, Lin KI, Griffin DE. Regulation of brain-derived T cells during acute central nervous system inflammation. *J Immunol.* 1997;158:2318-2326
97. Liou AK, Clark RS, Henshall DC et al. To die or not to die for neurons in ischemia, traumatic brain injury and epilepsy: a review on the stress-activated signaling pathways and apoptotic pathways. *Prog Neurobiol.* 2003;69:103-142
98. Efstathiou SP, Tsioulos DI, Zacharos ID et al. A new classification tool for clinical differentiation between haemorrhagic and ischaemic stroke. *J Intern Med.* 2002;252:121-129
99. Montaner, Alvarez-Sabin J, Abilleira S et al. [Acute phase response after stroke: differences between ischemic stroke and intracerebral hemorrhage]. (in Spanish) *Med Clin (Barc).* 2001;116:54-55

100. Bestue-Cardiel M, Martin-Martinez J, Iturriaga-Heras C et al. [Leukocytes and primary intracerebral hemorrhage]. (in Spanish) *Rev Neurol.* 1999;29:968-971
101. Bednar MM, Gross CE, Howard DB, Lynn M. Neutrophil activation in acute human central nervous system injury. *Neurol. Res.* 1997;19:588-592
102. Paul DA, Leef KH, Stefano JL. Increased leukocytes in infants with intraventricular hemorrhage. *Pediatr. Neurol.* 2000;22:194-199
103. Lee MC, Heaney LM, Jacobson RL, Klassen AC. Cerebrospinal fluid in cerebral hemorrhage and infarction. *Stroke.* 1975;6:638-641
104. Castillo J, Davalos A, Alvarez-Sabin J et al. Molecular signatures of brain injury after intracerebral hemorrhage. *Neurology.* 2002;58:624-629
105. Dziedzic T, Bartus S, Klimkowicz A et al. Intracerebral hemorrhage triggers interleukin-6 and interleukin-10 release in blood. *Stroke.* 2002;33:2334-2335
106. Csuka E, Morganti-Kossmann MC, Lenzlinger PM et al. IL-10 levels in cerebrospinal fluid and serum of patients with severe traumatic brain injury: relationship to IL-6, TNF-alpha, TGF-beta1 and blood-brain barrier function. *J Neuroimmunol.* 1999;101:211-221
107. Ferrarese C, Mascarucci P, Zoia C et al. Increased cytokine release from peripheral blood cells after acute stroke. *J Cereb Blood Flow Metab.* 1999;19:1004-1009
108. Ulfig N. Expression of leukemia inhibitory factor in the ganglionic eminence of the human fetal brain after bleedings. *Neurosci. Lett.* 2001;299:153-155

109. Winking M, Deinsberger W, Jodicke A, Boker DK. [Leukotriene synthesis after intracerebral hemorrhage: a further indicator for their pathophysiologic significance in the CNS]. (in German) *Zentralbl Neurochir.* 1998;59:113-120
110. Hedqvist P, Lindbom L. Lipid mediator of inflammation. In: Ley K, ed. *Physiology of Inflammation.* New York: Oxford University Press, 2001:111-130
111. Zhou H, Chen M, Wang D. [Change of serum soluble vascular cell adhesion molecule-1 in patients with acute cerebral infarction and its clinical significance]. (in Chinese) *Zhonghua Nei Ke Za Zhi.* 1997;36:748-750
112. Takasugi S, Ueda S, Matsumoto K. Chronological changes in spontaneous intracerebral hematoma - an experimental and clinical study. *Stroke.* 1985;16:651-658
113. Anderson RM, Opeskin K. Timing of early changes in brain trauma. *Am. J. Forens. Med. Pathol.* 1998;19:1-9
114. Loberg EM, Torvik A. Brain contusions: the time sequence of the histological changes. *Med. Sci. Law.* 1989;29:109-115
115. Holmin S, Biberfeld P, Mathiesen T. Intracerebral inflammation after human brain contusion. *Neurosurgery.* 1998;42:291-299
116. Mackenzie JM, Clayton JA. Early cellular events in the penumbra of human spontaneous intracerebral hemorrhage. *J. Stroke Cerebrovasc. Dis.* 1999;8:1-8
117. Strassmann G. Formation of hemosiderin and hematoidin after traumatic and spontaneous cerebral hemorrhages. *Arch. Pathol.* 1949;47:205-210

118. Del Bigio MR, Deck JH, Davidson GS. Glial swelling with eosinophilia in human post-mortem brains: a change indicative of plasma extravasation. *Acta Neuropathol (Berl)*. 2000;100:688-694
119. Damska M. Encephalic necrosis and inflammatory reaction in fetuses and newborns. *Pol. Med. J.* 1968;7:404-434
120. Darrow VC, Alvord ECJ, Mack LA, Hodson WA. Histologic evaluation of the reactions to hemorrhage in the premature human infant's brain. A combined ultrasound and autopsy study and a comparison with the reaction in adults. *Am. J. Pathol.* 1988;130:44-58
121. Sherwood A, Hopp A, Smith JF. Cellular reactions to subependymal plate haemorrhage in the human neonate. *Neuropathol Appl Neurobiol.* 1978;4:245-261
122. Back SA. Recent advances in human perinatal white matter injury. *Prog Brain Res.* 2001;132:131-147
123. Dropp JJ. Mast cells in the human brain. *Acta Anat (Basel)*. 1979;105:505-513
124. Adachi N, Itoh Y, Oishi R, Saeki K. Direct evidence for increased continuous histamine release in the striatum of conscious freely moving rats produced by middle cerebral artery occlusion. *J Cereb Blood Flow Metab.* 1992;12:477-483
125. Esposito P, Chandler N, Kandere K et al. Corticotropin-releasing hormone and brain mast cells regulate blood-brain-barrier permeability induced by acute stress. *J Pharmacol Exp Ther.* 2002;303:1061-1066
126. Arvin B, Neville LF, Barone FC, Feuerstein GZ. Brain injury and inflammation. A putative role of TNF alpha. *Ann N Y Acad Sci.* 1995;765:62-71

127. Arvin B, Neville LF, Barone FC, Feuerstein GZ. The role of inflammation and cytokines in brain injury. *Neurosci Biobehav Rev.* 1996;20:445-452
128. Burger D, Dayer JM. Cytokines, acute-phase proteins, and hormones: IL-1 and TNF-alpha production in contact-mediated activation of monocytes by T lymphocytes. *Ann N Y Acad Sci.* 2002;966:464-473
129. Munoz-Fernandez MA, Fresno M. The role of tumour necrosis factor, interleukin 6, interferon-gamma and inducible nitric oxide synthase in the development and pathology of the nervous system. *Prog. Neurobiol.* 1998;56:307-340
130. Mayne M, Ni W, Yan HJ et al. Antisense oligodeoxynucleotide inhibition of tumor necrosis factor- alpha expression is neuroprotective after intracerebral hemorrhage. *Stroke.* 2001;32:240-248
131. Qureshi AI, Suri MF, Ling GS et al. Absence of early proinflammatory cytokine expression in experimental intracerebral hemorrhage. *Neurosurgery.* 2001;49:416-420
132. Carlos TM, Clark RS, Franicola-Higgins D et al. Expression of endothelial adhesion molecules and recruitment of neutrophils after traumatic brain injury in rats. *J. Leukoc. Biol.* 1997;61:279-285
133. Connolly ES, Jr., Winfree CJ, Prestigiacomo CJ et al. Exacerbation of cerebral injury in mice that express the P-selectin gene: identification of P-selectin blockade as a new target for the treatment of stroke. *Circ. Res.* 1997;81:304-310
134. Whalen MJ, Carlos TM, Kochanek PM, Heineman S. Blood-brain barrier permeability, neutrophil accumulation and vascular adhesion molecule expression

- after controlled cortical impact in rats: a preliminary study. *Acta Neurochir. Suppl.* 1998;71:212-214
135. Isaksson J, Lewen A, Hillered L, Olsson Y. Upregulation of intercellular adhesion molecule 1 in cerebral microvessels after cortical contusion trauma in rat model. *Acta Neuropathol.* 1997;94:16-20
136. Wang X, Feuerstein GZ. Induced expression of adhesion molecules following focal brain ischemia. *J. Neurotrauma.* 1995;12:825-832
137. Gong C, Hoff JT, Keep RF. Acute inflammatory reaction following experimental intracerebral hemorrhage in rat. *Brain Res.* 2000;871:57-65
138. Savill J, Haslett C. Resolution of inflammation. In: Ley K, ed. *Physiology of Inflammation.* New York: Oxford University Press, 2001:496-525
139. Jenkins A, Maxwell WL, Graham DI. Experimental intracerebral hematoma in the rat: sequential light microscopical changes. *Neuropathol. Appl. Neurobiol.* 1989;15:477-486
140. Koeppen AH, Dickson AC, Mcevoy JA. The cellular reactions to experimental intracerebral hemorrhage. *J. Neurol. Sci.* 1995;134 Suppl.:102-112
141. Hartl R, Schurer L, Schmid Schonbein GW, del Zoppo GJ. Experimental antileukocyte interventions in cerebral ischemia. *J. Cereb. Blood Flow Metabol.* 1996;16:1108-1119
142. Pantoni L, Sarti C, Inzitari D. Cytokines and cell adhesion molecules in cerebral ischemia: experimental bases and therapeutic perspectives. *Arterioscler Thromb Vasc Biol.* 1998;18:503-513

143. Schnell L, Fearn S, Klassen H et al. Acute inflammatory responses to mechanical lesions in the CNS: differences between brain and spinal cord. *Eur. J. Neurosci.* 1999;11:3648-3658
144. Holmin S, Mathiesen T, Shetye J, Biberfeld P. Intracerebral inflammatory response to experimental brain contusion. *Acta Neurochir.* 1995;132:110-119
145. Boje KM, Arora PK. Microglial-produced nitric oxide and reactive nitrogen oxides mediate neuronal cell death. *Brain Res.* 1992;587:250-256
146. Nagata K, Takei N, Nakajima K et al. Microglial conditioned medium promotes survival and development of cultured mesencephalic neurons from embryonic rat brain. *J Neurosci Res.* 1993;34:357-363
147. Engel S, Schluesener H, Mittelbronn M et al. Dynamics of microglial activation after human traumatic brain injury are revealed by delayed expression of macrophage-related proteins MRP8 and MRP14. *Acta Neuropathol.* 2000;100:313-322
148. Pongvarin N, Bhoopat W, Viriavejakul A et al. Effects of dexamethasone in primary supratentorial intracerebral hemorrhage. *N. Eng. J. Med.* 1987;316:1229-1233
149. Tellez H, Bauer RB. Dexamethasone as treatment in cerebrovascular disease. 1. A controlled study in intracerebral hemorrhage. *Stroke.* 1973;4:541-546
150. De Reuck J, De Bleecker J, Reyntjens K. Steroid treatment in primary intracerebral haemorrhage. *Acta Neurol Belg.* 1989;89:7-11
151. Schneider D, Berrouschot J, Brandt T et al. Safety, pharmacokinetics and biological activity of enlimomab (anti-ICAM-1 antibody): an open-label, dose

- escalation study in patients hospitalized for acute stroke. *Eur Neurol.* 1998;40:78-83
152. Furuya K, Takeda H, Azhar S et al. Examination of several potential mechanisms for the negative outcome in a clinical stroke trial of enlimomab, a murine anti-human intercellular adhesion molecule-1 antibody: a bedside-to-bench study. *Stroke.* 2001;32:2665-2674
153. Kane PJ, Modha P, Strachan RD et al. The effect of immunosuppression on the development of cerebral oedema in an experimental model of intracerebral haemorrhage: whole body and regional irradiation. *J. Neurol. Neurosurg. Psychiatr.* 1992;55:781-786
154. Peeling J, Yan H-J, Chen S-G et al. Protective effects of free radical inhibitors in intracerebral hemorrhage in rat. *Brain Res.* 1998;795:63-70
155. Del Bigio MR, Yan HJ, Campbell TM, Peeling J. Effect of fucoidan treatment on collagenase-induced intracerebral hemorrhage in rats. *Neurolog. Res.* 1999;21:415-419
156. Peeling J, Yan HJ, Corbett D et al. Effect of FK-506 on inflammation and behavioral outcome following intracerebral hemorrhage in rat. *Exp. Neurol.* 2001;167:341-347
157. Power C, Henry S, Del Bigio MR et al. Intracerebral hemorrhage induces macrophage activation and matrix metalloproteinases. *Ann Neurol.* 2003;53:731-742
158. Xi G, Hua Y, Keep RF et al. Systemic complement depletion diminishes perihematomal brain edema in rats. *Stroke.* 2001;32:162-167

159. Schwartz M, Moalem G. Beneficial immune activity after CNS injury: prospects for vaccination. *J. Neuroimmunol.* 2001;113:185-192
160. Schwartz M. T cell mediated neuroprotection is a physiological response to central nervous system insults. *J. Molec. Med.* 2001;78:594-597
161. Nilsson OG, Lindgren A, Brandt L, Saveland H. Prediction of death in patients with primary intracerebral hemorrhage: a prospective study of a defined population. *J Neurosurg.* 2002;97:531-536
162. Yuan J, Lipinski M, Degtarev A. Diversity in the mechanisms of neuronal cell death. *Neuron.* 2003;40:401-413
163. Klionsky DJ, Emr SD. Autophagy as a regulated pathway of cellular degradation. *Science.* 2000;290:1717-1721
164. Johnston MV, Trescher WH, Ishida A, Nakajima W. Neurobiology of hypoxic-ischemic injury in the developing brain. *Pediatr Res.* 2001;49:735-741
165. Yuan JY, Yankner BA. Apoptosis in the nervous system. *Nature.* 2000;407:802-809
166. Hickenbottom SL, Grotta JC, Strong R et al. Nuclear factor-kappaB and cell death after experimental intracerebral hemorrhage in rats. *Stroke.* 1999;30:2472-2477; discussion 2477-2478
167. Gong C, Boulis N, Qian J et al. Intracerebral hemorrhage-induced neuronal death. *Neurosurgery.* 2001;48:875-882
168. Qureshi AI, Suri MF, Ostrow PT et al. Apoptosis as a form of cell death in intracerebral hemorrhage. *Neurosurgery.* 2003;52:1041-1047; discussion 1047-1048

169. Eldadah BA, Faden AI. Caspase pathways, neuronal apoptosis, and CNS injury. *J. Neurotrauma*. 2000;17:811-829
170. Stennicke HR, Jurgensmeier JM, Shin H et al. Pro-caspase-3 is a major physiologic target of caspase-8. *J Biol Chem*. 1998;273:27084-27090
171. Li P, Nijhawan D, Budihardjo I et al. Cytochrome c and dATP-dependent formation of Apaf-1/caspase-9 complex initiates an apoptotic protease cascade. *Cell*. 1997;91:479-489
172. Daugas E, Susin SA, Zamzami N et al. Mitochondrio-nuclear translocation of AIF in apoptosis and necrosis. *Faseb J*. 2000;14:729-739
173. Daugas E, Nochy D, Ravagnan L et al. Apoptosis-inducing factor (AIF): a ubiquitous mitochondrial oxidoreductase involved in apoptosis. *FEBS Lett*. 2000;476:118-123
174. Dumont C, Durrbach A, Bidere N et al. Caspase-independent commitment phase to apoptosis in activated blood T lymphocytes: reversibility at low apoptotic insult. *Blood*. 2000;96:1030-1038
175. Mort JS, Recklies AD. Interrelationship of active and latent secreted human cathepsin B precursors. *Biochem J*. 1986;233:57-63
176. Isahara K, Ohsawa Y, Kanamori S et al. Regulation of a novel pathway for cell death by lysosomal aspartic and cysteine proteinases. *Neuroscience*. 1999;91:233-249
177. Sorimachi H, Saido TC, Suzuki K. New era of calpain research. Discovery of tissue-specific calpains. *FEBS Lett*. 1994;343:1-5

178. Chan SL, Mattson MP. Caspase and calpain substrates: Roles in synaptic plasticity and cell death. *J. Neurosci. Res.* 1999;58:167-190
179. Knepper-Nicolai B, Savill J, Brown SB. Constitutive apoptosis in human neutrophils requires synergy between calpains and the proteasome downstream of caspases. *J Biol Chem.* 1998;273:30530-30536
180. Debiase RL, Squier MK, Pike B et al. Reovirus-induced apoptosis is preceded by increased cellular calpain activity and is blocked by calpain inhibitors. *J Virol.* 1999;73:695-701
181. Squier MK, Cohen JJ. Calpain, an upstream regulator of thymocyte apoptosis. *J Immunol.* 1997;158:3690-3697
182. Young LH, Klavinskis LS, Oldstone MB, Young JD. In vivo expression of perforin by CD8+ lymphocytes during an acute viral infection. *J. Exp. Med.* 1989;169:2159-2171
183. Reed JC. Double identity for proteins of the Bcl-2 family. *Nature.* 1997;387:773-776
184. Tsujimoto Y. Role of Bcl-2 family proteins in apoptosis: apoptosomes or mitochondria? *Genes Cells.* 1998;3:697-707
185. Vande Velde C, Cizeau J, Dubik D et al. BNIP3 and genetic control of necrosis-like cell death through the mitochondrial permeability transition pore. *Mol Cell Biol.* 2000;20:5454-5468
186. Schmidt-Kastner R, Aguirre-Chen C, Kietzmann T et al. Nuclear localization of the hypoxia-regulated pro-apoptotic protein BNIP3 after global brain ischemia in the rat hippocampus. *Brain Res.* 2004;1001:133-142

187. Henson PM, Bratton DL, Fadok VA. Apoptotic cell removal. *Current Biology*. 2001;11:R795-805
188. Charriaut-Marlangue C, Ben-Ari Y. A cautionary note on the use of the TUNEL stain to determine apoptosis. *NeuroReport*. 1995;7:61-64
189. Schmued LC, Albertson C, Slikker W, Jr. Fluoro-Jade: a novel fluorochrome for the sensitive and reliable histochemical localization of neuronal degeneration. *Brain Res*. 1997;751:37-46
190. Schmued LC, Hopkins KJ. Fluoro-Jade: Novel fluorochromes for detecting toxicant-induced neuronal degeneration. *Toxicol. Pathol*. 2000;28:91-99
191. Levy R, Benchaib M, Cordonier H et al. Annexin V labelling and terminal transferase-mediated DNA end labelling (TUNEL) assay in human arrested embryos. *Mol. Hum. Reprod*. 1998;4:775-783
192. Hausmann R, Biermann T, Wiest I et al. Neuronal apoptosis following human brain injury. *Int J Legal Med*. 2004;118:32-36
193. Ng I, Yeo TT, Tang WY et al. Apoptosis occurs after cerebral contusions in humans. *Neurosurgery*. 2000;46:949-956
194. Matsushita K, Meng W, Wang X et al. Evidence for apoptosis after intracerebral hemorrhage in rat striatum. *J. Cereb. Blood Flow Metab*. 2000;20:396-404
195. Yang G-Y, Betz AL, Chenevert TL et al. Experimental intracerebral hemorrhage: relationship between brain edema, blood flow, and blood-brain barrier permeability in rats. *J. Neurosurg*. 1994;81:93-102

196. Wang X, Mori T, Sumii T, Lo EH. Hemoglobin-induced cytotoxicity in rat cerebral cortical neurons: caspase activation and oxidative stress. *Stroke*. 2002;33:1882-1888
197. Felberg RA, Grotta JC, Shirzadi AL et al. Cell death in experimental intracerebral hemorrhage: the "black hole" model of hemorrhagic damage. *Ann Neurol*. 2002;51:517-524
198. Matz PG, Copin JC, Chan PH. Cell death after exposure to subarachnoid hemolysate correlates inversely with expression of CuZn-superoxide dismutase. *Stroke*. 2000;31:2450-2459
199. Qureshi AI, Ling GS, Khan J et al. Quantitative analysis of injured, necrotic, and apoptotic cells in a new experimental model of intracerebral hemorrhage. *Crit Care Med*. 2001;29:152-157
200. Dihanich M, Kaser M, Reinhard E et al. Prothrombin mRNA is expressed by cells of the nervous system. *Neuron*. 1991;6:575-581
201. Sharon R, Abramovitz R, Miskin R. Plasminogen mRNA induction in the mouse brain after kainate excitation: codistribution with plasminogen activator inhibitor-2 (PAI-2) mRNA. *Brain Res Mol Brain Res*. 2002;104:170-175
202. Basham ME, Seeds NW. Plasminogen expression in the neonatal and adult mouse brain. *J Neurochem*. 2001;77:318-325
203. Yoshida S, Shiosaka S. Plasticity-related serine proteases in the brain. *Int. J. Molec. Med*. 1999;3:405-409
204. Citron BA, Zhang SX, Smirnova IV, Festoff BW. Apoptotic, injury-induced cell death in cultured mouse murine motor neurons. *Neurosci. Lett*. 1997;230:25-28

205. Loret C, Sensenbrenner M, Labourdette G. Differential phenotypic expression induced in cultured rat astroblasts by acidic fibroblast growth factor, epidermal growth factor, and thrombin. *J Biol Chem.* 1989;264:8319-8327
206. Gurwitz D, Cunningham DD. Thrombin modulates and reverses neuroblastoma neurite outgrowth. *Proc Natl Acad Sci U S A.* 1988;85:3440-3444
207. Armao D, Kornfeld M, Estrada EY et al. Neutral proteases and disruption of the blood-brain barrier in rat. *Brain Res.* 1997;767:259-264
208. Xi GH, Keep RF, Hua Y et al. Attenuation of thrombin-induced brain edema by cerebral thrombin preconditioning. *Stroke.* 1999;30:1247-1255
209. Gingrich MB, Traynelis SF. Serine proteases and brain damage - is there a link? *Trends Neurosci.* 2000;23:399-407
210. Wang J, Rogove AD, Tsirka AE, Tsirka SE. Protective role of tuftsin fragment 1-3 in an animal model of intracerebral hemorrhage. *Ann Neurol.* 2003;54:655-664
211. Lo EH, Wang X, Cuzner ML. Extracellular proteolysis in brain injury and inflammation: role for plasminogen activators and matrix metalloproteinases. *J Neurosci Res.* 2002;69:1-9
212. Lapchak PA, Chapman DF, Zivin JA. Metalloproteinase inhibition reduces thrombolytic (tissue plasminogen activator)-induced hemorrhage after thromboembolic stroke. *Stroke.* 2000;31:3034-3040
213. Gu Z, Kaul M, Yan B et al. S-nitrosylation of matrix metalloproteinases: signaling pathway to neuronal cell death. *Science.* 2002;297:1186-1190
214. Peeling J, Del Bigio MR, Corbett D et al. Efficacy of disodium 4-[(tert-butylimino)methyl]benzene-1,3-disulfonate N-oxide (NXY-059), a free radical

- trapping agent, in a rat model of hemorrhagic stroke. *Neuropharmacology*. 2001;40:433-439
215. Del Bigio MR, Yan HJ, Xue M. Intracerebral infusion of a second-generation ciliary neurotrophic factor reduces neuronal loss in rat striatum following experimental intracerebral hemorrhage. *J Neurol Sci*. 2001;192:53-59
216. Rodrigues CM, Sola S, Nan Z et al. Tauroursodeoxycholic acid reduces apoptosis and protects against neurological injury after acute hemorrhagic stroke in rats. *Proc Natl Acad Sci U S A*. 2003;100:6087-6092
217. Kluck RM, Bossy-Wetzel E, Green DR, Newmeyer DD. The release of cytochrome c from mitochondria: a primary site for Bcl-2 regulation of apoptosis. *Science*. 1997;275:1132-1136
218. Yang J, Liu X, Bhalla K et al. Prevention of apoptosis by Bcl-2: release of cytochrome c from mitochondria blocked. *Science*. 1997;275:1129-1132
219. Altumbabic M, Peeling J, Del Bigio MR. Intracerebral hemorrhage in the rat. Effects of hematoma aspiration. *Stroke*. 1998;29:1917-1922
220. Altumbabic M, Del Bigio MR. Transplantation of fetal brain tissue into the site of intracerebral hemorrhage in rats. *Neurosci. Lett*. 1998;257:61-64
221. Niclou S, Suidan HS, Brown-Luedi M, Monard D. Expression of the thrombin receptor mRNA in rat brain. *Cell Mol Biol*. 1994;40:421-428
222. Del Bigio MR, Hosain S, Altumbabic M. Localization of urokinase-type plasminogen activator, its receptor, and inhibitors in mouse forebrain during postnatal development. *Int. J. Dev. Neurosci*. 1999;17:387-399

223. Del Bigio MR, Tchelingirian JL, Jacque CM. Expression of extracellular matrix degrading enzymes during migration of xenografted brain cells. *Neuropathol. Appl. Neurobiol.* 1999;25:54-62
224. Canete-Soler R, Gui YH, Linask KK, Muschel RJ. MMP-9 (gelatinase B) mRNA is expressed during mouse neurogenesis and may be associated with vascularization. *Dev. Brain Res.* 1995;88:37-52
225. Uhm JH, Dooley NP, Oh LYS, Yong VW. Oligodendrocytes utilize a matrix metalloproteinase, MMP-9, to extend processes along an astrocyte extracellular matrix. *Glia.* 1998;22:53-63
226. Cocks TM, Moffatt JD. Protease-activated receptors: sentries for inflammation? *Trends Pharmacol Sci.* 2000;21:103-108
227. Smith-Swintosky VL, Chéo-Isaacs CT, D'Andrea MR et al. Protease-activated receptor-2 (PAR-2) is present in the rat hippocampus and is associated with neurodegeneration. *J Neurochem.* 1997;69:1890-1896
228. Nicole O, Docagne F, Ali C et al. The proteolytic activity of tissue-plasminogen activator enhances NMDA receptor-mediated signaling. *Nat Med.* 2001;7:59-64
229. Krueger SR, Ghisu GP, Cinelli P et al. Expression of neuroserpin, an inhibitor of tissue plasminogen activator, in the developing and adult nervous system of the mouse. *J. Neurosci.* 1997;17:8984-8996
230. Choi BH, Suzuki M, Kim T et al. Protease nexin-1. Localization in the human brain suggests a protective role against extravasated serine proteases. *Am. J. Pathol.* 1990;137:741-747

231. Lorent K, Overbergh L, Moechars D et al. Expression in mouse embryos and in adult mouse brain of three members of the amyloid precursor protein family, of the alpha-2-macroglobulin receptor/low density lipoprotein receptor-related protein and of its ligands apolipoprotein E, lipoprotein lipase, alpha-2-macroglobulin and the 40,000 molecular weight receptor-associated protein. *Neuroscience*. 1995;65:1009-1025
232. Lorent K, Overbergh L, Delabie J et al. Distribution of mRNA coding for alpha-2-macroglobulin, the murinoglobulins, the alpha-2-macroglobulin receptor and the alpha-2-macroglobulin receptor associated protein during mouse embryogenesis and in adult tissues. *Differentiation*. 1994;55:213-223
233. Jaworski DM. Differential regulation of tissue inhibitor of metalloproteinase mRNA expression in response to intracranial injury. *Glia*. 2000;30:199-208
234. Kakita A, Goldman JE. Patterns and dynamics of SVZ cell migration in the postnatal forebrain: monitoring living progenitors in slice preparations. *Neuron*. 1999;23:461-472
235. Levers TE, Edgar JM, Price DJ. The fates of cells generated at the end of neurogenesis in developing mouse cortex. *J Neurobiol*. 2001;48:265-277
236. Liu X, Zhu XZ. Roles of p53, c-Myc, Bcl-2, Bax and caspases in serum deprivation-induced neuronal apoptosis: a possible neuroprotective mechanism of basic fibroblast growth factor. *Neuroreport*. 1999;10:3087-3091
237. Levison SW, Rothstein RP, Romanko MJ et al. Hypoxia/ischemia depletes the rat perinatal subventricular zone of oligodendrocyte progenitors and neural stem cells. *Dev Neurosci*. 2001;23:234-247

238. Duhaime AC, Margulies SS, Durham SR et al. Maturation-dependent response of the piglet brain to scaled cortical impact. *J. Neurosurg.* 2000;93:455-462
239. Del Bigio MR, Balasubramaniam J, Xue M. Reduced cell proliferation in germinal matrix following periventricular hemorrhage in humans and mice. *J. Neuropathol. Exp. Neurol.* Vol. 62, 2003:577 (abstract)
240. Xue M, Balasubramaniam J, Buist RJ et al. Periventricular / intraventricular hemorrhage in neonatal mouse cerebrum. *J. Neuropathol. Exp. Neurol.* Vol. 62, 2003:1154-1165
241. Dammann O, Leviton A. Maternal intrauterine infection, cytokines, and brain damage in the preterm newborn. *Pediatr Res.* 1997;42:1-8
242. Benjelloun N, Renolleau S, Represa A et al. Inflammatory responses in the cerebral cortex after ischemia in the P7 neonatal rat. *Stroke.* 1999;30:1916-1923
243. Perry VH, Hume DA, Gordon S. Immunohistochemical localization of macrophages and microglia in the adult and developing mouse brain. *Neuroscience.* 1985;15:313-326
244. Tanaka M, Marunouchi T, Sawada M. Expression of Ly-6C on microglia in the developing and adult mouse brain. *Neurosci Lett.* 1997;239:17-20
245. Nelson KB, Willoughby RE. Infection, inflammation and the risk of cerebral palsy. *Curr. Opin. Neurol.* 2000;13:133-139
246. Kolb B, Cioe J, Whishaw IQ. Is there an optimal age for recovery from motor cortex lesions? I. Behavioral and anatomical sequelae of bilateral motor cortex lesions in rats on postnatal days 1, 10, and in adulthood. *Brain Res.* 2000;882:62-

247. Kolb B, Cioe J. Recovery from early cortical damage in rats, VIII. Earlier may be worse: behavioural dysfunction and abnormal cerebral morphogenesis following perinatal frontal cortical lesions in the rat. *Neuropharmacology*. Vol. 39, 2000:756-764
248. Nagayama M, Aber T, Nagayama T et al. Age-dependent increase in ischemic brain injury in wild-type mice and in mice lacking the inducible nitric oxide synthase gene. *J Cereb Blood Flow Metab*. 1999;19:661-666
249. Cheng Y, Gidday JM, Yan Q et al. Marked age-dependent neuroprotection by brain-derived neurotrophic factor against neonatal hypoxic-ischemic brain injury. *Ann Neurol*. 1997;41:521-529
250. Tuor UI, Chumas PD, Del Bigio MR. Prevention of hypoxic-ischemic damage with dexamethasone is dependent on age and not influenced by fasting. *Exp Neurol*. 1995;132:116-122
251. Sidhu RS, Tuor UI, Del Bigio MR. Nuclear condensation and fragmentation following cerebral hypoxia-ischemia occurs more frequently in immature than older rats. *Neurosci Lett*. 1997;223:129-132
252. Lawson LJ, Perry VH. The unique characteristics of inflammatory responses in mouse brain are acquired during postnatal development. *Eur J Neurosci*. 1995;7:1584-1595
253. Thakker JC, Splaingard M, Zhu J et al. Survival and functional outcome of children requiring endotracheal intubation during therapy for severe traumatic brain injury. *Crit Care Med*. 1997;25:1396-1401

254. Emanuelson I. Preliminary data from a 10-year follow-up of children and adolescents with serious traumatic brain injury after road traffic accidents. (abstract). *Dev. Med. Child Neurol.* 2000;42 Suppl. 84:5
255. Roohey T, Raju TN, Moustogiannis AN. Animal models for the study of perinatal hypoxic-ischemic encephalopathy: a critical analysis. *Early Hum Dev.* 1997;47:115-146
256. Jenkins A, Mendelow AD, Graham DI et al. Experimental intracerebral haematoma: the role of blood constituents in early ischaemia. *Br. J. Neurosurg.* 1990;4:45-51
257. Leder LD. Uber die selektive fermentcytochemische Darstellung von neutrophilen myeloischen Zellen und Gewebsmatzellen im Paraffinschnitt. *Klin. Wochenschr.* 1964;42:553.
258. Torres-Nagel N, Kraus E, Brown MH et al. Differential thymus dependence of rat CD8 isoform expression. *Eur. J. Immunol.* 1992;22:2841-2848
259. Mendelow AD. Mechanisms of ischemic brain damage with intracerebral hemorrhage. *Stroke.* 1993;24 (Suppl. I):I-115-I-117
260. Suzuki J, Ebina T. Sequential changes in tissue surrounding ICH. In: Zierski J, ed. *Spontaneous Intracerebral Hematomas.* Berlin: Springer, 1980:121-128
261. Ikeda Y, Long DM. The molecular basis of brain injury and brain edema: the role of oxygen free radicals. *Neurosurgery.* 1990;27:1-11
262. Popko B, Baerwald KD. Oligodendroglial response to the immune cytokine interferon gamma. *Neurochem. Res.* 1999;24:331-338

263. Gehrmann J, Banati RB, Wiessnert C et al. Reactive microglia in cerebral ischaemia: an early mediator of tissue damage? *Neuropathol. Appl. Neurobiol.* 1995;21:277-289
264. Chopp M, Li Y, Jiang N et al. Antibodies against adhesion molecules reduce apoptosis after transient middle cerebral artery occlusion in rat brain. *J. Cereb. Blood Flow Metab.* 1996;16:578-584
265. Bullock R, Mendelow AD, Teasdale GM, Graham DI. Intracranial hemorrhage induced at arterial pressure in the rat. Part 1: Description of technique, ICP changes and neuropathologic findings. *Neurol. Res.* 1984;6:184-188
266. Funnell WR, Maysinger D, Cuello AC. Three-dimensional reconstruction and quantitative evaluation of devascularizing cortical lesions in the rat. *J. Neurosci. Methods.* 1990;35:147-156
267. Sensharma GC, Singh S, Deb S. Changes in the brain following experimental extirpation of pia. *Indian J. Med. Res.* 1979;69:338-343
268. Holmin S, Gahm C, Mathiesen T. Intracerebral inflammatory response in traumatic brain injury. *Research And Practice In Alzheimer's Disease.* 1999;2:48-54
269. Mannoji H, Yeger H, Becker LE. A specific histochemical marker (lectin Ricinus communis agglutinin-1) for normal human microglia, and application to routine histopathology. *Acta Neuropathol.* 1986:341-343
270. Poirier JL, Capek R, De Koninck Y. Differential progression of dark neuron and Fluoro-Jade labelling in the rat hippocampus following pilocarpine-induced status epilepticus. *Neuroscience.* 2000;97:59-68

271. Herrera DG, Cuello AC. Glial fibrillary acidic protein immunoreactivity following cortical devascularizing lesion. *Neuroscience*. 1992;49:781-791
272. Narayanan S. Multifunctional roles of thrombin. *Ann Clin Lab Sci*. 1999;29:275-280
273. Murphy P. *The Neutrophil*. New York: Plenum Medical Book Co., 1976:217
274. Nishimura T, Itoh T. Higher level expression of lymphocyte function-associated antigen-1 (LFA-1) on in vivo natural killer cells. *Eur J Immunol*. 1988;18:2077-2080
275. Johnson KJ, Varani J, Smolen JE. Neutrophil activation and function in health and disease. In: Coffey RG, ed. *Granulocyte Responses to Cytokines*. New York: Marcel Dekker Inc., 1992:1-46
276. Shiga Y, Onodera H, Kogure K et al. Neutrophil as a mediator of ischemic edema formation in the brain. *Neurosci. Lett*. 1991;125:110-112
277. Matsuo Y, Onodera H, Shiga Y et al. Correlation between myeloperoxidase-quantified neutrophil accumulation and ischemic brain injury in the rat. Effects of neutrophil depletion. *Stroke*. 1994;25:1469-1475
278. Emerich DF, Dean RL, 3rd, Bartus RT. The role of leukocytes following cerebral ischemia: pathogenic variable or bystander reaction to emerging infarct? *Exp Neurol*. 2002;173:168-181
279. Thomaidou D, Mione MC, Cavenagh JF, Parnavelas JG. Apoptosis and its relation to the cell cycle in the developing cerebral cortex. *J. Neurosci*. 1997;17:1075-1085

280. Chuaqui R, Tapia J. Histologic assessment of the age of recent brain infarcts in man. *J Neuropathol Exp Neurol.* 1993;52:481-489
281. Newcomb JK, Zhao X, Pike BR, Hayes RL. Temporal profile of apoptotic-like changes in neurons and astrocytes following controlled cortical impact injury in the rat. *Exp. Neurol.* 1999;158:76-88
282. Czurko A, Nishio H. 'Collapsed' (argyrophilic, dark) neurons in rat model of transient focal cerebral ischemia. *Neurosci. Lett.* 1993;162:71-74
283. Taylor CL, Selman WR, Ratcheson RA. Brain attack: the emergent management of hypertensive hemorrhage. *Neurosurg. Clin. North. Am.* 1997;8:237-244
284. Matz PG, Weinstein PR, Sharp FR. Heme oxygenase-1 and heat shock protein 70 induction in glia and neurons throughout rat brain after experimental intracerebral hemorrhage. *Neurosurgery.* 1997;40:152-162
285. Peng Z-C, Li XQ, Li QH et al. Induction of NADPH-diaphorase activity in the forebrain in a model of intracerebral hemorrhage and its inhibition by the traditional Chinese medicine complex Nao Yi An. *Brain Res. Bull.* 1997;42:119-128
286. Nath FP, Jenkins A, Mendelow AD et al. Early hemodynamic changes in experimental intracerebral hemorrhage. *J. Neurosurg.* 1986;65:697-703
287. Clasen RA, Brown DVL, Leavitt S, Hass GM. The production by liquid nitrogen of acute closed cerebral lesions. *Surg. Gynecol. Obstetr.* 1953;96:605-616
288. Hass GM, Taylor CB. A quantitative hypothermal method for the production of local injury of tissue. *Arch. Pathol.* 1948;45:563-580

289. Klatzo I, Piraux A, Laskowski EJ. The relationship between edema, blood-brain-barrier and tissue elements in a local brain injury. *J. Neuropathol. Exp. Neurol.* 1958;17:548-564
290. Elliott PJ, Garofalo L, Cuello AC. Limited neocortical devascularizing lesions causing deficits in memory retention and choline acetyltransferase activity--effects of the monosialoganglioside GM1. *Neuroscience.* 1989;31:63-76
291. Russell IS, Hobbelen JF, Van Hof MW, Pereira SC. The effect of devascularization of the visual cortex on visual function in the rabbit. *Behav. Brain Res.* 1984;14:69-80
292. Vengelen-Tyler V, ed. *Technical Manual* 12th ed. Bethesda MD: American Association of Blood Banks, 1996
293. Parkinson D, Stephensen S. Leukocytosis and subarachnoid hemorrhage. *Surg. Neurol.* 1984;21:132-134
294. Spallone A, Acqui M, Pastore FS, Guidetti B. Relationship between leukocytosis and ischemic complications following aneurysmal subarachnoid hemorrhage. *Surg. Neurol.* 1987;27:253-258
295. Suzuki S, Kelley RE, Dandapani BK et al. Acute leukocyte and temperature response in hypertensive intracerebral hemorrhage. *Stroke.* 1995;26:1020-1023
296. Herrera DG, Robertson HA. Unilateral induction of c-fos protein in cortex following cortical devascularization. *Brain Res.* 1989;503:205-213
297. Lee KR, Kawai N, Kim S et al. Mechanisms of edema formation after intracerebral hemorrhage: effects of thrombin on cerebral blood flow, blood-brain

- barrier permeability, and cell survival in a rat model. *J. Neurosurg.* 1997;86:272-278
298. Colbourne F, Sutherland GR, Auer RN. Electron microscopic evidence against apoptosis as the mechanism of neuronal death in global ischemia. *J. Neurosci.* 1999;19:4200-4210
299. Majno G, Joris I. Apoptosis, oncosis, and necrosis. An overview of cell death. *Am. J. Pathol.* 1995;146:3-15
300. Roy M, Sapolsky R. Neuronal apoptosis in acute necrotic insults: why is the subject such a mess? *Trends Neurosci.* 1999;22:419-422
301. Bona E, Andersson AL, Blomgren K et al. Chemokine and inflammatory cell response to hypoxia-ischemia in immature rats. *Pediatr. Res.* 1999;45:500-509
302. Lindsberg PJ, Ohman J, Lehto T et al. Complement activation in the central nervous system following blood- brain barrier damage in man. *Ann. Neurol.* 1996;40:587-596
303. Mathew P, Graham DI, Bullock R et al. Focal brain injury: histological evidence of delayed inflammatory response in a new rodent model of focal cortical injury. *Acta Neurochir. Suppl.* 1994;60:428-430
304. Soares HD, Hicks RR, Smith D, McIntosh TK. Inflammatory leukocytic recruitment and diffuse neuronal degeneration are separate pathological processes resulting from traumatic brain injury. *J. Neurosci.* 1995;15:8223-8233
305. Jean WC, Spellman SR, Nussbaum ES, Low WC. Reperfusion injury after focal cerebral ischemia: the role of inflammation and the therapeutic horizon. *Neurosurgery.* 1998;43:1382-1396

306. del Zoppo GJ, Von Kummer R, Hamann GF. Ischaemic damage of brain microvessels: inherent risks for thrombolytic treatment in stroke. *J. Neurol. Neurosurg. Psychiatr.* 1998;65:1-9
307. Montero-Menei CN, Sindji L, Pouplard-Barthelaix A et al. Lipopolysaccharide intracerebral administration induces minimal inflammatory reaction in rat brain. *Brain Res.* 1994;653:101-111
308. Schroeter M, Jander S, Witte OW, Stoll G. Local immune responses in the rat cerebral cortex after middle cerebral artery occlusion. *J. Neuroimmunol.* 1994;55:195-203
309. Weiss L. The blood. In: Weiss L, ed. *Cell and Tissue Biology*, 6th Ed. Baltimore, MD: Urban and Schwarzenberg, 1988:425-443
310. Schwarz S, Hafner K, Aschoff A, Schwab S. Incidence and prognostic significance of fever following intracerebral hemorrhage. *Neurology.* 2000;54:354-361
311. Lee JY, Lee MY, Chung SM, Chung JH. Chemically induced platelet lysis causes vasoconstriction by release of serotonin. *Toxicol. Appl. Pharmacol.* 1998;149:235-242
312. Akopov S, Sercombe R, Seylaz J. Cerebrovascular reactivity: role of endothelium/ platelet/leukocyte interactions. *Cerebrovasc. Brain Metab. Rev.* 1996;8:11-94
313. Cole DJ, McKay LD, Drummond JC et al. Subarachnoid molecular hemoglobin after subarachnoid hemorrhage in rats: effect on the area of hypoperfusion. *J. Neurosurg. Anesthesiol.* 1998;10:153-159

314. Clasen RA, Cooke PM, Pandolfi S et al. Experimental cerebral edema produced by focal freezing. 1. An anatomic study utilizing vital dye techniques. *J. Neuropathol. Exp. Neurol.* 1962;21:579-596
315. Lee KR, Betz AL, Keep RF et al. Intracerebral infusion of thrombin as a cause of brain edema. *J Neurosurg.* 1995;83:1045-1050
316. Ware JH, Dibenedetto AJ, Pittman RN. Localization of tissue plasminogen activator mRNA in adult rat brain. *Brain Res. Bull.* 1995;37:275-281
317. Figueroa BE, Keep RF, Betz AL, Hoff JT. Plasminogen activators potentiate thrombin-induced brain injury. *Stroke.* 1998;29:1202-1207
318. Wang YMF, Tsirka SE, Strickland S et al. Tissue plasminogen activator (tPA) increases neuronal damage after focal cerebral ischemia in wild-type and tPA-deficient mice. *Nature Med.* 1998;4:228-231
319. Schaller C, Rohde V, Meyer B, Hassler W. Stereotactic puncture and lysis of spontaneous intracerebral hemorrhage using recombinant tissue-plasminogen activator. *Neurosurgery.* 1995;36:328-335
320. Nishino A, Suzuki M, Yoshimoto T et al. A novel aspect of thrombin in the tissue reaction following central nervous system injury. *Acta Neurochir.* 1994;60 Suppl.:86-88
321. Cohen J. *Statistical Power Analysis for the Behavioral Sciences.* Revised Edition. Orlando FL: Academic Press, 1977:474
322. Kim WG, Mohny RP, Wilson B et al. Regional difference in susceptibility to lipopolysaccharide-induced neurotoxicity in the rat brain: Role of microglia. *J. Neurosci.* 2000;20:6309-6316

323. Bartha K, Domotor E, Lanza F et al. Identification of thrombin receptors in rat brain capillary endothelial cells. *J Cereb Blood Flow Metab.* 2000;20:175-182
324. McKinney M, Snider RM, Richelson E. Thrombin binding to human brain and spinal cord. *Mayo Clin. Proc.* 1983;58:829-881
325. Deschepper CF, Bigornia V, Berens ME, Lapointe MC. Production of thrombin and antithrombin III by brain and astroglial cell cultures. *Mol Brain Res.* 1991;11:355-358
326. Striggow F, Riek M, Breder J et al. The protease thrombin is an endogenous mediator of hippocampal neuroprotection against ischemia at low concentrations but causes degeneration at high concentrations. *Proc. Natl. Acad. Sci. USA.* 2000;97:2264-2269
327. Colon GP, Lee KR, Keep RF et al. Thrombin-soaked gelatin sponge and brain edema in rats. *J Neurosurg.* 1996;85:335-339
328. Castellino FJ. Plasmin. In: Woessner JF, ed. *Handbook of Proteolytic Enzymes.* San Diego CA: Academic Press, 1998:190-199
329. Fenton JWI. Thrombin specificity. *Ann N Y Acad Sci.* 1981;370:468-495
330. Lijnen HR, Collen D. t-plasminogen activator. In: Woessner JF, ed. *Handbook of Proteolytic Enzymes.* San Diego CA: Academic Press, 1998:184-190
331. Stone SR, le Bonniec BF. Thrombin. In: Woessner JF, ed. *Handbook of Proteolytic Enzymes.* San Diego CA: Academic Press, 1998:168-174
332. Donovan FM, Pike CJ, Cotman CW, Cunningham DD. Thrombin induces apoptosis in cultured neurons and astrocytes via a pathway requiring tyrosine kinase and RhoA activities. *J Neurosci.* 1997;17:5316-5326

333. Smirnova IV, Zhang SX, Citron BA et al. Thrombin is an extracellular signal that activates intracellular death protease pathways inducing apoptosis in model motor neurons. *J Neurobiol.* 1998;36:64-80
334. Cardell LO, Uddman R, Edvinsson L. Endothelins: a role in cerebrovascular disease? *Cephalalgia.* 1994;14:259-265
335. Ehrenreich H, Costa T, Clouse KA et al. Thrombin is a regulator of astrocytic endothelin-1. *Brain Res.* 1993;600:201-207
336. Hamann GF, Isenberg E, Strittmatter M et al. Big endothelin in spontaneous intracerebral hemorrhage. *Eur. Neurol.* 1994;34:99-102
337. Indyk JA, Chen ZL, Strickland S. Proteases and degradation of extracellular matrix in neurodegeneration. *Fibrinol. Proteol.* 1999;13:64-71
338. Higuchi M, Ito T, Imai Y et al. Expression of the  $\alpha$ 2-macroglobulin-encoding gene in rat brain and cultured astrocytes. *Gene.* 1994;141:155-162
339. Simpson CS, Johnston HM, Morris BJ. Neuronal expression of protease-nexin 1 mRNA in rat brain. *Neurosci. Lett.* 1994;170:286-290
340. Vivien D, Buisson A. Serine protease inhibitors: novel therapeutic targets for stroke? *J Cereb Blood Flow Metab.* 2000;20:755-764
341. Sappino AP, Madani R, Huarte J et al. Extracellular proteolysis in the adult murine brain. *J. Clin. Invest.* 1993;92:679-685
342. Ahn MY, Zhang ZG, Tsang W, Chopp M. Endogenous plasminogen activator expression after embolic focal cerebral ischemia in mice. *Brain Res.* 1999;837:169-176

343. Nagai N, De Mol M, Lijnen HR et al. Role of plasminogen system components in focal cerebral ischemic infarction - A gene targeting and gene transfer study in mice. *Circulation*. 1999;99:2440-2444
344. Tsirka SE, Gualandris A, Amaral DG, Strickland S. Excitotoxin-induced neuronal degeneration and seizure are mediated by tissue plasminogen activator. *Nature*. 1995;377:340-344
345. Chen ZL, Indyk JA, Bugge TH et al. Neuronal death and blood-brain barrier breakdown after excitotoxic injury are independent processes. *J Neurosci*. 1999;19:9813-9820
346. Kubo Y, Suzuki M, Kudo A et al. Thrombin inhibitor ameliorates secondary damage in rat brain injury: Suppression of inflammatory cells and vimentin-positive astrocytes. *J. Neurotrauma*. 2000;17:163-172
347. Berne RM, Levy MN. Blood and hemostasis. In: Stanton BA, ed. *Physiology*, 4th Edition: Harcourt / Mosby, 1998:1232
348. Colman RW, Hirsh J, Marder VJ, Salzman EW, eds. *Hemostasis and Thrombosis. Basic Principles and Clinical Practice.*: J.B. Lippincott Co., 1994
349. Gilles FH, Price RA, Kevy SV, Berenberg W. Fibrinolytic activity in the ganglionic eminence of the premature human brain. *Biol Neonate*. 1971;18:426-432
350. McDonald MM, Johnson ML, Rumack CM et al. Role of coagulopathy in newborn intracranial hemorrhage. *Pediatrics*. 1984;74:26-31

351. Van de Bor M, Briet E, Van Bel F, Ruys JH. Hemostasis and periventricular-intraventricular hemorrhage of the newborn. *Am J Dis Child.* 1986;140:1131-1134
352. MacDonald BK, Cockerell OC, Sander JW, Shorvon SD. The incidence and lifetime prevalence of neurological disorders in a prospective community-based study in the UK. *Brain.* 2000;123:665-676
353. Rubin RJ, Gold WA, Kelley DK, Sher JP. *The Cost of Disorders of the Brain.* Washington DC: National Foundation for Brain Research / Lewin-ICF, 1992:71
354. Hagberg G, Hagberg B. Antecedents. In: Goodman R, ed. *Congenital Hemiplegia.* Vol. 150. Cambridge UK: MacKeith Press, 2000:5-17
355. Towbin A. Mental retardation due to germinal matrix infarction. *Science.* 1969;164:156-161
356. Zhu Y, Li H, Zhou L et al. Cellular and molecular guidance of GABAergic neuronal migration from an extracortical origin to the neocortex. *Neuron.* 1999;23:473-485
357. Lemire RJ, Loeser JD, Leech RW, Alvord EC. *Normal and Abnormal Development of the Human Nervous System.* Hagerstown,MD: Harper and Row, 1975:421
358. Sturrock RR, Smart IH. A morphological study of the mouse subependymal layer from embryonic life to old age. *J Anat.* 1980;130:391-415
359. Doty FD, Entzminger G, Jr., Hauck CD, Staab JP. Practical aspects of birdcage coils. *J Magn Reson.* 1999;138:144-154

360. Leo O, Foo M, Sachs DH et al. Identification of a monoclonal antibody specific for a murine T3 polypeptide. *Proc Natl Acad Sci U S A*. 1987;84:1374-1378
361. Brown DC, Gatter KC. Ki67 protein: the immaculate deception? *Histopathology*. 2002;40:2-11
362. Tramontin AD, Garcia-Verdugo JM, Lim DA, Alvarez-Buylla A. Postnatal development of radial glia and the ventricular zone (VZ): a continuum of the neural stem cell compartment. *Cereb Cortex*. 2003;13:580-587
363. Woodhams PL, Basco E, Hajos F et al. Radial glia in the developing mouse cerebral cortex and hippocampus. *Anat Embryol (Berl)*. 1981;163:331-343
364. Papile LA, Burstein J, Burstein R, Koffler H. Incidence and evolution of subependymal and intraventricular hemorrhage: a study of infants with birth weights less than 1,500 gm. *J Pediatr*. 1978;92:529-534
365. Felderhoff-Mueser U, Rutherford MA, Squier WV et al. Relationship between MR imaging and histopathologic findings of the brain in extremely sick preterm infants. *AJNR Am J Neuroradiol*. 1999;20:1349-1357
366. Maalouf EF, Duggan PJ, Counsell SJ et al. Comparison of findings on cranial ultrasound and magnetic resonance imaging in preterm infants. *Pediatrics*. 2001;107:719-727
367. Hudgins RJ. Posthemorrhagic hydrocephalus of infancy. *Neurosurg Clin N Am*. 2001;12:743-751
368. Volpe JJ. Intraventricular hemorrhage in the premature infant - current concepts. Part 1. *Ann. Neurol*. 1989;25:3-11

369. Barakat I, Labourdette G, Sensenbrenner M. Inhibitory effects of fetal calf serum on proliferation of chick neuroblasts in culture. *Dev Neurosci*. 1983;6:169-183
370. Cameron HA, Hazel TG, McKay RD. Regulation of neurogenesis by growth factors and neurotransmitters. *J Neurobiol*. 1998;36:287-306
371. Luk KC, Sadikot AF. GABA promotes survival but not proliferation of parvalbumin-immunoreactive interneurons in rodent neostriatum: an in vivo study with stereology. *Neuroscience*. 2001;104:93-103
372. Lee SC, Dickson DW, Brosnan CF. Interleukin-1, nitric oxide and reactive astrocytes. *Brain Behav Immun*. 1995;9:345-354
373. Agrawal HC, Davis JM, Himwich WA. Developmental changes in mouse brain: weight, water content and free amino acids. *J Neurochem*. 1968;15:917-923
374. Anthony D, Dempster R, Fearn S et al. CXC chemokines generate age-related increases in neutrophil-mediated brain inflammation and blood-brain barrier breakdown. *Curr Biol*. 1998;8:923-926
375. Yu CC, Filipe MI. Update on proliferation-associated antibodies applicable to formalin-fixed paraffin-embedded tissue and their clinical applications. *Histochem J*. 1993;25:843-853
376. Scott RJ, Hall PA, Haldane JS et al. A comparison of immunohistochemical markers of cell proliferation with experimentally determined growth fraction. *J Pathol*. 1991;165:173-178
377. Nosarti C, Al-Asady MH, Frangou S et al. Adolescents who were born very preterm have decreased brain volumes. *Brain*. 2002;125:1616-1623

378. Mansuy IM, Vanderputten H, Schmid P et al. Variable and multiple expression of protease nexin-1 during mouse organogenesis and nervous system development. *Development*. 1993;119:1119-1134
379. Bayer S. Embryology. In: Duckett S, ed. *Pediatric Neuropathology*. Malvern, PA: Williams and Wilkins, 1995:54-107
380. Morell P, Greenfield S, Costantino-Ceccarini E, Wisniewski H. Changes in the protein composition of mouse brain myelin during development. *J Neurochem*. 1972;19:2545-2554
381. Sacher GA, Staffeldt EF. Relation of gestation time to brain weight for placental mammals: implication for the theory of vertebrate growth. *AM Naturalist*. 1974;108:593-615
382. Arand AG, Sawaya R. Intraoperative chemical hemostasis in neurosurgery. *Neurosurgery*. 1986;18:223-233
383. O'Shaughnessy CT, Lodge D. N-methyl-D-aspartate receptor-mediated increase in intracellular calcium is reduced by ketamine and phencyclidine. *Eur J Pharmacol*. 1988;153:201-209
384. Kolb B, Cioe J, Whishaw IQ. Is there an optimal age for recovery from motor cortex lesions? II. behavioural and anatomical consequences of unilateral motor cortex lesions in perinatal, infant, and adult rats. *Restor Neurol Neurosci*. 2000;17:61-70
385. Kolb B, Cioe J. Recovery from early cortical damage in rats, VIII. Earlier may be worse: behavioural dysfunction and abnormal cerebral morphogenesis following perinatal frontal cortical lesions in the rat. *Neuropharmacology*. 2000;39:756-764

386. De Felice C, Toti P, Laurini RN et al. Early neonatal brain injury in histologic chorioamnionitis. *Journal Of Pediatrics*. Jan. 2001;138:101-104
387. Bannerman DD, Goldblum SE. Direct effects of endotoxin on the endothelium: barrier function and injury. *Lab Invest*. 1999;79:1181-1199
388. Bohatschek M, Werner A, Raivich G. Systemic LPS injection leads to granulocyte influx into normal and injured brain: effects of ICAM-1 deficiency. *Exp Neurol*. 2001;172:137-152
389. Doukas J, Cutler AH, Mordes JP. Polyinosinic:polycytidylic acid is a potent activator of endothelial cells. *Am J Pathol*. 1994;145:137-147
390. Popko B, Corbin JG, Baerwald KD et al. The effects of interferon-gamma on the central nervous system. *Mol Neurobiol*. 1997;14:19-35
391. Watanabe Y, Morita M, Akaike T. Concanavalin A induces perforin-mediated but not Fas-mediated hepatic injury. *Hepatology*. 1996;24:702-710
392. Watanabe T, Yamamoto T, Abe Y et al. Differential activation of microglia after experimental spinal cord injury. *J. Neurotrauma*. 1999;16:255-265
393. Schuligoi R, Ulcar R, Peskar BA, Amann R. Effect of endotoxin treatment on the expression of cyclooxygenase-2 and prostaglandin synthases in spinal cord, dorsal root ganglia, and skin of rats. *Neuroscience*. 2003;116:1043-1052
394. Paul L, Fraifeld V, Kaplanski J. Evidence supporting involvement of leukotrienes in LPS-induced hypothermia in mice. *Am J Physiol*. 1999;276:R52-58
395. Burch RM, Noronha-Blob L, Bator JM et al. Mice treated with a leumedin or antibody to Mac-1 to inhibit leukocyte sequestration survive endotoxin challenge. *J Immunol*. 1993;150:3397-3403

396. Dommergues MA, Patkai J, Renauld JC et al. Proinflammatory cytokines and interleukin-9 exacerbate excitotoxic lesions of the newborn murine neopallium. *Ann. Neurol.* 2000;47:54-63
397. Benveniste EN. Cytokine actions in the central nervous system. *Cytokine Growth Factor Rev.* 1998;9:259-275
398. Cannella B, Raine CS. The adhesion molecule and cytokine profile of multiple sclerosis lesions. *Ann Neurol.* 1995;37:424-435
399. Watson DL, Colditz IG, Andrew M et al. Age-dependent immune response in Merino sheep. *Res Vet Sci.* 1994;57:152-158
400. Morin MJ, Karr SM, Faris RA, Gruppuso PA. Developmental variability in expression and regulation of inducible nitric oxide synthase in rat intestine. *Am J Physiol Gastrointest Liver Physiol.* 2001;281:G552-559
401. Martin TR, Ruzinski JT, Wilson CB, Skerrett SJ. Effects of endotoxin in the lungs of neonatal rats: age-dependent impairment of the inflammatory response. *J Infect Dis.* 1995;171:134-144
402. Cusumano V, Mancuso G, Genovese F et al. Neonatal hypersusceptibility to endotoxin correlates with increased tumor necrosis factor production in mice. *J Infect Dis.* 1997;176:168-176
403. Jiang Y, Wu J, Keep RF et al. Hypoxia-inducible factor-1alpha accumulation in the brain after experimental intracerebral hemorrhage. *J Cereb Blood Flow Metab.* 2002;22:689-696

404. Junge CE, Sugawara T, Mannaioni G et al. The contribution of protease-activated receptor 1 to neuronal damage caused by transient focal cerebral ischemia. *Proc Natl Acad Sci U S A*. 2003;100:13019-13024
405. Rigatto H, Rehan V, Lemke RP et al. Respiratory pacemaker cells responsive to CO(2) in the upper medulla: dose response and effects of mediators. *Pediatr Pulmonol*. 2000;30:359-367
406. Fox WM. Reflex-ontogeny and behavioural development of the mouse. *Anim Behav*. 1965;13:234-241
407. Wang H, Reiser G. Thrombin signaling in the brain: the role of protease-activated receptors. *Biol Chem*. 2003;384:193-202
408. Coughlin SR. Thrombin signalling and protease-activated receptors. *Nature*. 2000;407:258-264
409. Suo Z, Wu M, Citron BA et al. Persistent protease-activated receptor 4 signaling mediates thrombin-induced microglial activation. *J Biol Chem*. 2003;278:31177-31183
410. Muszbek L, Hauck M. Fragmentation of actin by thrombin-like snake venom proteases. *Biochim Biophys Acta*. 1979;577:34-43
411. Quinton TM, Kim S, Derian CK et al. Plasmin-mediated activation of platelets occurs by cleavage of protease-activated receptor 4. *J Biol Chem*. 2004;279:18434-18439
412. Domotor E, Bartha K, Machovich R, Adam-Vizi V. Protease-activated receptor-2 (PAR-2) in brain microvascular endothelium and its regulation by plasmin and elastase. *J Neurochem*. 2002;80:746-754

413. Barone FC, Willette RN, Yue TL, Feurestein G. Therapeutic effects of endothelin receptor antagonists in stroke. *Neurol Res.* 1995;17:259-264
414. Kreutzberg GW. Microglia: a sensor for pathological events in the CNS. *Trends Neurosci.* 1996;19:312-318
415. Billiau A. Interferon-gamma: biology and role in pathogenesis. *Adv Immunol.* 1996;62:61-130
416. Li HL, Kostulas N, Huang YM et al. IL-17 and IFN-gamma mRNA expression is increased in the brain and systemically after permanent middle cerebral artery occlusion in the rat. *J Neuroimmunol.* 2001;116:5-14
417. Kitaoka T, Hua Y, Xi G et al. Delayed argatroban treatment reduces edema in a rat model of intracerebral hemorrhage. *Stroke.* 2002;33:3012-3018